Water Technology and Sciences

Included in Thomson Reuters Science Citation Index® (ISI) • Expanded Thomson Reuters Research Alert® (ISI) • EBSCO • ProQuest • Elsevier • Redalyc

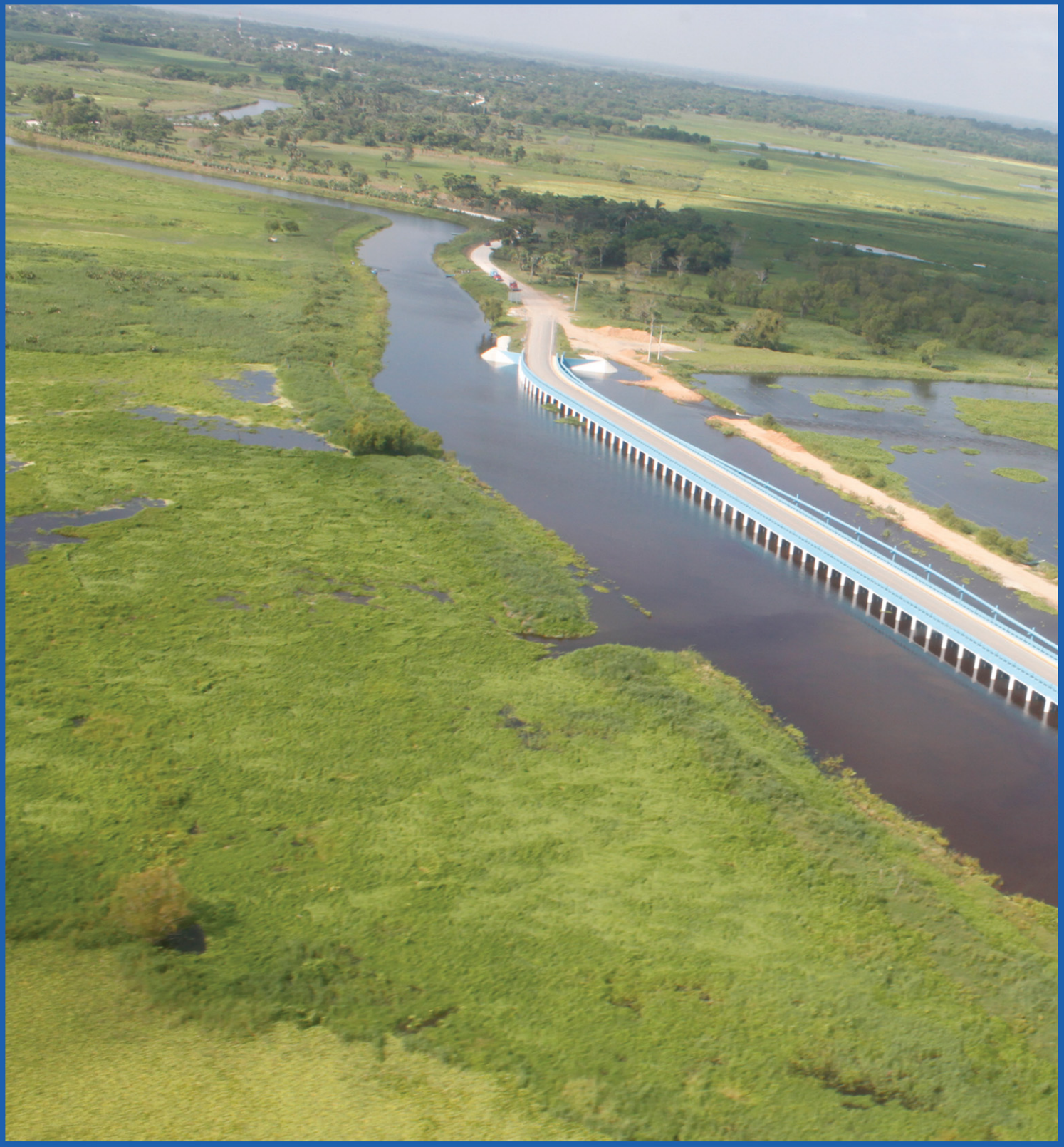

Vol. V, No. 3, May-June, 2014

Water Technology and Sciences

Edit Board

Editorial coordination and careful editing: Helena Rivas-López • **Editorial assistance and editorial layout:** Luisa Guadalupe Ramírez-Martínez • **Figures design:** Luisa Guadalupe Ramírez-Martínez and Rosario Castro-Rivera • **Coordination arbitration:** Elizabeth Peña and Bibiana Bahena • **Proofreading English:** Ellen Weiss • **Logo design and cover:** Oscar Alonso-Barrón • **Design format:** Gema Alín Martínez-Ocampo • **Marketing:** Marco Antonio Bonilla-Rincón.

Editorial Committee

©***Water Technology and Sciences.*** Vol. V, No. 3, May-June, 2014, is a bimonthly publication edited by the Instituto Mexicano de Tecnología del Agua, Paseo Cuauhnáhuac 8532, Colonia Progreso, Jiutepec, Morelos, C.P. 62550, telephone +52 (777) 3 29 36 00, extension 474, www.imta.gob.mx/tyca, fsalinas@tlaloc.imta.mx. Responsible editor, Nahún Hamed García Villanueva; Copyright No. 04-2013-121014514100-203, granted by the Instituto Nacional de Derechos de Autor. ISSN pending. Responsible for the latest update of this issue: Sub-Department of Dissemination and Circulation, Francisco José Salinas Estrada, Paseo Cuauhnáhuac 8532, Colonia Progreso, Jiutepec, Morelos, C.P. 62550.

Water Technology and Sciences is the traslation of *Tecnología y Ciencias del Agua*, which is the continuation of the following journals: *Irrigación en México* (1930-1946); *Ingeniería hidráulica en México* (1947-1971); *Recursos hidráulicos* (1972-1978), and *Ingeniería hidráulica en México*, second period (1985-2009).

For subscriptions, click here

Water Technology and Sciences

Vol. V, No. 3, May-June, 2014

Coordination for editorial comments, click here give

Home: pouring structure in the municipality of Buenavist Center in Tabasco. In the argo in its history, the Tabasco plain has suffered extensive flooding. The population initially occupied the highlands less susceptible to flooding, but population growth, lack of planning territorial, deforestation in the upper watershed and false sense of security associated with the construction of large dams on the Grijalva River has become very vulnerable populations and productive areas of Tabasco. Article "Analysis of flooding in Tabasco plain in the period 1995-2010 "(pp. 5-32) Philip I. Arreguin Cortés *et al*., the factors affecting the floods are analyzed the Tabasco plain, such as the absence of order appropriate land, deforestation in uptown watershed, a false concept of reduction scheme hydrological associated with the construction of large dams in the Grijalva River and climate change. It is also made a review of rainfall, runoff management dams Grijalva River basin and floods; present actions taken to reduce risks Flood the population during 1995-2010, including the Comprehensive Flood Control Programme and Programme Integral Water Tabasco, noting the conceptual difference among them.

Photo provided by Horacio Rubio Gutiérrez.

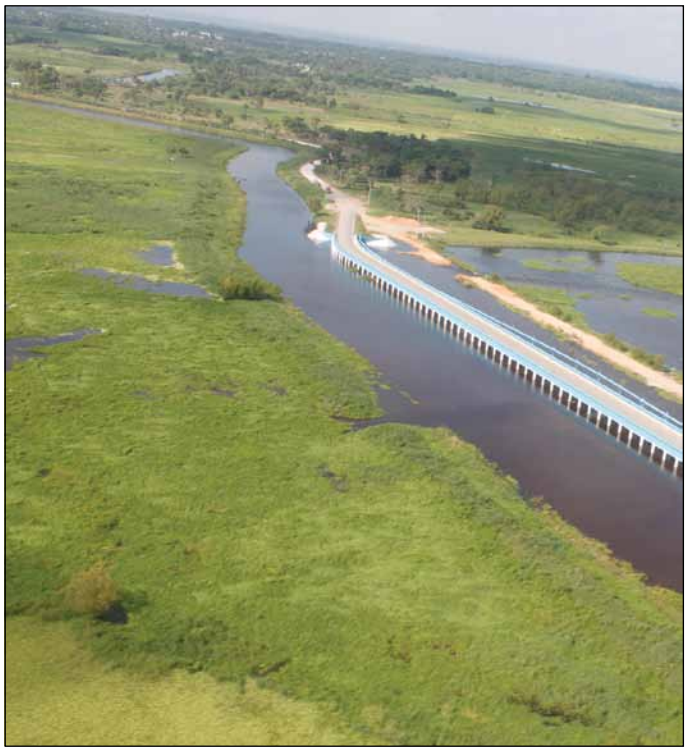

Change sequence flow conditions in a channel.

Photo: Jorge Izurieta.

Contents

Technical articles

Contenido

Artículos técnicos

Analysis of Floods in the Tabasco Plains from 1995-2010

• Felipe I. Arreguín-Cortés* • Horacio Rubio-Gutiérrez •
Comisión Nacional del Agua, México
*Corresponding Author

• Ramón Domínguez-Mora • Faustino de Luna-Cruz •
Universidad Nacional Autónoma de México

Abstract

ARREGUÍN-CORTÉS, F.I., RUBIO-GUTIÉRREZ, H., DOMÍNGUEZ-MORA, R. & DE LUNA-CRUZ, F. Analysis of Floods in the Tabasco Plains from 1995-2010. *Water Technology and Sciences* (in Spanish). Vol. V, No. 3, May-June, 2014, pp. 5-32.

The factors that influence floods in the plains of Tabasco are analyzed, including the lack of adequate land planning, deforestation of the upper basins, and a mistaken idea about decreases in the hydrological regime associated with the construction of large dams in the Grijalva River and climate change. A review of precipitation, runoff, management of dams in the Grijalva River basin and floods was conducted for the period 1995 – 2010. The actions taken to reduce flood risks for the population during that period are presented, including the Comprehensive Flood Control Program and the Tabasco Comprehensive Water Program. The conceptual differences between these are indicated. The objective of the present article is to describe the evolution of approaches to reduce flood disasters in the Tabasco plains, the management of reservoirs and a proposal for land management based on the application of a two-dimensional numerical hydraulic model and a nomogram for prevention of rollovers.

Keywords: Grijalva-Usumacinta, flood management, floods, structural and non-structural actions, risk mitigation.

Resumen

ARREGUÍN-CORTÉS, F.I., RUBIO-GUTIÉRREZ, H., DOMÍNGUEZ-MORA, R. & DE LUNA-CRUZ, F. Análisis de las inundaciones en la planicie tabasqueña en el periodo 1995-2010. Tecnología y Ciencias del Agua. *Vol. V, núm. 3, mayo-junio de 2014, pp. 5-32.*

Se analizan los factores que influyen en las inundaciones de la planicie tabasqueña, como la ausencia de ordenamiento territorial adecuado, la deforestación de la parte alta de las cuencas, un falso concepto de disminución del régimen hidrológico asociado con la construcción de las grandes presas en el río Grijalva y el cambio climático. Para el periodo 1995-2010 se hace una revisión de las precipitaciones, escurrimientos, manejo de las presas de la cuenca del río Grijalva e inundaciones; se presentan las acciones que se han tomado para reducir los riesgos de inundación a la población durante ese periodo, incluyendo el Programa Integral de Control de Inundaciones y el Programa Hídrico Integral de Tabasco, señalando la diferencia conceptual entre ellos. El objeto del presente artículo es describir la evolución de las aproximaciones de solución al problema de reducción de desastres por inundación en la planicie Tabasqueña, la gestión de embalses y una propuesta de gestión del territorio basado en la aplicación de un modelo numérico hidráulico bidimensional y un nomograma de resistencia al vuelco.

Palabras clave: *Grijalva-Usumacinta, manejo de crecientes, inundaciones, acciones estructurales y no estructurales, mitigación del riesgo.*

Introduction

Historically, The Tabasco plains has experienced large floods (see Table 1). The population began to occupy the high regions which are less susceptible to flooding, nevertheless population growth, lack of land planning, deforestation of the upper basins and a false sense of security associated with the construction of large dams in the Grijalva River have made the populations and production regions of Tabasco vulnerable.

The Economic Commission for Latin America and the Caribbean (CEPAL, Spanish acronym) and the National Center for Disaster Prevention (Cenapred, Spanish acronym)

Table 1. Major flooding in Tabasco plain. (Rivera-Trejo, 2011; Ortiz-Pérez *et al.*, 2005).

Year	Reference of floods registered in the state of Tabasco
1782	Santa Rosa Flood
1820	Large Flood
1868	Continuous Rain
1879	800 houses flooded
1886	Level: 13.71 masl
1888	Hurricane floods Villahermosa
1889	155 houses flooded, deaths and boats disappeared
1909	2 953 victims
1912	Grijalva River overflows
1936	Grijalva River overflows
1944	Rivers and lagoons overflow
1955	Ciclone *Janet*
1969	Grijalva River overflows
1973	Grijalva River overflows
1980	Historical rains

estimate losses from floods over the past five years at more than $57 000 million pesos (2007-2011) (CEPAL-CENAPRED-SEPLAN, 2012). Although large investments have been made by the federal government and infrastructure has been built which has alleviated the impact of floods on the city of Villahermosa, comprehensive proposals are needed in order to protect the population of Tabasco given the lack of control works in the La Sierra and Usumacinta Rivers, the particular morphology of the region, the invasion of the river channels (the weir in the Peñitas dam is designed to release 18 700 cubic meters per second of water and only 1 100 m^3/s flows through the river without causing damage) and a lack of land planning and reforestation policies. The already evident impact of climate change on the region should also be considered.

Physical Context

Physiography

Most of Tabasco is located in the physiographic province of the "Southern Gulf Coastal Plains" and a smaller portion is in the "Chiapas and Guatemala Mountain Range" (INEGI, 1986). The coastal plains is composed of marine and lacustrine basins filled with earth materials transported by surface currents, leading to the formation of the delta complex formed by the Mezcalapa-Grijalva-Usumacinta rivers and the fluvial deltaic plain of the Tonala River (Figure 1). The delta complex is subject to subsidence due to the consolidation of large amounts of sediments which are compacted and create sinks in this portion of the coastal plains.

Morphology of Rivers

The basin drains towards the north, and in the hillside the rivers are naturally diverted to the east. The morphology of the rivers is meandering in the plains, with rivers converting from their mountain geoform into networks of rivers and floodplains (see Figure 2).

Since this fluvial deltaic plain is in development, the orientation and direction of the rivers change as sediment drifting in the upper basin surpasses the sediment

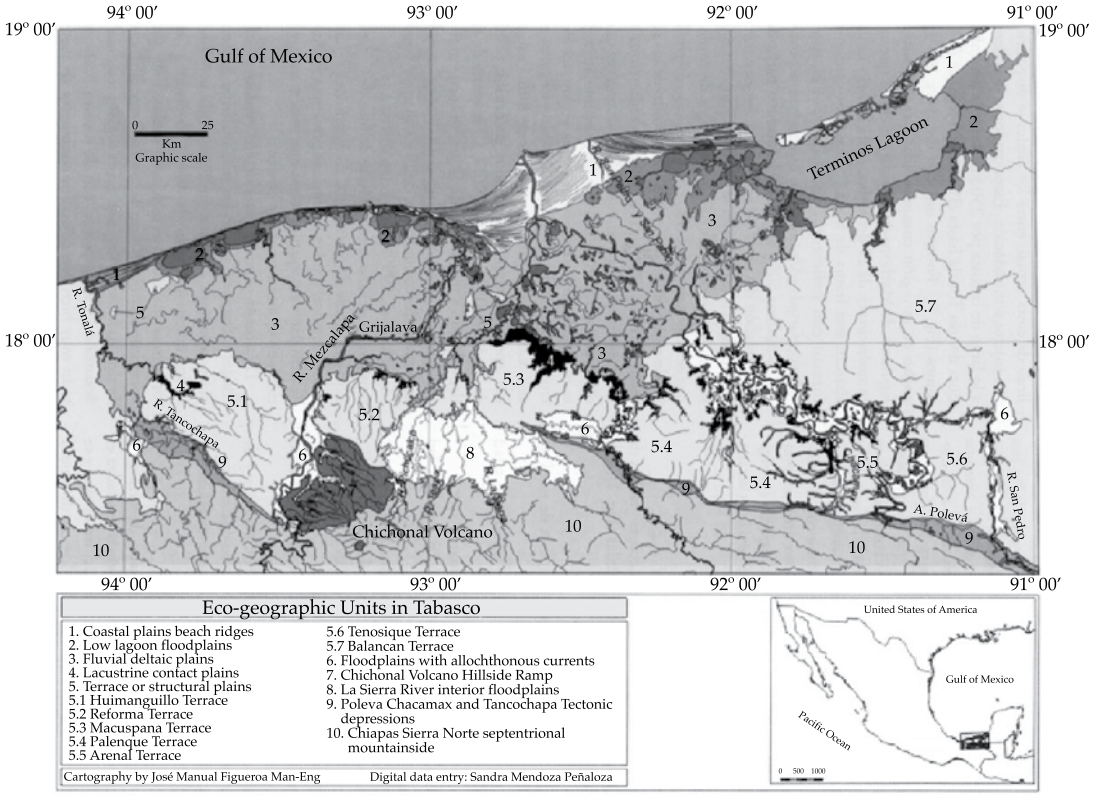

Figure 1. Eco-geographic units in Tabasco.

Figure 2. Hydrograph of the Grijalva-Usumacinta basin.

transport capacity. This divagation or avulsion are known in the region as "breaks".

Climatology

The state has a hot climate which is influenced by the sea. The annual mean temperature is 22°C. Rains occur nearly year-round, with a dry season in March and April.

There are three predominant sources of rainfall in the region: tropical cyclones and waves from the Caribbean Sea and Atlantic Ocean; the inter-tropical convergence zone whose latitude rises in summer, affecting the upper Grijalva basin; and cold fronts resulting in significant rainfall in the northern portion of the basin from September to February (Figure 3).

It is important to mention that the tropical rainfall regime significantly decreases in the upper Grijalva River basin, in the regions supplying the Chicoasen and Angostura dams. In the middle basin, where Malpaso and Peñitas are located, an intense regime continues from September through October and November.

Hydrology

The Grijalva River begins in Guatemala in the Cuchumatanes mountains. It enters Mexico by passing through the central depression in Chiapas, where its supply is regulated by the Angostura dam. Downstream, the river borders the city of Tuxtla Gutierrez, the capital of the state of Chiapas, and later reaches the Chicoasen dam, which has the largest electric generation capacity in the country. Afterwards, the Grijalva receives water on the left from the La Venta River and on the right from the Chocoasen and Yamonho Rivers, where the Malpaso dam is located. Several currents then converge to form the Mezcalapa River, the local name

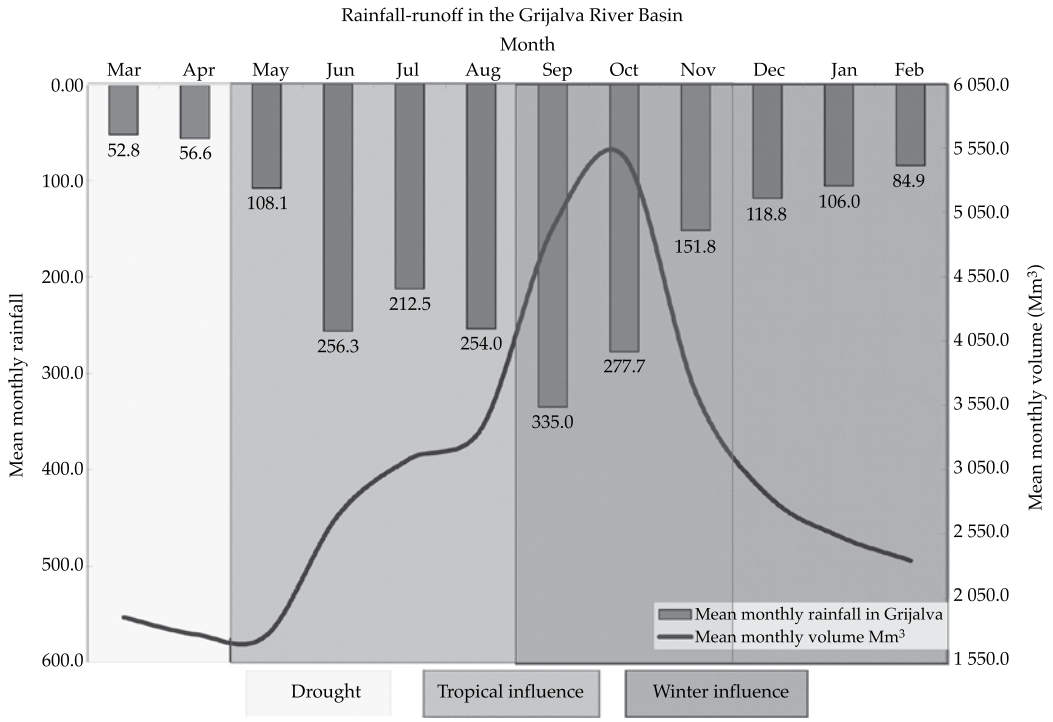

Figure 3. Rainfall-runoff regime in the Grijalva River Lower Basin.

of the Grijalva River. This splits into the Samaria River to the left (which flows into the Gulf of Mexico at Barra de Chiltepec) and the Carrizal River to the right, which runs through the city of Villlahermosa, capital of the state of Tabasco, where it receives water from the rivers flowing out of the mountains, with headwaters in the Altos de Chiapas. At this confluence is where it gets the name Grijalva River, and after running through the city of Villahermosa it joins with the Usamacinta River and then flows into the Gulf of Mexico. It is important to mention again that the rivers overflow in the lower plains nearly every year.

The annual mean volume that runs into the mouth of the Grijalva River is roughly 36 500 million m^3. When adding the volume from the Usumacinta River, the amount of freshwater discharged into the Gulf of Mexico is roughly 100 000 million cubic meters. It is worth mentioning that the river control infrastructure of dams in the Grijalva River can only regulate 23% of the annual mean runoff of the entire basin.

The floods in the region are seasonal. Those occurring from May through November are caused by rainfall generated by tropical systems; from July through September they are caused by the inter-tropical convergence zone; and after September the runoff in the basin is created by the incidence of cold fronts that continue through the last week of February. The months with the most intense rainfall and floods are September and October, when these three systems combine.

Recent Historical Floods

In order to analyze the primary floods that occurred during the years 1995 to 2010, accumulated rainfall will be described next according to contour line, the limnigraphs from the hydrometric stations El Muelle, Samaria, González and Boca del Cerro, and the functioning of the reservoirs at the Angostura, Chicoasen, Malpaso and Peñitas dams from June 1 through October 31, for each case.

Year 1995

This rainy season was characterized by the occurrence of hurricanes Opal and Roxanne, with an average accumulated rainfall of 1792 mm during the period mentioned above.

At the El Muelle station (see Figure 2 for location of stations), the Grijalva River rose above the *Ordinary High Water Level* (OHWL) during two periods: from September 3 to 19 and from September 30 to October 26. The OHWL was not exceeded at the Gonzalez station in the Carrizal and the Samaria station in the Samaria River, or at the Boca del Cerro station in the Usamacinta River (Figure 4).

In terms of the functioning of the dams, the largest amounts entered during September, with maximum flows of 2 661, 1 083 and 2 493 m^3/s, in the Angostura, Chicoasén and Malpaso dams, respectively. Only the Angostura dam operated in excess of the OHWL, as of September 17th. It was not necessary to operate weirs in any of these cases. The maximum extraction was 1 350 m^3/s from Peñitas (Figure 5).

Year 1999

Mean rainfall in the basin during the same period was 1720 mm, with most of the contour line concentrated in the Peñitas basin, of roughly 2 450 mm. This was due to the combination of the tropical waves depressions 26 to 30, tropical depression 11 and cold fronts 4 and 7, which caused three floods in mountain rivers without controls, with overflowing in the area of the city of Villahermosa. Another relevant effect of this hydrological event was a morphological

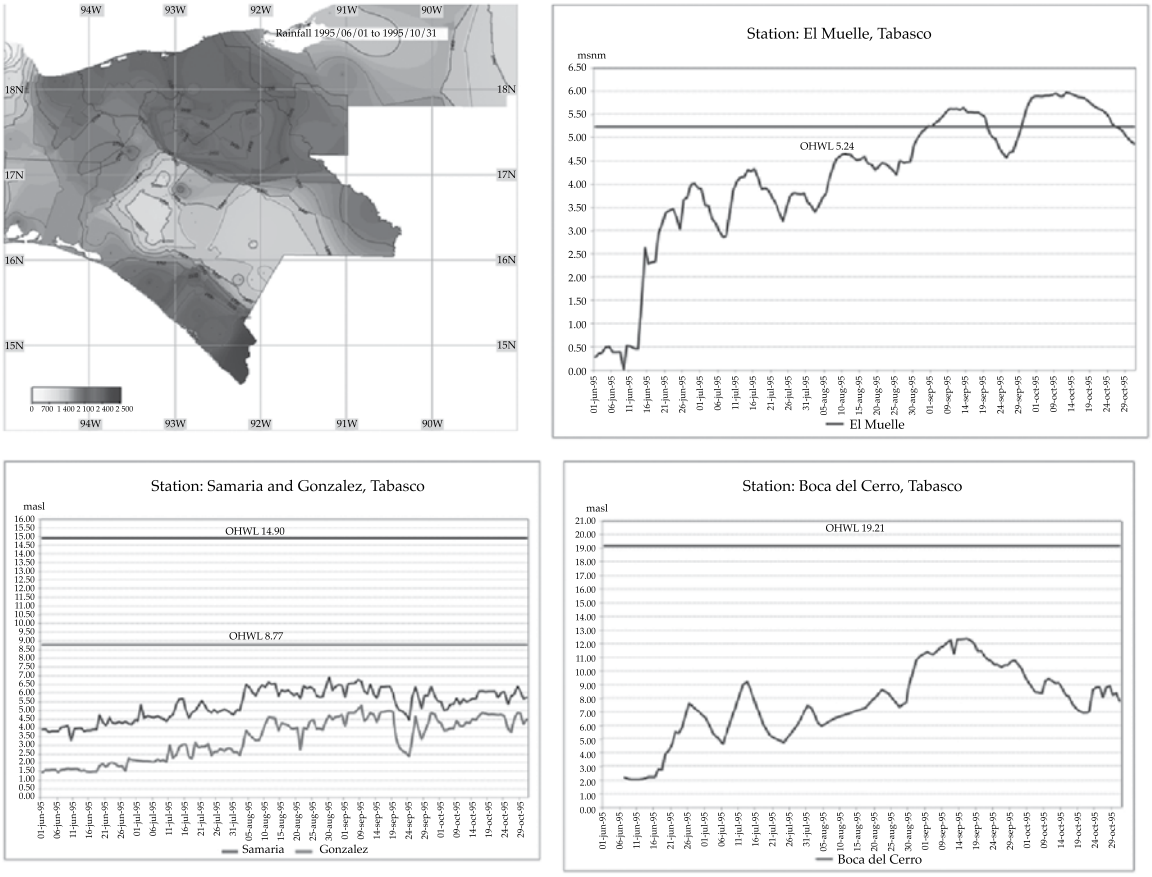

Figure 4. Limnigraphs for the stations El muelle, Samaria, Gonzalez and Boca del Cerro, 1995.

change in the branching of the Mezcalapa River into the Samaria and Carrizal rivers which, unlike in 1997, sent 60% of the flow down the Carrizal River which runs through Villahermosa. To restore the percentage share of the flow, the need to build a control structure at the site known as Macayo was suggested.

During this event, in the city of Villahermosa, the OHWL of the river was exceeded at the El Muelle hydrometric station on September 13 and remained above that mark until November 25. At the Gonzalez stations in the Carrizal and the Samaria station in the Samaria River, the free water surface was above their OHWLs from October 6 through 31. The Usumacinta River remained above this level from September 14 to October 27 and from November 9 to 19 (see Figure 6). The length of time that the level of the Grijalva River remained above the OHWL, as compared to the Gonzalez station in the Carrizal River, confirms that most of the water contributing to this flood came from the system of mountain rivers.

The Angostura dam stored increasing volumes over the entire period. The OHWL was exceeded on September 20, the supply to the dam from September 9 to October 24 remained above 1 000 m^3/s, with a daily maximum of 3 036 m^3/s. During the regulation of the floods, the Agonstura registered the highest storage, with 538.20 masl on October 25 of that year.

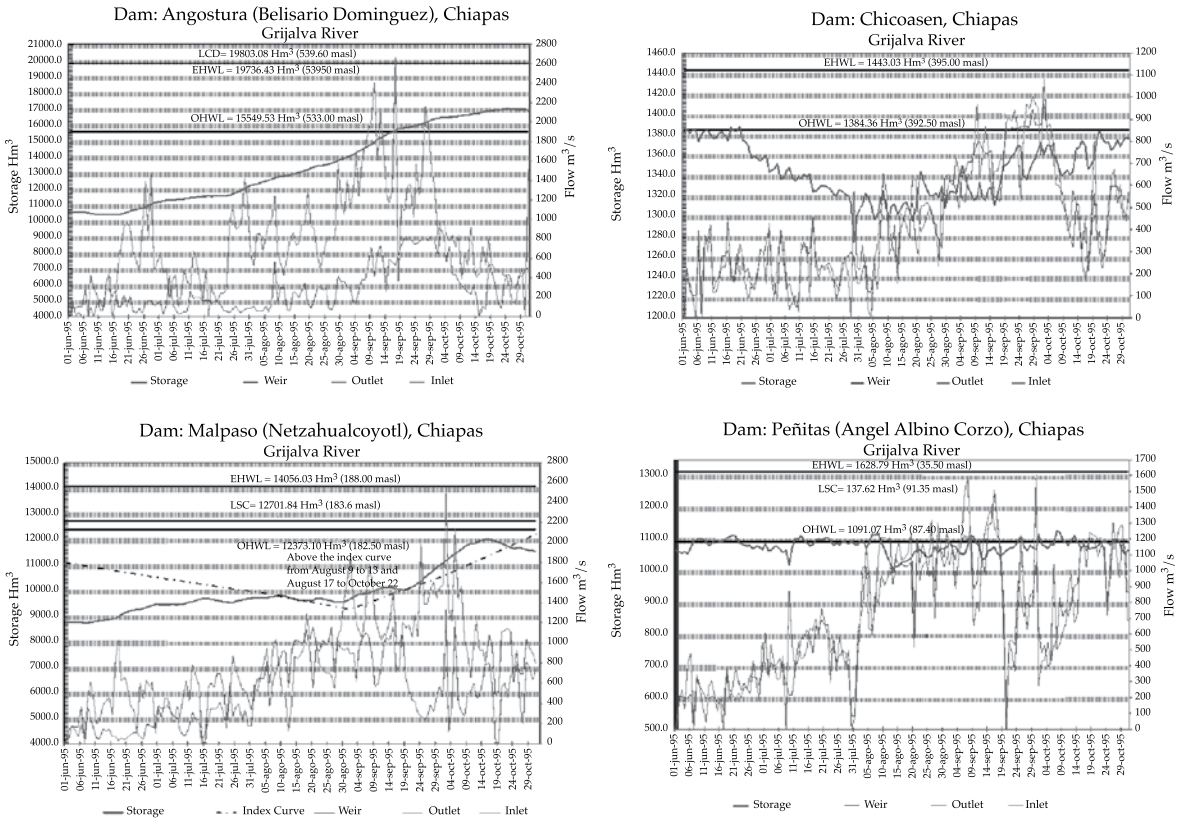

Figure 5. Functioning of the reservoirs in the Angostura, Chicoasen, Malpaso and Peñitas Dams, 1995.

The storage in the Malpaso dam during the period of analysis was above the guideline curve from June 23 to 29, July 2 to 30, August 12 to September 7 and September 15 to the end of the period. This dam was closed from September 15 to October 2. After rainfalls from cold front 4 and tropical depression 11, extractions were resumed at the full capacity of the turbines. At the end of October, with the impossibility of closing the Malpaso dam to reduce the storage in Peñitas, the weir was operated with flows up to 1 274 m^3/s (Figure 7).

The floods in Villahermosa led to the construction of perimeter walls around the entire city and along the banks of the urban rivers over the follow year. They were also the reason for the study of the technical feasibility of flood protection for the lower Grijalva River basin (Conagua, 2000). This later became the Comprehensive Flood Control Program (Programa Integral de Control de Inundaciones; PICI, Spanish acronym). These floods also resulted in the guideline storage curve that has governed the Angostura dam since the year 2000 and in the formation of the first Mexican Technical Operations Committee for Regional Hydraulic Works (Comité Técnico de Operación de Obras Hidráulicas Regional; CTOOH-R, Spanish acronym).

Year 2007

This year there was an abrupt and intense cooling of the Pacific Ocean, which caused a cold phase event of the El Niño Southern Oscillation (ENSO). The rainy season began early with the impact of the hurricane Barbara in the upper Grijalva on June

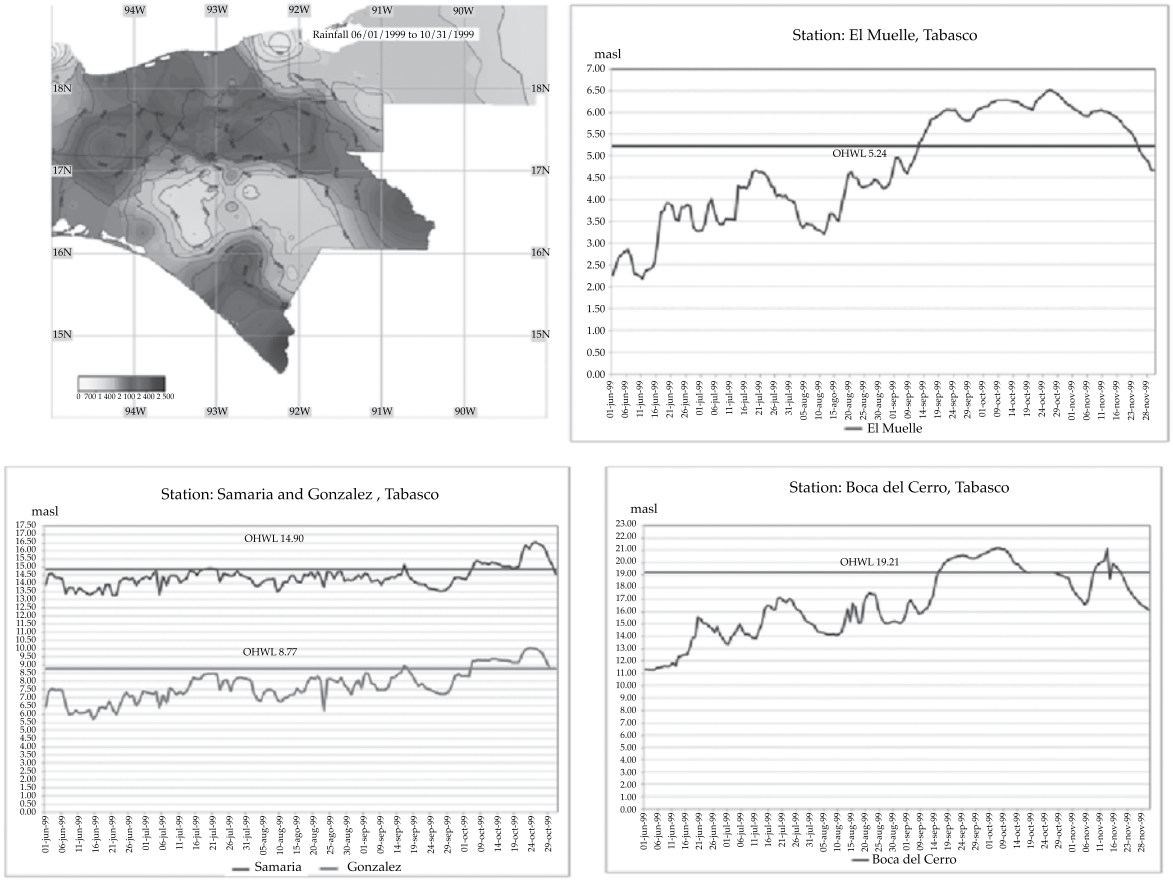

Figura 6. Limnigraphs for the El Muelle, Samaria, Gonzalez and Boca del Cerro stations, 1999.

2. The rainfall regime remained intense until the end of October, finishing with an accumulated flow in the basin of 1 423 mm, with concentrated cores in the Peñitas of 2 500 mm. This event was produced by cold fronts 4 and 7, strengthened four days later by hurricane Noel which caused roughly 1 000 mm of rain to accumulate in the Peñitas basin in less than 72 hours.

At the El Muelle station, the Grijalva River was above its OHWL from October 24 to November 13. During the week of October 29 to November 3, the water overflowed the dike's crown. In the Samaria and Gonzalez Rivers, the OHWLs were exceeded from October 29 to November 3. And although flooding was registered in the Usumacinta River, it did not exceed its OHWL (Figure 8).

The average supply flows to the Angostura and Malpaso dams during August and September were around 680 and 540 m^3/s, respectively. The regime increased considerably by October, reaching average values of 840 and 1 122 m^3/s, with daily maximums of 2 932 and 3 652 m^3/s, respectively.

By the beginning of September, storage at Angostura reached a height of 526.54 masl, 0.54 m above the index curve, whereas storage at Malpaso remained at 167.33 masl, 3.17 meters below the index curve. The supply to the Angostura reservoirs was

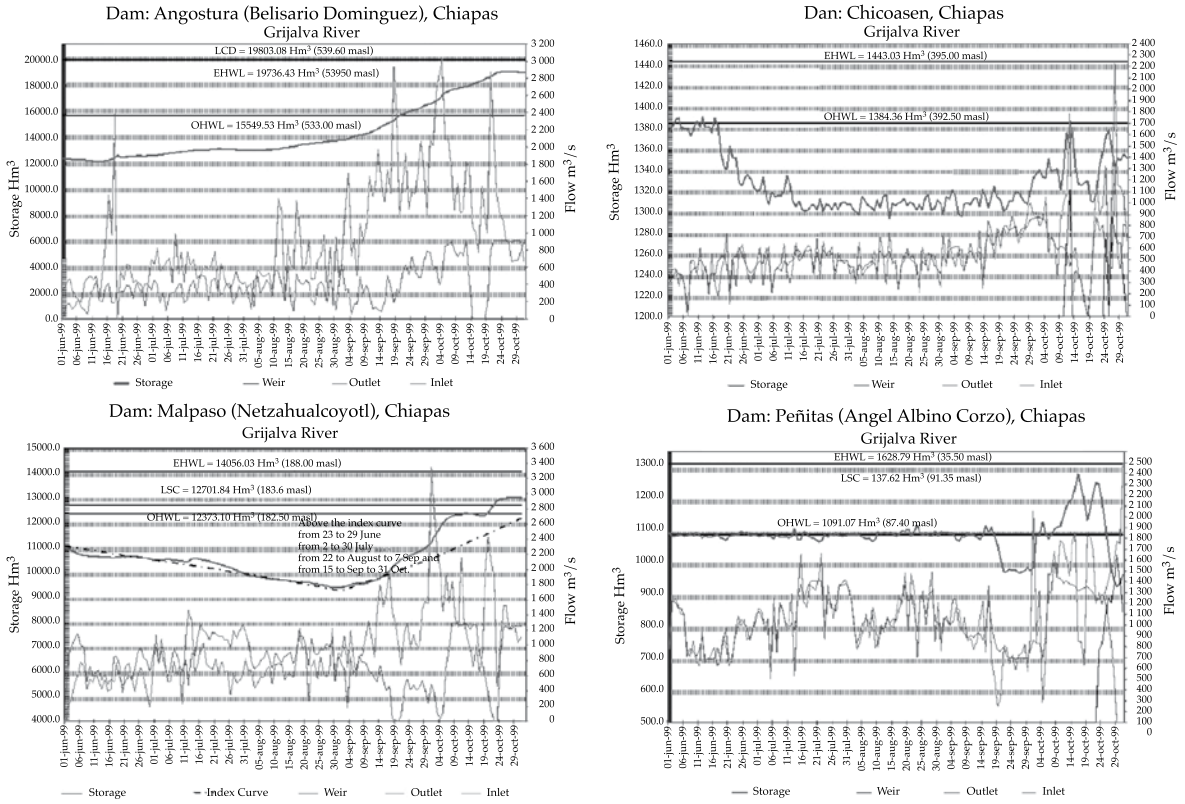

Figure 7. Functioning of the reservoirs in the Angostura, Chicoasen, Malpaso and Peñitas Dams, 1999.

classified as an average month with 2 178.63 Hm^3 and Malpaso was classified as a very dry month with 581.99 Hm^3.

By the first of October, Angostura was at a level of 529.33 masl, 0.67 meters below the storage amount established as safe according to the index curve, and Malpaso was at a height of 172.4 masl, 3.78 meters below the index curve.

During management of the floods caused by cold fronts 2 and 4 and the strengthening of the latter from the polar air mass and its interaction with hurricane Noel, enough space was created in the dams for Malpaso to stop extraction on October 23 and Angostura on October 29, which lasted until December 18. Thus, the upper Grijalva did not contribute to flooding in Tabasco.

The flooding of the Peñitas reservoir, even with the Malpaso dam being closed, required increasing the extraction of 550 m^3/s to a maximum of 2 000 m^3/s on the 29th of that month and the following days (Senate of the Republic, Commission of Hydraulic Affairs, 2008), until November 4 when a landslide blocked the Peñitas reservoir (Figure 9). The river levels that exceeded their OHWLs, at the El Muelle station, were higher than those at the Gonzalez station because the rivers in the mountains do not have control structures upstream from the station.

Two-thirds of the city of Villahermosa was flooded for roughly 40 days which, along with the landslide mentioned, constitutes one of the largest natural disasters in the history of Mexico. In April 2008, the PICI flood

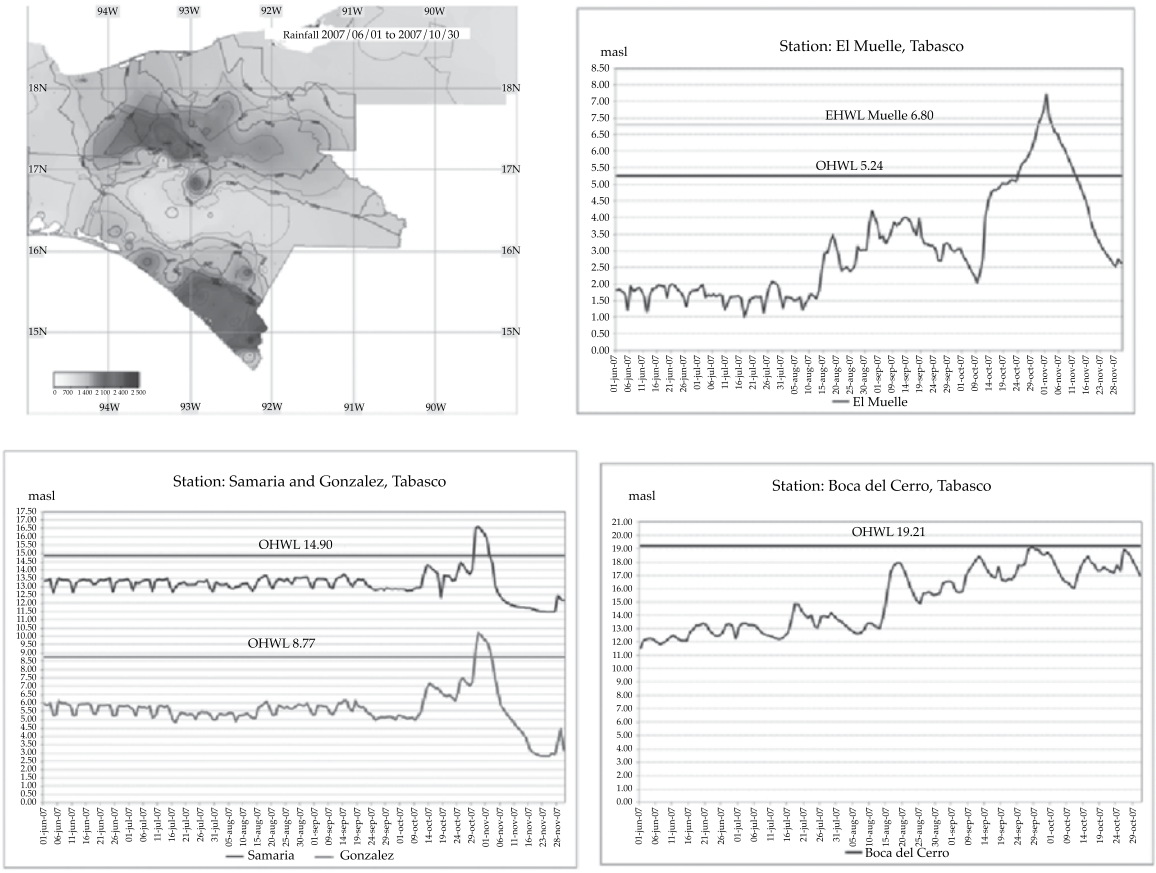

Figure 8. Limnigraphs for the El Muelle, Samaria, Gonzalez and Boca del Cerro stations, 2007.

management strategy was again proposed, later becoming the Tabasco Comprehensive Water Program (Programa Hídrico Integral de Tabasco; PHIT, Spanish acronym).

Year 2008

Most of the rainfall occurred in the tributary of the Usumacinta River. The Grijalva basin registered an accumulated rainfall of 1 510 mm, higher than the previous year. The level at the El Muelle station exceeded the OHWL from September 23 to October 29. The dikes built in the year 2000 did not reach their EHWL, although placing sacks for that rainy season was planned. The Samaria and Carrizal rivers did not exceed their OHWLs and the Usumacinta River levels were above the OHWL from September 21 to November 4, causing significant flooding in the floodplains of the Usumacinta River (Figure 10). A disaster such as the one in 2007 was not repeated due to adequate operations of the dams and the construction of the first notches included in the PHIT.

At the beginning of the rainy season, the average daily flow entering the Angostura in June was 513 m^3/s, with a maximum of 1 168 m^3/s on June 28. For July-September, the daily average reached 918 m^3/s and the maximum reached 2 212 m^3/s. The daily average was 905 m^3/s and the maximum was 1 675 m^3/s on day 4.

In Malpaso, the daily average flow in June was 934 m^3/s, with a maximum of 2 633 m^3/s on day 1. From July to September,

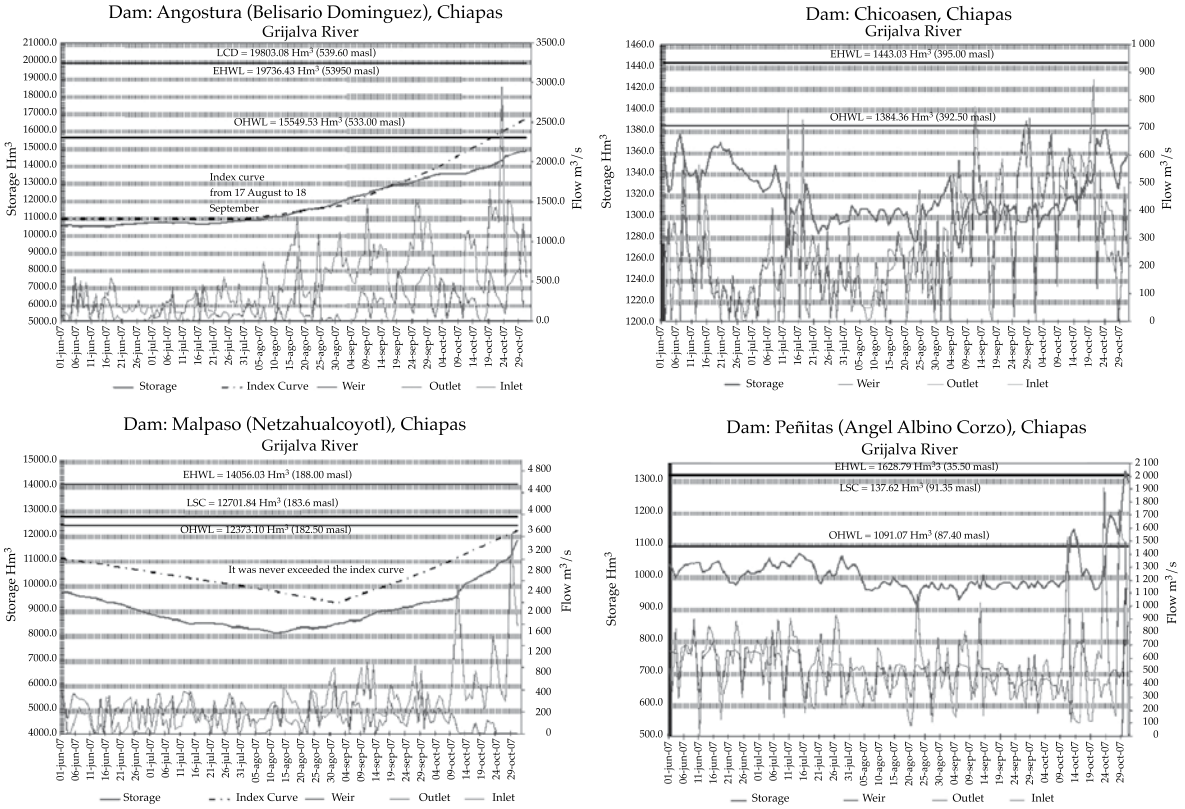

Figure 9. Functioning of the reservoirs in the Angostura, Chicoasen, Malpaso and Peñitas Dams, 2007.

the average flow was 963 m^3/s, with a maximum of 2 251 m^3/s on September 24. For the month of October, the average flow was 990 m^3/s and the maximum reached 1 657 m^3/s on day 15.

With regard to turbine extractions, the average was 508 m^3/s from June to October in Angostura, operating at full capacity only during the first few days of June. The average extracted from June to October in Chicoasen was 652 m^3/s and the maximum was 1 093 m^3/s. An extraction of 1 000 m^3/s was exceeded on a few days. In Malpaso, the average was 849 m^3/s, with extraction at full capacity during the three first weeks in August. In Peñitas, flows over 1 000 m^3/s were generated during nearly the entire period. Extractions using weirs were not needed from June to October at any dam throughout the entire period.

In terms of dam management, the hydraulic conditions imposed by the channel in Juan de Grijalva required extractions of 800 m^3/s to manage floods in the Peñitas reservoir, and based on the TMWL(typical minimum water level) of the dam, up to 600 mm can be managed over 24 hours without immediately increasing extraction at Peñitas (Figure 11).

Year 2010

This rainy season was very similar to that of 1999, dominated by the presence of the inter-tropical convergence zone in the upper Grijalva basin for more than 40 days, along with hurricanes Karl and Mathew, with an accumulated rainfall during the analysis period of 1 572 mm, more than the 2007 and 2008 rainy seasons.

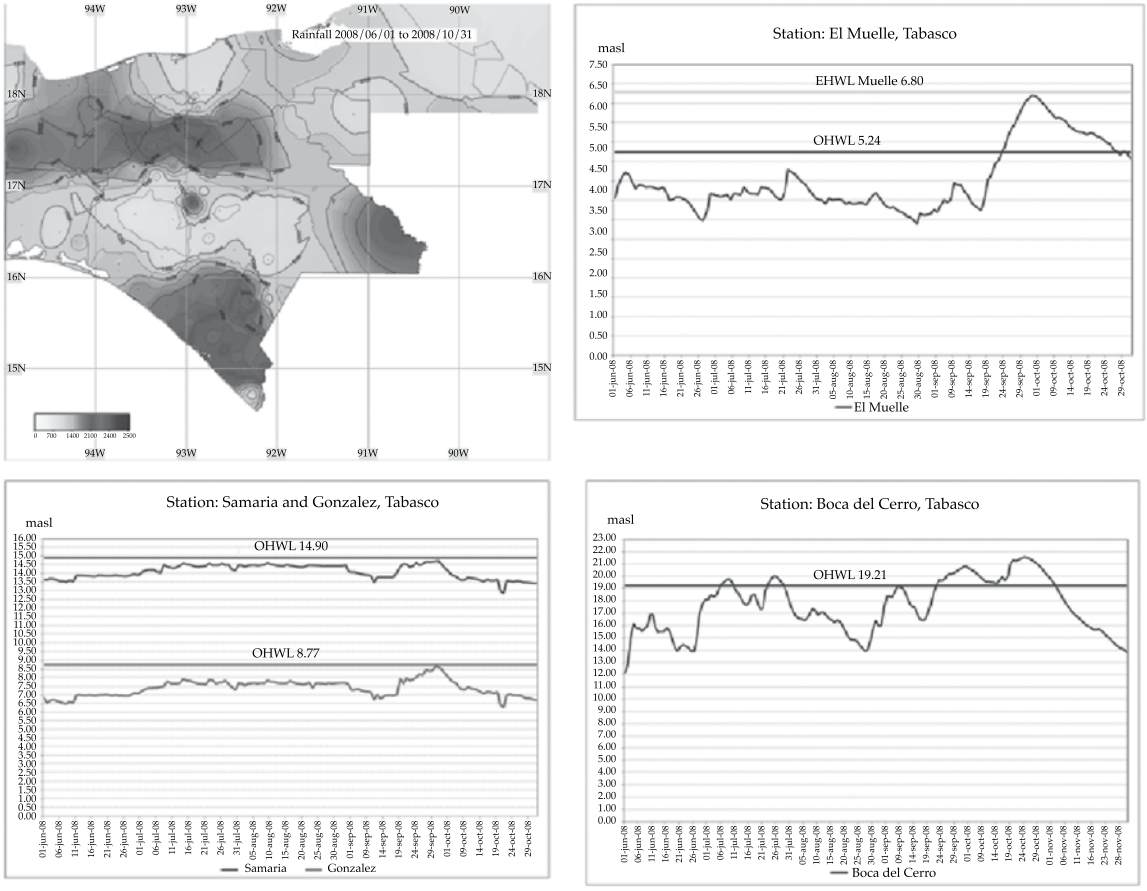

Figure 10. Limnigraphs for the El Muelle, Samaria, Gonzalez and Boca del Cerro stations, 2008.

When the rainy season began, the daily average flow entering the Angostura dam in June was 390 m^3/s, with a maximum of 743 m^3/s on day 27. From July through September, the daily average reached 1 500 m^3/s and the maximum was 3 461 m^3/s on September 27. In October, the daily average was 609 m^3/s with a maximum of 1 855 m^3/s on day 1. In the Malpaso dam, there was a daily average flow in June of 584 m^3/s, with a maximum of 2 201 m^3/s on day 28. From July to September, the average was 1 644 m^3/s and the maximum was 6 284 m^3/s on September 28. In October the average was 1 603 m^3/s and the maximum was 2 747 m^3/s on day 3.

With regard to turbine extractions, in Angostura from June to October an average of 475 m^3/s was extracted and more than 900 m^3/s from September 4 to 27. In Chicoasen, the average from June to October was 810 m^3/s and the maximum reached 418 m^3/s on several days. In Malpaso, the average was 945 m^3/s with extraction at full capacity in September and October. In Peñitas the average was 643 m^3/s, with values over 1 000 m^3/s in July, August and the first few days of September.

Weir extractions occurred in the four dams as follows: In Angostura from September 10 to October 14, with an average of 716 m^3/s and a maximum of 897 m^3/s on Oc-

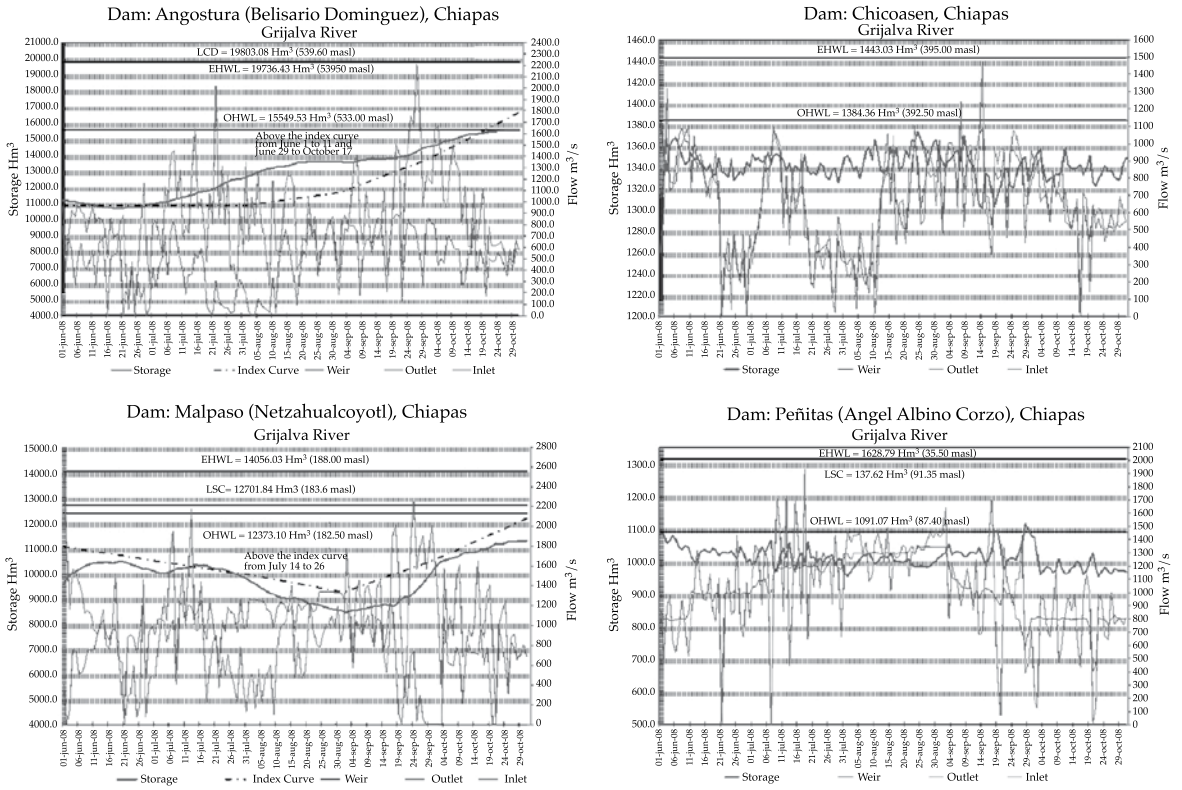

Figure 11. Functioning of the reservoirs in the Angostura, Chicoasen, Malpaso and Peñitas Dams, 2008.

tober 3; in Chicoasen the average was 818 m^3/s from September 16 to October 14 and the maximum was 1 710 m^3/s on September 28; in Malpaso the average was 961 m^3/s from September to October with a maximum of 1 496 m^3/s on October 3; and in Peñitas extractions were made with the weir from September 1 to October 31 with an average of 913 m^3/s and a maximum of 2 450 m^3/s on October 5.

The large dams received significant amounts beginning in July and it was determined in advance that extraction from the Peñitas dam would need to be increased to balance out the filling of the system without losing available space to manage flooding. The amount of water stored in the Angostura dam exceeded OHWL by August 25 and on September 9 the weirs were operated for the first time in history. Malpaso operated depending on the extractions from Peñitas which eased the Grijalva system, which in turn depended on the speed at which the sacks were placed along the urban sections of the Carrizal and Grijalva rivers. An jetty was also built at the bifurcation to divert more flow to the Samaria. In September, with half of the flood regulating capacity used in Angostura, a decision was made to take the turbines in Peñitas dam out of operation to increase the volume regulated. The floods from Karl and Mathew had already been managed and Richard was developing in the Caribbean. The extractions from Peñitas for this year measured 2 450 m^3/s from October 14 to 19. Afterwards, because of a blockage by a high pressure system that prevented the

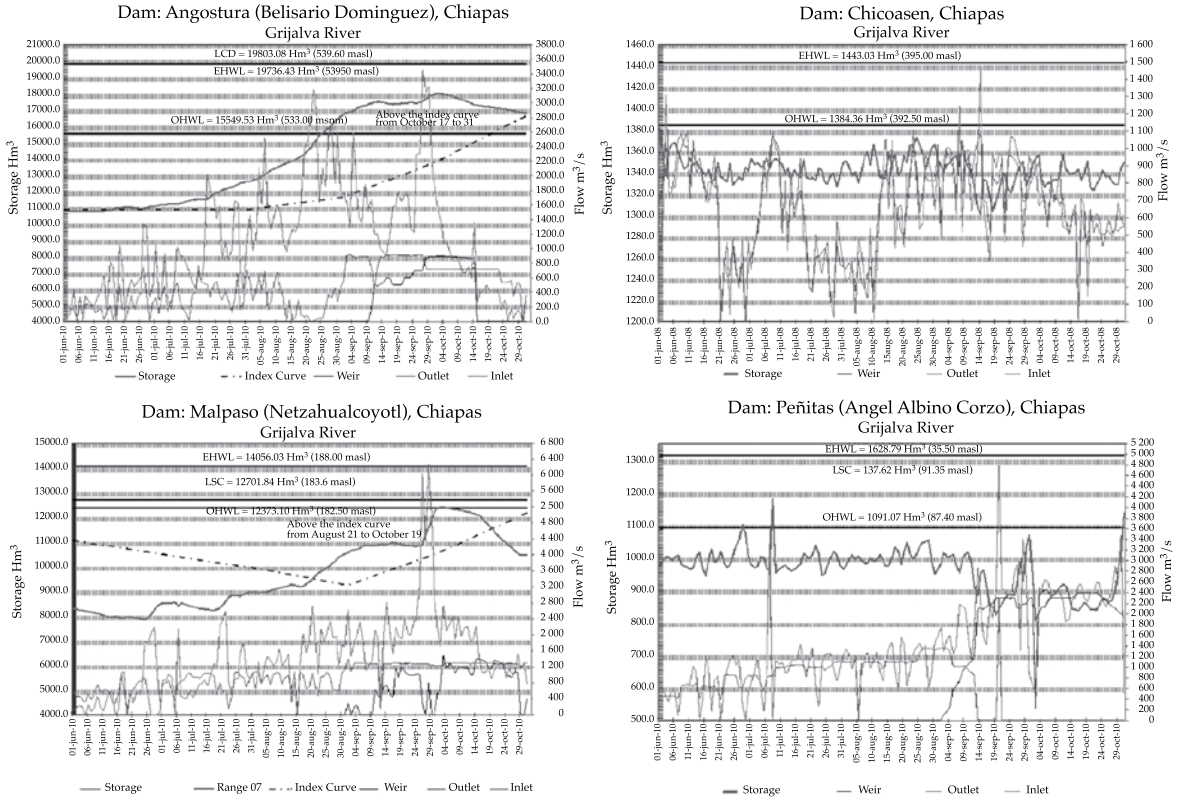

Figure 12. Functioning of the reservoirs in the Angostura, Chicoasen, Malpaso and Peñitas Dams, 2010.

moisture from the Caribbean from entering the country, a decrease in the extraction from the Peñitas dam began (Figure 12).

During this season four other notches were built. The Grijalva River levels were above OHWL at the El Muelle station from August 5 to October 20. The Carrizal and Samaria rivers were above this mark from August 26 to October 31 and the Usumacinta River fluctuated around the OHWLfrom July 20 to October 11 (Figure 13).

Due to this extended flood management period, the CTOOH met 15 times and the CTOOHR Southern Border met 37 times. The ongoing evaluation of the evolution of the hydrological phenomena throughout the basin showed that Villahermosa had not flooded by the end of the season because of coordination in management among the basins upstream, the execution of new control works in the lower basin and civil protection actions.

Flood management in 2010 involved a review and updating of all the protocols for the managing dams and rivers.

Climate Change

In terms of the analysis of floods in Tabasco, climate change will have two significant effects —an increase in the sea level and changes in the rainfall regime. According to the IPCC, the scenario for 2050 shows an increase in the mean sea level of as much as 1.5 meters, which would cause an intrusion of a mass of water for at least 40 km, moving the boundary of the basin discharge and the mouth of the Samaria Oxciacaque channel

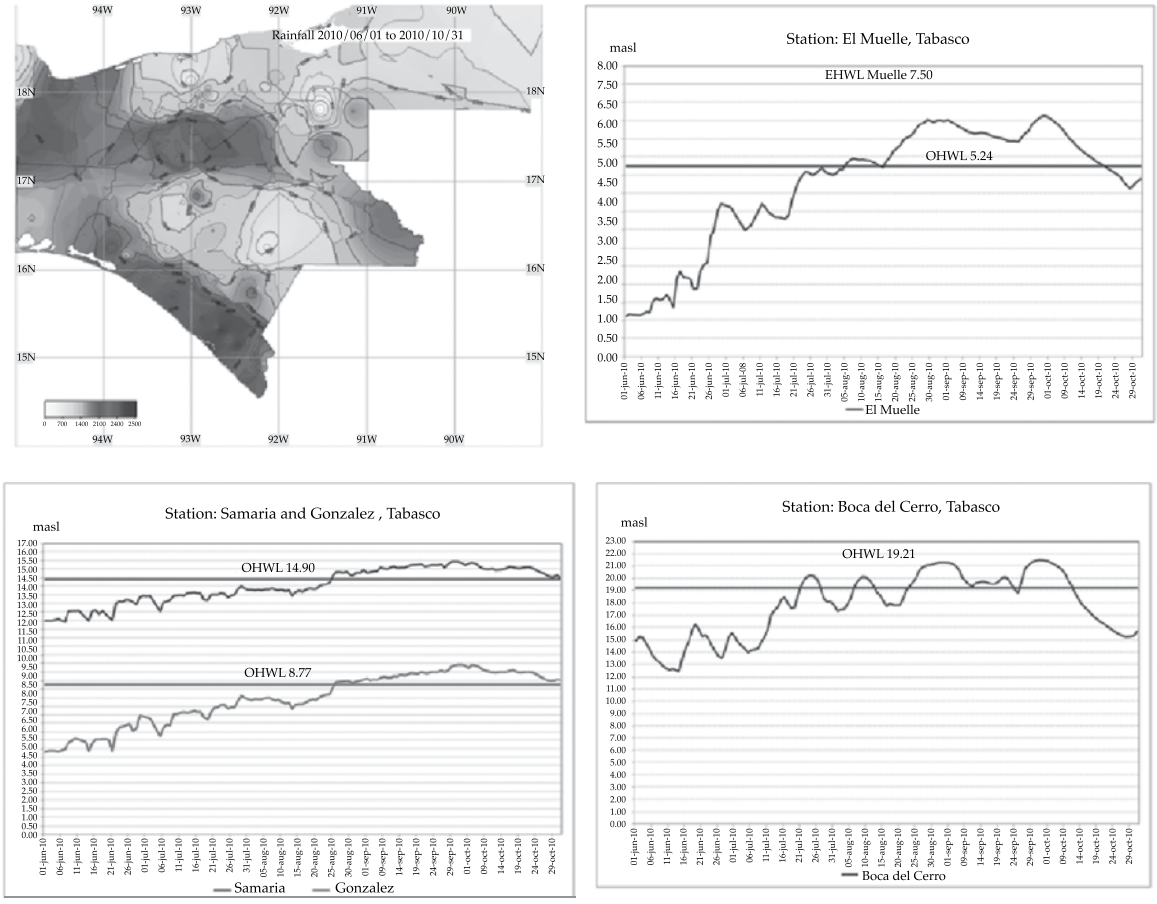

Figure 13. Limnigraphs for the El Muelle, Samaria, Gonzalez and Boca del Cerro stations, 2010.

quite close to Villahermosa (see Figure 14). This would result in increases in water depths and restrict the discharge of rivers.

Another relevant effect is a wider fluctuation in the magnitude of annual accumulated rainfall between dry and wet years. As can be seen in Figure 15, according to the scenarios modeled by the IPCC, these effects would not be noticeable until after the year 2030 (IMTA, 2007). For example, if scenario A1B were to happen, the rainfall regime will decrease and moisture events will become more intense and spaced out over time. This would involve updating the policies for operating the dams in the basin, as well as an increase in floods.

Modern Chronology of a Mitigation Process

Table 2 shows the key actions taken in the Grijalva River basin in relation to large hydrological events, the development of infrastructure and flood management (Rubio and Triana, 2006).

Comprehensive Flood Control Project (PICI, Spanish acronym)

The PICI involved building works in three systems as shown in Figure 16. The Mezcalapa-Samaria enables excess runoff from the upper Grijalva River basin to reach

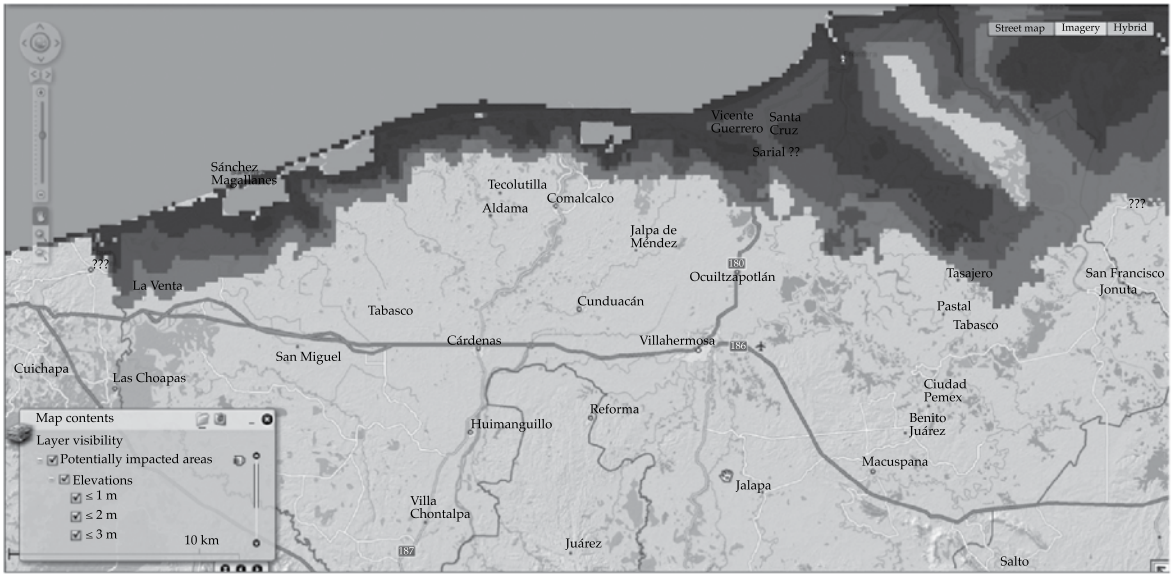

Figure 14. Continent incursion of sea based on various scenarios of increased mean sea levels (Overpeck and Weiss, 2011).

Source: SEDEPECC 2007 (IMTA-Conagua)

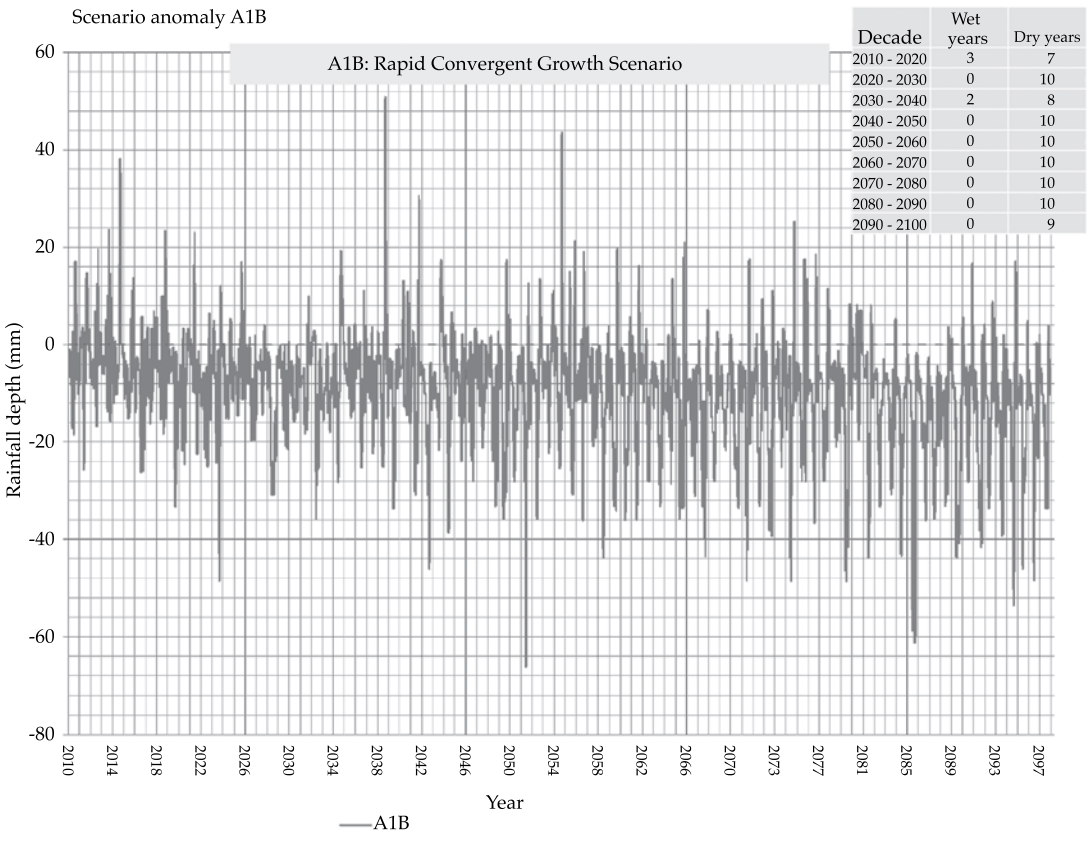

Decade	Wet years	Dry years
2010 - 2020	3	7
2020 - 2030	0	10
2030 - 2040	2	8
2040 - 2050	0	10
2050 - 2060	0	10
2060 - 2070	0	10
2070 - 2080	0	10
2080 - 2090	0	10
2090 - 2100	0	9

Figure 15. Rainfall anomaly forecasted for scenario A1B for the Grijalva-Usumacinta basin.

Table 2. Main actions taken in the Grijalva River related to large hydrological events, development of infrastructure and flood management.

Year	Structural measure	Non-structural measure
1993		Test hydraulic capacity of the Mezcalapa River with a controlled extraction from the Peñitas dam; corroborated no effect downstream from the dam with 1 400 m^3/s.
1995	Flood caused by hurricanes *Opal* and *Roxane*.	
1996	The hydrometric scales for the flow measurement stations in the lower basin were referenced to mean sea level.	Study of the overall vision of the Comprehensive Flood Control Project (PICI, Spanish acronym).
1998		Pre-project study of the PICI
1999	Flood caused by the combination of a flood train resulting from tropical waves 26-30, tropical depression 11 and cold front 4, plus cold front 7 of the season.	
1999	Building of the hydraulic squeezing of the Carrizal River. The building of protection dikes is initiated in the urban zone of the city of Villahermosa.	Short- and medium-term forecasting model constructed for dam levels for the upper and middle Grijalva for decision-making. The national CTOOH determines an index curve for the Angostura dam.
2000		Hydrometric, climatological and reservoir information is published in newspaper with large circulation in the state of Tabasco and on the regional website. The precipitation forecast Integrates medium term storages of dams Grijalva. The weather forecast is regionalized level basin longer state. Feasibility studies are completed Project Comprehensive Flood. The technical feasibility study of CIIP is concluded.
2001	The building of 80 km of longitudinal dikes is completed in the metropolitan zone of the city of Villahermosa.	
2002	Building of the right dike of the Carrizal River.	The Regional Hydraulics Works Operations Committee (CTOOHR, Spanish acronym) is established —a collegiate, technical and advisory committee of the regional water authority, with the participation of the state governments of Chiapas and Tabasco. Studies for PICI executive projects are developed.
2003	Building begins of longitudinal dikes in the mountain system of rivers. Automated stations are installed in the lower Grijalva River basin, first stage.	The Grijalva dams are managed under severe drought and flash floods caused by hurricane *Larry*. In April, the Tabasco state government and federal government sign an agreement to develop the Comprehensive Flood Control Project for the lower plains.
2004	Automated stations are installed in the Grijalva River basin, second stage, to cover 17 telemetry stations.	Test of hydraulic capacity of the Mezcalapa River.

Table 2 (continuation). Main actions taken in the Grijalva River related to large hydrological events, development of infrastructure and flood management.

Año	Medida estructural	Medida no estructural
2005	Building of the flood control work in the Carrizal River is begun.	Effects of tropical storm Stan are managed in terms of alerts and flood management, largest flood volume registered in the upper Grijalva basin.
2006	Ten automated stations are installed in the upper Grijalva and Chiapas coast.	
2007	Year dominated by La Niña. Another large flood caused by the combination of tropical and winter systems. The unfinished PICI works do not withstand the floods, primarily those related to rivers without control structures. A landslide occurs in the Peñitas dam reservoir which blocks the free flow from the the upper Grijalva.	
2007	The flow from the upper Grijalva is reconnected by excavating an open air channel in the body of the landslide, in a record time of 38 days.	The measures taken by the CTOOHR to obtain space in the dams in the upper Grijalva, management of the Grihalva dams, make it possible to finish the reconnection of the Grijalva River during the first strage.
2008	The channel built in the landslide is widened to connect the Peñitas reservoir with better flood management conditions	The CTOOHR establishes the organized emptying of the Grijalva system to manage the 2008 rainy season.
	The persistence of La Niña in the Pacific creates conditions for another intense rainy season, with values similar to the rainfall in 2007.	
	The first two notches are built (Censo and Tintillo) in the lower Grijalva, with the new flood management approach facilitating the drainage of the basin.	The Tabasco Comprehensive Water Plan is implemented.
2009	The construction of the weir on the left bank of the Carrizal River control structure is completed.	
2010	A flood train occurs in the upper and middle Grijalva basins, which has a greater volume than all previous historical floods.	
	Six additional notches are built and operations are begun: Tintillo II, Acachapan y Colmena I, II and III, Sabanilla and Buenavista. During management of the July-October flood, a jetty is built in the bifurcation of the Samaria and Carrizal rivers, and sacks are placed in the channel that passes through the urban zone of Villahermosa.	Management by the CTOOHR of inflow into to the Grijalva dam and the plains, as well as the coordination with structural actions and the PHIT project enables handling a larger increase in volume without flooding in Villahermosa.
2011	The curtain of the control structure in the Carrizal River is closed. The building of Zapote III, PHIT's largest notch is initiated.	The CTOOHR operations rules are refined. The index curves for the Grijalva dams are revised, lowering the normal storage level by 600 Hm^3. For a rainy season higher than normal in the Grijalva basin, the capital city does not undergo damages from floods due of the management of the dams and the functioning of the works built (Conagua, 2011).

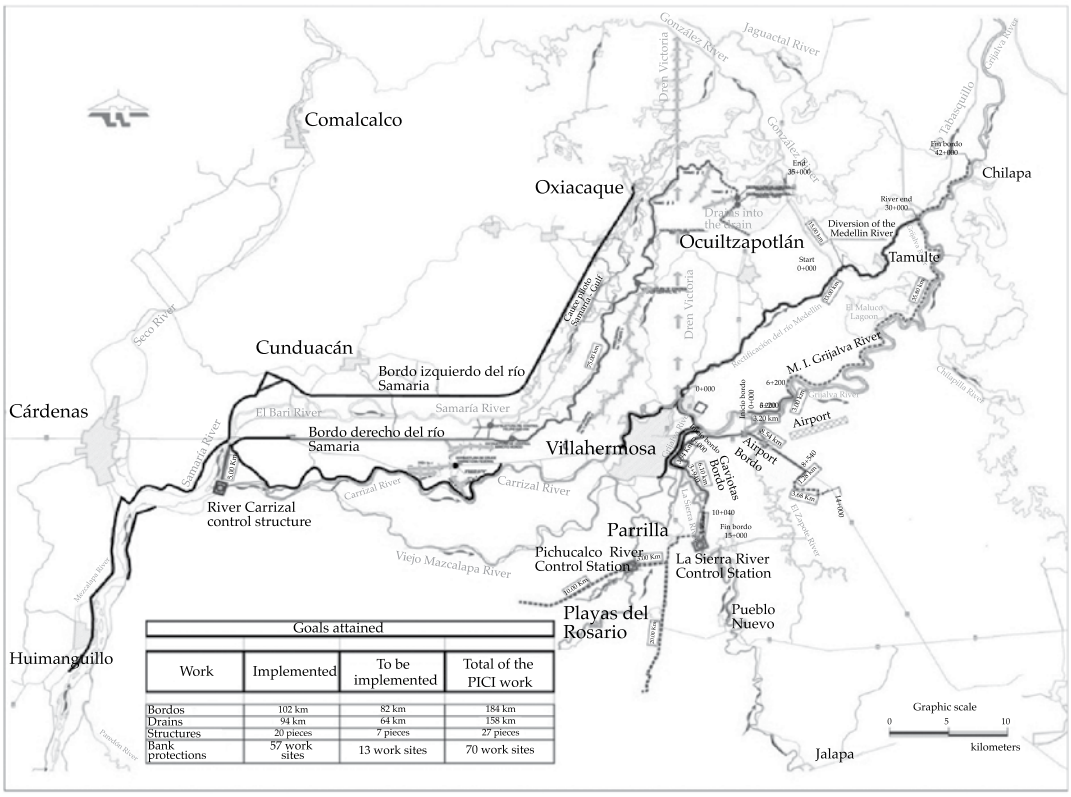

Figure 16. Components of the Comprehensive Flood Control Project.

the sea by means of the Samaria-Gulf relief channel and other secondary diversion works.

The river system in the mountains carries the overflow from those channels to the lagoon region in the lower basins of the Grijalva and Usumacinta rivers. It is important to mention the planning of the control structures in the Pichucalco and La Sierra rivers, which divert all the runoff to the lagoon in Zapotes. A significant area of the Parrilla and Zapotes lagoons is segmented by the dike line of protection that are embedded in both control structures.

Finally, the El Carrizal-Medellín system carries the controlled runoff from the Carrizal River and the rivers in the mountains to the sea through the rehabilitated Medellin River channel and the Victoria drain which ends at the Carrizal River in Villahermosa.

The PICI included the construction of 27 works and 184 kilometers of longitudinal dike. The most important work in this comprehensive project was the control structure in the Carrizal River, whose operation would ensure flexibility and independence in managing floods in the Mezcalapa-Samaria systems, which is part of the mountain river system.

Hydraulic Works Technical Operations Committee (CTOOH, Spanish acronym)

Operating increasingly more complex hydraulic systems requires the participation of the water authority, the institutions that operate or are benefited or affected by the hydraulic works and the leading specialists on the subject. The Secretary of Agriculture

and Hydraulic Resources has been meeting regularly with the Federal Electric Commission (FEC) to reach agreements on the operations of hydroelectric dams. Given the increasing importance of managing the hydraulic infrastructure, the Dam Operations Committee was formally created in 1991 as part of the National Water Commission (Conagua, Spanish acronym). This committee became the Hydraulic Works Technical Operations Committee (CTOOH, Spanish acronym) in 1994, which continues to operate to-date and is composed of the National Water Commission, the Federal Electric Commission, the Secretary of Agriculture, Livestock and Fishing, the National Autonomous University of Mexico, the Mexican Institute of Water Technology and the National Center for the Prevention of Disasters. Institutions interested in the subject are invited to participate when analysis is required.

Over 1,000 sessions of analysis have been held by the CTOOH, which meets regularly 50 times per year, on Tuesdays, and holds extra sessions when needed. During these sessions, the meteorological and hydrological conditions and forecasts are analyzed for the basins containing the main dam systems in the country. According to their state and forecast, the best operating policies to be followed and applied by basin organizations are discussed and determined.

Because of the management complexity and short-term needs with regard to regulating their operations, some basins and dam systems in the country have required the creation of Regional Hydraulic Works Technical Operating Committees, such as the one in Frontera Sur (CTOOHR-FS, Spanish acronym) created in August 2002. Among other issues, this organization addresses the

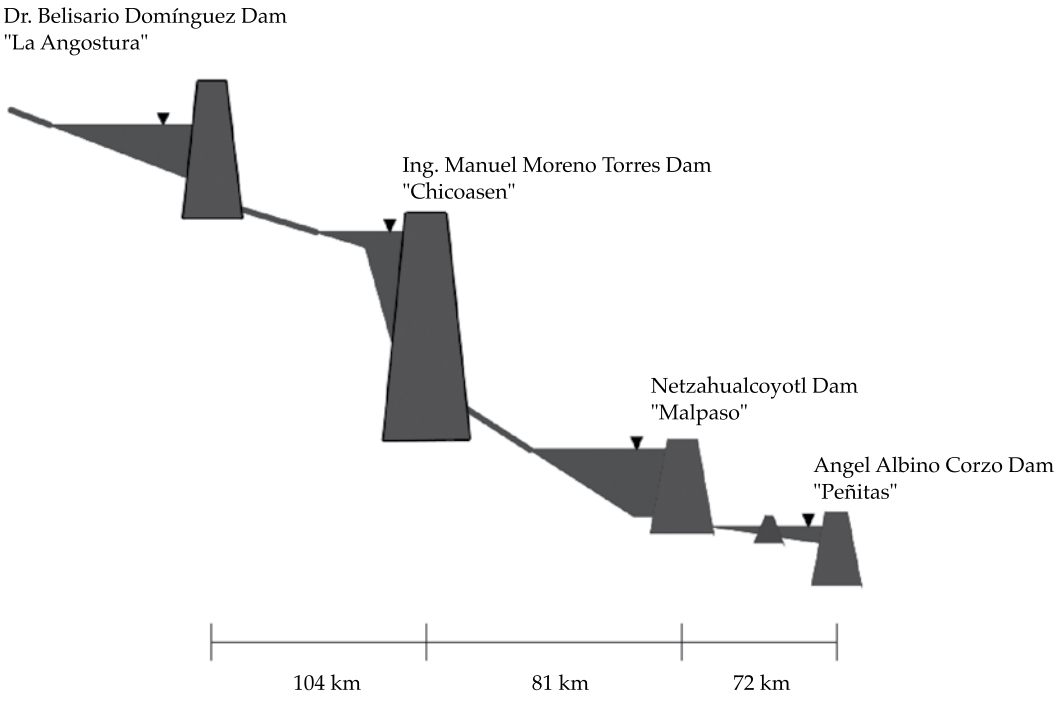

Figure 17. Profile of the Grijalva River and location of the Angostura, Chicoasen, Malpaso and Peñitas dams.

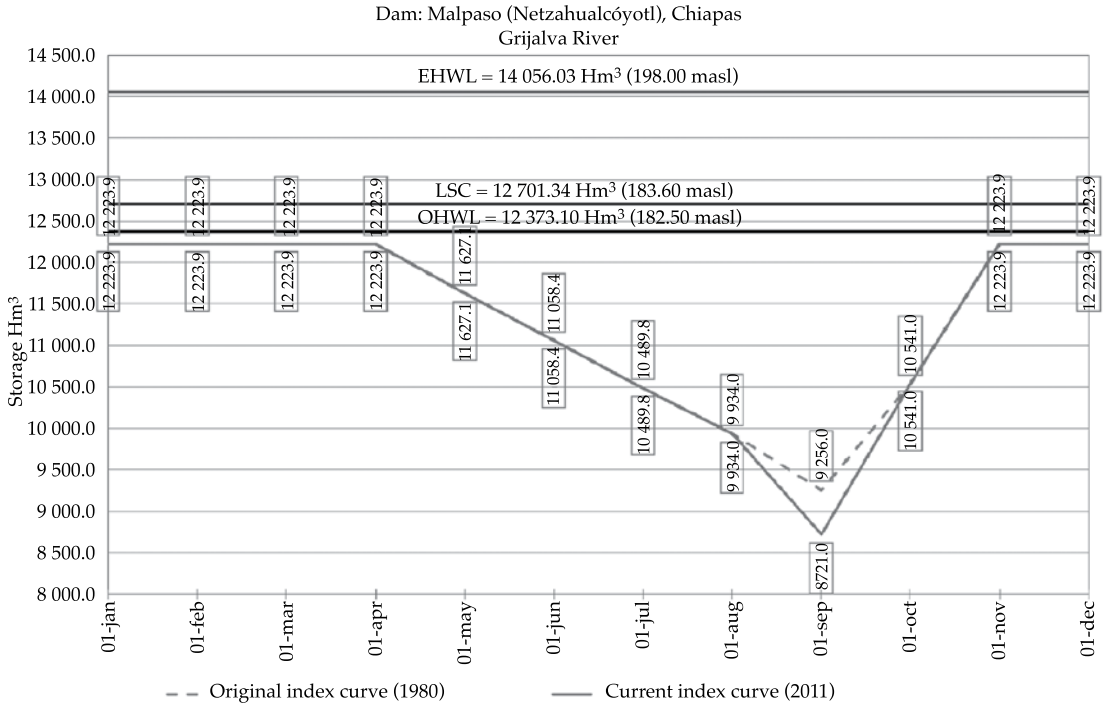

Figure 18. Index curves adopted to regulate the storage of the Malpaso dam.

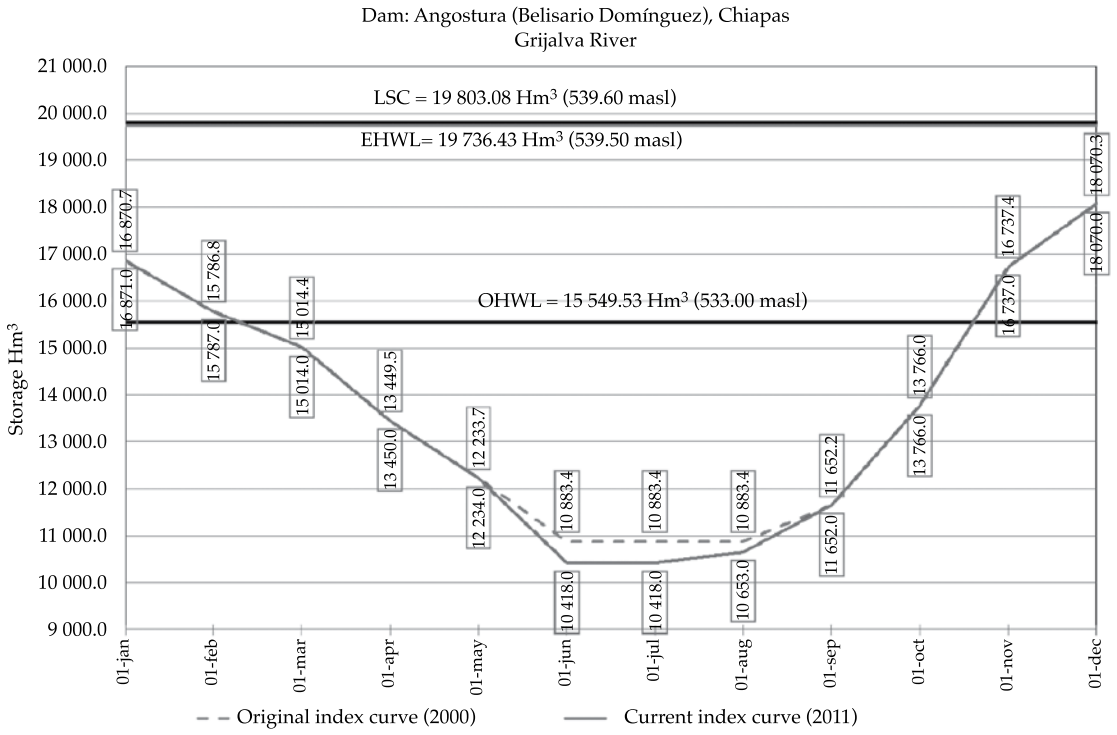

Figure 19. Index curves adopted to regulate the storage of the Angostura dam.

operations of the dam system in the Griajlva River. The CTOOHR in the northwest is responsible for the dam systems in the Yaqui and Mayo basins, and has operated since 2005.

Management of Dams

The adequate operations of the dams systems in the Grijalva River (Figure 17) is the basis for the safety of the Tabasco plains. The operations has varied over time, as shown in the guidelines curves or index. In the year 1980, the curve for the Malpaso, Chiapas dam was approved jointly by the FEC and the then Secretary of Agriculture and Hydraulic Resources (Figure 18) before building the Peñitas dam, for a discharge of 3 000 m^3/s with return periods of 100 years, which was the capacity of the channels at that time. The index curve for the Angostura dam (Figure 19) was agreed to in 2000 by the CEF and Conagua, establishing that a weir would not be used with a return period of 100 years, only generation at a full capacity of 900 m^3/s.

In the beginning of 2011, considering the changes in the Tabasco plains and as a consequence of the floods over the previous 10 years, the index curves for Angostura and Malpaso were reevaluated using dynamic stochastic programming to optimize operations policies.

When dynamic programming is applied to reservoir systems, the state variables are the storage levels, stages, and time intervals (months, biweekly, weekly). The decision variables are the discharge from the reservoir. The random variable is generally the inflow volume and can be represented as a function of the probability distribution, making it possible to proceed with the dynamic stochastic programming.

The continuity equation governs the functioning of a dam, applied to a time interval (stage), and is expressed as (Domínguez, 2000):

$$S_j = S_i + VI_j - VS_j \tag{1}$$

where:

S_j = storage and the end of the stage, in L^3.
S_i = storage and the beginning of the stage, in L^3.
VI_j = inflow volume during the stage, in L^3.
VS_j = extracted volume during the stage, in L^3.

The dynamic stochastic programming takes into account the random nature of the inflow volume in reservoir *VI*, represented with a probability distribution function which primarily depends on the season of the year of the time interval. That is, it is the uncontrollable variable in the system, and VS_j is the variable in the system that can be controlled. S_i defines the initial condition and determines the state of the system.

The storage S_j and the extractions VS_j pertaining to the system are subject to the following restrictions:

$$VS_{\min} \leq VS_j \leq VS_{\max} \tag{2}$$

$$S_{\min} \leq S_j \leq S_{\max} \tag{3}$$

The reservoir has a useful volume that is divided by *NS* intervals of magnitude ΔV, as seen in Figure 20. If the same interval is used to discretize all the variables, the continuity equation (1) takes the form:

$$j = i + x - k \tag{4}$$

Subject to:

$$1 \leq j \leq NS \tag{5}$$

$$0 \leq k \leq NK \tag{6}$$

$$1 \leq x \leq NK \tag{7}$$

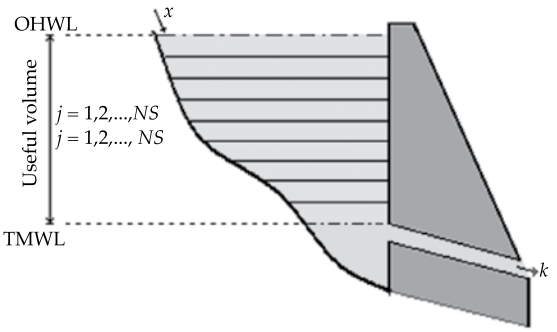

Figure 20. Discretized values in a reservoir.

Where:

$i = 1, 2, 3\ldots, NS \rightarrow$ storage volume (per unit ΔV) at the beginning of the stage.

$j = 1, 2, 3\ldots, NS \rightarrow$ storage volume (per unit ΔV) at the end of the stage.

$x = 1, 2, 3\ldots, NX \rightarrow$ inflow volume(per unit ΔV) during the stage.

$k = 1, 2, 3\ldots, NK \rightarrow$ extraction volume (per unit ΔV) during the stage.

When considering the variables discretely, the benefit corresponding to any stage n depends on the extracted volume k and storage volumes i and j at the beginning and the end of the stage. That is, the benefits during the stage can be expressed as $b_n^k(i,j)$.

Since it is a hydroelectric dam, one objective is the generation of energy. Therefore, each time there is a spill or a deficit, penalties are applied, which will depend on the damage caused by spilling water downstream or not meeting demand. The objective function takes the form:

$$F.O = \sum_{n=1}^{n} b_n^k(i,j) - \sum \text{Csp}(\text{spill}) - \sum \text{Cdef}(\text{deficit}) \quad (8)$$

where:

$b_n^k(i,j)$ = benefit obtained from generation of electric energy.

Csp (spill) = product of the spill multiplied by its respective penalization coefficient.

Cdef (deficit) = product of the deficit multiplied by its respective penalization coefficient.

For the particular case of the two large dams in the Grijalva River basin, the objective function to be optimized (8) is expressed as:

$$\text{OF} = \text{Max E } (-C1\ \text{SpAng} - C2\ \text{SpMalp} - C3\ \text{DEFAng} - C4\ \text{DEFMalp} - C5\ \text{DEFCiAng} - C6\ \text{DEFCiMalp} + \text{GAng} + \text{GMalp}) \quad (9)$$

where:

OF: objective function.

E: energy.

*C*1 and *C*2: penalization coefficients for spills.

*C*3 and *C*4: penalization coefficients for volumes under OMWL.

*C*5 and *C*6: penalization coefficients for volumes over those indicated by the index curve.

SpAng: volumes spilled in Angostura.

SpMapl: volumes spilled in Malpaso.

DEFAng: deficit volume in Angostura.

DEFMalp: deficit volume in Malpaso.

GAng: annual generation in Angostura.

GMalp: annual generation in Malpaso.

The long-term optimization is obtained using a recursive equation to integrate the benefits over time.

The result of the analysis is a reduction in overall storage of 600 Hm^3 for the beginning

of June and September (Figures 18 and 19).

Model for Planning for Land Exposed to Floods

As indicated previously, one of the factors that most greatly influences floods is a lack of land-use planning. Next, a model is presented which enables determining high flood risk areas, thereby providing certainty as to land uses that involve non-assumable losses of life and property.

The model is based on the water's capacity to drag structures, vehicles and persons due to the amount of movement generated by the water depth and velocity. A simplified model is shown in Figure 21.

The water depths that can occur in a channel or on land are represented by the horizontal axis and the velocities by the vertical axis. The areas are the combination of water depth and velocity that can cause a human being of average weight to lose their balance, a vehicle to become unstable or structures to be placed at risk.

The flood risk model is applied to a severity map, resolving amount of movement (10)(11) and continuity (12) equations for two-dimensional flow (Fuentes and Franco, 1997):

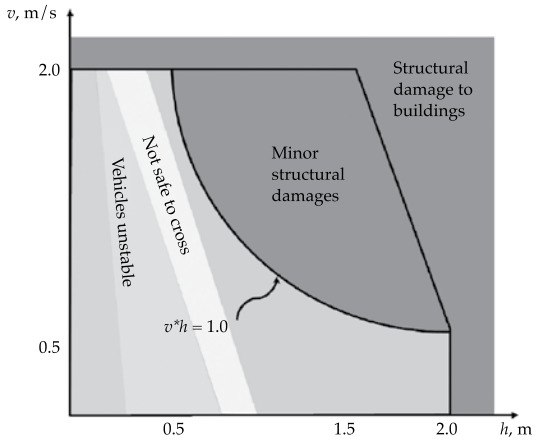

Figure 21. Flood Risk Model from water depth and velocity.

$$\frac{1}{g}\frac{\partial u}{\partial t}+\frac{n^2|u|u}{h^{4/3}}=-\frac{\partial h}{\partial x}-\frac{\partial z}{\partial x} \quad (10)$$

$$\frac{1}{g}\frac{\partial v}{\partial t}+\frac{n^2|v|v}{h^{4/3}}=-\frac{\partial h}{\partial y}-\frac{\partial z}{\partial y} \quad (11)$$

$$\frac{\partial h}{\partial t}+\frac{\partial}{\partial x}uh+\frac{\partial}{\partial y}vh=0 \quad (12)$$

where:

$S_{fx}=\frac{n^2|u|u}{h^{4/3}}$, $S_{fy}=\frac{n^2|v|v}{h^{4/3}}$, "friction" slope in the dimensionless x and y directions.

g = acceleration of gravity, in m/s^2.

u, v = components of velocity in the dimensionless x and y directions.

h = free surface level of water with respect to the level of land, in m.

n = roughness factor, according to the Manning formula, in $s/m^{1/3}$.

x, y, z = directions of the right cartesian axis systems.

t = time, in s.

The solutions to the equations for amount of movement and two-dimensional continuity of flow for the Lower Grijalva are presented in Figures 22 and 23 and the flood risk model in figure 24. The latter explicitly shows where the building of infrastructure is not recommended, represented by sites located inside the red polygon. The orange and yellow polygons represent areas where the circulation of vehicles is not recommended and the green polygons areas through which people are not recommended to pass.

While the depths are the main problem in the study area, the hydraulic depth and magnitude of the vectors resulting from the velocity modules of the two-dimensional model need to be taken into account for de-

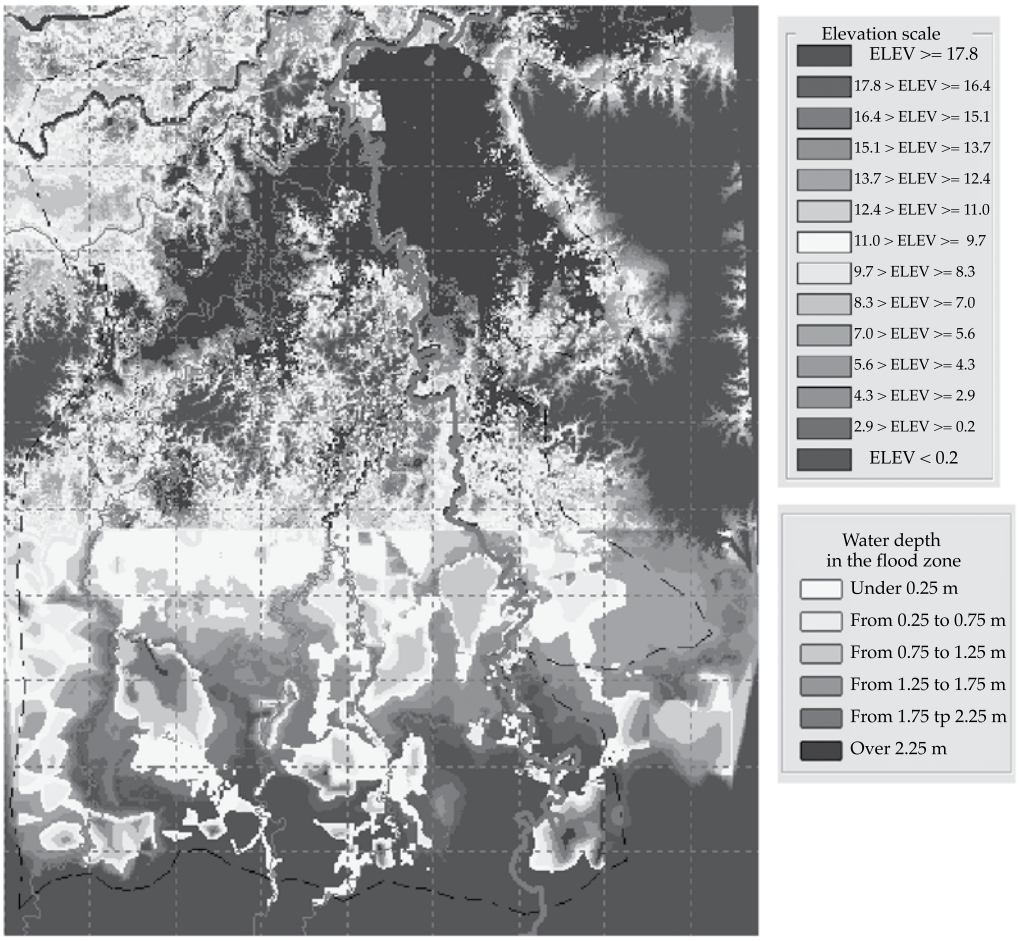

Figure 22. Map of water depth for the lower Grijalva.

cision-making, since in some areas where the lagoons are connected the movement of persons is not recommended due to the velocities that can develop.

These flood risk scenarios have a high probability of occurring during certain months and years when the weather conditions can produce floods. Since not being able to use the land all the time is impractical, flood risk variables need to be transformed into assumable risks using financial tools such as flood insurance premiums, which allow using and developing the land with the ability to replace exposed goods through insurance.

Thus a severity or flood risk map is obtained which provides the advantage of knowing which sites in the space are suitable to building structures and which are not recommended for vehicular or pedestrian traffic because of the possibility of being dragged by the current. This methodology also has the advantage of being able to determine how to redistribute the flood risk with the development of infrastructure, as shown in Figures 25 and 26. For flood plains, the policy of making higher dikes and building perimeters to protect populations in

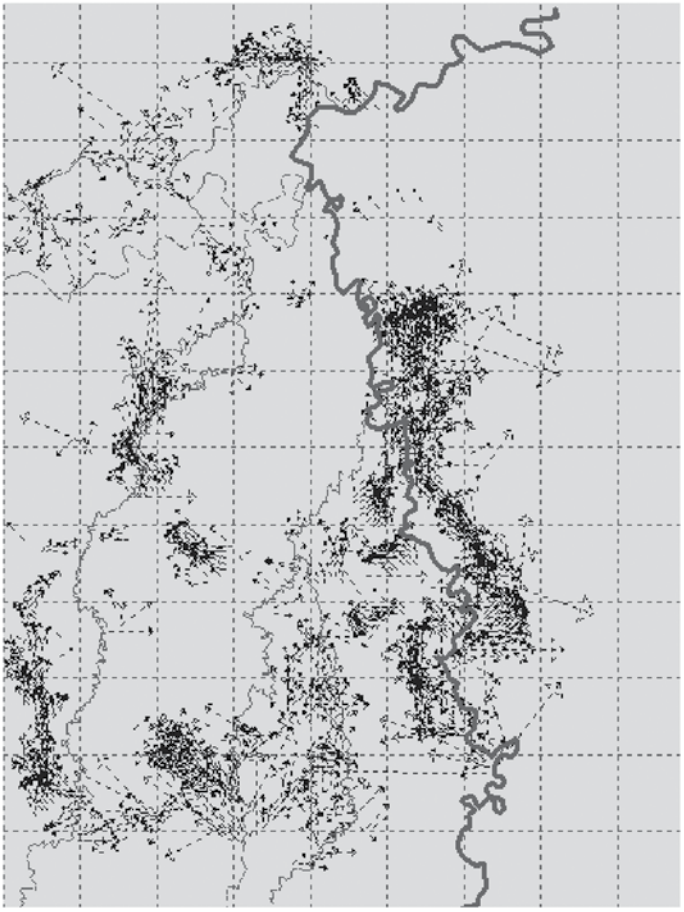

Figure 23. Vectors map for water velocity for the lower Grijalva.

flood zones increases and worsens flood risk areas, and also affects drainage time since the hydrological systems take longer to remove volumes equal to the runoff. Flood periods can also be extended, thereby adding to prior events that have not yet drained.

Conclusions

The Tabasco plains has historically been subject to large floods. Adding to this a lack of land-use planning, deforestation in the upper basins and a false sense of safety associated with the construction of large dams in the Grijalva River, the high vulnerability of populations located in these plains is understandable.

Climate change will have two significant impacts: increase in the sea level and changes in rainfall regimes. In one of the scenarios presented for the year 2050, the mean increase in sea level can be as much as 1.5 meters, which would cause at least a 40 km intrusion of a mass of water into the continent, which would put the boundary of the new discharge of the basin quite close to Villahermosa and the mouth of the Samaria Oxciacaque channel.

The Tabasco Comprehensive Water Program seeks to return river levels to normal after a flood in a short period so that the river systems, regulated areas and dikes

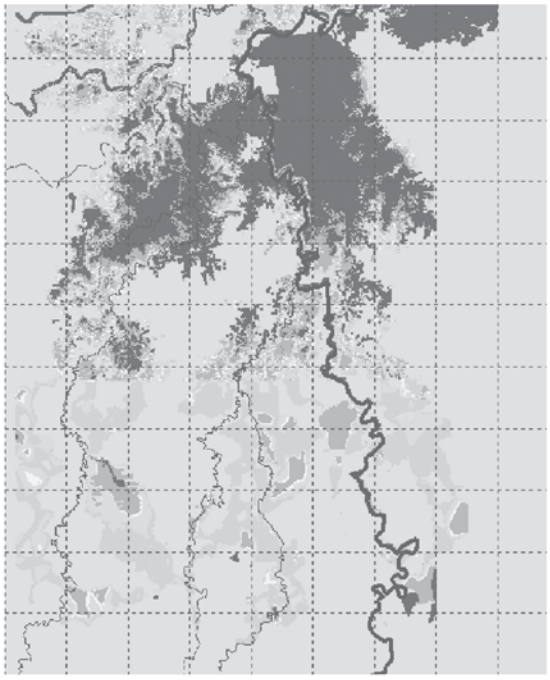

Figura 24. Peligro de inundaciones para la planicie tabasqueña.

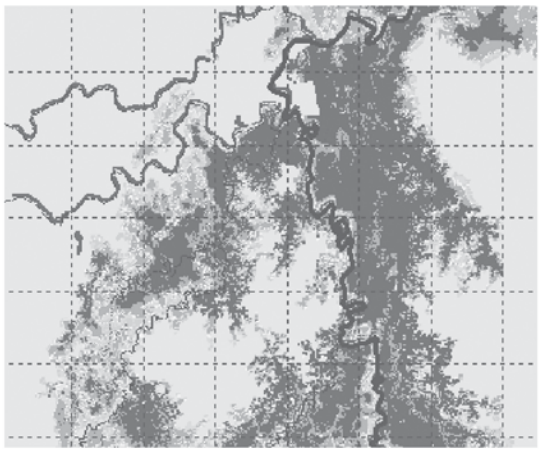

Figura 25. Mapa de peligro de inundación, privilegiando el drenaje de la cuenca.

are able to receive new floods in conditions equal or near to the first condition affecting the Grijalva basin.

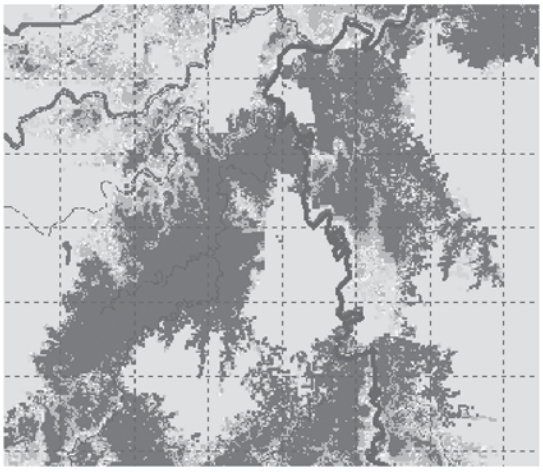

Figura 26. Mapa de peligro por inundación, privilegiando la construcción de bordos y muros.

Undoubtedly, the adequate operations of the dam system in the Grijalva River is crucial to the safety of the Tabasco plains. The operations have varied over time and have been shown by guidelines curves since 1980.

The model presented to analyze the flood risk zones can be used as a tool to support land-use planning in a flood plain, in terms of which land uses are compatible with the combined effect of water depth and velocity, conditions which can produce a flood in the territory.

Received: 17/02/12
Accepted: 01/08/13

References

CEPAL-CENAPRED-SEPLAN. *Impacto socioeconómico de las inundaciones registradas en el estado de Tabasco de septiembre a noviembre de 2011*. México, DF: Comisión Económica para América Latina y el Caribe-Centro Nacional de Prevención de Desastres-Secretaría de Planeación y Desarrollo Social del Estado de Tabasco, 2012, pp. 132 y 138.

CONAGUA. *Se confirma efectividad de las obras de protección del PHIT, construidas por la Conagua en Tabasco* [en línea]. México, DF: Comisión Nacional del Agua octubre, 2011. Disponible en *World Wide Web*: http://www.conagua.gob.

mx/CONAGUA07/Comunicados/Comunicado%20de%20Prensa%20358-11%20(Tabasco).pdf.

CONAGUA. *Estudio de Factibilidad del Proyecto Integral contra Inundaciones en Tabasco*. México, DF; Comisión Nacional del Agua, 2000.

FUENTES, O. y FRANCO, L. *Modelo matemático de áreas de inundación* [en línea]. CENAPRED. *Cuadernos de investigación*. Núm. 41, México, D.F., mayo, 1997, pp. 3-6. Disponible en *Word Wide Web*: http://www.cenapred.gob.mx/es/Publicaciones/archivos/3112011modelomat.pdf.

ORTIZ-PÉREZ, M.S., SIEBE, C. y CRAM, S. Diferenciación Geográfica de Tabasco. Capítulo 14 305-322. En Bueno, J., Álvarez, E. y Santiago, S. (editores). *Biodiversidad del Estado de Tabasco*. México, D.F.: Instituto de Biología, Universidad Nacional Autónoma de México, Comisión Nacional para el Conocimiento y Uso de la Biodiversidad, 2005, 386 pp.

RIVERA-TREJO, F. *Inundaciones en Tabasco*. Asociación Nacional de Protección Civil, AC. Foro: Los Retos de la Protección Civil [en línea]. Querétaro, marzo, 2011, pp. 9. Disponible en *World Wide Web*: http//www.anpcmexico.org/documents/eventos/fotolosretosdelaproteccioncivilqueretaromarzo2011/inundacionestabascofabinriveratrejopdf.

RUBIO, H. y TRIANA, C. *Gestión integrada de crecientes, estudio del caso Grijalva*. [en línea] Associated Programme on Flood Management, septiembre de 2006, p. 8. Disponible en *World Wide Web*: http//www.apfm.info/publications/casestudies/cs_mexico_full.pdf.

IMTA. *Sistema para la Exhibición de Datos del Ensamble Ponderado de Escenarios de Cambio Climático para México* (SEDEPECC) [en línea]. Consultada en junio de 2007. Disponible en *World Wide Web*: http//galileo.imta.mx/aplisedepecc.php?entrar=1.

SENADO DE LA REPÚBLICA, COMISIÓN DE ASUNTOS HIDRÁULICOS. *Informe de las inundaciones del 2007 en el estado de Tabasco Diagnóstico preliminar*. México, DF: Senado de la República, Comisión de Asuntos Hidráulicos, marzo, 2008, pp. 23. Disponible en *World Wide Web*: http://www.imta.gob.mx/gaceta/anteriores/g12-04-2008/informe-tabasco.pdf.

Institutional Address of the Authors

Dr. Felipe I. Arreguín-Cortés

Subdirector General Técnico
Comisión Nacional del Agua, México
Insurgentes Sur 2416, Colonia Copilco el Bajo,
Delegación Coyoacán
04340 México, D.F., México
Teléfono: +52 (55) 5174 4400
felipe.arreguin@conagua.gob.mx

M.I. Horacio Rubio-Gutiérrez

Gerencia de Aguas Superficiales e Ingeniería de Riegos
Comisión Nacional del Agua, México
Insurgentes Sur 2416, Colonia Copilco el Bajo,
Delegación Coyoacán
04340 México, D.F., México
Teléfono: +52 (55) 5174 4400, extensiones 1687 y 1688
horacio.rubio@conagua.gob.mx

Dr. Ramón Domínguez-Mora

Instituto de Ingeniería
Coordinación de Hidráulica
Universidad Nacional Autónoma de México
Circuito Escolar s/n, Ciudad Universitaria,
Delegación Coyoacán,
04510 México D.F., México
Teléfono: +52 (55) 5623 3675
rdm@pumas.iingen.unam.mx
rdominguezm@iingen.unam.mx

M.I. Faustino de Luna-Cruz

Instituto de Ingeniería
Universidad Nacional Autónoma de México
Ciudad Universitaria, Avenida Universidad 3000,
Delegación Coyoacán
04510 México D.F., México
Teléfono: +52 (55) 5623 3600
Fax: +52 (55) 5616 2164
fluc@pumas.iingen.unam.mx

Click here to write the autor

Determination of Environmental Flows in the Yuna River Basin, Dominican Republic

• Quyen Melina Bautista-de-los-Santos* •
Universidad Iberoamericana, República Dominicana
*Corresponding Author

Abstract

BAUTISTA-DE-LOS-SANTOS, Q.M. Determination of Environmental Flows in the Yuna River Basin, Dominican Republic. *Water Technology and Sciences* (in Spanish). Vol. V, No. 3, May-June, 2014, pp. 33-40.

Environmental flows were estimated using a range of variability analysis (RVA) and hydrological alterations indicators (HAI) at three points in the Yuna River basin (Hatillo, Rincón and Blanco reservoirs), located in the Dominican Republic. The series of daily flows for each study site were obtained using a combination of synthetically generated monthly flows and disaggregated daily flows. The 33 parameters calculated for each point were used to determine environmental flow regimes, demonstrating that the application of the method is feasible at the local level, in spite of the difficulties found to survey and process the data.

Keywords: Environmental flows, ecological flows, hydrological alterations, variability of range approach, Yuna.

Resumen

BAUTISTA-DE-LOS-SANTOS, Q.M. Determinación de caudales ambientales en la cuenca del río Yuna, República Dominicana. Tecnología y Ciencias del Agua. *Vol. V, núm. 3, mayo-junio de 2014, pp. 33-40.*

Se han estimado los caudales ambientales utilizando el método del análisis del Rango de Variabilidad (RVA, por sus siglas en inglés) y los Indicadores de Alteración Hidrológica (IHA), en tres puntos de la cuenca del río Yuna (Embalses de Hatillo, Rincón y Blanco), localizada en República Dominicana. Las series de caudales diarios para cada sitio de estudio fueron obtenidas mediante una combinación de generación sintética de caudales mensuales y desagregación en caudales diarios. Los treinta y tres (33) parámetros calculados en cada punto fueron utilizados para prescribir regímenes de caudales ambientales, demostrando que la aplicación del método es factible en el contexto local, pese a las dificultades encontradas en el levantamiento y procesamiento de los datos.

***Palabras clave**: caudales ambientales, caudales ecológicos, alteración hidrológica, Enfoque del Rango de Variabilidad, Yuna.*

Introduction

"Environmental flows" or "ecological flows" are flow regimes that can maintain the functioning, composition and structure of the river ecosystem of a channel through which they flow in natural conditions (García-de-Jalón and González-de-Tánago, 1998). An overall review of the subject indicated the existence of 207 methodologies to estimate ecological flows, which have been proposed since the 1940s (Tharme, 2003). These methodologies have been classified and described be several authors (Arthington and Zalucki, 1998; Tharme, 2003; Acreman and Dunbar, 2004). Currently, the application of methods that take into account the natural variability of flows and their impact on ecosystems are favored over the earlier methods proposed that assign a fixed value to the environmental flow for the entire year; for example, the Montana de Tennant method, 1976, cited by Tharme, 2003, which considers the ecological flow as 10% of the annual mean flow. This method is still used in the Dominican Republic. Therefore, the investigation herein proposes calculating environmental flows in the Dominican Republic using broader methods that are

consistent with current recommendations. This estimate was performed for three sites in the Yuna River basin (5 630 km^2), the largest in the country, corresponding to the three largest regulating works having the greatest impact on the basin— Hatillo, Rincón and Blanco reservoirs, with storage capacities of 441, 75.50 and 0.73 Mm^3, respectively.

Methodology

Ecological flows were calculated by applying the Range of Variability Approach (RVA) (Richter *et al*., 1997), which is based on the use of Indicators of Hydrologic Alteration (IHA) (Richter *et al*., 1996). To characterize ecological flows, the IHA includes 33 ecological parameters divided into five groups according to five key characteristics of hydrologic regimes: magnitude, synchronization, frequency, duration and rate of change. The RVA methodology has been widely used (Richter *et al*., 1998; Bragg *et al*., 1999; Black *et al*., 2002; Brunke, 2002; Baeza-Sanz y García-del- Jalón, 2004; Opperman, 2006; Limbrunner, 2010) because it is easier to apply and more flexible than methods that simulate habitats. The following steps, indicated by Richter *et al*. (1997), were taken to apply the method:

1. Generation of a daily flow series. For the study sites, the daily flow series found in the institutions that record this type of data were incomplete and did not cover the length of time required (20 years or more). Therefore, three 50-year daily flow series (one for each study site) were synthetically generated using the following methodology:

a) Data analysis (calculation of basic statistics).
b) Normalization of monthly flow series using transformations. The transformation included logarithmic, gamma, Box Cox and Potential, which were evaluated using the Filliben test (correlation coefficients must be greater than 0.987 for $n > 100$; Rodríguez, 2012) and the bias test (values between +0.5 and -0.5 to accept the normality of the data; Brown, 2012).
c) Fitting the periodic univariate ARMA (p,q) model or the univariate PARMA (p,x) to the flow series using the least squares method.
d) Stochastic generation of monthly flow series using the fitted PARMA (p,q). Series were generated for 50 years using the fitted model for each one of the study sites. The PARMA model (Periodic Autoregressive-Moving-Average) has been widely used to generate seasonal and periodic (monthly) flows, especially the low-order models (PARMA(1,0) and PARMA(1,1); (Salas *et al*., 1997).
(e) Disaggregation of monthly flows to daily flows using the Acharya and Ryu method (2012), which conserves the balance of mass and the statistical characteristics of the historical series.

The monthly flows described above were generated using *Stochastic Analysis, Modeling, and Simulation* (SAMS) *software*, version 2007, developed by Sveinsson *et al*. in the year 2007. The monthly flows were disaggregated into daily flows using a spreadsheet and by developing macros in *Visual Basic for Applications* (VBA).

2. Characterization of the natural range of variation in flows using 33 hydrologic parameters known as Indicators of Hydrologic Alteration (IHA; Richter *et al*., 1996). The software developed by The Nature Conservancy was used to estimate the IHA (The Nature Conservancy, 2011).

3. Selection of 33 ranges of variation, one for each IHA, as targets for the management system. The range of variation chosen for the non-parametric analysis (percentile statistics) was 25% to 75%, in accordance with recommendations by Armstrong and Parker (2003).

Results

The IHA analysis for the Hatillo dam resulted in a monthly mean flow for the period 1950-1999 as shown in Figure 1, normalized by area. An increase in monthly mean flows in May and from October to December was verified. The dry period was from January to April, and a period of receding flows occurred in June and July. The range of variability of the monthly mean flows, annual low flows and other measurements used in the RVA as management targets are shown in Table 1. Figure 2 shows the monthly mean flow for the period 1950-1999, normalized by area, for the Rincon reservoir. An increase in monthly mean flows was observed in May and from October to January. The dry period was from February to April and a period of receding flows was observed from June to September. The range of variability of the monthly mean flows, annual low flows and other measurements used as targets in the RVA are shown in Table 1. Figure 3 shows the results from the IHA analysis for the Blanco reservoir, indicating the monthly mean flow for the period 1950 – 1999, normalized by area. An increase in the monthly mean flows was observed from May to July and from September to November. The dry period was from December to April, and a period of receding flows was observed in July and August. Table 1 shows the range of variability of monthly mean flows, annual low flows and other measurements used as management targets in the RVA.

Discussion

Data Collection/Acquisition

The daily flow series available for the Yuna River were missing data for days as well as years, and the data for time periods did not coincide, requiring more work to adapt these series for later use. The flow series records were provided in .txt format with an inconsistent configuration (many skips and spaces, in a non-standardized format), making it difficult to work with them since they first needed to be organized.

Generation of Daily Flows

In the process to generate flows, it was difficult to apply simple techniques for daily flows, such as linear regression, because the hydrometric stations had many missing data and data over time periods did not coincide.

The next best option was to synthetically generate the flows, a technique used by the present study to obtain the daily flow series. Nevertheless this technique has limitations when low flows are generated and, therefore, the results obtained with respect to the estimate of indicators, rate increases and decreases, and number of reversals must be interpreted with care (Richter *et al.*, 1997). The third recommended technique, which is hydrologic modeling, requires many data in order to correctly apply it and validate the results. Therefore, its application would be much more difficult in our context. Another option would be to use different techniques to generate flows for dry periods (or low flows) versus flows for the high volume period, in order to find documentation in the literature and generate good estimates.

Generation of ecological flows

The ecological flow regimes estimated with the method used herein are undoubtedly

Table 1. Range of variability in flows, Hatillo, Rincon and Blanco reservoirs. Period of analysis 1950-1999 (50 years).

	Hatillo					Rincón					Blanco				
	10%	25%	50%	75%	90%	10%	25%	50%	75%	90%	10%	25%	50%	75%	90%
Group 1 Parameters															
March	3.829	11.75	19.84	29.85	35.07	1.94	3.875	6.73	9.635	14.48	2.035	2.237	2.458	3.388	5.539
April	9.539	14.43	22.32	32.25	36.23	2.84	5.3	8.183	10.88	12.81	2.012	2.132	2.574	3.353	5.839
May	10.11	15.87	27.2	51.16	80.91	5.282	7.178	9.58	16.78	22.9	2.311	3.114	4.071	7.57	9.743
June	6.725	13.93	19.04	29.31	92.5	2.912	5.978	8.755	13.43	18.02	4.483	4.716	5.29	7.362	10.56
July	6.065	9.567	18.03	29.59	67.3	3.175	5.9	7.535	8.858	12.43	3.559	3.964	5.052	5.927	7.463
August	9.666	19.51	21.82	42.52	67.67	3.348	4.343	6.495	9.825	11.61	2.309	2.925	3.76	4.573	5.331
September	6.264	11.55	25.54	42.39	65.59	4.314	6.06	7.768	8.984	10.46	3.693	4.252	5.668	6.381	6.921
October	15.56	22.75	29.71	41.84	58.02	4.545	6.295	8.49	11.05	12.67	4.492	6.045	7.061	8.285	9.99
November	7.067	24.6	43.83	61.03	77.5	3.37	6.778	9.055	11.28	17.49	6.187	6.74	7.644	10.03	12.43
December	10.83	18.26	38.16	70.57	89	1.86	4.405	14	17.43	21.54	2.508	2.999	5.656	7.204	8.131
January	8.749	13.95	25.58	31.81	37.65	2.143	3.155	11.71	17.44	23.44	2.37	3.652	4.928	6.202	7.284
February	4.285	12.46	18.23	22.86	28.28	0.9	2.414	7.71	10.94	17.59	2.534	3.002	4.066	4.818	5.373
Group 2 Parameters															
1-day minimum	2.544	2.798	4.291	6.38	7.806	0.418	0.87	1.615	2.113	3.607	1.064	1.41	1.673	1.962	2.358
3-days minimum	2.653	2.945	4.406	7.211	10.48	0.494	0.8817	1.688	2.317	3.976	1.064	1.457	1.755	2.006	2.489
7-days minimum	2.72	3.143	4.514	8.181	13.21	0.7216	0.935	1.834	2.595	4.656	1.064	1.484	1.792	2.122	2.632
30-days minimum	3.898	4.621	9.249	13.42	19.9	0.9857	1.88	2.373	4.718	6.422	1.835	2.11	2.293	2.738	3.335
90-days minimum	7.024	9.892	16.39	22.3	27.71	2.503	3.74	5.683	7.912	9.383	2.892	3.364	4.079	4.347	4.765
1-day maximum	125	193	241.8	458.1	852.5	36.56	54.91	70.75	98.86	171.2	18.96	22.59	27.24	37.09	60.29
3-days maximum	109.2	142.3	181.3	247.9	367.6	27.52	39.34	49.74	73.09	94.76	15.31	15.89	19.51	31.53	36.22
7-days maximum	72.04	106.1	127.9	179.3	230.9	22.78	28.68	38.35	52.86	68.2	12.77	13.53	14.44	19.49	21.77
30-days maximum	37.3	56.33	82.78	116.8	171.7	13.74	17.83	23.25	29.71	36.41	8.27	9.266	11.33	13.61	15.85
90-days maximum	27.82	41.66	58.07	78.48	116.1	9.969	11.47	16.83	22.03	25.98	7.04	7.369	8.419	10.73	12.11
No. days/zero flow	0	0	0	0	0	0	0	0	0	0	0	0	0	0	0
Baseline Flow Index	0.07558	0.09556	0.1478	0.2172	0.3273	0.06601	0.111	0.1853	0.2322	0.3732	0.1749	0.2658	0.3189	0.381	0.4225
Group 3 Parameters															
Date of min. flow	330.9	32	84.5	107	215.8	341	34	64	119	227.2	25.2	33	91	122	123
Date of max. flow	160.9	244	305.5	350	26.2	130.1	144	335	346.5	47.9	152.6	242	270	322	323
Group 4 Parameters															
Low pulse count	3	5	10	14	18	4	6	10	13	14.9	4.2	6	9	11	15.8
Duration of low pulses	2	3	4.75	7	11.8	2	3	5	7	10.8	2.6	3	4	6.5	9
High pulse count	6.1	9	14	18	22.7	10	13	16	21	23	9	11	14	17	19
Duration of high pulses	1	2	2.25	3.125	5	1	2	2	3	4	1.1	2	3	3.625	5
Group 5 Parameters															
Rate of increase	2.253	3.304	4.268	5.881	7.986	0.546	0.6475	0.86	1.171	1.684	0.4159	0.4852	0.5897	0.7034	0.8057
Rate of decrease	-4.325	-3.172	-1.949	-1.584	-1.118	-0.89	-0.7387	-0.6	-0.495	-0.4005	-0.3685	-0.3366	-0.2985	-0.2413	-0.2132
Number of reversals	118.2	127	131.5	139.3	147.9	132.1	137	143	151	156.8	112	120	126	131	135

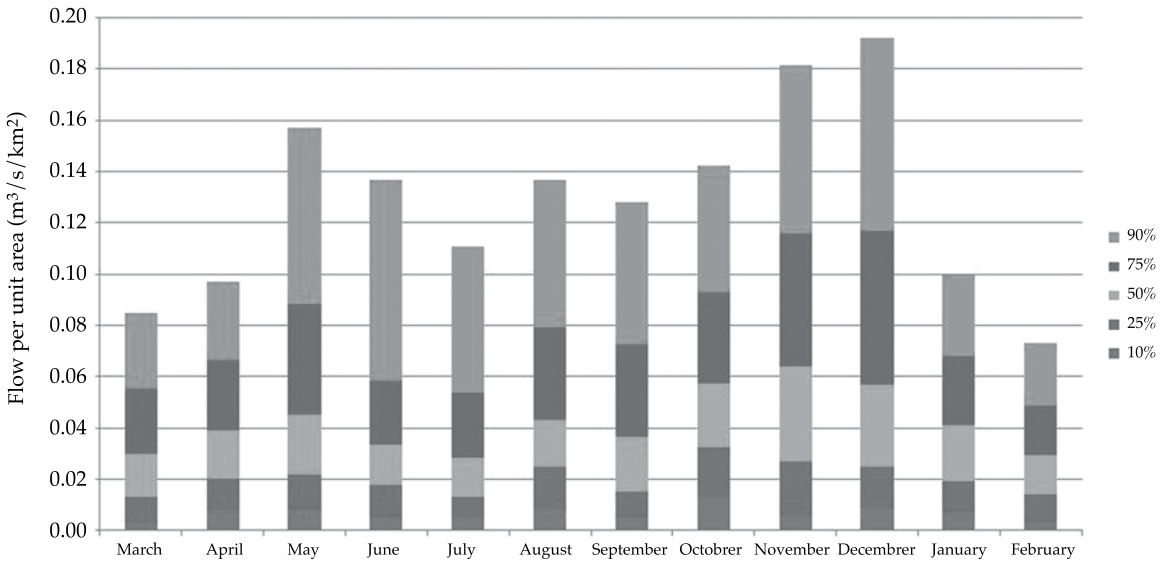

Figure 1. Distribution of monthly mean flows normalized by area. Study site: Hatillo dam (1950-1999) (legend in percentiles).

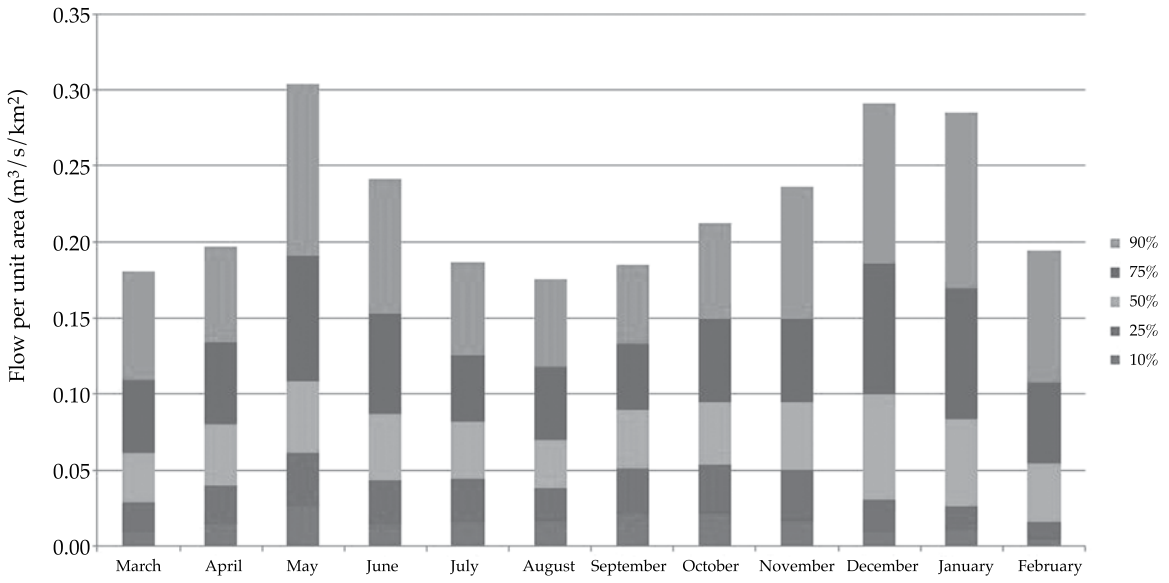

Figure 2. Distribution of monthly mean flows normalized by area. Study site: Rincon dam (1950-1999) (legend in percentiles).

better than the results obtained with the current method used in the country (the Montana de Tennant method(1976) cited by Tharme, 2003). Once the methodology is established (as was done in the present study), it can be used for all later studies to estimate ecological flows.

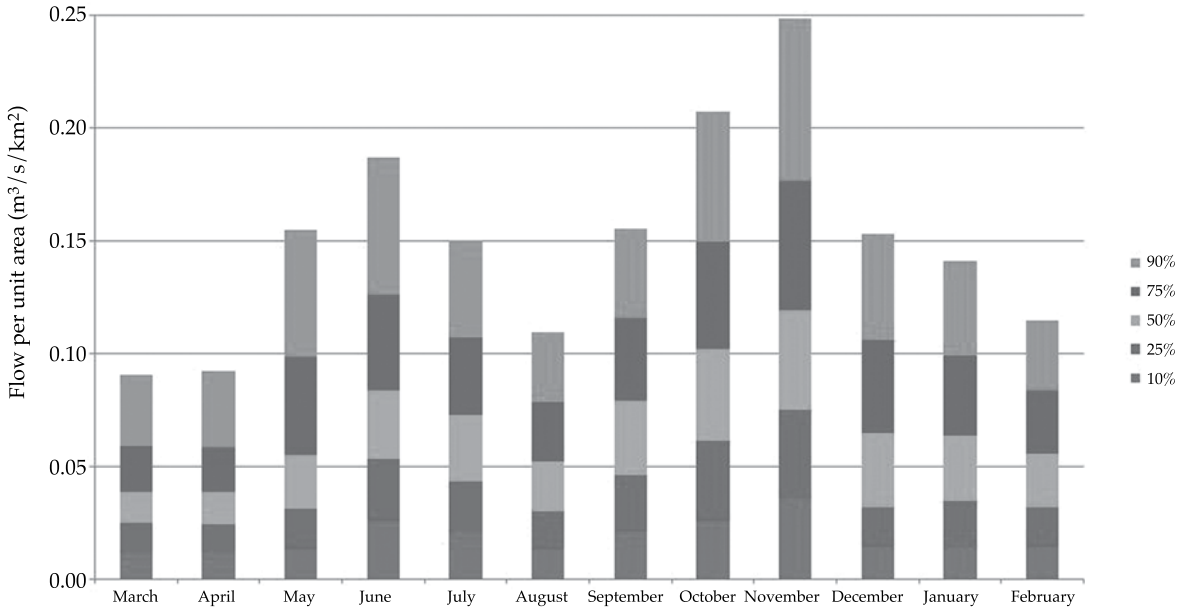

Figure 3. Distribution of monthly mean flows normalized by area. Study site: Blanco dam (1950-1999) (legend in percentiles).

Operation of Reservoirs

According to the operations data supplied by the Hydroelectric Generation Company (Empresa de Generación Hidroeléctrica; EGEHID Spanish acronym), the Hatillo and Rincon reservoirs did not use bottom drains, except for a few times during the year. Therefore, in the case of Hatillo, the ecological flow was managed with turbines and was later spilled into the river. In the case of Rincon, because of a compensating reservoir that diverts the turbined water for irrigation, the flow managed for ecological purposes for the entire system (reservoir+compensating reservoir) was determined according to the outflows from the compensating reservoir. According to the data provided by the EGEHID, the Blanco hydroelectric releases a volume that is nearly equal to the inflow, and therefore there is no hydrologic alteration. This is because the Blanco reservoir is completely sedimented and has therefore lost its storage capacity (Jiménez-Ramírez and Farías, 2012).

Conclusions

The application of the RVA methodology and the IHA to determine ecological flows is a feasible option for the Dominican Republic, given the current limited knowledge of the subject and application in the country. It is a more complete and broader methodology than the one traditionally used and is recommended for estimating ecological flows, despite the limitations and difficulties. The results obtained by the present study can be used to develop an operations program for reservoirs, agreed to by the appropriate institutions, in order to coordinate the different uses of the reservoirs with the need to protect the habitat downstream from the works. This program should be accompanied by an ecological monitoring program to

verify the effectiveness of the flow regimes adopted and modify them when necessary.

Acknowledgements

This investigation was conducted thanks to the financial support of the Fondo de Investigación Competitiva UNIBE, 2011.

Received: 17/10/12
Accepted: 12/07/13

References

ACHARYA, A. and RYU, J. *Stream Flow Disaggregation for Regulated and Unregulated Waterways* [on line] 2012. World Wide Web: http://www.idahoepscor.org/Uploads/Acharya,%20Anil.pdf.

ACREMAN, M. and DUNBAR, M. Defining Environmental River Flow Requirements - A Review. *Hydrology and Earth System Sciences*. Vol. 8, No. 5, 2004, pp. 861-876.

ARMSTRONG, D.S. and PARKER, G.W. *Assessment of Habitat and Stream Flow Requirements for Habitat Protection, Usquepaug-Queen River, Rhode Island, 1999-2000* [on line]. U.S. Geological Survey Open-File Report 02-438, 2003. Fecha de acceso: 27/05/2011, 78 pp. World Wide Web: http://dodreports.com/pdf/ada441417.pdf.

ARTHINGTON, A.H. and ZALUCKI, J.M. *Comparative Evaluation of Environmental Flow Assessment Techniques: Review of Methods*. Australia: Land and Water Resources Research and Development Corporation, 1998.

BAEZA-SANZ, D. and GARCÍA-DEL-JALÓN, D. *The Natural Variability Approach. Application to Five Rivers in the Ebro Basin, Spain* [on line]. Fecha de acceso: 29/05/2011, 2004. World Wide Web: http://www2.montes.upm.es/Dptos/DptoIngForestal/Hidrobiolog%C3%ADa/Publicaciones/Flow_Variability-Baeza.pdf.

BLACK, A.R., BRAGG, O.M., DUCK, R.W., and ROWAN, J.S. Development of a Method to Assess Ecological Impact Due to Hydrological Regime Alteration of Scottish Rivers. *IAHS* Publ. No. 276, 2002, pp. 45-51.

BRAGG, O.M., BLACK, A.R., and DUCK, R.W. *Anthropogenic Impacts on the Hydrology of Rivers and Lochs: Literature Review and Proposed Methods*. Report No. W98 (50)I1. Dundee, United Kingdom: University of Dundee, 1999.

BROWN, S. *Measures of Shape: Skewness and Kurtosis* [on line]. Fecha de acceso: 7/10/2012. World Wide Web: http://www.tc3.edu/instruct/sbrown/stat/shape.htm.

BRUNKE, M. Floodplains of a Regulated Southern Alpine River (Brenno, Switzerland): Ecological Assessment and Conservation Options. *Aquatic Conservation: Marine and Freshwater Ecosystems*. Vol. 12, No. 6, 2002, pp. 583-599.

GARCÍA DE JALÓN, D. y GONZÁLEZ DEL TÁNAGO, M. *El concepto de caudal ecológico y criterios para su aplicación en los ríos españoles* [on line]. Departamento de Ingeniería Forestal, Escuela de Ingenieros de Montes, Universidad Politécnica de Madrid, 1998. Fecha de acceso: 27/05/2011. World Wide Web: http://ocw.um.es/ciencias/ecologia/ejercicios-proyectos-y-casos-1/jalon-tanago-1998.pdf.

JIMÉNEZ-RAMÍREZ, H. y FARÍAS, H.D. *Problemática de la sedimentación del embalse de Valdesia, República Dominicana*. Fecha de acceso: 15/10/2012. World Wide Web: http://irh-fce.unse.edu.ar/Rios2003/TC/TC_2_5.pdf.

LIMBRUNNER, J. *IHA Applications* [on line]. 2010. Fecha de acceso: 29/05/2011. World Wide Web: http://conserveonline.org/workspaces/iha/documents/iha-apps/view.html.

OPPERMAN, J. *Indicators of Hydrologic Alteration Analysis for the Patuca River* [on line]. 2006. Fecha de acceso: 29/05/2011. World Wide Web: http://conserveonline.org/workspaces/iha/documents/opperman1106/view.html.

RICHTER, B.D., BAUMGARTNER, J.V., POWELL, J.M., and BROWN, D.P. A Method for Assessing Hydrologic Alteration within Ecosystems. *Conservation Biology*. Vol. 10, No. 4, 1996, pp. 1163-1174.

RICHTER, B.D., BAUMGARTNER, J.V., BRAUN, D.P., and POWELL, J. A Spatial Assessment of Hydrologic Alteration within a River Network. *Regulated Rivers: Research and Management*. Vol. 14, 1998, pp. 329-340.

RICHTER, B.D., BAUMGARTNER, J.V., WIGINGTON, R., and BRAUN, D.P. How Much Water does a River Need? *Freshwater Biology*. Vol. 37, 1997, pp. 231-249.

RODRÍGUEZ, G. *Generalized linear models* [on line]. Fecha de acceso: 7/10/2012. Disponible en: http://data.princeton.edu/wws509/notes/c2s9.html.

SALAS, J.D., DELLEUR, J.W., YEVJEVICH, V., and LANE, W.L. *Applied Modeling of Hydrologic Time Series*. Colorado: Water Resources Publications, 1997, 485 pp.

SVEINSSON, O.G.B., SALAS, J.D., LANE, W.L., and FREVERT, D.K. *Stochastic Analysis, Modeling, and Simulation (SAMS), Version 2007. User's Manual*. December, 2007. Fecha de acceso: 16/10/2012. World Wide Web: http://www.engr.colostate.edu/Sams-CSU-USBR/SAMS/Resources/SAMS2007_User_Manual.pdf.

THARME, R.E. A global Perspective on Environmental Flow Assessment: Emerging Trends in the Development and Application of Environmental Flow Methodologies for Rivers. *River Research Applications*. Vol. 19, 2003, pp. 397-441.

THE NATURE CONSERVANCY. *Indicadores de alteración hidrológica, versión 7.1. Manual del usuario* [en línea]. Junio de 2011. Fecha de acceso: 16/10/2012. World Wide Web: http://www.conservationgateway.org/Files/Pages/indicadores-de-alteraci%C3%B3n.aspx.

Author's address institutional

Quyen Melina Bautista de los Santos

Universidad Iberoamericana (UNIBE)
Ave. Francia 129, Gazcue
Santo Domingo, D.N., República Dominicana
Teléfono: +1 809 6885 983, extensión 1198
q.bautista@unibe.edu.do

Click here to write the autor

Electrocoagulación para eliminar sílice del agua de torres de enfriamiento

• Iván Emmanuel Villegas-Mendoza* • Alejandra Martín-Domínguez •
• Sara Pérez-Castrejón • Silvia Lucila Gelover-Santiago •
Instituto Mexicano de Tecnología del Agua
*Autor de correspondencia

Resumen

VILLEGAS-MENDOZA, I. E., MARTÍN-DOMÍNGUEZ, A., PÉREZ-CASTREJÓN, S. & GELOVER-SANTIAGO, S.L. Electrocoagulación para remover sílice en agua de torres de enfriamiento. Tecnología y Ciencias del Agua. *Vol. V, núm. 3, mayo-junio de 2014, pp. 41-51.*

El presente artículo muestra los resultados de un estudio que se llevó a cabo para evaluar el efecto de la calidad del agua en la remoción de sílice disuelto mediante un proceso de electrocoagulación utilizando electrodos de aluminio. El sílice se encuentra en el agua de repuesto (RW) y de purga de las torres de enfriamiento (CTBW). Las pruebas se hicieron a escala semipiloto a flujo continuo en un tren de tratamiento consistente de electrocoagulación (EC), floculación, sedimentación y filtración en arena. Se estudiaron dos RW y CTBW, con características fisicoquímicas diferentes. Las variables de respuesta analizadas fueron las siguientes: eficiencia del aluminio para remover sílice (relación mgl^{-1} de Al^{3+} dosificado/mgl^{-1} de sílice removido), eficiencia de remoción de Al^{3+} dosificado, pérdida de carga hidráulica a través del reactor electroquímico y el voltaje. Se calculó el costo del tratamiento de los cuatro tipos de agua. La relación mgl^{-1} de Al^{3+} dosificado /mgl^{-1} de sílice removido osciló de 1.09 ± 0.06 a 1.33 ± 0.05 al tratar RW, mientras que para CTBW fue de 0.85 ± 0.1. Los costos de energía, sustancias químicas y consumo de electrodos para el tratamiento de RW osciló de US$ 0.52 a US$ 0.74 m^{-3}, y el costo del tratamiento de CTBW fue de aproximadamente US$ 0.53 m^{-3}.

Palabras clave: *aluminio, purga, torre de enfriamiento, electrocoagulación, agua de repuesto, sílice, calidad del agua, ciclos de concentración.*

Abstrac

VILLEGAS-MENDOZA, I. E., MARTÍN-DOMÍNGUEZ, A., PÉREZ-CASTREJÓN, S. & GELOVER-SANTIAGO, S.L. Electrocoagulation to Remove Silica from Cooling Towers Water. *Water Technology and Sciences* (in Spanish). Vol. V, No. 3, May-June, 2014, pp. 41-51.

This paper presents the results of a study carried out about the effect of water quality on the removal of dissolved silica using an electrocoagulation process with aluminum electrodes. Silica is found in replacement water (RW), usually known as make up water, and in cooling tower blowdown water (CTBW). Tests were conducted on a small pilot scale (~2 $lmin^{-1}$) with a continuous flow device. The treatment train consisted of electrocoagulation (EC), flocculation, sedimentation and sand filtration. Two distinct RW and two CTBW with different physicochemical characteristics were studied. The response variables analyzed were: efficiency of aluminum to remove silica (ratio mgl^{-1} of dosed Al^{3+}/mgl^{-1} SiO_2 removed), removal efficiency of dosed Al^{3+}, hydraulic head loss throughout the electrochemical reactor and voltage. The cost of the treatment for the four types of water is discussed. The ratio mgl^{-1} Al^{3+} dosed /mgl^{-1} silica removed ranged from 1.09 ± 0.06 to 1.33 ± 0.05 when treating RW and 0.85 ± 0.1 when treating CTBW. The consumption costs of energy, chemicals and electrodes for RW treatment ranged from US$ 0.52 to 0.74 m^{-3}, and was approximately US$0.53 m^{-3} for CTBW.

Keywords: Aluminum, blowdown, cooling tower, electrocoagulation, make-up, silica, water quality, concentration cycles.

Introducción

Una de las estrategias más efectiva para reducir la demanda de agua en las industrias es reducir la sustitución de agua o el consumo del agua de repuesto (RW) en las torres de enfriamiento (TE), ya que estos equipos consumen grandes cantidad de agua (Hinrichs y Kleinbach, 2012). La elevada concentración de sílice (hasta 100 mgl^{-1}) contenida en el agua subterránea usada comúnmente como RW en ciertas regiones en México y Latinoamérica (Demadis y Neofotistou, 2004) provoca que las TE operen en bajos ciclos de concentración (CC), los cuales corresponden al número de veces que una especie química de referencia

(en este caso la sílice) puede aumentar su concentración antes que una porción del agua se deseche para evitar precipitación en el equipo de transferencia de calor. Si X es la sustancia de referencia, entonces:

CC = (concentración de X en purgado/ concentración de X en el agua de repuesto) (1)

El RW en una TE puede calcularse empleando la ecuación (2), si el arrastre (figura 1) se considera cercano a cero

$$RW = E*CC/(CC-1) \quad (2)$$

Donde E es la cantidad de agua evaporada y CC representa los ciclos de concentración.

Por otro lado, el agua purgada de la torre de enfriamiento (CTBW) puede estimarse con la ecuación (3).

$$CTBW = RW/CC \quad (3)$$

De acuerdo con estas ecuaciones, si aumenta el CC, el RW requerida disminuyo al igual que la CTBW (Seneviratne, 2007). La figura 1 ilustra las principales corrientes en una TE.

Existen varios métodos de tratamiento para remover la sílice; sin embargo, el más común ha sido la coagulación química (CQ), el cual es eficiente en la remoción de sílice soluble y coloidal (Sheikholeslami y Bright, 2002), aunque tiene problemas inherentes en el costo, mantenimiento y producción de lodo (Emamjomeh y Sivakumar, 2009). Chuang *et al*. (2006) reportaron que la eficiencia de remoción era alrededor de 7.4 mg de Al_2O_3/ mg de SiO_2 cuando se dosificaba cloruro de polialuminio (CLPA) o alumbre en un intervalo de 150 kg/L como Al_2O_3, lo que representa una relación de masa de 4:1 (aluminio:sílice). Existen otros métodos que pueden remover la sílice eficientemente; estos incluyen la nanofiltración, la ósmosis inversa, intercambio de iones y electrodesionización. Sin embargo, los costos de estos métodos son más altos que los de los métodos químicos (Zeng *et al*., 2007).

La electrocoagulación (EC) es una técnica electroquímica que se ha sugerido como una alternativa para la coagulación convencional, y se caracteriza por su baja producción de lodo, la no adición de compuestos químicos y la fácil operación (Emamjomeh y Sivakumar, 2009; Pérez-Castrejón *et al*., 2012). La principal diferencia entre EC y la CQ es la manera en la que los iones metálicos se añaden al agua. La EC produce bandadas de hidróxidos metálicos por electrodisolución de ánodos solubles, integrados usualmente por hierro o aluminio, mientras que la CQ promueve la formación de hidróxidos usando sales metálicas como el sulfato de aluminio o el cloruro férrico (Comninellis y Chen, 2010).

Se han realizado varios estudios utilizando EC para remover la sílice: Den y Wang (2006), Kin *et al*. (2006); Wang *et al*. (2009); Liao *et al*. (2009); Schulz *et al*. (2009) sin embargo, solo los dos últimos autores trabajaron con agua representativa de torres de enfriamiento. Por otro lado, hasta donde se sabemos, no hay estudios donde se haya analizado la conveniencia de tratar el agua de repuesto con respecto al tratamiento del agua purgada de la torre de enfriamiento.

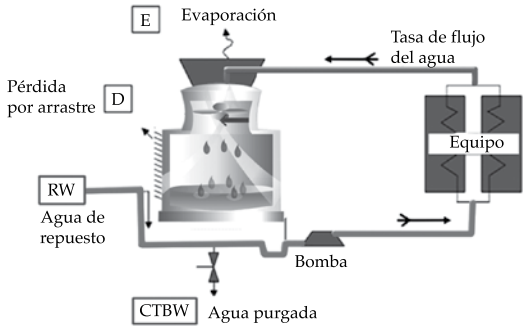

Figura 1. Balance de masa del agua en una torre de enfriamiento.

Este artículo presenta los resultados de tratamiento del agua de repuesto de pozos (RW) y el agua purgada de la torre de enfriamiento (CTBW) a una pequeña escala piloto. Los resultados se usaron para determinar la factibilidad técnica y económica de tratar RP o CTBW en un proceso de EC combinado con un sistema de clarificación convencional para la remoción de sílice.

Metodología

Tipo de agua utilizada

El agua utilizada en este estudio se obtuvo de dos pozos de suministro (RW1, RW2); la calidad del agua es diferente cuando proviene de dos lugares distintos. Por otro lado, dos diferentes muestras de purga de torre de enfriamiento proveniente de dos industrias diferentes (CTBW1, CTBW2) fueron las otras matrices estudiadas. Los parámetros de calidad relevantes de las cuatro fuentes de agua se muestran en la tabla 1.

La matriz RW1 ha sido estudiada ampliamente por nuestro grupo de trabajo bajo diferentes condiciones de operación, y los resultados obtenidos previamente en forma consistente aseguran que el sistema es estable y que los resultados son estadísticamente reproducibles (Villegas-Mendoza, 2009, 2011; Gelover-Santiago *et al*., 2012). El agua de RW2 y CTBW1 provienen de la misma torre de enfriamiento.

Descripción del equipo experimental y de las variables de respuesta

Los experimentos se realizaron utilizando un sistema piloto EC de pequeña escala, con un reactor electroquímico de flujo conectado unido de manera directa a un floculador mecánico de tres etapas seguido por un estabilizador de alta velocidad y un filtro de arena alimentado por gravedad.

El reactor se hizo de acrílico con la forma de un paralelepípedo rectangular con una dimensión de altura de 10 cm, longitud de 78 cm y ancho de 15 cm. Situados dentro del reactor estuvieron 60 electrodos de aluminio que median cada uno 8 × 4 × 0.5 cm, conectados como pantallas deflectoras en un arreglo monopolar (figura 2), obligando al agua a comportarse como un tapón de flujo a través del reactor. El espacio entre los electrodos fue de 0.6 cm y el área anódica activa total de los electrodos correspondió a 0.19 m^2. La pérdida de carga hidráulica en el reactor se midió mediante un manómetro diferencial de mercurio, permitiendo una evaluación del bloqueo causado por la formación de depósitos en la superficie de los electrodos.

La potencia eléctrica requerida para establecer la concentración teórica deseada de Al^{3+} en cada uno de los experimentos se calculó utilizando la ley de Faraday (Comninellis y Chen, 2010; Pérez-Castrejón *et al*. 2012). Fue suministrada utilizando una fuente de poder Sorensen modelo DLM 40-

Tabla 1. Calidad del agua analizada.

	RW1	RW2	CTBW1	CTBW2
pH	7	8.64	8.6	7.13
Conductividad (µS/cm)	200	795	1 625	1 290
Sílice (mgL^{-1})	50	83	164	195
Sulfatos (mgL^{-1})	25.2	83	250	298
Cloruros (mgL^{-1})	8.38	43.1	111	338
Turbidez (NTU)	0.05	0.05	14	35.1

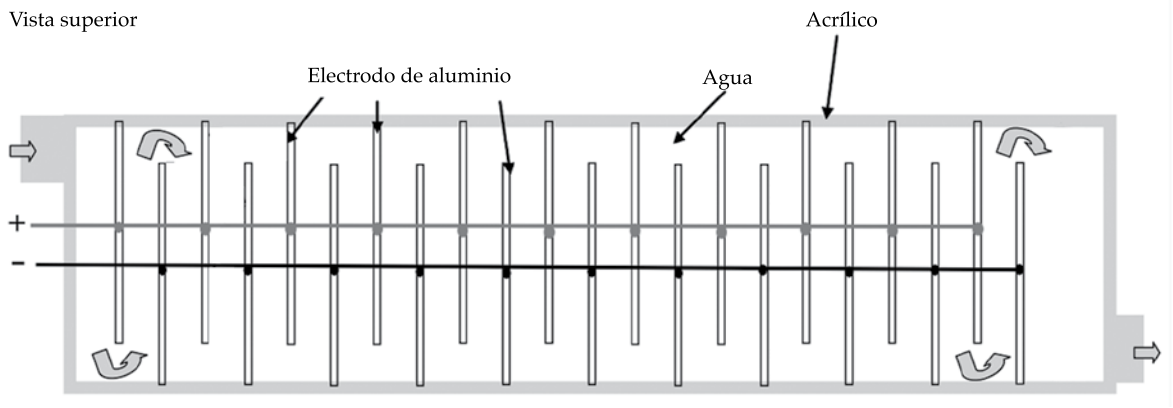

Figura 2. Reactor electroquímico.

15 y la polaridad de los electrodos se cambió cada hora. La densidad de corriente y la tasa de flujo de operación fueron de 71 Am^{-2} y 1.7 $Lmin^{-1}$, respectivamente. Con el fin de remover los depósitos formados durante las pruebas anteriores, al principio de cada experimento el reactor se lavó químicamente con una solución a 30% de producto comercial con ácido hidroclórico como el ingrediente activo. Las variables de respuesta fueron:

- Eficiencia del aluminio para remover sílice (mgl^{-1} de Al^{3+}dosificado/mgl^{-1} de sílice removida), después de estabilizar y filtrar.
- Remoción eficiente del aluminio dosificado, después de estabilizar y filtrar.
- Pérdida de carga hidráulica (medición indirecta de la obstrucción por depósitos en el reactor).
- Variación de voltaje (medición indirecta de la pasivación de los electrodos).

Los datos de la eficiencia de remoción de sílice se analizaron estadísticamente. Antes que nada, los datos para RW1 se compararon con los datos previamente publicados por nuestro grupo (Gelover-Santiago *et al.*, 2012), para la misma matriz de agua (RW1) utilizando la misma planta piloto, cátodos de aluminio y ánodos, aplicando densidades de corriente similares y cambiando la polaridad durante la prueba. Después de esto, se aplicó una prueba t de Student para comparación de medios para contrastar el valor de la remoción de sílice para los cuatro tipos de agua considerados.

Determinaciones analíticas

La concentración de sílice y aluminio se determinó por medio de un colorímetro con un espectrómetro Hach DR/2010 mediante los métodos de Aluver y Molibdato, respectivamente. El pH se determinó con un modelo de potenciómetro Orión 420A y la conductividad con un modelo Orión 145.

La película en los electrodos pasivados se caracterizó utilizando un difractómetro de Rayos-X Rigaku DMAX-2200 con una radiación K alfa de cobre. Las intensidades se midieron en el rango de of 2θ entre 3° a 100°, con un paso de dos teta de 0.02° y una velocidad de escaneo de 1°/min, 36 kV y 30 mA. La identificación de fases de cristal se realizó con el software Jade 6.5 y la base de datos de los patrones de difracción de polvo (PDP) del International Centre for Diffraction Data (ICDD).

Descripción de las pruebas

Efecto de la calidad del agua en la remoción de sílice. Habiendo encontrado las mejores condiciones de pH y gradientes de velocidad en el reactor y el floculador (Villegas-Mendoza, 2011), datos no mostrados en este artículo, se efectuaron corridas continuas para cada tipo de agua utilizando la pequeña EC piloto. Los valores de pH que optimizan la formación de bandadas de aluminio y consecuentemente la remoción de sílice fueron como sigue: RW1 = 7, RW2 = 6, CTBW1 = 5.5 y CTBW2 = 5, y se advirtió que la concentración de sulfato aumenta el valor de pH y que cuando la concentración de sulfato aumenta el valor de pH debe disminuir para alcanzar la precipitación más alta de hidróxido de aluminio.

Las dosis de aluminio se estableció en ~60 mgl^{-1}, lo cual corresponde a la concentración más alta que puede obtenerse con la fuente de poder utilizada. Esto se hizo para analizar la eficiencia de altas dosis de aluminio para remover sílice. Las variables de respuesta se midieron cada una o dos horas a lo largo de la duración de las pruebas, lo cual proporcionó entre 6 y 8 datos de operación en un sistema de estado estable. Esto permitió obtener suficientes datos para llevar a cabo un análisis estadístico aplicando una prueba de Student (comparación de dos medios), y para comparar los resultados entre los diferentes tipos de agua.

Cuando la pérdida de carga en el reactor EC empezó a aumentar (figura 3b), el flujo se incrementó con el fin de extraer hidráulicamente depósitos que se formaron en la superficie del electrodo, excepto en el caso de CTBW2, que se usó como referencia para ver cuál es el resultado cuando esta condición de operación no se implementó.

La operación del sistema se interrumpió cuando el voltaje empezó a aumentar. El incremento en el voltaje se considera como un indicador de la pasivación de los electrodos. El incremento en la pérdida de carga sugiere obstrucción mecánica en el reactor.

Costo del tratamiento. Una vez que se analizó el comportamiento de los cuatro tipos de agua, se calcularon para cada matriz los costos de energía de la oxidación de aluminio, así como el del propio desbaratamiento de aluminio y de los químicos necesarios para fijar el pH en los valores óptimos de operación.

Se consideraron estos factores debido a que son los principales contribuyentes y pueden variar ampliamente dependiendo de las características de calidad del agua. El costo de la oxidación del aluminio

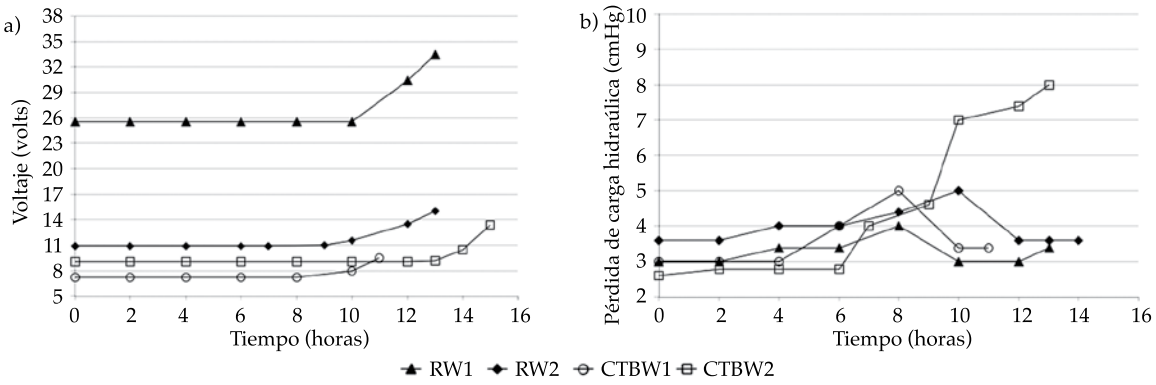

Figura 3. Variación de a) voltaje y b) pérdida de carga hidráulica en relación con los tiempos de operación.

depende del voltaje, el cual es una función de la conductividad. Las dosis de aluminio requeridas dependen de la concentración de sílice y la cantidad de ácido necesario para alcanzar el pH que maximice la remoción de sílice depende de características de agua como la alcalinidad.

Los siguientes datos se consideraron para el cálculo de costos: a) energía eléctrica = 0.12 dólares por KW-h; b) placas de aluminio = 4.85 dólares/kg de aluminio; c) ácido hidroclórico para ajustar el pH = 0.16 dólares/L; a la tasa de cambio de 14.00 pesos mexicanos = 1 dólar.

Resultados y discusión

Análisis del efecto de la calidad del agua

Los cuatros tipos de agua se probaron utilizando el pequeño sistema piloto EC continuo entre ocho y diez horas al día y los datos se graficaron con respecto a horas reales de trabajo. La figura 3a muestra el voltaje con respecto al tiempo de operación. Este es el voltaje suministrado necesario para garantizar la corriente eléctrica requerida para la producción buscada de aluminio. Pueden hacerse dos observaciones de acuerdo con la tendencia de esta variable: el voltaje con los electrodos limpios depende inversamente de la conductividad, y la pasivación empieza en general después de aproximadamente 10 horas de trabajo. La pasivación es un fenómeno caracterizado por el aumento gradual en la potencia eléctrica requerida para fijar la corriente deseada en la celda electrolítica durante la operación del sistema. En este caso, la pasivación no depende de manera significativa de la calidad del agua, sino de la densidad de corriente, que fue un parámetro fijo similar para los cuatro tipos de agua.

La figura 3b muestra la pérdida de carga hidráulica, medida con el manómetro de mercurio, con respecto al tiempo de operación. En la totalidad de las pruebas la pérdida de carga aumentó de manera significativa entre la cuarta y la sexta hora de operación. Una vez que la pérdida de carga aumentó, se buscó reducirla mediante flujo hidráulico, incrementando de manera drástica el flujo de operación por ~ 10 segundos, (excepto en la prueba del CTBW2, donde este método de lavado no fue implementado como medida de comparación). Esto permitió una recuperación temporal de la pérdida de carga inicial y la limpieza de la mayoría de

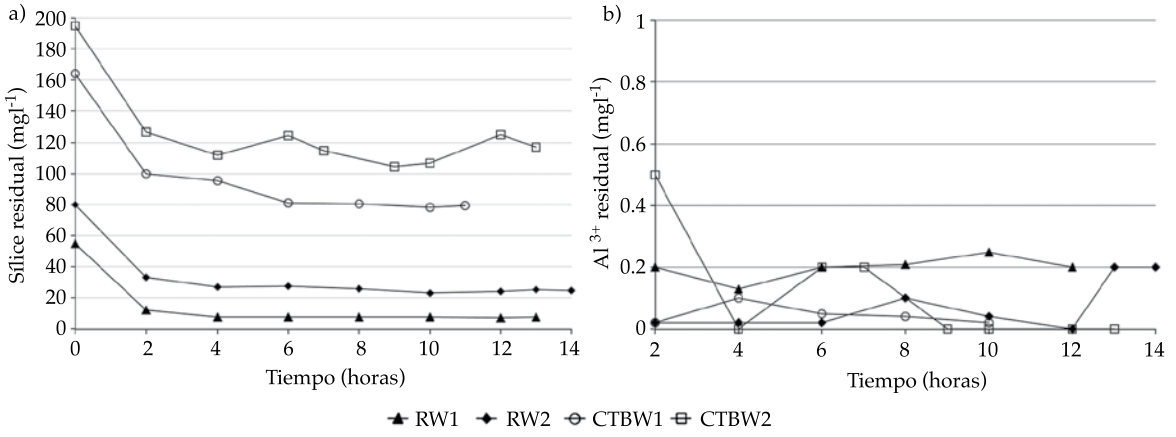

Figura 4. Variación de a) sílice residual y b) Al^{3+} residual, en el afluente del filtro, con respecto al tiempo de operación.

los depósitos suaves y esponjosos presentes en los electrodos; sin embargo, eso no ayudó a parar el proceso de pasivación, lo que indica que este fenómeno se asocia con la presencia de depósitos fuertemente adheridos a la superficie de los electrodos. A través de estudios de difracción de rayos X de muestras en polvo, el principal componente de la incrustación fue identificado como bayerita insoluble $Al(OH)_3$ cuando se usó agua de pozo en las pruebas.

Este segundo tipo de depósito puede removerse parcialmente con lavado químico y removerse por completo solo mediante abrasión mecánica.

Se ha observado consistentemente durante lo presentado aquí y en los experimentos previos que un incremento en la pérdida de carga siempre es seguido por un aumento en el voltaje. Esto es impactante porque una vez que se incrementa la pérdida de carga, se puede esperar que la pasivación de los electrodos empiece en breve.

En la figura 4, las concentraciones de sílice y aluminio en la salida del filtro se muestran como una función del tiempo. Solo los datos de la segunda hora y más allá se han considerado para el análisis estadístico, debido a que el tiempo de residencia hidráulica para el agua tratada en el sistema es alrededor de 2 h. Como puede observarse en la figura 4b, debido a la optimación efectuada con el estabilizador-filtro buscando concentraciones por debajo de 0.2 mgl^{-1}, el aluminio casi se removió totalmente en cada caso, correspondiendo a una eficiencia de remoción de más de 99%.

Del estudio de Gelover-Santiago *et al.*, (2012), los valores para la relación mgl^{-1} de Al^{3+} dosificado / mgl^{-1} del SiO_2 removido, medido a la salida del estabilizador, se encontraron en el intervalo 1.22 ± 0.12 mientras que para el presente trabajo fueron de 1.36 ± 0.05. De acuerdo con la prueba t, ambos valores de medios pertenecieron al mismo intervalo en un nivel de confianza de 95%. Esta es una indicación de la reproducibilidad del sistema.

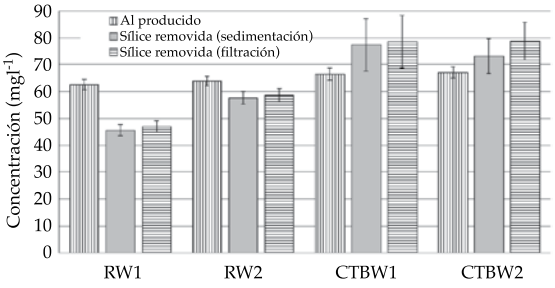

Figura 5. Aluminio producido y sílice removida. Los valores promedio y los intervalos de confianza se muestran en cada caso para cada uno de los cuatro tipos de agua estudiados.

La cantidad de la sílice disuelta residual y la relación Al^{3+} dosificado / SiO_2 removido tienen valores más reproducibles a lo largo del tiempo de experimentación para las pruebas con el agua de repuesto (agua subterránea) que los observados en el purgado de la torre de enfriamiento (figura 4a). En la misma figura puede observarse que se removió más sílice del agua purgada que del agua subterránea.

El análisis estadístico demostró que la sílice removida en ambas muestras purgadas no tuvo diferencias significativas (95% de confianza), pero una situación diferente ocurrió para la sílice removida en las dos muestras de agua subterránea, donde la sílice removida de RW1 fue diferente a la de RW2. Además las cantidades de sílice removida fueron estadísticamente diferentes entre el agua subterránea y el agua purgada (figura 5).

Este comportamiento no tiene nada que ver con el aluminio producido, debido que los medios de este parámetro son significativamente iguales entre los cuatro tipos de agua estudiada, contrario a lo que se esperaría con base a su concentración de cloruro, debido a que como se reportó en la literatura (Vargel, 2004), estos iones favorecen la oxidación del aluminio y por lo tanto su producción. Sin embargo, no se observó una relación clara con respecto a este ion. Otros

autores reportan el efecto combinado de la presencia de iones de sulfato y cloruro. En nuestro caso las cuatro matrices contenían cierta cantidad de sulfatos, y de acuerdo con Trompette y Vergnes, 2008, y Huang *et al*. (2009), los sulfatos pueden preservar la película de alumina pasiva (Al_2O_3) presente naturalmente sobre la superficie de aluminio, situación que puede contrarrestar el efecto corrosivo de los iones cloruro.

La mayor remoción de sílice observada con los dos tipos de agua purgada, con respecto a los dos tipos de agua de pozo, se explica más bien por el hecho de que el paso de sedimentación es más eficiente cuando el agua contiene sólidos suspendidos, como en el caso del agua purgada. Sin embargo, la eficiencia mayor en RW2 con respecto a RW1 solo puede explicarse por una conductividad superior, o porque RW2 empieza con una concentración mayor de sílice. Este comportamiento requiere un estudio adicional, pero nuestro grupo de trabajo ha observado que cuando hay menor concentración de sílice el sistema es menos eficiente.

La sílice disuelta después de la sedimentación y después de la filtración fue casi la misma y algo similar ocurrió con las concentraciones finales de aluminio, hecho que significa que el paso de sedimentación fue altamente eficiente al remover las bandadas, y que la filtración es un paso de pulido.

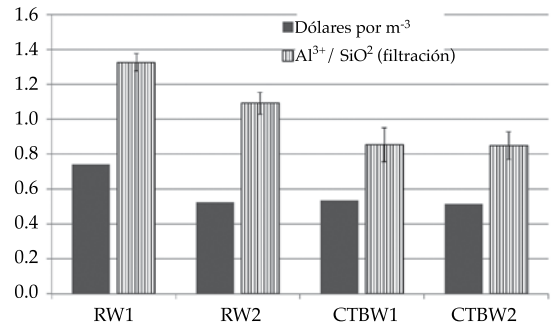

Figura 6. Relación del aluminio producido-sílice removida y costo unitario por metro cúbico.

El análisis de la relación Al^{3+} dosificado/ SiO_2 removido confirma que la remoción de sílice es más eficiente para el agua purgada que para la subterránea. La cantidad de aluminio necesaria para remover una unidad de sílice es mayor que la unidad en el caso de agua subterránea, mientras que es de alrededor de 0.8 para el agua purgada. La complejidad de las matrices de agua purgada, ricas en sales y con la presencia de diversos químicos tales como dispersantes, biocidas e inhibidores de corrosión es un factor importante que debe estudiarse por separado para identificar su impacto en los procesos propuestos.

Costo del tratamiento

Después de cuantificar el costo del tratamiento, donde se consideraron la cantidad de aluminio producido, el ácido consumido y la energía eléctrica, fue claro que la conductividad del agua es un parámetro muy importante por considerar, ya que afecta fuertemente el precio final del tratamiento (figura 6). En el estudio presente RW1 (0.74 dólares por m^3) tuvo el costo de tratamiento más alto debido a su baja conductividad, la cual aumenta de manera significativa el consumo de energía eléctrica. Los costos para los otros tres tipos de agua fueron RW2 (0.52 dólares por m^3), CTBW1 (0.53 dólares por m^3) y CTBW2 (0.52 por m^3), es decir, casi el mismo precio para dosis similares de aluminio. Debe saberse que los precios unitarios serán más altos para concentraciones mayores de sílice, ya que se demandarán dosis superiores de aluminio por metro cúbico de agua tratada y luego más corriente eléctrica.

Costos para el tratamiento CTBW

Además del costo y eficiencia del tratamiento, otro factor por considerar al decidir la matriz por tratar, es la concentración final deseada de sílice y las posibilidades para rehusar el

agua recuperada. En el presente estudio, RW2 es el agua de repuesto utilizada en la torre de enfriamiento cuya corriente purgada es CTBW1; esta TE trabaja a CC = 1.97 (164 mgL s^{-1} de sílice en la purga y 83 mgL s^{-1} de sílice en el repuesto). La aplicación del tratamiento propuesto a CTBW1 nos permitió alcanzar una concentración de sílice similar a la presente en la fuente de agua de repuesto. En esta situación es posible recuperar toda el agua de la purga y reusarla en el sistema como agua de repuesto manejando el mismo CC, ahorrando la primera agua usada y sin descarga de purga.

Como forma de ilustración si E = 100 Ls^{-1}, RW2 = 203 L s^{-1} y CTBW1 =103 L s^{-1}, de acuerdo con las ecuaciones 2 y 3. El tratamiento de CTBW1 tiene un costo de 0.53 dólares por metro cúbico, la conveniencia o no de tratar una corriente de este tipo depende del precio del agua subterránea; esto es, de si es más caro extraer el agua subterránea o tratar la purga.

En contraste, si se decide tratar la corriente RW2 en vez de CTBW1, la concentración inicial de sílice puede disminuirse de 83 hasta ~25 mg/L haciendo entonces posible alcanzar hasta 6.44 CC. En este caso, empleando las ecuaciones 2 y 3 para la situación hipotética del párrafo anterior, será necesario tratar 118.5 Ls^{-1} de agua de repuesto a un costo de 0.52 dólares por metro cúbico con una tasa de purga de 18.5 Ls^{-1}. Esto significa que para este ejemplo particular la opción más económica es tratar la corriente de purga.

En el segundo caso, donde la purga de la CT tuvo características CTBW2 y el requerimiento hipotético para reusarse como agua de repuesto fue alcanzar un contenido de sílice final de 50 mgl^{-1}, el tratamiento no permitiría dicha condición, por lo que sería muy alto el costo para bajar la concentración de sílice de 195 mgl^{-1} a 50 mgl^{-1}. Bajo estas condiciones el dilema es si tratar la purga o continuar utilizado el agua subterránea como repuesto. La decisión final dependerá de la disponibilidad y precio del agua.

Conclusiones

La electrocoagulación es una opción técnicamente factible para reducir la concentración de sílice en el agua de las torres de enfriamiento. La aplicación de este tratamiento podría ayudar a reducir la enorme cantidad de agua de repuesto usualmente demandada por el proceso de enfriamiento.

Los resultados obtenidos en este trabajo nos permiten concluir que el costo del tratamiento es una función inversa de la conductividad del agua; sin embargo, la función no es lineal y para las conductividades exploradas en este trabajo, mayores que para el agua del RW1, no hubo diferencias significativas en el consumo de energía asociado con la conductividad.

La cantidad de sílice por removerse es otro parámetro importante por considerar en el costo, ya que este determina la cantidad de aluminio que se tiene que dosificar. Existe una función lineal entre la cantidad de aluminio y la corriente eléctrica requerida (energía). Para este parámetro la relación del aluminio dosificado-energía requerida es lineal para un régimen de flujo constante.

La sobreproducción del aluminio debe controlarse estrictamente pues en otro caso la relación Al^{3+} dosificado/SiO_2 removido aumenta significativamente haciendo solo el tratamiento más costoso sin ningún beneficio adicional.

La relación estequiométrica encontrada en este trabajo entre el aluminio y la sílice es casi 1:1 (masa:masa). Este valor es significativamente menor que el reportado en la literatura para la aplicación convencional de sales de aluminio, donde la relación es 4:1 aluminio:sílice.

En las condiciones estudiadas el tratamiento propuesto fue más eficiente en términos de la relación Al^{3+} dosificado/SiO_2 removido cuando se aplicó al agua purgada y se asoció con el mayor contenido de solo sólidos suspendidos para esta matriz,

aun cuando este hecho requiere estudios adicionales. Sin embargo trabajar con agua purgada ocasiona una mayor variabilidad en el sistema y puesto que la calidad del agua de esta matriz puede ser muy variable a lo largo de una base diaria, el control del sistema de tratamiento se vuelve complicado.

La decisión de cuál de las matrices tratar, agua de repuesto o purgada, con el fin de aumentar los ciclos de concentración para ahorrar agua depende en gran medida de la concentración de sílice de ambas matrices, de la calidad del agua de repuesto y de la disponibilidad y precio del agua. El tratamiento de las purgas podría ser conveniente para zonas de alta escasez de agua.

El proceso resultará atractivo para sistemas con un valor bajo de CC. En el caso de CC realmente elevado, la relación de sílice en el agua de purgado/sílice en el agua de repuesto se espera que sea alta y como se ha mostrado la remoción de una alta concentración de sílice será muy costosa sin ningún beneficio adicional.

Reconocimientos

Este trabajo fue apoyado por el FSIDTE-CONACYT, proyecto CFE-2008-CO7-89054.

Recibido: 11/12/12
Aceptado: 09/08/13

Referencias

CHUANG, S.H., CHANG, T.C., OUYANG, C.F., and LEU, J.M. Colloidal Silica Removal in Coagulation Processes for Wastewater Reuse in High-Tech Industrial Park. *Water Science and Technology*. Vol. 55, No. 1-2, 2006, pp. 187-195.

COMNINELLIS, C. and CHEN, G. *Electrochemistry for the Environment*. New York: Springer, 2010, 564 pp.

DEMADIS, K. and NEOFOTISTOU, E. Inhibition and Growth Control of Colloidal Silica: Designed Chemical Approaches. *Materials Performance*. Vol. 43, No. 4, 2004, pp. 38-42.

DEN, W. and WANG, C. Parameter Optimization and Design Aspect for Electrocoagulation of Silica Nanoparticles in Water Polishing Wastewater. *Water Science and Technology*. Vol. 53, No. 6, 2006, pp. 187-194.

EMAMJOMEH, M.M. and SIVAKUMAR, M. Review of Pollutants Removed by Electrocoagulation and Electrocoagulation/flotation Processes. *Journal of Environmental Management*. Vol. 90, No. 5, 2009, pp. 1663-1679.

GELOVER-SANTIAGO, S.L., PÉREZ-CASTREJÓN, S., MARTÍN-DOMÍNGUEZ, A., and VILLEGAS-MENDOZA, I.E. Electrogeneration of Aluminium to Remove Silica in Water. *Water Science and Technology*. Vol. 65, No. 3, 2012, pp. 434-439.

HINRICHS, R.A. and KLEINBACH, M.H. *Energy: Its Use and the Environment*. Fifth edition. Boston: Cengage Learning, 2012, 640 pp.

HUANG, C., CHEN, L., and YANG, C. Effect of Anions on Electrochemical Coagulation for Cadmium Removal. *Separation and Purification Technology*. Vol. 65, No. 2, 2009, pp. 137-146.

KIN, K., TANG, H., RAGHAVAN, S., and MARTINEZ, S. Treatment of Chemical-Mechanical Planarization Wastes by Electrocoagulation/ElectroFenton Method. *IEEE Transactions on Semiconductor Manufacturing*. Vol. 19, No. 2, 2006, pp. 208-215.

LIAO, Z., GU, Z., SCHULZ, M.C., DAVIS, J.R., BAYGENTS, J.C., and FARRELL, J. Treatment of Cooling Tower Purge Water Containing Silica, Calcium and Magnesium by Electrocoagulation. *Water Science and Technology*. Vol. 60, No. 9, 2009, pp. 2345-2352.

PÉREZ-CASTREJÓN, S., RIVERA-HUERTA, M.L., MARTÍN-DOMÍNGUEZ, A., GELOVER-SANTIAGO, S.L., PIÑA-SOBERANIS, M., GÓMEZ-ROJAS, A., HERNÁNDEZ-YÁÑES, C., y CORTÉS-MUÑOZ, J.E. Technical and Economic Comparison of Chemical Coagulation and Electrocoagulation to Remove Arsenic from Drinking Water. *Water Technology and Sciences (in Spanish)*. Vol. 3, 2012, pp. 5-21.

SCHULZ, M.C., BAYGENTS, J.C., and FARRELL, J. Laboratory and Pilot Testing of Electrocoagulation for Removing Scale-Forming Species from Industrial Process Waters. *International Journal of Environmental Science and Technology*. Vol. 6, No. 4, 2009, pp. 521-526.

SENEVIRATNE, M. *A Practical Approach to Water Conservation for Commercial and Industrial Facilities*. Oxford: Elsevier, 2007, 400 pp.

SHEIKHOLESLAMI, R. and BRIGHT, J. Silica and Metals Removal by Pretreatment to Prevent Fouling of Reverse Osmosis Membranes. *Desalination*. Vol. 143, No. 3, 2002, pp. 255-267.

TROMPETTE, J.L. and VERGNES, H. On the Crucial Influence of Some Supporting Electrolytes during

Electrocoagulation in the Presence of Aluminum Electrodes. *Journal of Hazardous Materials*. Vol. 163, No. 2-3, 2008, pp. 1282-1288.

VARGEL, C. *Corrosion of Aluminium*. Oxford: Elsevier, 2004, 626 pp.

VILLEGAS-MENDOZA, I.E. *Silica Removal from Water for Cooling Towers Using an Electrochemical Method*. Graduate Thesis (In Spanish). Cuernavaca, México: Autonomous University of the State of Morelos, 2009.

VILLEGAS-MENDOZA, I.E. *Influence of Physicochemical and Hydraulic Parameters in the Efficiency of Silica Removal using an Electrocoagulation System*. Master Degree Thesis (In Spanish). Mexico, D.F.: National Autonomous University of Mexico, 2011.

WANG, C., CHOU, W., CHEN, L., and CHANG, S. Silica Particles Settling Characteristics and Removal Performances of Oxide Chemical Mechanical Polishing Wastewater Treated by Electrocoagulation Technology. *Journal of Hazardous Materials*. Vol. 161, No. 1, 2009, pp. 344-350.

ZENG, Y., YANG, C., PU, W., and ZHANG, X. Removal of Silica from Heavy Oil Wastewater to be Reused in a Boiler by Combining Magnesium and Zinc Compounds with Coagulation. *Desalination*. Vol. 216, No. 1-3, 2007, pp. 147-159.

Dirección institucional de los autores

M.C. Iván Emmanuel Villegas-Mendoza
Ph.D. Alejandra Martín-Domínguez
M.C. Sara Pérez-Castrejón
Ph.D. Silvia Lucila Gelover-Santiago

Instituto Mexicano de Tecnología del Agua
Paseo Cuauhnáhuac 8532, colonia Progreso
62550 Jiutepec, Morelos, México
Teléfono: +52 (777) 3293 600
mr.villegass@hotmail.com
alejandra_martin@tlaloc.imta.mx
sara_perez@tlaloc.imta.mx
sgelover@tlaloc.imta.mx

Click here to write the autor

Crater Lake, La Preciosa, Puebla, Mexico.

Photo provided by Óscar Raúl Mancilla Villa.

Industrial Water Use in Mendoza, Argentina: Coefficients for the Food Industry

• Alicia Elena Duek* • Graciela Elena Fasciolo •
Instituto Nacional del Agua, Argentina
*Corresponding Author

Abstract

DUEK, A.E. & FASCIOLO, G.E. Industrial Water Use in Mendoza, Argentina: Coefficients for the Food Industry. *Water Technology and Sciences* (in Spanish). Vol. V, No. 3, May-June, 2014, pp. 53-64.

Approximately 50% of the industries in the province of Mendoza, Argentina are related to food and drinks. In arid regions such as this one, the consumption and efficient use of water requires special attention by all demand sectors, including domestic, irrigation, industrial and environmental. The industries in Mendoza mostly use groundwater, including for cooling, as a prime material or for cleaning during different parts of the productive process. In this latter case, returning it to the hydric system. Knowledge about the water volume used by these industries is important for diverse applications, such as calculating virtual water products and obtaining water balances that incorporate the uses by sector at the basin level. To identify the water consumed by the food industry in Mendoza, the present work proposed using coefficients relating water volume with the prime material processed or the produced product. These can be applied to perform estimates per basin of the volume of water used by these industries. The main coefficients were obtained based on in-person interviews in industries with different production scales, such as warehouses, producers of beer and non-alcoholic drinks and fruit and vegetable preservers. In addition, the use of the water in the process is explained for each branch of activity. The coefficient values obtained from the interviews were compared with those reported by the local and international literature.

Keywords: Water uses, food industries, coefficients, Mendoza.

Resumen

DUEK, A.E. & FASCIOLO, G.E. Uso industrial del agua en Mendoza, Argentina: coeficientes para la industria alimenticia. Tecnología y Ciencias del Agua. *Vol. V, núm. 3, mayo-junio de 2014, pp. 53-64.*

Aproximadamente el 50% de los establecimientos industriales de la provincia de Mendoza, Argentina se concentra en los rubros de alimentos y bebidas. En zonas áridas como ésta, el consumo y la eficiencia en el uso del agua requieren de especial atención en todos los sectores de la demanda: doméstico, riego, industrial y ambiental. Las industrias de Mendoza utilizan fundamentalmente agua subterránea, ya sea para refrigerar, como materia prima o para la limpieza en distintas partes del proceso productivo; en este último caso, con retorno al sistema hídrico. El conocimiento del volumen de agua que utilizan tales industrias es importante para diversas aplicaciones, como el cálculo del agua virtual de los productos, y para la realización de balances hídricos que incorporan los usos sectoriales en el nivel de cuenca. Para conocer el consumo de agua por parte de la industria alimenticia de Mendoza, el presente trabajo propone utilizar coeficientes que relacionen volumen de agua con materia prima procesada o producto elaborado. Éstos se pueden aplicar para efectuar las estimaciones por cuenca del volumen de agua utilizada por tales industrias. Los coeficientes primarios se obtuvieron a partir de entrevistas presenciales en industrias con diferentes escalas de producción, tales como bodegas, cerveceras, elaboradoras de bebidas no alcohólicas, y conserveras de frutas y hortalizas. Asimismo, para cada rama de actividad se explica el uso de agua en el proceso. Los valores de coeficientes obtenidos a partir de las entrevistas se compararon con aquellos provenientes de bibliografía local e internacional.

***Palabras clave**: usos del agua, industrias alimenticias, coeficientes, Mendoza.*

Fundamentals, background and objectives

Water plays a very important role in the processing of foods. The manufacturing industry uses it in a variety of stages involved in the processes, including heat transfer (heat or cool), cleaning, and as a component of the product itself. Its use can be consumptive or discarded as wastewater.

Some authorities differentiate between the concept of "consumption" and "extraction" to distinguish between consumptive uses versus waste. Also notable is that the total surface and groundwater extracted worldwide by the industry is usually much greater than the amount consumed (United Nations Organization for Education, Science and Culture, 2006).

In addition, the volume of water that produces a flow that is returned to the water system at some point within or outside the industrial establishment is considered part of the water circuit, though it is not a consumptive use.

For the province of Mendoza, Argentina, there are no accurate estimates of the amount of water used by the industrial sector. The Physical Environmental Diagnostics by the Mendoza Strategic Framework, developed by the National University of Cuyo (2004) presents a water balance which shows irrigation as the sector using the majority of the water in the province's basins, followed by potable water. That study also notes the little information available regarding the industrial use of water. In addition, it is important to remember that the industrial sector in Mendoza grew considerably over recent years and after the 2001 economic crisis as a result of the drive towards wine making.

Table 1 shows the manufacturing industry in the province of Mendoza representing 15% of the geographic gross product (GGP) of the province. It is composed of a wide variety of activities, the most representative of which are the extraction and processing of oil and the manufacturing of foods and drinks. The latter sector is the subject of this study herein.

Roughly half of the establishments (49.8%) in the manufacturing industry correspond to foods and drinks, including winemaking and other drinks as well as preserved and unpreserved foods. Table 2 shows the number of industrial establishments per activity, according to information from the Institute for Industrial Development, Technology and Services (Instituto de Desarrollo Industrial, Tecnológico y de Servicios ; IDITS, Spanish acronym).

With regard to the geographic distribution of the water used by the industrial food and drink establishments, Table 3 shows that the majority are located in the lower basins of the Mendoza and Tunuyan Rivers, that is, in the North Oasis. This again provides evidence of the pressure on the water resource in these basins as compared to the others (UNCuyo, 2004).

Table 1. Distribution of the provincial GGP according economic sector, Mendoza, Argentina, 2010.

Economic Sector	Percentage of GGP
Business, restaurants and hotels	25%
Community, social and personal services	16%
Industrial manufacturing	15%
Mining and quarries	14%
Financial establishments	11%
Agriculture and livestock	8%
Transportation and communications	7%
Construction	2%
Electricity, gas and water	2%
Total	**100%**

Source: DEIE Mendoza.

Table 2. Industrial manufacturing establishments by industry in Mendoza, Argentina, 2003 in number and percentage.

Activity	Amount	Percentage
Winemaking	684	24%
Preserved foods	344	12.1%
Non-preserved foods	289	10.1%
No vínicas drinks	103	3.6%
Metal mechanics	658	23.1%
Paper and graphics	233	8.2%
Woods and furniture	225	7.9%
Mining	96	3.4%
Textile and leather	85	3.0%
Chemical and petrochemical	78	2.7%
Plastics	58	2.0%
Total	**2 853**	**100%**

Source: IDITS.

Table 3. Distribution of establishments related to winemaking and other drinks, preserved and non-preserved foods, by basin, Mendoza, Argentina, 2003, as percentage.

Basin	Winemaking s/684 establishments	Preserved foods, s/344 establishments	Non-conserved foods, s/289 establishments	No vínicas drinks, s/103 establishments
Mendoza River	35.4%	42.4%	69.9%	50.5%
Tunuyan Lower River	45.3%	20.6%	7.3%	13.6%
Tunuyan Upper River	6.6%	4.4%	4.8%	16.5%
Diamante, Atuel and Malargue Rivers	12.7%	32.6%	18.0%	19.4%
	100%	**100%**	**100%**	**100%**

Source: developed based on the IDITS database.

The work presented below calculates the coefficients associated with the use of water, as a processed prime material or finished product, by establishments related to preserved foods and winemaking and certain other drinks.

Methodology

To address the issue of water used by the industrial sectors in Mendoza and obtain elements to quantify it, interviews were conducted with technical representatives and managers in different establishments using a semi-structured questionnaire. The measurement instrument used to collect the data was designed specifically for this investigation in order to determine the volumes of water used in the industrial establishments, per unit of prime material or per finished product. The unit of analysis was the establishment and the informant was the technician representative of the establishment. This instrument well reflects the contents of the concepts to be measured.

In terms of the accuracy of the instrument, the information obtained about extraction and consumption of water varies according

to the technology used by each establishment, since some had flow meters to measure the water at different points in the process while other responses were based on the knowledge and experience of the informant.

The activities included are: wineries, preserved tomato and fruit manufactures, beer producers, and soda and mineral water establishments.

The establishments studied were located in the province's North and Central Oasis. A directed sample was selected through non-probabilistic samplings of representative establishments of different sizes, using databases supplied by the IDITS General Department of Irrigation (DGI, Spanish acronym) and Statistics. Table 4 presents a summary of the number of establishments included in the sample.

The interviews of the establishments selected were agreed to by the technical representative by telephone and conducted by three researchers at a rate of one per day. The average length of the interviews was 2.5 hours and they were conducted during the year 2012.

There were difficulties in obtaining agreements to be interviewed due to the sectors themselves and to fears by the companies about providing information, as well as the inconveniences involved in making time available to be interviewed. Nevertheless, once the informants agreed to be interviewed, they were very friendly with the investigators and very willing to provide information and show the interviewers the facilities.

The objective of the directed sample was to obtain data from representative establishments that could be applied to production in the province, based on the calculation of coefficients. This sample of interviews is considered a first approach to obtaining the values of the coefficients.

The following variables were included in the interviews:

- Volume of prime material processed
- Volume of production
- Number of employees
- Installed and consumed electric power
- Electric energy consumed
- Water supply source
- Destination of water used
- Volume of water used
- Wastewater treatment
- Innovations related to efficient use of water
- Suggestions and comments.

While respecting the questionnaire guide, the interviews were also open and therefore permitted incorporating other variables that were not included and arose spontaneously. While it is not always possible to obtain all of the quantitative information for these pre-selected variables, it was possible to obtain valuable approximations for the purposes of this study.

Coefficients were calculated for the amount of water used per volume of prime

Table 4. Establishments interviewed by activity, Mendoza, Argentina, 2012.

Activity	Amount
Wineries	Three (two large and one small)
Beer producers	One (large)
Soda manufacturers	One (large)
Bottled mineral water manufacturers	Two (large)
Preserved Fruit and vegetable manufacturers	Three (two large and one medium)
Total	**10**

material processed or finished product based on the information provided by the interviewees at the establishments. Upper and lower limits are presented and compared to those obtained by other local and international studies.

To have an idea of the amount of water returned to the system, an indicator was designed which measures the relationship between volume of water returned to the system and volume of water extracted. Ranges were determined using the ratio "volume returned / volume extracted x 100."

The individual results and identification of the establishments visited are not presented herein so as to honor the commitment to statistical confidentiality.

Results and Discussion

This section presents the results and discussion for each of the industries analyzed, as seen in Table 4. For each industrial activity, the primary stages in which water is used are identified and the consumption coefficients obtained from both interviews as well as local and international literature are shown.

Elaboration and bottling of wine

The process to manufacture and bottle wine shows some differences depending on the types— white, rose, red, aged, young. Nevertheless, the stages can be summarized as: reception and crushing, maceration, fermentation, transfer, pressing, malolactic fermentation, clarification and filtering, stabilization and bottling.

The use of water by wineries can be divided according to two stages — production and bottling. The former uses water to clean the grinders and presses and the latter to clean bottles and demijohns. There are two cleanings, external with hard water and internal with soft water requiring a conditioning system. It is worth mentioning that water is also used to clean basins, tanks, filters, floors, etc throughout the year. In all, these uses correspond to the concept of "water extracted," that is, nearly all the water used is discarded as wastewater.

In relation to the water consumption coefficient obtained through interviews of wineries, the ranges were between 1.5 and 20 liters of water per liter of wine produced. The lower limit of this range corresponds to large and medium wineries with more awareness about environmental sustainability. In addition, a recent study on the use of water by this industry reported an average coefficient of 3 liters of water per liter of wine produced (Duek and Fasciolo, 2012).

The local and international literature presents coefficients consistent with those in the range just mentioned, such as that calculated by Nazrala *et al.* (2003) of 3.08 liters of water per liter of wine produced. Meanwhile, Smith (2010) estimated that certain wineries may use as much as 20 liters per liter of wine produced. Lastly, the range found by the Beverage Industry Environmental Roundtable (2011) is between 1.46 and 14.83 liters of water per liter of wine produced.

Beer Production

The production of beer requires four key prime materials: water, barley, hop and yeast. The first step in the production process is to convert the barley into malt. Nevertheless, it is worth mentioning that this stage is not conducted by the majority of the industrial plants that produce beer, but rather, by establishments that are specially dedicated to this activity.

The following stages in the production process are: crushing, maceration, filtering, boiling, decanting, fermentation, settling and filtering, and bottling. Of these, most of

the water is used for maceration, boiling or cooking, filtration and fermentation.

The interviews indicated coefficients between 3.8 and 4.5 liters of water used per liter of beer produced. This activity involves both water consumption and extraction, with approximately 75% of the total water resulting in wastewater.

PVassolo and Döll (2005) report coefficients between 3.4 and 25 liters of water per liter of beer produced, with an average of 9.5, and the Beverage Industry Environmental Roundtable (2011) reports a range between 3.44 and 9.13.

In the case of beer producing industries, the coefficients obtained from the interviews were on the lower limits of those cited by the international literature. This is because the these types of industries located in the province of Mendoza belong to multinational companies that have rigorous environmental sustainability objectives.

Production of Sodas

The production of sodas can be summarized by the following stages: water treatment, production of syrups, mixing, carbonation and filling. Unlike the prior processes, water is consumed in all of the stages. It is worth mentioning that mixing the syrup with treated water has the highest consumption, around 70%.

With regard to the coefficients found for this industry, the interviews resulted in values between 1.5 and 2 liters of water per liter of soda produced. This activity involves predominantly "consumed water."

The Beverage Industry Environmental Roundtable (2011) presents a range between 1.56 and 4.55 liters of water per liter of soda produced.

In this case, the coefficients provided by the primary sources of information are also found to be at the lower limit of those cited by the international literature. Although the difference is less, the explanation is the same as that described for beer producers, that is, the companies adopt international standards for environmental indicators.

Bottling of mineral water

Bottling of mineral water is the simplest production process described herein. It involves the following stages: collection and transfer, storage, filtration, microfiltration, bottling and packaging. The water is primarily used as a prime material; that is, it represents a consumptive use as in the case of soda. It is also used for overall sterilization of industrial warehouses and, as in any other establishment, for dining and bathroom services. In this case, approximately 35% of the water used is discarded.

Stages that could use water that have not yet been mentioned include cleaning glass bottles if they were part of production as well as refrigeration compressors and blowers if polyethylene terephthalate (PET) bottles were manufactured in the plant.

The coefficients obtained from the interviews were between 1.62 and 1.84 liters of water per liter of bottled water. In addition, the interviewees provided coefficients between 2.1 and 1.2 liters of water per liter of bottled water for other bottling plants in the country and internationally.

The international literature presents coefficients in a range that coincides with those just mentioned, of 1.22 a 2.57 liters of water per liter of bottled water (Beverage Industry Environmental Roundtable, 2011).

Production of preserved fruits and vegetables

Production processes for preserved vegetables are very similar, though small differences naturally exist.

In the case of the production of preserved vegetables, the primary stages are reception

and selection of the prime material, cleaning, conditioning, inspection, classification, packaging, adding the covering liquid, eliminating inside air, sealing, sterilizing and cooling. The production of preserved fruit involves reception and cleaning of the prime material, cleaning, peeling, cutting and coring, inspection, cooling, precooking, packaging, producing the syrup, adding the syrup, sterilization and cooling. Some of these processes require a second peeling of fruits or vegetables. Packaging is another factor to keep in mind, since depending on the type used it may need to be washed, sealed, sterilized, etc.

The stages that require the most amount of water in the production of preserved vegetables are cleaning the prime material, cooling of the packaging after sterilization, and the concentration and transportation of the product within the plant. Nearly all of this corresponds to "extracted water", that is, results in wastewater.

The coefficients estimated by the interviews for the preserved vegetable production industry are between 19.85 and 29.76 liters of water per kilo of prime material processed, and between 29.76 and 32.72 liters of water per kilo of finished product.

The local literature cites values between 14.95 and 26.60 liters of water discarded per kilo of prime material processed and an average coefficient of 18.9 liters of water discarded per kilo of prime material processed (Zoia *et al*., 1983). Meanwhile, the international literature presents a range of 4.16 to 14.01 liters of water discarded per kilo of finished product (North Carolina Department of Environment and Natural Resources, 1998). In addition, those who were interviewed stated that their establishments consumed much more water than foreign companies. In effect, they indicated that they have an average coefficient of 5 liters of water per kilo of prime material processed.

The local values indicated by the interviews are considerably higher than those cited by international literature, and those interviewed mentioned not using the water resource in a reasonable manner because the price of water in Argentina is much lower than in other countries. Therefore, these companies do not invest highly in sustainability technologies.

In terms of the production of preserved fruits, the stages that use the most water are cleaning and peeling the fruits, sterilizing and transferring the product to the different stages in the production process. This also involves "extracted" water.

One interview was conducted for this activity and a coefficient of 18 liters of water per kilo of prime material processed was obtained. This can be compared to findings by Zoia *et al*. (1983), which reported a range of 20.6 to 57.3 of water discarded per prime material processed. The international literature indicates a range of 5.30 to 23.85 liters of water discarded per kilo of finished product (North Carolina Department of Environment and Natural Resources, 1998).

In this case, the coefficient obtained from the interview is located near the upper limit of the range found in the international literature. While those interviewed mentioned that their use was high because of the low price of water, they showed interest in decreasing these volumes. In fact, they had recently installed flow meters to measure their water use and develop a reduction plan.

Table 5 shows a summary of the results presented by the above discussion.

The coefficient units were standardized in order to make comparisons, since the international literature uses different units. For both production of preserved fruits as well as vegetables, the coefficients in the local and international literature correspond to liters of water discarded. Since consumptive

Table 5. Coefficients for water consumed by industrial activity, Mendoza, Argentina, 2012.

Activity	Coefficients obtained from interviews (2012)	Coefficients from local literature review	Coefficients from international literature	Local and international coefficients mentioned in the interviews (2012)
Wine Production and bottling	1.5 to 20.0 liters of water/liter of wine produced	3.0 to 3.1 liters of water/liter of wine (2003/2010/2012)	1.5 to 20.0 liters of water/liter of wine produced (2010/2011)	s/d
Beer production	3.8 to 4.5 liters of water/liter of beer produced	s/d	3.4 to 20.0 liters of water/liter of beer produced (2005/2011)	s/d
Soda production	1.5 to 2.0 liters of water/liter of soda produced	s/d	1.6 to 4.5 liters of water/liter of soda produced (2011)	s/d
Bottling of mineral water	1.6 to 1.8 liters of water/liter of water bottled	s/d	1.2 to 2.6 liters of water/liter of water bottled (2011)	1.2 to 2.1 liters of water/liter of water bottled
Production of preserved vegetables	19.9 to 29.8 liters of water/kilo of prime material processed, 29.8 to 32.7 liters of water/kilo of finished product	14.9 to 26.6 liters of water discharged/kilo of prime material processed (1983)	4.2 to 14.0 liters of water discharged/kilo of finished product (1998)	5.0 liters of water/kg of prime material processed
Production of preserved fruits	18.0 liters of water/kilo of prime material processed	20.6 to 57.3 liters of water discharged/kilo of prime material processed (1983)	5.3 to 23.9 liters of water discharged/kilo of finished product (1998)	s/d

Source: prepared and from appointments in text.

water use is low for these activities, these coefficients can be used for comparisons.

The range of water used, per unit of product, by the establishments interviewed which produce preserved fruits and vegetables is observed to be much higher than others in the food industry, including those with consumptive water use (as much as 20 times the lower limit of the range and twice the upper limit).

The amount of water used by the beer industry establishments interviewed is slightly lower than those reported in the international literature. Sodas and bottled water manufacturers interviewed have the same levels. Preserved vegetable producers are higher and fruit and wineries are within the ranges.

Applications: volumes of water used, ratio of volume returned /volume extracted for the food industries in Mendoza, and water balance

The coefficients for water used by the food industries make it possible to estimate the volumes of water they use. Table 6 presents the results of this application for the three primary hydrogeological basins located in the Oasis production region of the province of Mendoza. The estimates were based on the results from the interviews conducted

Table 6. Volumes of water used by industry industrial activity and basin in Mendoza, Argentina, 2013 in hectometres per year.

Activity	Basin		
	Mendoza River and Lower Tunuyan	Upper Tunuyan	Atuel, Diamante and Malargue
Wine production and bottling	2.91	0.22	0.28
Beer Production	0.66	0	0
Bottling of mineral water	1.31	0.18	0
Production of preserved vegetables (*)	2.15	0.96	0.20
Production of preserved fruits (**)	1.34	1.16	2.14
Basin Total	**8.37**	**2.52**	**2.62**

Source: Based on stastical information from the province.

(*) Values correspond to preserving tomatoes, which represents the largest of the vegetable preserving in the province of Mendoza.

(**) Values correspond to industries preserving peaches, representing the largest of fruit preservation in the province of Mendoza.

with the industrial establishments, applied to provincial statistics such as volume of wine produced, areas of tomato and peach crops for industrial use and average yield of crops per hectare.

From an analysis of Table 6, it can be inferred that, for the food industry, the northern Mendoza basin demands 62% of the province's water demanded by this sector. It is worth mentioning that most of the urban/industrial area and most of the crop areas are located in this basin.

The ratio of volume returned/volume extracted resulted from the interviews and were grouped into three ranges. Table 7 shows the volume of water returned to the system to be within the range. Most of the water used by the wine, fruit and vegetable producers is returned to the system, while a significant amount of water used for beer and bottled mineral water production is retained in the process, that is, its use is consumptive.

The estimate of water demanded by food industries is quantitatively important information to determine the demand generated by industrial usage in Mendoza. The sectors in Mendoza that use water are primarily irrigation, domestic, industrial and environmental. Knowledge about the water demanded by each of these sectors provides information to attain a water balance, which is the difference between the water available and the sum of the demands by the sectors. In Mendoza, availability is determined by the basin's water inflows, which come primarily from snow in the high mountains and groundwater accumulated through natural recharge processes. The water balance at the basin or sub-basin levels is an indicator of the availability of water and, therefore, a tool for comprehensive management of the resource in the territory.

Llop and Fasciolo (2011), in their article about the state of water resources in Mendoza, determined a water demand of 5 626 hm^3/year by irrigation, the population and the environment. Without including reuse, the water availability was determined to be 5 282 hm^3/year; that is, an average deficit of 156 hm^3/year. These authors considered this deficit to be related to the pumping of water, which creates the problem of overexploitation of the aquifers.

Irrigated crops represent the largest demand (89%) in this province, as is the case for the entire arid region. According to the results presented in Table 7, the food industry establishments in Mendoza use

Table 7. Volumes of water used and ratio of volume returned/volume extracted, by industrial activity in Mendoza, Argentina, 2013, in cubic hectometers per year and percentage.

Activity	Volumes of water used (hm^3/year) (*)	Ratio of volume extracted (%)
Wine production and fraccionamiento	3.41	> 80%
Beer Production	0.66	40 a 80%
Bottling of mineral water	1.49	< 40%
Production of preserved vegetables (*)	3.31	> 80%
Production of preserved fruits (**)	4.64	> 80%
Total	13.51	

(*) Values calculated based on Table 6.

13.5 hm^3/year, which represents only 2.4% of the demand. Although this value is small in relative terms, it represents a significant volume. In the northern basin, the deficit is higher than the average (445 hm^3/year), and demand by these industries is 8.37 hm^3/year, as shown in Table 6. On the other hand, when analyzing Table 7, it can be interpreted that the highest volume demanded by this sector comes from industries with high extractive values and within ranges for the percentage ratio of volume returned/volume extracted, over 80%. This implies that the sustainability and efficiency policies for use of industrial wastewater for irrigation crops which are being applied in the province of Mendoza have a positive impact on the water balance by increasing the availability of water for irrigation.

To obtain a water balance that takes into account the total demand by the manufacturing industry, it would be important to estimate the water volumes used by other activities conducted by the industry, which has not yet been studied.

Conclusions

In Mendoza, wineries use between 1.5 and 20 liters of water per liter of wine produced. The lower limit of this range corresponds to larger establishments and those with more awareness about environmental sustainability. This range is consistent with that found in the local and international literature. For these establishments, the percentage ratio of volume returned to water extracted is over 80%, which indicates significant extractive use.

Beer producers use 3.8 to 4.5 liters of water per liter of beer produced. These values are at the lower limit of the range presented by international sources. This is also the case for sodas. The coefficients for use of water by this industry are between 1.5 and 2.0 liters of water per liter of soda produced. The percentage ratio of volume returned to extracted is average, with somewhat more than half of the demand used in the process and the rest returned to the system.

The coefficient obtained for bottling of mineral water is between 1.6 and 1.8 liters of water per liter of bottled water, which is also within the range of international sources. Consumptive use is significant in these establishments, where the percentage ratio of volume returned to extracted is under 40%.

The preserved fruit and vegetable industries use the most water per unit of production in relation to the other food industries analyzed in this work. The preserved vegetable production establishments interviewed used 19.8 to 29.7 liters of water per kilo of prime material processed, and between 29.7 and 32.7 liters of water per kilo of finished product. These

values are higher than the coefficients reported by the international literature. The coefficient for the preserved fruit establishment is less, with 18 liters of water per kilo of prime material processed, and is within the range cited by the international literature. For both types of establishments, the percentage ratio of volume returned to extracted is over 80%, which indicates significant extractive use.

The differences between the local coefficients obtained and those cited in local and international literature can be explained by a series of factors. These include awareness regarding environmental sustainability, belonging to multinational groups and lower water prices in Argentina.

The foods industry in Mendoza uses 13.51 hm^3/year. Most of this water is returned to the hydric system.

Received: 01/02/13
Accepted: 22/08/13

References

BEVERAGE INDUSTRY ENVIRONMENTAL ROUNDTABLE. *Water use benchmarking in the beverage industry. Trends and observations, 2010* [en línea]. St. Paul, Estados Unidos. Anteagroup, 2011 [citado el 20 de octubre de 2012]. Disponible para World Wide Web: http://bieroundtable.com/files/BIER%20Benchmarking%20Publication%202011.pdf.

DUEK, A.E. y FASCIOLO, G.E. Uso de agua en las bodegas de Mendoza. *Revista de la Facultad de Ciencias Agrarias, Universidad Nacional de Cuyo.* Tomo 44, núm. 2, año 2012, pp. 263-268.

LLOP, A. y FASCIOLO G.E. *Estado de los recursos hídricos en Mendoza.* Informe ambiental. Mendoza: Secretaría de Medio Ambiente, Gobierno de Mendoza (coord.), 2011, pp. 68-75.

NAZRALA, J., VILA, H., GARCÍA, R., JAIT, R., y DESPOUS, G. Gestión de efluentes y consumo de agua en bodega. *Revista de la Facultad de Ciencias Agrarias, Universidad Nacional de Cuyo.* Tomo 35, núm. 1, año 2003, pp. 35-42.

NORTH CAROLINA DEPARTMENT OF ENVIRONMENT AND NATURAL RESOURCES. *Water efficiency. Manual for Commercial, Industrial and Institutional Facilities* [en línea]. North Carolina, Estados Unidos. Land-of-sky Regional Council, 1998 [citado el 11 de octubre de 2012]. Disponible para World Wide Web: http://www.docstoc.com/docs/376400/Water-Efficiency-Guide-for-Business-Managers-and-Facility-Engineers.

ORGANIZACIÓN DE LAS NACIONES UNIDAS PARA LA EDUCACIÓN, LA CIENCIA Y LA CULTURA. *Agua e industria. El Agua, una responsabilidad compartida*. 2° Informe de las Naciones Unidas sobre el Desarrollo de los Recursos Hídricos en el Mundo [en línea]. Zaragoza, España. Sociedad Estatal Expoagua Zaragoza, 2006 [citado el 3 de octubre de 2012]. Disponible para World Wide Web: http://d7.rirh.org/documentos/insumos/informe_naciones_unidas2.pdf.

SMITH, M.H. *Water efficiency opportunities drink processing. Wine making best practice guide* [en línea]. Departament of Sustainability, Environment, Water, Population and Communities. Australian Government. The Australian National University, 2010 [citado el 17 de febrero de 2012]. Disponible para World Wide Web: http://www.environment.gov.au/water/publications/urban/weo-wineries-guide.html.

UNIVERSIDAD NACIONAL DE CUYO. *Marco Estratégico para la provincia de Mendoza: Diagnóstico físico-ambiental* [en línea]. Mendoza, Argentina. Universidad Nacional de Cuyo, 2004 [citado el 14 de marzo de 2012]. Disponible para World Wide Web: http://www.uncu.edu.ar/contenido/index.php?logout=true&tid=101.

VASSOLO, S. y DÖLL, P. Global-scale gridded estimates of thermoelectric power and manufacturing water use. *Water Resources Research*. Vol. 41, W04010, 2005, doi:10.1029/2004WR003360,

ZOIA, O., MANGHISI, S. y BERTRANOU, A. *Estimación de caudales y calidad de efluentes industriales. Elaboración de conservas de frutas y hortalizas: durazno, tomate, coctel de frutas y pimiento. Costos del control de la contaminación en áreas urbanas. Área de influencia del Canal Pescara, Maipú, Mendoza*. Mendoza, Argentina: Instituto Nacional de Ciencia y Técnica Hídricas, Centro de Economía, Legislación y Administración del Agua, 1983 (informe inédito).

Institutional Address of the Authors

Ing. Alicia Elena Duek

Consejo Nacional de Investigaciones Científicas y Técnicas
Centro de Economía, Legislación y Administración
del Agua
Instituto Nacional del Agua
Belgrano 210 Oeste
M55500FIF Mendoza, Argentina
Teléfono: +54 (261) 4285 282
danaduek@hotmail.com

Ing. Graciela Elena Fasciolo

Facultad de Ciencias Agrarias,
Universidad Nacional de Cuyo
Centro de Economía, Legislación y Administración
del Agua
Instituto Nacional del Agua
Belgrano 210 Oeste
M55500FIF Mendoza, ARGENTINA
Teléfono: +54 (261) 4285 282
gfasciolo@hotmail.com

Click here to write the autor

Characterization of Groundwater Flows According to Salinity

• Juan R. Fagundo-Castillo •
Universidad de La Habana, Cuba

• Margarita M. Alconada-Magliano* •
Universidad Nacional de La Plata, Argentina
*Corresponding Author

• J. Joel Carrillo-Rivera •
Universidad Nacional Autónoma de México

• Patricia González-Hernández •
Universidad de La Habana, Cuba

Abstract

FAGUNDO-CASTILLO, J.R., ALCONADA-MAGLIANO, M.M., CARRILLO-RIVERA, J.J. & GONZÁLEZ-HERNÁNDEZ, P. Characterization of Groundwater Flows According to Salinity. *Water Technology and Sciences* (in Spanish). Vol. V, No. 3, May-June, 2014, pp. 65-82.

The relationships among elements in the landscape can be explained using the theory of groundwater flow systems, which recognizes the different flows and their discharge and recharge zones, demonstrating their hydrological functioning. Characterizing the different flows is crucial to identifying their potential, salinity and possible use for different agricultural and forestry management practices. This definition implicitly includes characteristics related to quantity and depth of circulation. In environments where the water table is shallow, defining flow is key to selecting agricultural and forestry management practices that help in a given situation, such as water excess or deficit. The flows are defined according to the water quality and environmental indicators. The costs of the chemical analysis of water are high and it is difficult to analyze large areas. Nevertheless, electrical conductivity (*EC*) can be used to estimate the chemical composition of water in an area if the principles through which they acquire their composition are known and mathematical relationships with major ions are determined. The objective of the present study is to determine the feasibility of using the proposed hydrogeochemical models to calculate the chemical composition of water based on its electrical conductivity. Sources of water from wells, phreatimeters and lagoons in northwest Buenos Aires, Argentina were studied to identify the geology of the site and apply hydrogeochemical pattern recognition models to identify patterns (*HIDROGEOQUIM*, *GEOQUIM*, *SAMA*, *MODELAGUA*). The hydrogeochemical patterns and mathematical relationships between the ionic composition and *EC* were obtained. The best fit was obtained using the polynomial (parabola) equation that passes through the origin of the coordinates, having previously grouped the data using the pattern recognition model. It is concluded that the chemical composition of the water can be defined with mathematical calculations based on the value of electrical conductivity, which along with pH, temperature and other elements of the landscape enable defining types of flow and related soil management.

Keywords: Groundwater flows, electrical conductivity, water quality, recharge, discharge, soil management, landscape, shallow phreatic surface.

Resumen

FAGUNDO-CASTILLO, J.R., ALCONADA-MAGLIANO, M.M., CARRILLO-RIVERA, J.J. & GONZÁLEZ-HERNÁNDEZ, P. Caracterización de los flujos de agua subterránea a partir de su salinidad. Tecnología y Ciencias del Agua. *Vol. V, núm. 3, mayo-junio de 2014, pp. 65-82.*

*La vinculación entre elementos del paisaje puede ser explicada mediante la teoría de los sistemas de flujo de agua subterránea, que reconoce los diferentes flujos y sus zonas de descarga y recarga, que manifiestan en forma complementaria su funcionamiento hidrológico. Es esencial la caracterización de los diferentes flujos para conocer su potencialidad, salinidad y su posibilidad de uso en diferentes prácticas de manejo agropecuario y forestal; en esta definición quedan implícitas sus características de cantidad y profundidad de circulación. En ambientes donde la superficie de agua freática es poco profunda, definir los flujos constituye un procedimiento esencial al seleccionar las prácticas de manejo agropecuario y forestal que coadyuven en una situación dada, tales como excesos o déficit hídricos. Los flujos se definen a partir de la calidad del agua e indicadores ambientales. Los costos de los análisis químicos de agua son elevados y resultan difíciles de abordar en grandes áreas. Sin embargo, puede utilizarse la conductividad eléctrica (CE) para estimar la composición química del agua en un área si se conocen los principios mediante los cuales adquiere su composición y se establecen las relaciones matemáticas con los iones mayoritarios. El objetivo del presente estudio es establecer la factibilidad de utilizar los modelos hidrogeoquímicos propuestos para estimar la composición química del agua a partir de su conductividad eléctrica. Se estudió el origen del agua de pozos, freatímetros y lagunas del noroeste de la provincia de Buenos Aires, Argentina, conociendo el referente geológico del sitio, y aplicando modelos hidrogeoquímicos de reconocimiento de patrones (*HIDROGEOQUIM, GEOQUIM, SAMA, MODELAGUA*). Se obtuvieron los patrones hidrogeoquímicos y las relaciones matemáticas entre la composición iónica y CE. El mejor ajuste se obtuvo utilizando la ecuación polinomial (parábola), que pasa por el origen de coordenadas, habiendo agrupado previamente los datos mediante el modelo de reconocimiento de patrones. Se concluye que es posible definir la composición química del agua mediante estimaciones matemáticas a partir del valor de la conductividad eléctrica, la cual, junto al pH, temperatura y otros elementos del paisaje, permiten definir tipos de flujo y manejo del suelo asociado.*

***Palabras clave**: flujos de agua subterránea, conductividad eléctrica, calidad del agua, recarga, descarga, manejo de suelos, paisaje, superficie freática somera.*

Introduction and Background

The elements that make up the landscape are part of an integral system responsible for the functioning of a region. They are related in such a way that the actions of one affects the overall functioning. Although the need for comprehensive studies of ecosystems is well known, groundwater is often omitted from studies because its incidence is underestimated or it is considered that only specialists can study it. Nonetheless, both natural ecosystems and farming and forestry practices affect groundwater in many ways and also are affected by it. Thus the need for a broader group of professionals with knowledge about hydrogeological functioning, that understands the flow systems that affect a site and how their local and regional routes and physical and chemical characteristics are related to management practices. This is particularly important in regions where the water table is not very deep (1.0 to 3.5 m) and is subject to changes due to the climate as well as farming and forestry practices such as those occurring in the study region, the Northwestern (NW) portion of the province of Buenos Aires, Argentina. This area is characterized by the occurrence of cyclical floods and droughts recorded from 1576 to the present (Moncaut, 2003).

In general, groundwater in this region is unconfined. The flows circulate through a granular medium with a thicknesses that can exceed 5 000 m, which composes the plains that extend from the Andes mountains to Tandil, near the Atlantic coast (Figure 1). The direction of the movement of the groundwater across the horizontal plains is generally towards the study region, from the northwest, given the groundwater hydraulic communications with the outlet on the eastern boundary with the Atlantic Ocean. No supply is observed after the southern boundary (Tandil mountain range) (Guillermo-Hernández in Alconada, 2008). The presence of each vertical flow component depends on its recharge (downward flow) or discharge (upward flow) characteristics. The international literature indicates that it is useful to define farming and forestry practices that can help with excess or deficit water conditions and the control of salinity by applying bio-drainage, in which vegetation affects the water table through evapotranspiration (Heuperman *et al*., 2002; Tomar, 2007). This is recommendable if information is known about how the water flows affecting a site function, the type of flows (local, intermediate or regional) and the type of zones in which they are located (recharge, transit or discharge), as explained by Toth (2000). The zones through which a flow runs are also complemented by their hydrogeological functioning, depending on whether they are recharge, transit or discharge zones, as well as management practices (Tóth, 2000). The functioning of groundwater and its interaction with surface water can be estimated based on the chemical characteristics of the water (cations, anions, pH, salinity, CO_2 and temperature) and relationships with the geology, geomorphology, soils and vegetation in the study region (Tóth, 2000; Carrillo-Rivera, 2000).

In the present study region and based on the concept of bio-drainage (Heuperman et al., 2002; Tomar, 2007) mentioned previously, Alconada et al.(2009) proposed addressing situations of extreme droughts and floods by planting tree species, primarily silvopastoral, and herbaceous species that contribute to reducing the water table to a depth compatible with the growth of vegetation and/or decreasing overall excess water in an area. This uses knowledge of the hydrogeological behavior as a factor which integrates all the elements in the landscape, as explained by Toth's groundwater flow systems theory (2000).

While information about the geology, soil and vegetation of an area is often available, at least on small scales, there are few studies about the overall characterization of water. The studies that are conducted tend to focus

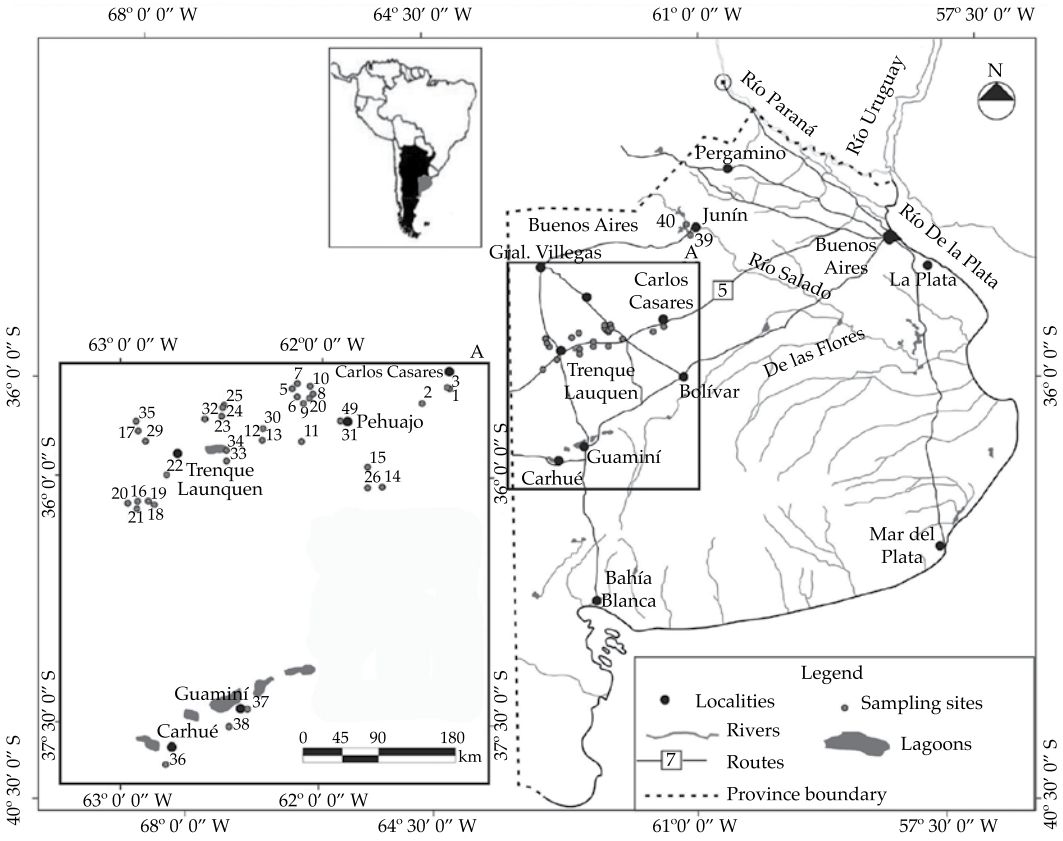

Figure 1. Location of the study area and groundwater sampling sites.

on identifying its potential use for human consumption or farming. This may occur for different reasons. For example, the usefulness of studying groundwater for the purposes of farming-forestry management may not be recognized. Or when it is recognized, the technical and economic infeasability is often raised of conducting a study needing a large number of water analyses to characterize the areas involved in the overall dynamic responses, which require recording changes in water excess, droughts and associated soil degradation processes. The physio-chemical procedures to analyze the water end up being relatively expensive and usually take a long time. Therefore, simple and low-cost methods are needed that can contribute to decision-making about management of the landscape.

Fagundo (1985, 1990), and Fagundo and Rodríguez (1991, 1992) studied the water-rock (limestone and dolostone) interaction processes in the laboratory and the field (open and closed systems) in order to simulate natural processes for acquiring the chemical composition of water circulating through carbonated areas. In Cuba, these authors found that the concentration of ions related to a system in equilibrium, CO_2-H_2O-$CaCO_3$, as well as the pH, electrical conductivity (*EC*), concentrations of HCO_3^-, Ca^{2+}, Mg^{2+}; $CaCO_3$ and total dissolved solids (*TDS*) increase according to a first-order kinetics exponential function (equation 1)

until reaching chemical equilibrium. The *EC* will at all times depend on the concentration of the ions HCO_{3^-}, Ca^{2+} and Mg^{2+} dissolved in the kinetic process and, to a lesser degree, on the ions acquired from the atmosphere (Fagundo *et al*., 1992, 2004). The speed at which a mineral dissolves depends on its composition in the rock as well as the temperature and CO_2 contents of the circulating water:

$$C_t = C_{eq}\left(1 - e^{kt^n}\right) \text{ (open and close systems with respect to } CO_2) \quad (1)$$

Where C_t is the ionic concentration (HCO_{3^-}, Ca^{2+}, Mg^{2+}) for time *t*; and C_{eq} is the ionic concentration in chemical equilibrium; *k* is the kinetic constant (speed) and *n* is the experimental coefficient which takes values between 0 and 1. Since the magnitudes of *k* for the same value of *t* are of the same order for all ions and the *EC*, the correlations between C_t and *EC* are linear.

Miller *et al*. (1988) found that the theoretical electrical conductivity EC_t (equation (2)) is approximately equal to the sum of the product of the concentration of each dissolved ion (C_i) in the system, multiplied by the specific equivalent conductivity of each ion at infinite dilution (S_i) and by the fraction of free ions that contribute to the electrical conductivity (α), which in turn depends on the empirical exponent *f* which varies according to the ionic concentration and type of water:

$$EC_t = \sum_{i=1}^{n}\left(\alpha_i C_i S_i\right)^f \quad (2)$$

Based on these studies and field information from different regions in Cuba, Fagundo *et al*. (1992, 2005, 2006) and Álvarez *et al*. (1993) developed hydrogeochemical models that define correlations between measured and calculated hydrochemical variables, as well as mathematical relations between these variables and electrical conductivity.

Nevertheless, the relations mentioned must be established for each study area and, therefore, it is necessary to know the processes through which the water acquires its chemical composition, since the type of mathematical correlation model to be used depends on that.

The physio-chemical characteristics of water results from a complex interaction process between the water and the geological units of the medium through which it circulates (most importantly: acquisition and escape of gases, dissolution-precipitation of minerals, hydrolysis, oxidation-reduction, ionic exchange, the common ion effect, salinity effect, mixing effect). Although other factors are involved —including the geomorphology, edaphology, climate and microbiology of a site— their effects are constant and, thus, knowing the mineral composition of the geological stratum through which the water circulates and the physio-chemical characterization of that water is sufficient to establish the relationships mentioned (Fagundo, 1990).

The objective of the present study is to establish the feasibility of using the proposed hydrogeochemical models to calculate the chemical composition of water based on its electrical conductivity, in order to obtain a low-cost method to monitor water quality and indicate the usefulness of the relationship between water quality and other elements in the landscape to define interventions that are more appropriate to the dominant environmental components.

Characterization of the Study Area and Sampling

The study area is called the Northwestern Bonaerense or Pampa Arenosa (PA), which covers some 5 500 000 ha, and includes the Medanos Longitudinales area of the Argen-

tine Pampeana Plains. The study area primarily covers the administrative political districts of Pehuajo and Trenque Lauquen, in Buenos Aries province, and to a lesser extent, neighboring districts that are hydrogeologically connected (Carlos Casares, Nueve de Julio, Guaminí, Carhué and Junín) (Figure 1).

The PA is characterized by a geomorphology dominated by longitudinal and parabolic sand dunes with lagoons between them. The area is approximately 20 000 ha, and the characteristics and distribution are related to the climate, topography, lithology and geological structure (Dangavs, 2005). The water table is between 1.1 and 3.5 m deep and is subject to alternating droughts and floods characteristic of the region, which determine the flood area and sizes of the lagoons. The region is under 100 masl, with the Salado River on the N-NE boundary (which was connected to it by artificial canals (PMI, 1999)), and the hydrological system of Las Encadenadas lagoons on the southern boundary (Figure 1). Geologically, it is characterized by a Precambrian crystalline rock base with outcroppings in the higher portions of the southern area of the study zone (Tandilia and Ventania systems with elevations between 500 and 1 100 masl), which become progressively buried towards the north by younger sediments between 2 and 6 km thick (Etchichury *et al*., 1988; PMI, 1999; Zárate and Rabanesse, 2005).

Water samples were taken from phreatimeters and wells between 20 and 40 m deep as well as lagoons. Local and intermediate groundwater flow recharge, transit and discharge zones were included, as defined by Alconada (2008), according to criteria by Toth (2000).

Materials and Methods

Physio-Chemical Field Measurements

Field measurements were taken for pH, temperature (HANNA pH meter model HI-8424), electrical conductivity (*EC*) (ORISON model 524 conductivity meter) and total alkalinity (HCO_{3^-} and CO_3^{2-}). The major ions (HCO_{3^-}, Cl^-, SO_4^{2-}, Ca^{2+}, Mg^{2+}, Na^+, K^+; $CaCO_3$) were analyzed with an ICP-MS (inductively coupled plasma - mass spectrometry) (APHA, AWWA, WEF, 1989, in Alconada, 2008).

Hydro-geochemical Modeling and Information Processing

The *MODELAGUA* (Fagundo-Sierra *et al*., 2001) informatics system, which is based on hydrogeochemical pattern recognition models, balance of masses and water mixing, was used to explain the geochemical processes affecting the chemical composition of the water. This was determined according to the lithology presented in Table 1 (adapated from PMI, 1999 and González, 2005). The minerals considered to be primarily responsible for the composition of the water were halite (sodium chloride), gypsum, calcite, quartz, plagioclase (albite y anorthite), feldspars-K, biotite and clay. The geochemical processes that cause the weathering of these materials are managed by the algorithm in the *MODELAGUA* system. The number of data assigned in the tables resulted from grouping the samplings by hydrogeochemical pattern, according the most number of data, thereby joining samples having common characteristics and, thus, enabling a better fit to the equations than directly using all of the data together.

The hydrochemical variables were processed using informatics systems that complemented each other: *HIDROGEOQUIM*, *GEOQUIM* and *SAMA*. These models perform calculations, relations between variables, validate data, define hydrogeochemical patterns, classify water and calculate ionic coefficients (slope of equations (3), (4) and (5)) which indicate the

Table 1. Mineral Composition in the pA (adapted from PMI, 1999 and Gonzalez, 2005).

Formation	Age	Lithology (salinity of water)	Reported or inferred minerology
Medano Invasor	Holocene	Fine to silty sand, clayey silt with volcanic ash (TDS 500 - 2 000 mg/l)	Quartz, plagioclase, K-feldspar, calcite, clay, mineral with magnesium (augite, hypersthene, and hornblende), halite
Pampeano	Pleistocene	Sandy silt, clayey and calcareous silt, gypsum clay, loess (TDS 1 000 - 30 000 mg/l)	Quartz, plagioclase, K-feldspar, calcite, clay, mineral with magnesium (augite, hypersthene, and hornblende), halite
Araucano	Plio-Pleistocene	Clayey sandstones, calcareous cement and a large amount of gypsum (TDS > 5 000 mg/l)	Gypsum, quartz, plagioclase, K-feldspar, calcite, clay mineral (kaolinite), halite
Arenas Puelches	Plio-Pleistocene	Fine to medium sand in clay matrix with some mica (TDS, 2 000 - 10 000 mg/l)	Quartz, plagioclase, K-feldspar, muscovite, halite, gypsum
Paraná (Superior e Inferior)	Higher Miocene	Green to blue clay, sand with calcareous (STD 2 000 - 10 000 a > 100 000 mg/l)	Quartz, plagioclase, K-feldspar, calcite, clay mineral (kaolinite), halite
Olivos	Lower Miocene	Sandstone, red clay, gypsum and anhydrite (STD, 6 000 - 60 000 mg/l)	Halite, plagioclase, feldspar, chalcedony, gypsum, anhydrite, clay mineral (kaolinite)
Las Chilcas	Paleoceno	Marine siltstone and clay (High TDS)	Limonite, clay mineral (kaolinite), quartz, hatite, gypsum
G. Belgrano	Cretaceous	Consolidated sandstone and sandy limonite, and clay, calcareous and gypsum sandstone (TDS > 50 000 mg/l)	Quartz, limonite, clay mineral (kaolinite), plagioclase, K-feldspar, calcite, halite, gypsum
Hydrogeological Basement	Paleozoic	Quartzite and limestone	Quartz, calcite
	Precambrian	Granite y gneiss (very high TDS)	Quartz, halite, gypsum

ionic concentration of each of the variables based on the EC.

Using the *HIDROGEOQUIM* system (Fagundo *et al.*, 2005), the calculations required to validate the quality of the data were performed, and classify the water according to hydrogeochemical patterns and water type, based on the Kurlov method (Fagundo, 1998). The hydrogeochemical patterns consist of stoichiometric relations of the type $Na^{+}+K^{+}$: Ca^{+2}: Mg^{+2} and Cl^{-}: HCO_3^{-}: SO_4^{-2}, taking whole numbers between 0 and 8 which result in a numerical combination of anions and cations. Therefore, for example, the pattern 361-316 represents the approximate composition 30% $Na^{+}+K^{+}$, 60% Ca^{+2}, 10% Mg^{+2}, 30% Cl^{-}, 10% HCO_3^{-} and 60% SO_4^{-2}, a pattern corresponding to sodium-calcium-chloride-sodium water. Only ions with more than 20% meq.l^{-1} are considered in the denomination (Fagundo, 1998).

The graphic representations were created using a Piper-Hill diagram (Appelo y Postma, 1993), by grouping the waters into fundamental types, and with Stiff diagrams (1951) in order to determine similarities and differences among water groups, according to hydrogeochemical patterns.

Correlation matrices were generated for the hydrochemical variables using the *GEOQUIM* (Álvarez *et al.*, 1993) system, and the correlation equations were calculated using the straight line model with non-zero intercept:

$$Ci = a_0 + a_1 ... EC \qquad (3)$$

Equations for the mathematical dependence between ionic concentration and electrical conductivity were determined with the *SAMA* system (Álvarez *et al*., 1990, 1993) according to a first-order (straight line equation (4)) and a second-order (parabola equation (5)) polynomial regression model passing through the coordinate origin, and as indicated in *GEOQUIM* (equation (3)):

$$Ci = a_1.EC \quad (4)$$

$$Ci = a_1.(EC) + a_2.(EC)^2 \quad (5)$$

Where *Ci* is the concentration of ions *I*; a_0, a_1 and a_{22} are coefficients of the polynomial equations and *EC* is the electrical conductivity value of the sample.

The equation that best estimates the theoretical ionic concentration of each hydrochemical variable based on the *EC* was selected based on the similitude index (*SI*), which compares the hydrogeochemical patterns and determines the similitude between real data and those estimated by the modeling, using the expressions:

$$SI = \sum_{i=1}^{n}(R_1 R_2) \quad (6), \text{ where:}$$

$$R_1 = \frac{C_{ir}}{C_{im}} \quad (7)$$

$$R_2 = \frac{C_{ir}}{\sum_{i-1}^{n} C_{ir}} \quad (8)$$

Where *SI* is the similitude index, C_{ir} is the real ionic concentration and C_{im} is the ionic concentration obtained by modeling.

In classical statistics, the correlation coefficient (*r*) or the coefficient of determination (r^r) is the most commonly used. Nevertheless, these statistics provide good results when sufficient data are available and when they have a certain degree of linearity. The *SI* provides better results when less data are available or the points are concentrated.

Statistical Processing

The functional relations between hydrochemical variables and their relevance with water-rock interaction were selected based on regression analysis and linear correlation. The mathematical correlations between the *TDS* and *EC* values with ions Cl^-, SO_4^{2-}, Na^+ and K^+ enabled confirming what the *MODELAGUA* obtained for the geochemical processes that explain the source of the chemical composition of the water.

The significance of the correlation between hydrochemical variables was analyzed with the student-*t* for a probability level *p* of 0.005 and 0.05.

Data management and obtainment of water quality

The steps to define water quality are summarized below. Based on this and other variables related to the landscape, the hydrological functioning and management consistent with it are defined as follows.

1. The geochemical processes resulting in the chemical composition of water are determined using the *MODELAGUA* based on the geology representative of the site and by sampling water from sources representative of the area.
2. Ionic coefficients are calculated (slopes of the equations from the *HIDROGEOQUIM*, *GEOQUIM* and *SAMA* models) which indicate the ionic concentration of each of the variables based on the *EC*. The equation is selected which presents the best similitude index

(fit between real and estimated data) for the conditions at the site.

3. Field measurements are taken for *EC*, pH and temperature, as well as redox potential (Eh), dissolved oxygen and alkalinity.
4. Elements of the landscape at the site are recorded: vegetation patterns, type and degradation of soil, topographic position, geomorphology and general topography.
5. The hierarchy of water flow and the zones (recharge, transit or discharge) through which they run are defined by comparing physio-chemical variables in the area, type of soil, and topographic position, primarily in local studies; as well as the geomorphology and general topography in regional studies.
6. A technical-productive and socioeconomic analysis of feasible management practices is performed. In this regard, Alconada (2008) and Alconada *et al*. (2009) performed an exhaustive analysis in the study region and presented recommendations.

Note that in the definition of recharge and discharge components in flow systems with different hierarchies, piezometric measurements at different depths are needed to evaluate the components of the vertical water movement (recharge and discharge). Since this information was lacking, the present work only determined the different hierarchy of flows identified by the physio-chemical qualities of the water and temperature. The recharge and discharge conditions are identified by the depth of the water table (shallow for discharge, deep for recharge), and alkaline pH conditions represent discharge and acidic recharge.

Results and Discussion

Using the *MODELAGUA*, the prevalence of calcite precipitation and cationic exchange between Ca and Na (Ca increases at the expense of Na) were determined in water-rock interaction processes affecting the chemical composition of surface and groundwater in the study region. To a lesser degree, processes involving the dissolution of halite, gypsum, biotite, albite, anorthite and feldspars-K were found. The concentration for which precipitation of calcite occurs varies, with high *TDS* values in the range of 1 300 to 1 500 $mg.l^{-1}$. Cationic exchange occurs with high concentrations in the range of 500 to 12 000 $mg.l^{-1}$, depending on the site. In the case of the lagoons a high precipitation was found of halite, calcite, quartz, clay and occasionally dolomite. The detailed analysis obtained by *MODELAGUA* can be found in Alconada (2008) and Alconada *et al.* (2011).

Table 2 presents the main physio-chemical properties of the water studied from the province of Buenos Aires and indicates the flow hierarchy and discharge, transit and recharge zones through which these flows run, according to Toth's flow systems theory (2002) (Alconada, 2008). It is important to mention that this table is the result of integrating patterns and hydrogeochemical facies and incorporates the water's physical variables, such as pH and temperature, as well as chemical variables. In effect, Toth (2002) indicates that the relationship among anions relates to the residence time of the water and, consequently, can be considered representative of the type of flow. Recharge, transit and discharge zones were identified using additional criteria related to geomorphology and position of the water table, determining the type of flow identified.

Figure 2 presents the distribution of the hydrochemical data in the Piper-Hill diagram (Appelo y Postma, 1993), which suggests that the water samples belong to various groups according to a trend towards increased Cl^- and Na^+ contents. Based on the hydrogeochemical pattern and water type,

Table 2. Physio-chemical properties of water from phreatimeters (P), wells (W) and lagoons (L). Composition of ions in me.l^{-1}; $CaCO_3$ and TDS in mg l^{-1}, pH; T C; *EC* in µS/m; groups (G); Flow (F); intermediate (I) and local (L); zones: recharge (R), transit (T), discharge (D).

No.	M	pH	T	CE	TDS	HCO_3^-	Cl^-	SO_4^{2-}	Na^+	K^+	Mg^{2+}	Ca^{2+}	$CaCO_3$	G	F	Z
1	W	8.18	17.2	1 060	895	8.98	1.37	0.67	9.74	0.35	0.99	0.80	90	2	L	R
2	W	7.04	16.4	1 884	1 571	14.11	3.66	2.60	14.57	0.99	2.81	2.42	261	2	L	D
3	W	7.01	16.3	3 500	2 303	8.98	21.52	5.50	31.00	1.51	11.17	7.55	936	3	L	D
4	W	6.98	18.3	18 300	10 528	8.12	124.39	37.80	145.00	5.08	10.13	7.70	892	4	I	D
5	W	7.03	19.1	5 150	3 100	8.98	28.21	9.67	43.0	1.04	3.15	1.05	210	4	I	T
6	P	7.65	27.0	4 750	3 210	14.11	29.31	5.52	39.10	0.99	6.28	1.60	394	3	I	T
7	P	7.36	27.0	1 510	1 024	2.14	12.45	1.67	14.37	0.49	0.73	0.70	72	4	I	T
8	P	7.21	19.0	3 000	1 892	2.99	23.66	4.00	25.00	1.24	2.00	1.60	180	4	I	D
9	P	7.25	19.5	845	576	2.14	4.62	1.56	6.65	0.90	0.25	0.81	53	3	L	T
10	P	6.98	17.7	182	141	1.34	0.32	0.14	0.74	0.20	0.24	0.59	42	1	L	R
11	P	6.92	16.8	8 010	5 124	7.27	70.08	6.00	73.91	1.51	5.00	5.50	525	4	I	T
12	W	7.92	23.50	9 350	6 279	22.66	64.23	10.52	85.22	1.23	5.55	2.00	378	3	I	T
13	W	8.29	21.70	3 420	2 539	14.11	15.04	6.04	30.80	0.69	4.09	1.20	265	3	I	T
14	W	7.70	18.50	3 660	2 958	20.95	11.69	7.23	35.43	0.67	4.82	1.00	291	2	L	D
15	W	8.11	22.30	3 200	2 772	21.80	8.25	6.02	33.70	1.19	2.31	0.54	142	2	I	D
16	P	6.69	18.10	6 510	3 971	12.40	38.31	10.85	50.85	1.36	5.54	2.33	394	3	I	D
17	P	7.44	17.80	500	402	4.20	0.78	0.18	1.79	0.32	1.36	1.70	135	2	L	R
18	W	8.12	18.20	3 010	1 928	4.70	16.99	7.23	25.78	0.36	3.55	2.05	280	4	I	T
19	W	7.60	18.60	646	530	5.56	0.70	0.44	3.49	0.18	1.72	1.86	179	2	L	R
20	W	7.60	18.20	4 860	3 897	26.08	18.08	8.04	51.74	0.58	3.76	1.05	240	2	I	T
21	W	8.04	18.10	1 015	684	3.75	5.25	0.92	8.90	0.20	0.50	0.30	40	3	L	T
22	W	7.23	19.10	38 680	22 798	9.83	295.77	76.96	292.61	3.87	64.00	18.50	4 125	4	I	D
23	W	7.58	19.10	11 850	7 514	5.56	90.99	27.92	90.00	1.79	23.30	9.50	1 640	4	I	T
24	W	7.63	18.60	2 100	1 417	3.85	12.37	5.46	16.52	0.44	3.89	1.90	289	4	L	T
25	P	7.90	18.60	868	705	6.71	1.95	0.85	3.96	0.71	1.85	2.76	232	2	L	R
26	W	8.25	17.80	4 180	2 717	10.69	23.13	6.94	35.84	1.17	2.20	0.76	148	3	L	D
27	L	9.02	25.20	4 190	2 663	2.99	28.73	10.94	35.17	0.89	4.18	2.10	314	4	I	D
28	L	9.87	21.00	10 420	7 296	8.12	74.65	34.79	97.83	2.02	10.08	1.55	582	4	I	D
29	L	6.69	17.80	8 950	5 077	1.28	63.10	19.29	67.80	1.49	11.08	4.30	769	4	I	D
30	L	9.02	20.00	36 400	22 240	4.70	329.01	36.25	330.12	6.59	39.17	11.50	2 534	4	I	D
31	L	7.31	21.00	8 610	5 478	5.56	60.56	22.29	73.48	1.44	11.08	2.00	654	4	I	D
32	L	6.83	18.60	19 800	14 133	2.14	165.92	63.75	185.22	1.64	29.08	19.00	2 404	4	I	D
33	L	8.31	23.00	22 900	16 531	9.83	190.42	65.00	237.83	4.72	27.25	3.50	1 538	4	I	D
34	L	8.25	23.00	18 100	12 653	6.41	138.59	61.25	170.00	3.49	20.25	5.65	1 295	4	I	D
35	L	7.60	25.50	10 410	7 593	8.12	55.49	51.04	103.04	2.01	12.92	3.70	831	4	I	D
36	L	9.53	21.40	75 600	63 322	22.66	692.96	293.75	1 000.02	8.72	9.92	0.75	533	4	I	D
37	L	9.02	21.40	9 370	6 884	20.09	57.46	26.04	95.10	2.06	7.63	0.60	412	4	I	D
38	L	9.07	23.00	18 510	11 840	20.95	127.32	35.83	182.57	3.46	4.68	0.90	279	4	I	D
39	L	9.20	17.20	9 370	6 333	12.40	49.01	31.88	90.22	4.26	4.53	0.66	260	4	I	D
40	L	8.09	17.20	5 240	3 512	9.83	26.70	14.75	48.26	2.31	3.25	0.87	206	4	I	D

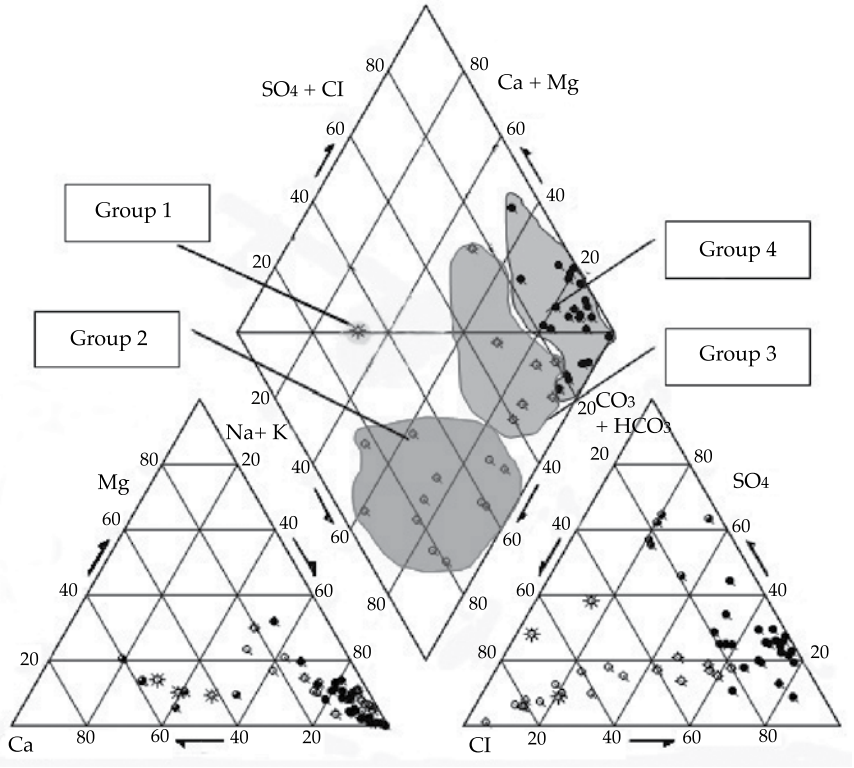

Figure 2. Distribution of hydrochemical data in the Piper-Hill diagram (Appelo and Postma, 1993).

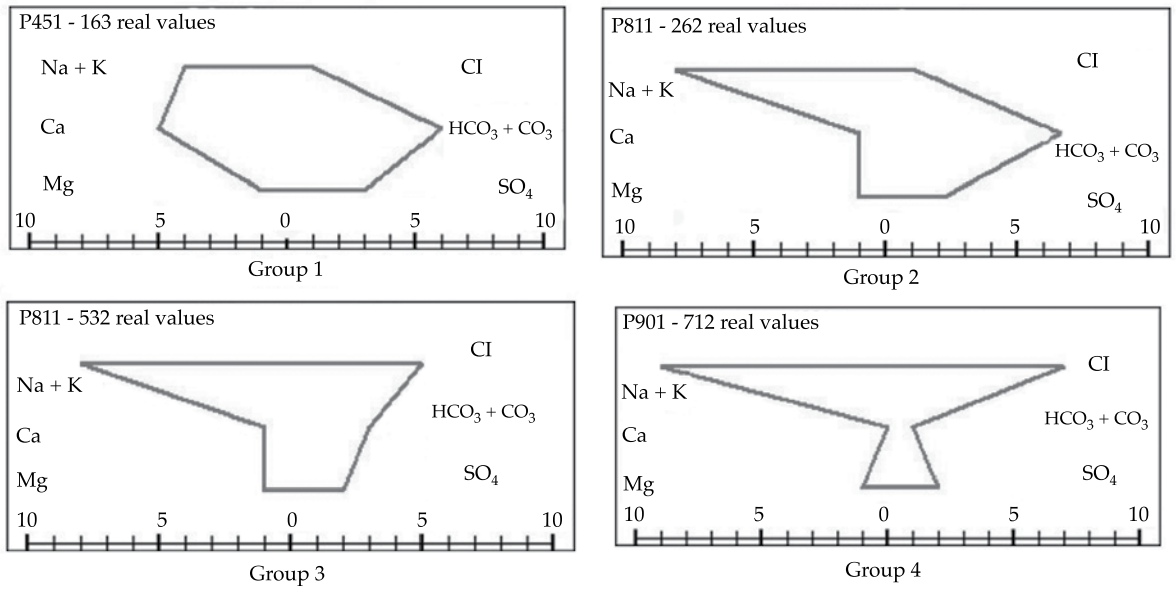

Figure 3. Average hydrogeochemical patterns for the water studied (Na^{+}+K^{+}: Ca^{+2}: Mg^{+2} - Cl^{-}: HCO_3^{-}: SO_4^{-2}).

according to the Kurlov criterion (Fagundo *et al*., 1996) obtained by the *HIDROGEOQUIM* model (Fagundo *et al*., 2005), four main water groups were determined. Figure 3 shows the Stiff diagrams (1951) for the average hydrogeochemical patterns. The representations of the individual samples are presented in Alconada (2008).

The chemical characteristics based on the Piper and Stiff diagrams and TSD values and hydrogeochemical patterns (HP) are summarized below, by water group:

- Group 1 (one sampling in a phreatimeter in Pehuajo) is sodium-calcium, chloride-bicarbonate (HCO_3 > Cl-Ca > Na); *TDS* of 141 mg.l^{-1}; *EC* of 182 µS.m^{-1}, and the hydrogeochemical pattern is 451-163.
- Group 2 (eight samples: 6 wells, 2 phreatimeters) is bicarbonate and sodium-chloride bicarbonate (HCO_3-Na y HCO_3 > Cl-Na, respectively); *TDS* between 530 and 3 897 mg.l^{-1}; *EC* between 500 and 4 860 µS.m^{-1}, and the hydrogeochemical pattern is 811-361.
- Group 3 (eight samples: 5 wells, 3 phreatimeters) is chloride -bicarbonate, primarily with sodium (Cl > HCO_3-Na); *TDS* between 531 and 4 201 mg.l^{-1}; *EC* between 268 and 6 510 µS.m^{-1}, and the hydrogeochemical pattern is 811-631.
- Group 4 (twenty-three samples: 5 wells, 3 phreatimeters, 15 lagoons) is chloride and sodium-sulfate and chloride (Cl > SO_4-Na); *TDS* between 930 and 67 356 µS.m^{-1}; *EC* between 1 510 and 75 600 µS.m^{-1}, and the hydrogeochemical pattern is 811-712.

All four groups of water were identified from the wells and phreatimeters, corresponding to different flows and zones, while all the lagoons belonged to group 4, with a predominance of Cl^- and Na^+, with groundwater discharge zones with intermediate flows (Table 2).

One result of the classification conducted by water groups suggests that two or more samples may be from different sources (*i.e.* well or phreatimeter) while belonging to the same flow, and are therefore the same potential supply source for farming or forestry management. In some cases, this classification will enable determining hydrogeological risk, by proposing a management practice in a zone that has been hydrogeologically connected with another. Being of the same type does not indicate that the water extracted is necessarily from the same source.

Calculation of the chemical composition of the water based on electrical conductivity

As mentioned in the introduction, while natural water acquires its chemical composition from a complex process involving different factors, in an area with a certain degree of homogeneity many of these factors are constant, and the relative chemical composition would vary within a determined water type and hydrogeochemical pattern. It would be altered only by precipitation, since mineralization in surface water during rainy periods is less than during dry periods.

Phreatimeters

After processing all the data corresponding to the phreatimeters sampled, applying the three mathematical correlation models calculated with *SAMA* and *GEOQUIM* (straight line with non-zero intercept(equation (3)), with a straight line through the origin of coordinates (equation (4)), parabola through the origin of coordinates (equation (5)), the resulting equations present very low mean SI for real and estimated data, which have less than 60% similitude. Better results can be obtained if the data area is processed after being grouped by water type, even if the amount of data is very small.

Table 3 presents the equations using the data from the samples from the

Table 3. Phreatimeters in Buenos Aires. Ionic concentration (*Ci*) adjusted by straight line equations with non-zero intercept (equation 3), straight line through origin pf corrdinates (equation 4) and parabola through origin of coordinates (equation 5), similitude index (*SI*).

Water groups 1 and 2 (*N* = 3)			
Ci	$Ci = a_1 (EC)$ (4)*	$Ci = a_0 + a_1 (EC)$ (3)**	$Ci = a_1 (EC) + A2 (EC)2$ (5)*
HCO_{3^-}	$y = 0.00791x$	$y = 0.1029 + 0.0078x$	$y = 0.0088502x - 1.2421 * 10 - 6x2$
Cl^-	$y = 0.00183x$	$y = -0.0727 + 0.0019x$	$y = 0.0013921x + 5.7231 * 10 - 7x2$
SO_4^{2-}	$y = 0.00082x$	$y = -0.1446 + 0.0010x$	$y = -0.0000570x + 1.1654 * 10 - 6x2$
Ca^{2+}	$y = 0.00326x$	$y = 0.0926 - 0.0031x$	$y = 0.003755x - 6.4986 * 10 - 7x2$
Mg^{2+}	$y = 0.00205x$	$y = -0.1899 + 0.0023x$	$y = 0.0014480x + 7.9794 * 10 - 7x2$
$Na^+ + K^+$	$y = 0.00492x$	$y = -0.0300 + 0.0053$	$y = 0.004919x + 5.0777 * 10 - 7x2$
SI	0.948	0.933	0.941
Water group 3 (*N* = 3)			
Ci	$Ci = a1 (EC)$	$Ci = a_0 + a_1 (EC)$	$Ci = a_1 (EC) + A2 (EC)2$
HCO_{3^-}	$y = 0.002278x$	$y = 1.4017 + 0.0020x$	$y = 0.004988x - 4.4838 * 10 - 7x2$
Cl^-	$y = 0.005978x$	$y = -1.1680 + 0.0060x$	$y = 0.06489x - 8.7366 * 10 - 8x2$
SO_4^{2-}	$y = 0.001495x$	$y = -0.2210 + 0.0015x$	$y = 0.000411x + 1.8554 * 10 - 7x2$
Ca^{2+}	$y = 0.000357x$	$y = 0.5416 + 0.0003x$	$y = 0.000506x - 2.5517 - 8x2$
Mg^{2+}	$y = 0.001007x$	$y = -0.1536 + 0.0010x$	$y = 0.001892x - 1.5151 * 10 - 7x2$
$Na^+ + + K^+$	$y = 0.008174x$	$y = 1.1723 + 0.0080x$	$y = 0.009426x - 2.1415 * 10 - 7x2$
SI	0.909	0.900	0.909
Water group 4 (*N* = 3)			
Ci	$Ci = a1 (EC)$	$Ci = a_0 + a_1 (EC)$	$Ci = a_1 (CE) + A2 (EC)2$
HCO_{3^-}	$y = 0.000934x$	$y = 0.8118 + 0.0008x$	$y = 0.001197x - 3.6441 * 10 - 8x2$
Cl^-	$y = 0.008631x$	$y = -2.9550 + 0.0096x$	$y = 0.007599x + 1.4301 * 10 - 7x2$
SO_4^{2-}	$y = 0.000830x$	$y = 2.3489 + 0.0007x$	$y = 0.001534x - 9.7619 * 10 - 8x2$
Ca^{2+}	$y = 0.000662x$	$y = -4.3398 + 0.0026x$	$y = 0.00043x + 3.1745 * 10 - 8x2$
Mg^{2+}	$y = 0.000625x$	$y = -5.3495 + 0.0031x$	$y = 0.00019x + 8.0430 * 10 - 10x2$
$Na^+ + K^+$	$y = 0.009252x$	$y = 12.0331 + 0.0042x$	$y = 0.00888x + 5.1209 * 10 - 8x2$
SI	0.934	0.812	0.871

**SAMA*, ***GEOQUIM*. *EC*: Electrical Conductivity uS/m.

phreatimeters in Buenos Aires, for each water group, based on three mathematical correlation models calculated using *SAMA* and *GEOQUIM*. This type of processing resulted in a mean similitude between 70 and 90%. As an example, Figure 4 shows the real and estimated patterns for two samples from groups 1 and 2 from the phreatimeters. A high similitude index (*SI*) can be seen among the individual samples as well as the index resulting from all the samples (0.89). This high relationship can also be seen in Figure 5, with a correlation between real and estimated values of close to 1.

Wells

By applying the three mathematical methods indicated to equations (3), (4) and (5), with all of the hydrochemical data, similitude indices from 80 to 94% were obtained for real and estimated data, respectively. As is the case for water from the phreatimeters, the *SI* is better when fitted by water group (table 2),

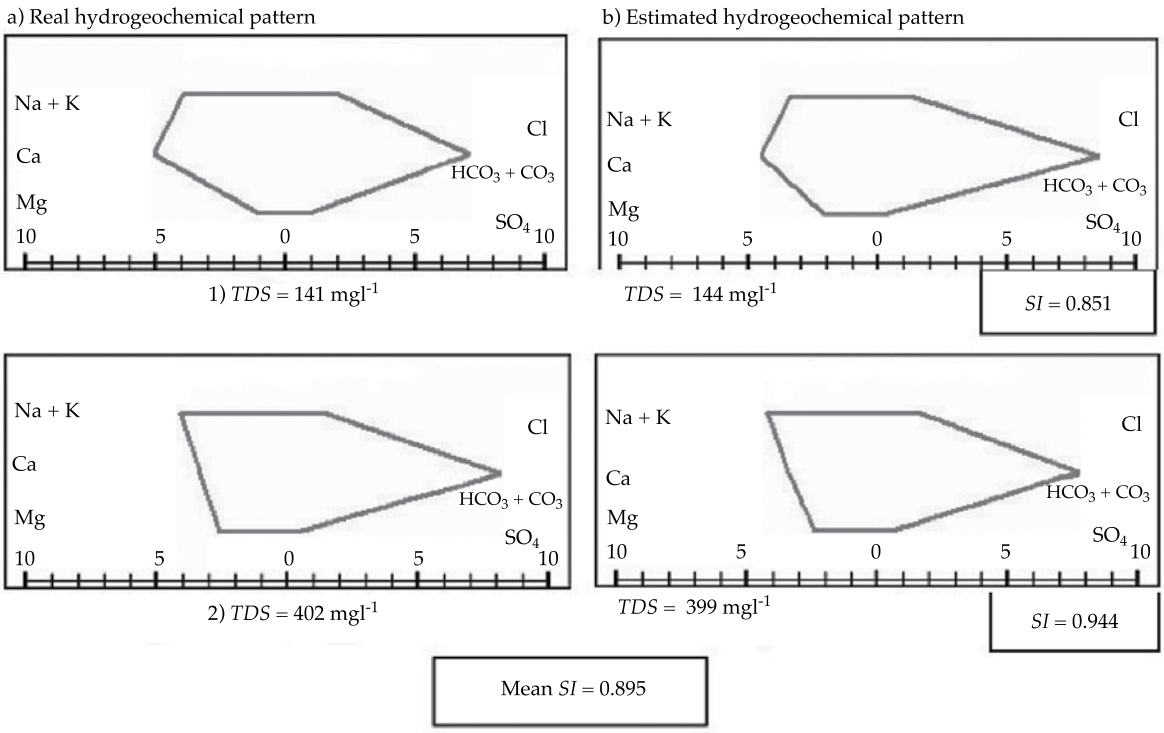

Figure 4. Comparison between real hydrogeochemical patterns and TDS and a) estimated b) hydrogeochemically modeled (model $y = a_1 x + a_2 x^2$). Samples 1) no 10 and 2) no. 17 (phreatimeters, groups 1 and 2, respectively). Similitude index (*SI*).

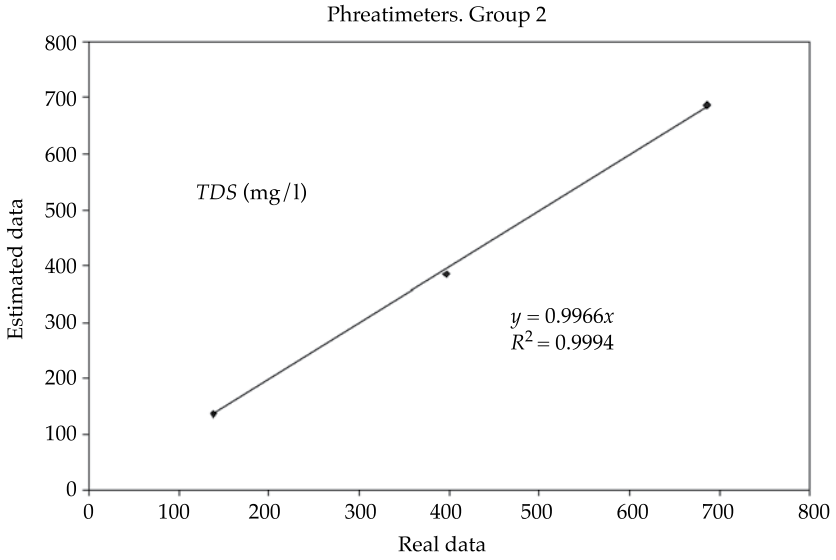

Figure 5. Relation between real values and those calculated with mathematical modeling. Phreatimeters, group 2.

Table 4. Wells in Buenos Aires. Ionic concentration (Ci) adjusted by straight line equations with non-zero intercept (equation 3), straight line through origin pf corrdinates (equation 4) and parabola through origin of coordinates (equation 5), similitude index (*SI*).

Water group 2 (*N* = 6)			
Ci	*Ci* = *a*1 (*EC*) (4) *	*Ci* = *a*0 + a1 (*EC*) (3) **	*Ci* = a1 (*EC*) + A2 (*EC*)2 (5) *
HCO_{3^-}	$y = 0.00598x$	$y = 3.9216 + 0.0048x$	$y = 0.008895x - 7.4612 * 10 - 7x2$
Cl^-	$y = 0.00317x$	$y = -3.1264 + 0.0041x$	$y = 0.000756x + 6.1756 * 10 - 7x2$
SO_4^{2-}	$y = 0.00173x$	$y = -1.0024 + 0.0020x$	$y = 0.001461x + 6.9267 * 10 - 8x2$
Ca2+	$y = 0.00033x$	$y = 1.5399 - 0.0001x$	$y = 0.001236x - 2.3244 * 10 - 7x2$
Mg2+	$y = 0.00097x$	$y = 1.0271 + 0.0007x$	$y = 0.001654x - 1.7498 * 10 - 7x2$
$Na^+ + K^+$	$y = 0.01032x$	$y = -3.5705 + 0.0114x$	$y = 0.00814x + 5.5879 * 10 - 7x2$
SI	0.824	0.910	0.922
Water group 3 (*N* = 5)			
Ci	*Ci* = *a*1 (*EC*)	*Ci* = *a*0 + *a*1 (*EC*)	*Ci* = *a*1 (*EC*) + *A*2 (*EC*)2
HCO_{3^-}	$y = 0.00254x$	$y = 2.5008 + 0.0021x$	$y = 0.003074x - 7.5711 * 10 - 8x2$
Cl^-	$y = 0.00623x$	$y = -5.7638 + 0.0072x$	$y = 0.004270x + 2.7615 * 10 - 7x2$
SO_4^{2-}	$y = 0.00139x$	$y = 1.6923 + 0.0011x$	$y = 0.002155x - 1.0716 * 10 - 7x2$
Ca^{2+}	$y = 0.00021x$	$y = 0.0945 + 0.0002x$	$y = 0.000227x - 1.0671 * 10 - 9x2$
Mg^{2+}	$y = 0.00063x$	$y = 0.4454 - 0.0006x$	$y = 0.000776x - 2.0243 * 10 - 8x2$
$Na^+ + K^+$	$y = 0.00908x$	$y = -0.7786 + 0.0092x$	$y = 0.008693x + 5.4919 * 10 - 8x2$
SI	0.898	0.883	0.918
Water group 4 (*N* = 5)			
Ci	*Ci* = *a*1 (*EC*)	*Ci* = *a*0 + *a*1 (*EC*)	*Ci* = *a*1 (*EC*) + *A*2 (*EC*)2
HCO_{3^-}	$y = 0.00035x$	$y = 5.2474 + 0.0001x$	$y = 0.00848x - 1.5648 * 10 - 8x2$
Cl^-	$y = 0.00747x$	$y = -6.4551 + 0.0077x$	$y = 0.00666x + 2.5261 * 10 - 8x2$
SO_4^{2-}	$y = 0.00204x$	$y = 2.2961 + 0.0019x$	$y = 0.00230x - 8.1702 * 10 - 9x2$
Ca^{2+}	$y = 0.00049x$	$y = 0.8168 + 0.0005x$	$V = 0.00055x - 1.5839 * 10 - 9x2$
Mg^{2+}	$y = 0.001456x$	$y = -3.7100 - 0.0016x$	$y = 0.00064x + 2.5504 * 10 - 8x2$
$Na^+ + K^+$	$y = 0.00761x$	$y = 3.4689 + 0.0075x$	$y = 0.00759x + 5.6518 * 10 - 10x2$
SI	0.855	0.889	0.869

* *SAMA*, ***GEOQUIM*. *EC*: Electrical Conductivity uS/m.

particularly when using the parabola model (mean *SI* between 0.90 and 0.94), as can be seen in Table 4. Figure 6 presents an example of real and estimated patterns for samples from group 4, from wells, with extreme *TDS* values. As in the case of phreatimeters, a very high similitude index can be observed for these samples as well as for all of the samples (0.9). The correlation coefficient between real and estimated values for the wells was also relatively high (Figure 7).

Lagoons

The water from all the lagoons corresponded to group 4. Therefore, it constitutes a homogeneous group, with Stiff diagrams similar to those presented by Figure 5 for the wells, which also represent group 4. The *SI* for real and estimated values was also very high (0.9). Table 5 presents the equations using the data from the samples from the lagoons based on the three mathematical

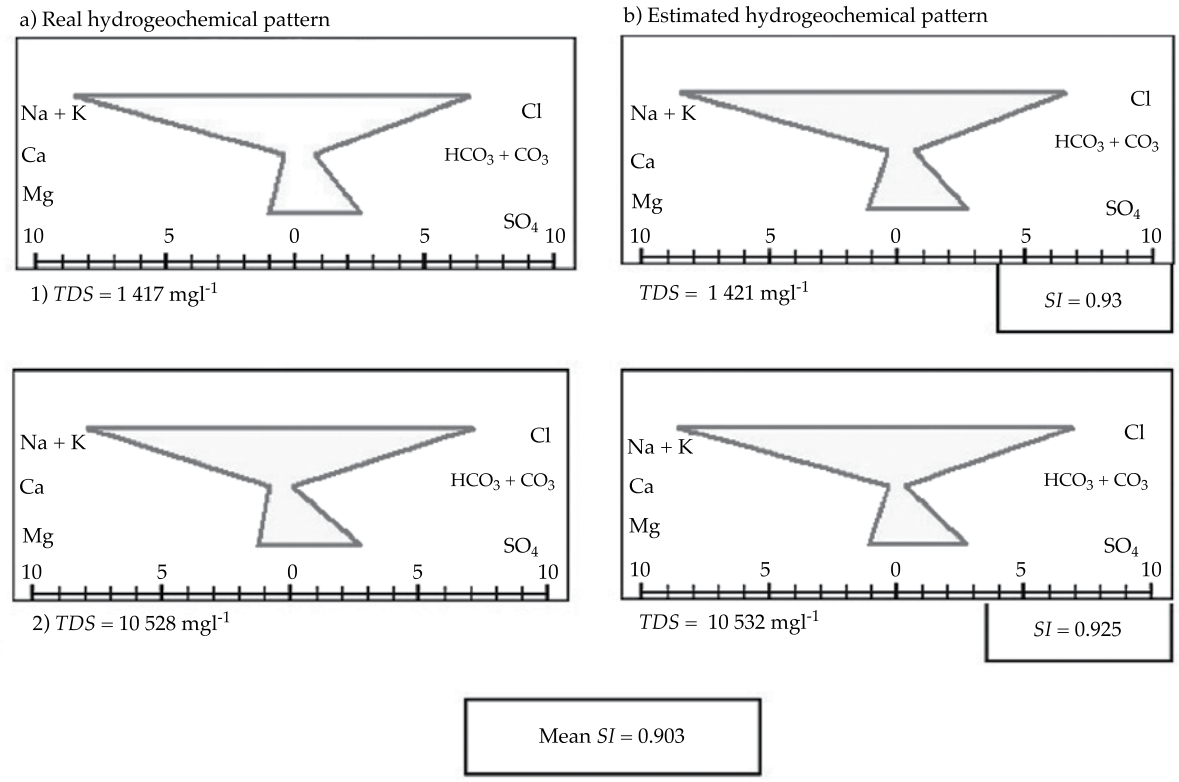

Figure 6. Comparison between real hydrogeochemical patterns and TDS and a) estimated b) hydrogeochemically modeled (model $y = a_1x + a_2x^2$). Samples 1) no 24 and 2) no. 4 (wells, group 4). Similitude index (*SI*).

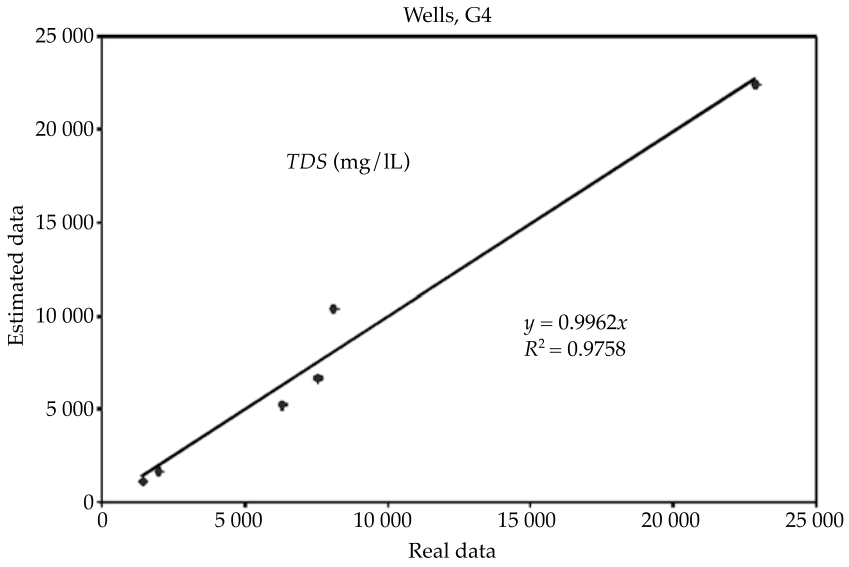

Figure 7. Relation between real values and those calculated with mathematical modeling of TDS. Wells, group 4.

Table 5. Lagoon water. Ionic concentration (*Ci*) adjusted by straight line equations with non-zero intercept (equation 3), straight line through origin pf corrdinates (equation 4) and parabola through origin of coordinates (equation 5), similitude index (*SI*).

Ci	*Ci* = *a*1 (*EC*) (4) *	*Ci* = *a*0 + *a*1 (*EC*) (3) **	*Ci* = *a*1 (*EC*) + *A*2 (*EC*)2 (5) *
HCO^{3-}	$y = 0.00033x$	$y = 3.3192 + 0.0002x$	$y = 0.00049x - 2.5599 * 10 - 9x2$
Cl^{-}	$y = 0.00881x$	$y = -27.0151 + 0.0095x$	$y = 000712x + 2.7357 * 10 - 8x2$
SO_4^{2-}	$y = 0.003721x$	$y = -8.9577 + 0.0039x$	$y = 0.00299x + 1.1822 * 10 - 8x2$
Ca^{2+}	$y = 0.000001x$	$y = 4.6755 - 0.00003x$	$y = 0.00051x - 6.5428 * 10 - 9x2$
Mg^{2+}	$y = 0.000378x$	$y = 13.2306 + 0.0005x$	$y = 0.00150x - 1.7989 * 10 - 8x2$
$Na^{+}+K^{+}$	$y = 0.01243x$	$y = -49.4665 + 0.0137x$	$y = 0.00872x + 5.9621 * 10 - 8x2$
SI	0.764	0.839	0.910

**SAMA*, ***GEOQUIM*. *EC: electrical conductivity* uS/m.

correlation models mentioned (*SAMA* and *GEOQUIM*) and the *SI* means.

The best fits were obtained with the second-order polynomial model (0.90 mean *SI* for real data versus data obtained by modeling).

While an adequate fit was found for all procedures used to estimate concentrations of ions based on the EC, in the case of the wells and lagoons better results were obtained using the second-order polynomial equation (parabola), followed by the straight line with non-zero intercept.

Fagundo *et al*. (1993a, 1996) found that in Cuba, the chemical composition of water from different sites, grouped according to common lithology, in the straight line model that passes through the origin of coordinates was satisfactory (*SI* 0.880 y 0.930). Nevertheless, Fagundo *et al*. (1993b) and Vinardell *et al*. (1999) found that when there is a mix of water, as occurs in extraction wells in coastal aquifers due to the effect of the intrusion of salt water, better results are obtained by applying the second-order polynomial model, previously grouping the samples using the pattern recognition method when a high number of hydrogeochemical patterns is present. These authors coincide with the results from the study herein, since the physio-chemical properties varied greatly among samples according to the water source, type of flows and whether they were in recharge or discharge zones.

A procedure can be used to estimate ionic concentration based on *EC*, considering the principles by Toth (2000) related to the functioning of groundwater. Regions that better adapt to farming-forestry management can be defined simply and at a low cost, as proposed by Heuperman *et al*. (2002), Tomar (2007) and Alconada *et al*. (2009). This is very important in environments subject to alternating droughts and floods, where the water table is shallow, as in the area studied by the work herein. Coinciding with Miller *et al.* (1988), in this study there was a satisfactory relationship between theoretical *EC* and field measurements, according to the lithology of the site and by applying the proposed programs.

Since the present study did not have systematic sampling data (at least monthly for one or two years), it was not possible to evaluate the effect of the hydrological cycle (precipitation-drought) on the chemical composition of the water from the different sources. It is recommended that this be investigated by future studies to more accurately determine the mathematical correlation models obtained herein.

Conclusions

The objective of the present study was achieved, which aimed to use hydrogeochemical models to estimate the chemical composition of water based on its electrical conductivity. In effect, the chemical composition of the water, its ion concentration, can be defined using mathematical calculations based on the electrical conductivity value. The best fits in Northwest Bonoaerense were obtained by processing hydrochemical data by water group using the pattern recognition method and the second-order polynomial mathematical model (parabola passing through the origin of coordinates). This procedure makes it possible to propose the most suitable management practices based on the definition of the type of groundwater flow, using simple and low-cost field measurements such as *EC*, temperature and pH, and by considering other elements in the landscape, such as soil, geomorphology and vegetation. This information enables obtaining knowledge about the flow system being sampled and its recharge, discharge and transit zones.

Received: 29/11/2011
Accepted: 23/08/2013

References

ALCONADA-MAGLIANO, M.M. *Procesos de inundación en el sector de Médanos Longitudinales del Noroeste de la provincia de Buenos Aires, Argentina. Su relación con vegetación, suelo, agua, y clima. Opciones de desarrollo*. Tesis de Doctorado en Geografía. México, DF: Universidad Nacional Autónoma de México, 2008, 598 pp. y anexos.

ALCONADA-MAGLIANO, M.M., BUSSONI, A., ROSA, R. y CARRILLO-RIVERA, J.J. El bio-drenaje para el control del exceso hídrico en Pampa Arenosa, Buenos Aires, Argentina. *Investigaciones Geográficas, Boletín*. Instituto de Geografía, UNAM. Núm. 68, 2009, pp. 50-72.

ALCONADA-MAGLIANO, M.M., FAGUNDO-CASTILLO, J.R., CARRILLO-RIVERA, J.J., and HERNÁNDEZ, P.G. Origin of Flooding Water through Hydrogeochemical Identification, the Buenos Aires Plain, Argentina. *Environmental Earth Sciences*. Vol. 64, No. 1, 2011, pp. 57-71.

ÁLVAREZ, E., VINARDEL, I., FAGUNDO, J.R., REGUERA, E. y CARDOSO M.E. Evolución química y relaciones empíricas en aguas naturales. II- Sistema Automatizado para el Monitoreo de las Aguas. *Voluntad Hidráulica*. Núm. 83, 1990, pp. 15-25.

ÁLVAREZ, E., VINARDELL, I., FAGUNDO, J.R. y RODRÍGUEZ, J.E. Sistemas para el procesamiento de datos hidroquímicos: SAPHIQ, GEOQUIM, SAMA y BATOMET. En *Libro de Comunicaciones I Taller sobre Cuencas Experimentales en el Karst, Matanzas*. Castellón, España: Editorial Universidad Jaume I, 1993, pp. 189-194.

APPELO, C.A.J. and POSTMA, D. *Geochemistry, Groundwater and Pollution*. Rotterdam: Ed. Balkema, 1993, 536 pp.

APHA, AWWA, WEF. *Standards Methods for the Examination of Water and Wasters*. Vol. 17. Washington, DC: American Public Health Association (APHA), the American Water Works Association (AWWA), and the Water Environment Federation (WEF), 1989.

CARRILLO-RIVERA, J.J. Application of the Groundwater-Balance Equation to Indicate Interbasin and Vertical Flow in Two Semi-Arid Drainage Basins. *Hydrogeology Journal*. Vol. VIII, No. 5, 2000, pp. 503-520.

DANGAVS, N. *Los ambientes acuáticos de la provincia de Buenos Aires*. XVI Congreso Geológico Argentino, La Plata, Capítulo XIII, 2005, pp. 219-236.

ETCHICHURY, M.C., TOFALO O.R. y FORZINETTI, M.E. Composición psamítica de sedimentos actuales de la provincia de Buenos Aires y su significado tectónico. *Actas Seg. Tour. Geológico Bonaerense*, Bahía Blanca, 1988, pp. 419-428.

FAGUNDO, J.R. Caracterización de acuíferos mediante relaciones entre contenidos iónicos y parámetros químico-físicos. *CENIC Ciencias Químicas*. Vol. XVI, núm. 2, 1985, pp. 321-325. http//www.redciencia.cu/geobiblio/paper/1990_Fagundo_Hidrogeological.pdf.

FAGUNDO, J.R. Evolución química y relaciones empíricas en aguas naturales. Efecto de los factores geológicos, hidrogeológicos y ambientales. *Hidrogeología*. Vol. 5. Granada, 1990, pp. 33-46.

FAGUNDO, J.R. Patrones hidrogeoquímicos y relaciones matemáticas en aguas naturales. *Ingeniería Hidráulica*. Vol. XIX, núm. 2, 1998, pp. 62-78.

FAGUNDO, J.R. y RODRÍGUEZ, J. Hydrogeochemical Pattern and Mathematical Correlations in Karst at the Examples of Cuba. *Proc. Int. Conference Environmental Changes in Karst Areas*, Italy, No. 13, 1991, pp. 361-369.

FAGUNDO, J.R. and RODRÍGUEZ, J. Hydrogeochemical Pattern and Mathematical Correlations in Karst at the Examples of Cuba. *Newsletter Geology, Climate and Karst Formation*. Guilin, China: Inst. of Karst Geology, 1992, pp. 41-45.

FAGUNDO, J.R., ÁLVAREZ, E., BENÍTEZ, G., FERRERA, V. y VEGA, J. *Simulación química y matemática de la disolución*

de rocas carbonatadas por las aguas naturales. Congreso Interamericano de Ingeniería Sanitaria y Ambiental, CUBAIDIS, La Habana, 1992, Vol. 1, pp. 152-157.

FAGUNDO, J.R., RODRÍGUEZ, J.E., PAJÓN, J.M., FRANCO, E., BENÍTEZ, G., RODRÍGUEZ, A.C., GÜERÓN, J. y ABELLÓ, I. Caracterización hidroquímica de las aguas del Pan de Guajaibón y otras áreas cársicas cercanas a la Sierra del Rosario. En *Libro de Comunicaciones. I Taller sobre Cuencas Experimentales en el Karst, Matanzas*. Castellón, España: Ed. Univ. Jaume I, 1993a, pp. 43-53.

FAGUNDO, J.R., RODRÍGUEZ-BENÍTEZ, G., MORERA, W., FERNÁNDEZ, C. y VEGA J. Caracterización hidroquímica y control de la calidad de las aguas del carso de la cuenca Zapata. En *Libro de Comunicaciones. I Taller sobre Cuencas Experimentales en el Karst, Matanzas*. Castellón, España: Ed. Univ. Jaume I, 1993b, pp. 73-81.

FAGUNDO, J.R., VALDÉS, J.J. y RODRÍGUEZ, J.E. *Hidroquímica del Karst*. Granada: Univ. Granada, 1996, pp. 304.

FAGUNDO, J.R., GONZÁLEZ, P., RODRÍGUEZ, M., SUÁREZ, M. y MELIÁN C. Aplicaciones de la Cinética en la Hidrogeología y el Medio Ambiente. *Contribución a la Educación y la Protección Ambiental*. Núm. 5, 2004, pp. 80-89.

FAGUNDO, J.R., GONZÁLEZ, P., SUÁREZ-MUÑOZ, M., FAGUNDO-SIERRA, J., MELIÁN, C. y ÁLVAREZ E. HIDROGEOQUIM. *Contribución a la Educación y Protección Ambiental*. Núm. 6, 2005, pp. 58-67.

FAGUNDO, J.R., GONZÁLEZ, P., FAGUNDO-SIERRA, J., ÁLVAREZ, E., SUÁREZ, M., and MELIÁN, C. Application of hidrogeochemical modeling to characterization and water quality control of coastal karst aquifer. In: (ed) S. Demuth, A. Gustard, E. Planos, F. Scatena, E. Servat. *Climate Variability and Change Hydrological impacts*. Netherlands: International Association of Hydrological Sciences Publication, 2006, pp. 596-600.

FAGUNDO-SIERRA, J., FAGUNDO, J.R., GONZÁLEZ, P. y SUÁREZ, M. Modelación de las aguas naturales. *Contribución a la Educación y la Protección Ambiental*. Vol. VII, núm. 2, 2001, pp. 1-8.

GONZÁLEZ, N. *Los ambientes hidrogeológicos de la provincia de Buenos Aires*. XVI Congreso Geológico Argentino, La Plata, Capítulo XXII, 2005, pp. 359-374.

HEUPERMAN, A.F., KAPOOR, A.S., and DENECKE, H.W. *Biodrainage. Principles, experiences and applications*. International Programme for Technology and Research in Irrigation and Drainage, Food and Agriculture Organization of the United Nations-FAO, 2002, 79 pp.

MILLER, R.L., BRADFORD, W.L., and PETERS, N.E. Specific Conductance: Theoretical Considerations and Application to Analytical Quantity Control. *U.S. Geological Survey Water-Supply*. No. 2311, 1988, pp. 1-21.

MONCAUT, C.A. Inundaciones y sequías tienen raíces añejas en la pampa bonaerense (1576-2001). En Maiola, O., Gabellone, N. y Hernández, M. (editores). *Inundaciones en la región pampeana*. La Plata, Argentina: Universidad Nacional de La Plata, 2003, pp. 27-48.

PMI. Informe Plan Maestro Integral Cuenca del Río del Salado. Informe tirada reducida. Ministerio de Economía de la Provincia de Buenos Aires-Halcrow-Banco Mundial, 1999, La Plata, Buenos Aires, Argentina, 1300 pp.

STIFF, H.A. The Interpretation of Chemical Water Analysis by Means of Pattern. *Petroleum Technology*. No. 3, 1951, pp. 15-17.

TÓTH, J. Las aguas subterráneas como agente geológico: causas, procesos y manifestaciones. *Boletín Geológico y Minero*. Instituto Geológico Geominero. Vol. III, núm. 4, 2000, pp. 9-25.

TOMAR, O.S. Bio-Drainage: Performance of Various Tree Species as Effective Bio-Drain Material. In: Ambast, S.K., Gupta, S.K., and Singh, Gurbachan (editors). *Agricultural Land Drainage: Reclamation of Waterlogged Saline Lands*. Karnal, India: Central Soil Salinity Research Institute, 2007, pp. 213-221.

VINARDELL, I., TILLÁN, G., FAGUNDO, J.R. y ONTIVERO, E. Un método para la clasificación e identificación de las aguas mediante patrones hidrogeoquímicos. *Revista Ciencias Químicas*. Vol. XXXI, núm.1, 1999, pp. 14-20.

ZÁRATE, M. y RABANESSE, J. *Geomorfología la provincia de Buenos Aires*. XVI Congreso Geológico Argentino, La Plata, 2005, capítulo VIII, pp. 119-138.

Institutional Address of the Authors

Dr. Juan R. Fagundo-Castillo
Dra. Patricia González-Hernández

Facultad de Química
Universidad de La Habana
Zapata s/n entre G y Carlito Aguirre,
Municipio Plaza de la Revolución
Provincia La Habana, Cuba
Teléfono: +53 (7) 2021 871
juanrfag@infomed.sld.cu
patricia@instec.cu

Dra. Margarita M. Alconada-Magliano

Facultad de Ciencias Agrarias y Forestales
Universidad Nacional de La Plata
y CISAUA (Ministerio de Asuntos Agrarios)
Calle 3, núm. 584 (1900) La Plata, Argentina
margaalconada@yahoo.com.ar
Teléfono: +54 (221) 4229 923

Dr. J. Joel Carrillo-Rivera

Departamento de Geografía Física
Instituto de Geografía
Universidad Nacional Autónoma de México
Circuito Exterior, Ciudad Universitaria, Coyoacán
04510 México, D.F., México
Teléfono: +52 (55) 5623 0222, extensión 45467
joeljcr@igg.unam.mx

Prediction of Gauge Readings of Filtration in Arch Dams Using Artificial Neural Networks

• David Santillán* • Jesús Fraile-Ardanuy • Miguel Ángel Toledo •
Universidad Politécnica de Madrid, España
*Corresponding Author

Abstract

SANTILLÁN, D., FRAILE-ARDANUY, J. & TOLEDO, M.A. Prediction of Gauge Readings of Filtration in Arch Dams Using Artificial Neural Networks. *Water Technology and Sciences* (in Spanish). Vol. V, No. 3, May-June, 2014, pp. 83-98.

Artificial neural networks are mathematical structures inspired by the brain of live beings which can generate relatively simple non-linear numerical calibration models. The present work models the flow of water filtered through the rocky base of a pilot arch dam using a multi-layer perceptron neural network. Seepage through a rock mass is difficult to model because it is impossible to obtain a detailed characterization of the medium through which it passes and because of the complexity of the process. The final result is a model composed of three hidden neurons grouped in a layer, using as input variables the water level in the reservoir and their three velocities from prior periods. The structure of the neural network is determined considering the influence of each of the input variables on the output variables. This is based on an extensive set of possible input variables extracted from analytical or conceptual models of the physical phenomenon to be modeled.

Keywords: Arch dams, seepage, artificial neural networks, dam monitoring.

Resumen

SANTILLÁN, D., FRAILE-ARDANUY, J. & TOLEDO, M.A. Predicción de lecturas de aforos de filtraciones de presas bóveda mediante redes neuronales artificiales. Tecnología y Ciencias del Agua. *Vol. V, núm. 3, mayo-junio de 2014, pp. 83-98.*

Las redes neuronales artificiales son estructuras matemáticas inspiradas en el cerebro de los seres vivos, capaces de generar modelos numéricos no lineales de calibración relativamente sencilla. En el presente trabajo se modela el caudal de agua filtrado a través del cimiento rocoso de una presa bóveda piloto con una red neuronal tipo perceptrón multicapa. La filtración a través de un macizo rocoso es un fenómeno difícil de modelar debido a la imposibilidad de caracterizar con detalle el medio en el que discurre y por la complejidad del propio fenómeno. El resultado final es un modelo compuesto por tres neuronas ocultas agrupadas en una capa y cuyas variables de entrada son el nivel de agua en el embalse y tres velocidades de la misma en periodos anteriores. La estructura de la red neuronal se determina teniendo en cuenta la influencia de cada una de las variables de entrada sobre las variables de salida. Para ello, se parte de un conjunto extenso de posibles variables de entrada extraídas de los modelos analíticos o conceptuales del fenómeno físico a modelar.

Palabras clave: *auscultación presas, filtraciones, presa bóveda, redes neuronales artificiales.*

Introduction

The filtration of water through solid rock is difficult to numerically model. The medium in which the solid rock is located is difficult to characterize because of the presence of joints hidden inside, and because of the heterogeneity of the characteristics of the rock mass and different degrees of fractures (Li *et al*., 2008). Adding to this is the complexity of filtration itself. Nevertheless, in certain situations a model is needed that can predict the filtration that could occur in a solid mass.

The most interesting of these situations include the reservoirs formed from the presence of a dam, since these structures are unique because of their dimensions, useful lifespan, impact on the land and, especially, the risk related to their presence. Thus existing concern has led to investigating the possible

problems with dams using new methods to monitor their behavior. For example, a problem in some dams built decades ago is the alkali-aggregate reaction, which deteriorates the mechanical characteristics of the concrete. To control this problem, calculation methods are developed to study how this reaction impacts the response of the dam, considering the actions to which it is subject (Comi *et al.*, 2009). Experiments also exist to evaluate the potential reactivity of the aggregates (Martín *et al.*, 2010; Campos *et al.*, 2010).

Readings of water filtration through the foundation of a dam are among the most useful data for identifying whether an alteration in the structure exists that will directly affect its behavior (ASCE, 2000). The usual strategy to monitor the structural behavior begins with compiling readings from particular devices installed in the dam that control certain variables that are representative of its behavior, such as flows filtrating through the foundation or movements at particular points in the structure. Qualitative information from visual inspections is also obtained for this purpose. The process then continues with the interpretation and evaluation of the compiled data and information. To this end, prediction models based on the readings of the devices are used, according to the conditions found in the dam at the time of the readings. Finally, decisions are made about actions to take if some type of anomaly is detected or suspected.

Artificial neural networks have been considered a useful tool given the need to numerically model complex phenomena that may have diverse causes, including when the laws governing them may be partially or totally unknown and characterizing the medium in which they occur is difficult (Rafiq *et al.*, 2001). Their applications extend to many branches of engineering, including software (Singh *et al.*, 2009), chemical (Jamal *et al.*, 2006) and civil (Flood, 2001).

The article herein describes the application of multilayer perceptron neural networks to the numerical modeling of water flow that filtrates through the foundation of an arch dam, which is measured at one of its gauges. Neural networks are considered a suitable tool for this. Therefore, the objective of the work herein is to apply and evaluate the ability of neural models to reproduce the phenomenon presented.

Background and Frame of Reference

Typical Models to Predict Dam Behavior

Prediction models to predict the behavior of dams are classified as non-deterministic, deterministic and hybrid. They all require two types of data or variables —response variables and external variables. The response variables include the physical magnitudes that are representative of an aspect of the behavior of the structure and are measured with an exploration device or sensor installed inside or outside the structure, such as DGPS to read movements (Galán-Martín *et al.*, 2011). Some of the most important variables are the flow of filtrated water, the movement of certain points in the structure and piezometric pressures registered at particular locations on the foundation (Marengo-Mogollón, 1996). The external variables include physical changes that result in a significant change in one or several response variables, such as the water level in the reservoir.

Non-deterministic models relate response variables with exterior variables through a set of functions that depend on the exterior variables. For example, a statistical model is a non-deterministic model in which the response variables are related to exterior variables through a set of shape functions

which are dependent on the latter. The shape functions are multiplied by coefficients that are usually calculated using the least squares method according to readings of both. From the statistical point of view, the values of the shape functions are the regressors or explicative variables in a multiple linear regression model and the coefficients are the estimators. It is important to mention that these statistical models are typically used to predict response variables related to movement (ICOLD, 2003).

Deterministic models relate response variables with external variables through physical laws. The geometric medium and mechanical, thermal and chemical processes are reproduced using mathematical models. They typically require the discretization of the medium into finite elements according to laws related to the behavior of the structure's body and foundation. This type of model is used primarily to calculate movements (ICOLD, 2003), although it has also been used to model filtrations through both fractured solid rock (Li *et al*., 2008; Yanqing, 2005) and alluvial materials (Tayfur *et al*., 2005).

Hybrid models are a combination of statistical and deterministic models. The functions are determined using deterministic models of the structure, with laboratory tests, or proposals in the statistical models are adopted. Both types of functions are multiplied by coefficients calculated with statistical techniques based on readings of diverse variables taken from explorations.

Artificial Neural Networks

Artificial neural networks are simplified models of the central nervous system. They contain a large number of highly interconnected simple processing elements (neurons) which work in parallel and can learn, adapt and generate solutions based on patterns, or training data (Martín del Brío and Sanz-Molina, 1997). Therefore these models are nonlinear.

Artificial Neural Networks and Prediction Models for Dam Behavior

Over recent years, models of dam behavior have been developed using multi-layer perceptron neural networks. These new models are non-deterministic. Ahmadi-Nedushan and Chouinard (2003) developed three neural networks to model the movement of a pendulum in a gravity dam in a spatial direction. The network architecture consists of a hidden layer with two or three hidden neurons, depending on the network. The procedure used to determine the number of neurons was trial and error. Mata (2011) modeled the radial movements of two pendulums in the Alto Rabagao dam located in Vila Real (Portugal) with a neural network composed of 12 hidden neurons in one single layer.

Other response variables that have been modeled using neural networks include piezometric readings in dams with loose material (Tayfur *et al*., 2005) and prediction of settlement (Kim and Kim, 2008). Other investigations have studied the possibilities of using neural networks to predict the response of gravity dams to seismic actions (Joghataie and Dizaji, 2009).

Other techniques recently used in the exploration of dams are fuzzy logic, genetic algorithms and cointegration theory. Rankovic *et al*. (2012) successfully used fuzzy logic to predict the radial movements of two pendulums in the Bocac arch dam located in the Vrbas River in the Republic of Srpska. The radial movements of one of those pendulums were also successfully modeled with a technique that combines statistical prediction models with genetic algorithms (Stojanovic *et al*., 2013). Initially, a large number of empty regressors exist and

those most suitable are selected using the genetic algorithms technique. The resulting statistical model is a compromise between the quality and complexity of prediction. The regressors of the statistical models traditionally used in the exploration of dams can only be used with static time series. Nevertheless, this condition does not usually occur in real cases. To solve this problem, Li *et al*. (2013) proposed using a new statistical model based on cointegration theory (Artis-Ortuño *et al*., 2009). The model was validated by applying it to the prediction of readings of pendulums in the Wanfu arch dam located in southern Zhejiang, China. The predictions obtained with the new technique are more precise than those resulting from traditional models.

Neural networks have also been successfully used for numerous facets of geology and geotechnology; for example, to determine the permeability of soil with fine grains, providing better results than multiple regression (Yusuf-Erzin *et al*., 2009). They have also been applied, with more satisfactory results than theoretical models, to calculate the last load of the surface foundation on soils without cohesion (Kalinli *et al*., 2011; Padmini *et al*., 2008) to evaluate changes in the temporal evolution of interstitial pressure in hillsides due to rainfall (Mustafa *et al*., 2012) and susceptibility to landslides (Pradhan y Lee, 2010). And they have been used to predict the movement of screen walls in clay soil (Kung *et al*., 2007).

Multi-layer Perceptron

Multi-layer perceptron (MLP) is a one-directional neural model composed of at least three neural layers: input, output and one or more hidden layers. This type of neural network is widely used in engineering (Rafiq *et al*., 2001; Meireles *et al*., 2003). An input pattern p made up of a set of values of input variables x_i is represented by the vector $x_p = [1, x_{p1,\ldots,} x_{pN}]^T$, where the first component of the vector has a value of 1 to include the bias b, and w_{ij} is the weight of the connection between the input neuron I and the hidden neuron j and v_{kj} is the connection between the hidden neuron j and the output k. In addition, n_{pj} and m_{pk} are the arguments for the neuron activation functions for the hidden layer and the output for a given pattern p, respectively; z_{pj} and y_{pk} are the output values corresponding to the output of the neuron j in the hidden layer and k in the output layer, respectively, for a given pattern p, as a result of applying the activation function F over the net input to the neuron.

A given neural network is composed of three layers, with N neurons in the input layer, L neurons in the hidden layer, M in the output layer, a matrix of weights and biases between neurons in the input layer and output layer W, and a matrix of weights and biases of the neurons in the hidden layer and the output V. For an input pattern x_p, the arguments n_{pj} for the neurons in the hidden layer are given by equation (1), the output values z_{pj} for the hidden layer by equation (2), the arguments m_{pk} for the neurons in the output layer by equation (3) and the output y_p of the neural network by equation (4):

$$n_{pj} = \sum_{i=1}^{N} w_{ji} x_{pi} + b_j; \quad \boldsymbol{n_p} = \boldsymbol{W} \cdot \boldsymbol{x_p} \tag{1}$$

$$z_{pj} = F\left(n_{pj}\right); \quad \boldsymbol{z_p} = \left(1, z_{p1}, \ldots, z_{pj}, \ldots, z_{pL}\right)^T \tag{2}$$

$$m_{pk} = \sum_{j=1}^{L} v_{kj} z_{pj} + c_k; \quad \boldsymbol{m_p} = \boldsymbol{V} \cdot \boldsymbol{z_p} \tag{3}$$

$$y_{pk} = F\left(m_{pk}\right); \quad \boldsymbol{y_p} = \left(y_{p1}, y_{p2}, \ldots, y_{pk}, \ldots, y_{pM}\right)^T \tag{4}$$

The neural networks are trained with a process that determines the value of the weights and biases using an algorithm. The topologies of the multilayer perceptron net-

works are trained using the retro-propagation algorithm (Haykin, 1998). There are many variations of this algorithm corresponding to different optimization techniques, such as the conjugated gradient or Newton's methods. The present work uses the variant proposed by Levenberg-Marquardt because of its execution speed (Beale and Hagan, 2012).

Initially, the values of the weights and biases are low and are randomly selected. The algorithm will provide the network with a set of input data, x_p, which will calculate the corresponding outputs, y_p. The algorithm will compute the differences between y_p and the target value that the network should have provided, y^*_p, attempting to minimize them, modifying the value of the weights and biases. Therefore, a set of input-output pairs ($x_{p,} y^*_p$) will be needed, called training data, with which the network can learn.

If the network is trained again, with other initial weights and biases, the solution will generally be different than the previous one. This occurs because the error hypersurface has different local minimums and depending on the value of the initial weights different final values will be reached. In practice, the intention is a network that provides some outputs with the degree of accuracy desired, not necessarily to search for the overall minimum but rather for a local minimum with the required accuracy (Meireles *et al.*, 2003).

In conclusion, for given input variables, designing the network architecture is the same as determining the number of hidden layers and neurons in each one. In addition, a sufficient number of trainings is needed, starting with different initial weights, until obtaining a network that produces sufficiently accurate solutions.

Selection of Input Variables

On advantage of neural networks is that the most important independent variables do not need to be selected. The weights of the synapses associated with irrelevant variables will be negligible and the weights of the relevant variables will be significant (Meireles *et al.*, 2003). This characteristic is used in the study herein to select the input variables that best characterize the phenomenon.

With regard to this idea, several authors have proposed procedures to determine the importance of each of the input variables to the neural network, in relation to each of the output variables; for example, the study by Garson (1991). The sensitivity analysis arose later, based on the Jacobian sensitivity matrix. Gedeon (1997) conducted a study that compared both methods, deducing that the Jacobian matrix provides better agreement with the technique described in the previous paragraph. Consequently, the sensitivity analysis based on the calculation by the Jacobian sensitivity matrix is more reliable than that based on the magnitude of the weights.

The elements that make up the Jacobian *S* matrix provide a measure of the sensitivity of the outputs to changes produced in each one of the input variables. In the Jacobian *S* of order *ixk*, each row represents an input to the network and each column represents an output, such that the matrix element S_{ik} is an index of the sensitivity of output k with respect to input i. Each S_{ik} element is calculated by applying the chain rule, with the following expression:

$$S_{ik} = \frac{\partial y_k}{\partial x_i} = F'\left(m_k\right)\sum_{j=1}^{L} v_{kj} F'\left(n_j\right) w_{ji} \qquad (5)$$

Therefore, the higher the absolute value of S_{ik} the greater the effect of the variable x_i on y_k. The sensitivity must be evaluated for all data patterns. Considering the sensitivity between i and k for pattern x_p as $S_{ik}(p)$, the sensitivity can be defined based on the

sampling mean, $E(S_{ik}(p))$, estimated with equation (6):

$$E\left(S_{ik}\left(p\right)\right)=\frac{1}{p}\sum_{p=1}^{P}S_{ik}\left(p\right) \qquad (6)$$

Number of Hidden Layers and Neurons

The optimal number of hidden layers and neurons in each one is a question that still needs to be solved. Currently, the most common way to determine this is by applying trial and error (Ahmadi-Nedushan and Chouinard, 2003), although some general suggestions and methods to optimize the neural structure exist.

Meireles *et al*. (2003) recommends increasing the number of hidden layers until reaching the desired training results or using three layers (in which case only one hidden layer would exist) and increasing the number of neurons in the hidden layer until the results achieve the accuracy desired. Rafiq *et al*. (2001) indicate that a single hidden layer with an adequate number of neurons is sufficient to model most of the practical problems.

In terms of the hidden layers, based on the Kolmogorov theorem (Hassoun, 1995), Hecht- Nielsen (1990) propose that the number should be less than or equal to twice the number of input variables in the network plus one.

The methods to optimize the structure of the neural network can be classified into two groups: neural pruning algorithms and neural growth algorithms. Both have the drawback of not being computationally efficient and not being able to guarantee that the result will be optimal (Ren and Zhao, 2002). In the same reference, a new algorithm is proposed with a different approach which combines the golden-section search technique (Gutiérrez, 2003) with the Akaike information criterion (AIC). The authors apply this to multi-layer neural perceptron networks with one hidden layer and one output. This information criterion has been applied to neural networks by other authors. For example, Kalin *et al*. (2010) used it to select the neural networks that are most suitable to predict water quality in hydrographic basins, and Zhao *et al*. (2008) used it to design the architecture of neural networks used in their investigations.

The golden-section search technique is used to find the *extremum* of a unimodal function, which consists of successively reducing the range of values, among which the solution is found. When applying the AIC to neural networks according to Ren *et al*. (2002) for the training data set, the value is calculated using equation (7), when $P/(Q+1) \leq 40$ or equation (8) when $P/(Q+1) > 40$:

$$AIC = P\log\left(\hat{\sigma}^2\right)+2\left(Q+1\right) \qquad (7)$$

$$AIC_c = P\log\left(\hat{\sigma}^2\right)+2\left(Q+1\right)\frac{P}{P-Q-2} \qquad (8)$$

where P is the number of training patterns, $\hat{\sigma} = \sum\sigma^2/P$ is the mean squared error between target outputs and those calculated by the network and Q is the number of the network's weights and biases, that is, the parameters. The AIC value makes it possible to select the optimal network among different architectures, where the lesser the value the better the network.

For a given problem, the number of training data P and the number of inputs and outputs in the neural network is fixed. Then, the first addend in the AIC expression given by equation (7) or (8) depends only on the mean squared error of the model and the second term from the number of parameters, for the purpose of penalizing for overfitting.

Ren Neural Architecture Optimization Algorithm

The application of the golden-section search technique to minimize the AIC values for various candidate networks requires the function that results in the unimodal value, which is comparable to finishing the process. For a given set of training data P, the minimum number of hidden neurons is 1 and the maximum must be less than P.

Given a neural network with one hidden layer, N inputs, L hidden neurons and M outputs, the architecture optimization algorithm consists of the following steps (Ren and Zhao, 2002):

1. Establish the minimum number of hidden neurons $N_0 = 1$ and the maximum number possible, $N_1 = (P - M)/(N + M + 1)$.

2. Calculate the golden-section points $N_2 = N_0 + \varphi(N_1 - N_0)$ y $N_3 = N_1 - \varphi(N_1 - N_0)$ where $\varphi = (\sqrt{5} - 1)/2$ is the radius of the golden section. N_2 and N_3 are rounded to the closest whole number.

3. Construct two neural networks. Both will have N input neurons and M output neurons, while the first will have N_2 hidden neurons and the second N_3.

4. Train each network architecture from the previous point several times with different initial weights and biases and, among all the resulting networks, obtain that which has the lowest minimum squared error when predicting the training data.

5. Calculate the AIC or AIC_c value, as applicable, for both networks, obtaining $AIC(N_2)$ and $AIC(N_3)$. Next:
   a) If $N_0 = N_1$, stop the algorithm.
   b) If $AIC(N_2) \leq AIC(N_3)$, then $N_0 = N_0$, $N_1 = N_3$ and the algorithm continues to step 2.
   c) If $AIC(N_2) > AIC(N_3)$, then $N_0 = N_2$, $N_1 = N_1$, and the algorithm continues to step 2.

Methodology

Pilot Case

The La Baells dam was selected as a pilot case. This is a three-centered arch dam with double curvature. Its height is 102 meters above the foundation and it was built in 1974-1975. It is located on the Llobregat River, in the Término Municipal de Cercs i Vilada (Bergueda), Barcelona, Spain.

The dam is located in an area with terrain corresponding to the Tertiary Oligocene period, which is made up of alternating conglomerates and sandstone with medium grain, and some thinly layered intercalations of clay sandstone and argillite. The conglomerate is more predominant than the sandstone. Both make up approximately 85% of the formation, the remaining are cemented alternations. The banks are flat and virtually vertical and perpendicular to the channel, with a slightly southern trend and an overall E-W direction. The position of the banks ensures impermeability and contributes favorably to the dam.

The conglomerates are made up of limestone, granite and quartzite with a rounded shape and mostly 10 cm in size. The matrix is calcareous sandstone. They are very hard and cemented, although they have been modified in one area. The sandstone with thick grain contain a very gross calcareous cement, generally having a lens shape. The set of argillite and finely grained sandstone, depending on the sand content, is made up of hard and compact sandy-clay rocks which are quite resistant to erosion.

In the dam, internal filtrations are controlled with gauges by measuring the flow filtrated through the concrete and

foundation. The gauge chosen for the modeling measures the water flow that collects in one of the side galleries excavated in the foundation.

Variables on which the Filtrated Flow Depends

Filtration through solid rock is affected by the hydraulic gradient, electrical conductivity of the medium through which the fluid flows and the tensional state of the solid rock. In turn, the tensional state depends on the stresses transmitted by the dam due to the hydraulic load generated by the reservoir and the temperature field of the concrete and solid rock in the dam.

Filtrated flow is also affected by the history of past loads because of the relaxation and contraction of the concrete, and the rock to a lesser extent. Consequently, thermal inertia and tensile strain slow down the changes.

The hydraulic gradient depends on the water depth in the reservoir. Temperature fields depend on the temperature of the solid rock and the water, and both of these depend on the air temperature. Therefore, the temperature field can be characterized by the *daily air temperature*, *T*. The available temperature data is measured at the location of the dam and can roughly be considered representative of the temperature throughout that day. The tensile field depends on the hydraulic load and the temperature field. Therefore, it can be characterized by the *water level in the reservoir*, H, *and the daily air temperature*, T.

The information related to past tensile and temperature fields is supplied to the neural network, quantifying the speed at which the *daily air temperature* and *water level in the reservoir* changes during past periods. The speed of change of variable *A* during period (*n*,*m*), $A_{n,m}$ is calculated using equation (9), which in mathematical terms corresponds to the expression for the rate of change of function *A* (*t*):

$$A_{n,m} = \frac{A_n - A_m}{n - m} \tag{9}$$

where A_n is the value of *A* on *n* days earlier (see Figure 1). The periods chosen correspond to (0,10), (10,20) and (20,30) days.

Available Data

After extracting the data from the readings of the instruments installed in the La Baells Dam, there were 1 021 days during which the flow in the study gauge was measured, between 15/02/1980 and 24/10/2008. The mean air temperature was recorded on 8 964 days, between 1/10/1979 and 29/10/2008 and the water level in the reservoir on 9 271 occasions, between 3/08/1979 and 29/10/2008. The high frequency of air and level readings made it possible to estimate the missing readings using linear interpolation.

Figure 2 represents the original and interpolated data, water level, air temperature and readings from the flow gauges, in descending order. The correlation coefficient matrix indicates an acceptable degree of correlation among the data (Table 1). The data used for the training of the networks are normalized using a linear transformation

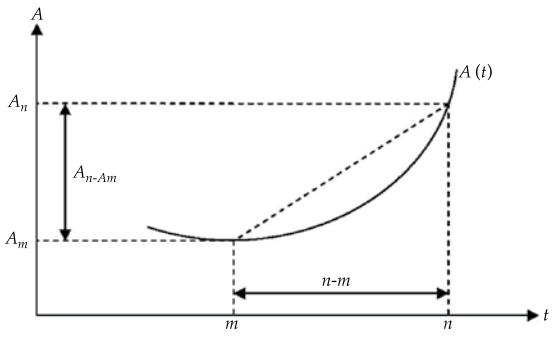

Figure 1. Field velocity for Variable A.

such that their maximums and minimums change to 1 and -1, respectively.

Design of the Neural Network

The methodology to define the neural architecture is composed of the steps graphically represented in the flow diagram in Figure 3. In the first step, the values of the network's input variables are calculated, which are *daily air temperature*, *water level in the reservoir* and the rate of change of both variables during the periods (0,10), (10,20) and (20,30) days. Then, the dates are selected

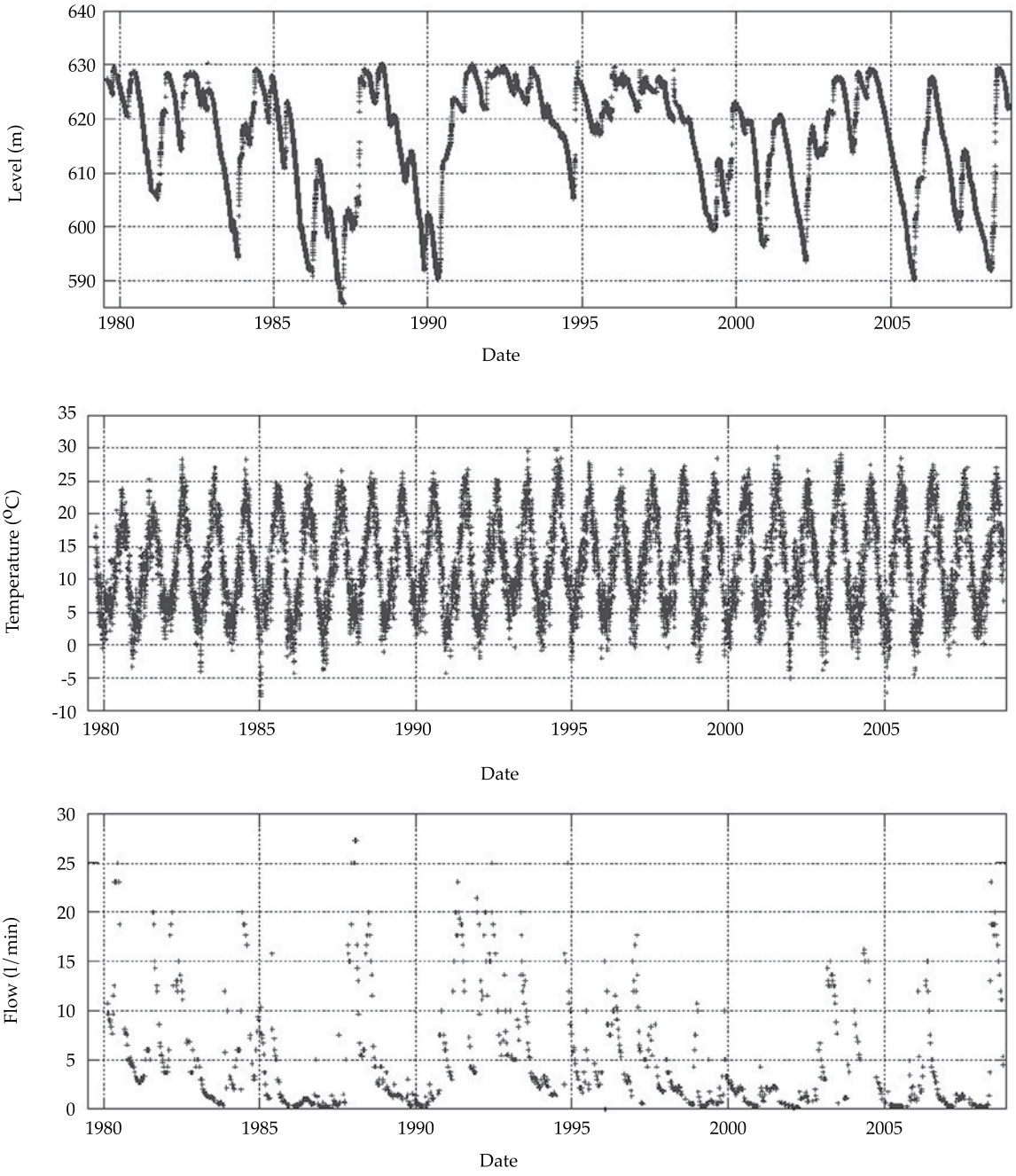

Figure 2. Data available and interpolated from the pilot dam.

Table 1. Linear Correlation Coefficients.

	H	$H_{0,10}$	$H_{10,20}$	$H_{20,30}$	T	$T_{0,10}$	$T_{10,20}$	$T_{20,30}$
H	1.00							
$H_{0,10}$	0.08	1.00						
$H_{10,20}$	0.14	0.56	1.00					
$H_{20,30}$	0.17	0.27	0.47	1.00				
T	0.06	-0.02	-0.02	0.01	1.00			
$T_{0,10}$	-0.03	0.03	0.05	0.01	0.37	1.00		
$T_{10,20}$	0.04	0.02	0.03	0.03	0.06	-0.37	1.00	
$T_{20,30}$	0.05	-0.03	-0.01	0.05	0.20	0.17	-0.37	1.00

which have data for filtrated flow. A total of 1 021 complete records with values for the neural network's input and output variables are available.

Next, the 1 021 records are divided into four subsets, named D1, D2, D3 and D4. The first (D1) is used to train the neural networks, the second (D2) is used along with the first to select the neural networks and input variables as explained in the following paragraphs, the third (D3) is used to choose among each one of the networks obtained by each iteration the one with which to model the phenomenon studied, and the fourth (D4) to evaluate the predictive capacity of the previously chosen network.

The 1 021 records are randomly divided into the four subsets described above. The first, D1, contains 608 records (59.7% of the total), the second contains 207 records (20.3%), the third 103 records (10.1%) and the fourth also contains 103 records. A homogeneity test is used to prove that these four samples are from the same population.

Then, the number of hidden neurons for some of the input variables is determined with the Ren algorithm. Each network architecture is trained 200 times with the Levenberg-Marquardt algorithm using different initial weights and biases and the D1 normalized data subset. Of these 200 networks with the same architecture, the one is chosen which has the lowest AIC value, determined with subsets D1 and D2, and which also results in a root mean squared error between 0.8 and 1.2 when predicting both subsets. The purpose of this last condition is to ensure the capability for generalization of the network and prevent over-training problems.

The next step is to analyze the importance of each one of the network's input variables resulting from the Ren algorithm. To this end, the importance matrix I is defined using the mathematical expectation values for sensitivity, $E(Sik(p))$, estimated using equation (6). The element I_{ik} quantifies the relative effect of the input variable I on the output k, in relation to the rest of the input variables. The elements of the matrix are calculated using the expression:

$$I_{ik} = \frac{E\left(S_{ik}(p)\right)}{\sum_{i=1}^{N} E\left(S_{ik}(p)\right)} 100 \qquad (10)$$

Once the importance matrix is calculated independently with the data subsets D1 and D2, the least important variable is eliminated and the process described in the previous paragraphs is repeated with the

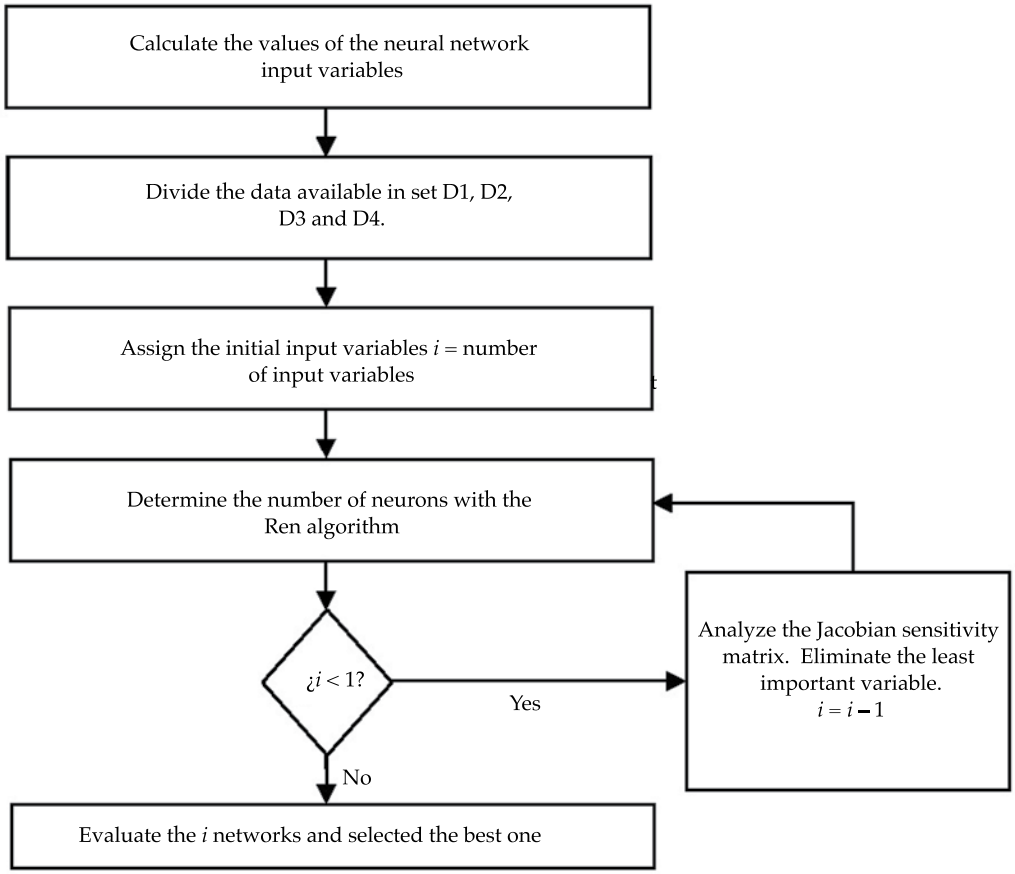

Figure 3. Flow diagram of the methodology.

new input variables. We will call the process to determine the best network architecture "iteration" according to the Ren algorithm for some of the fixed input variables and the evaluation of the importance of those variables.

The process terminates when there is only one input variable, obtaining in the end i neural networks, where i is the number of initial input variables.

From these networks, the one with the lowest AIC value is selected, which is calculated with subset D3, and its predictive capacity is determined with subset D4 according to the root mean squared error.

Results and Discussion

First Iteration

In the first iterations the neural network's input variables were *daily air temperature*, *water level in the reservoir* and rate of change of both variables during the periods (0,10), (10,20) and (20,30) days.

With the input variables fixed, the number of hidden neurons was determined using the Ren algorithm. Initially, the minimum number of hidden neurons, N_0, was 1 and the maximum possible number, N_1, was 61. The golden-section points were calculated, which

in this first step were $N_2 = 24$ and $N_3 = 38$. Next, 200 neural networks were trained with 24 hidden neurons and another 200 with 38, each one with different weights and biases. At the end of the training, the network with the least root mean squared error (RMSE) was chosen from each architecture, when predicting the subsets D1 and D2, and which also resulted in a root mean squared error between 0.8 and 1.2 when predicting both subsets. After the networks were selected, the AIC values of both were calculated, in this case, $AICc\ (N_2) = 1\ 860$ and $AICc\ (N_3) = 3\ 155$. $N_0 = 1$ and $N_1 = 38$ are taken since $AICc\ (N_2) < AICc\ (N_3)$. The nine golden-section points are calaculated and the process is repeated. Table 2 shows the results from these steps until reaching the optimal number of neurons. Note that the sixth column shows that the function that governs the AIC values is unimodal, with a minimum value of 1 113.

The optimal architecture has five hidden neurons with root mean squared error values when predicting subsets D1 and D2 of 2.28 and 2.58 l/min, respectively. The variable with the lowest value of importance is the rate of change in temperature in the interval (0,10), $T_{0,10}$ and therefore this was eliminated and was not included in successive iterations. Note that the values of importance are identical for both subsets, which was repeated in the rest of the iterations.

Iterative Process and Final Model

The process was repeated successively until only one network input value was obtained. Table 3 shows the RMSE when predicting the different subsets of data and their respective AIC values, as well as the number of hidden neurons contained in the networks resulting from each iteration. The process continued until only one input variable was obtained. The order of elimination of the variables was $T_{0,10}$, $T_{20,30}$, $T_{10,20}$, T, $H_{10,20}$, $H_{20,30}$, $H_{0,10}$ and H. Then, the network was chosen which had the number of inputs and hidden neurons resulting in the lowest AIC value when predicting subset D3. In this study case, the network selected was iteration 5, whose input variables are water level in the reservoir and their three rates for periods (0,10), (10,20) and (20,30) days. The network architecture was composed of three hidden neurons, with RMSE of 2.41, 2.65, 1.96 and 1.84 l/min when predicting the data subsets D1, D2, D3 and D4, respectively. Figure 4 shows the prediction obtained by the network according to the gauge reading.

Behavior of Neural Networks

The most suitable variables for modeling gauged flow has been determined based on an initial set. It is worth mentioning that

Table 2. Parameters for the first iteration.

Step	N_{0i}	N_{1i}	N_2	N_3	$AIC(N_2)$	$AIC(N_3)$	N_{0f}	N_{1f}
1	1	61	24	38	1 861	3 155	1	38
2	1	38	15	24	1 432	1 861	1	24
3	1	24	10	15	1 315	1 433	1	15
4	1	15	6	10	1 175	1 315	1	10
5	1	10	4	7	1 118	1 204	1	7
6	1	7	3	5	1 120	1 113	3	7
7	3	7	5	5	1 113	1 113	4	5
8	4	5	4	5	1 118	1 113	4	5

Table 3. Evolution of the architecture over the course of the iterations.

Iteration	1	2	3	4	5	6	7	8
$RMSE_{D1}$ (l/min)	2.27	2.34	2.38	2.41	2.41	2.27	2.39	2.52
$RMSE_{D2}$ (l/min)	2.58	2.80	2.79	2.79	2.65	2.83	2.75	2.75
$RMSE_{D3}$ (l/min)	2.29	2.58	1.73	1.93	1.96	2.25	2.43	2.21
$RMSE_{D4}$ (l/min)	1.90	2.20	1.81	1.86	1.84	2.95	1.67	2.14
AIC_{D1}	1 113	1 097	1 125	1 135	1 109	1 085	1 123	1 152
AIC_{D2}	533	495	507	496	449	537	490	449
AIC_{D3}	385	277	217	221	189	311	269	196
AIC_{D4}	346	244	225	213	176	367	195	190
Hidden Neurons	5	3	4	4	3	8	7	4

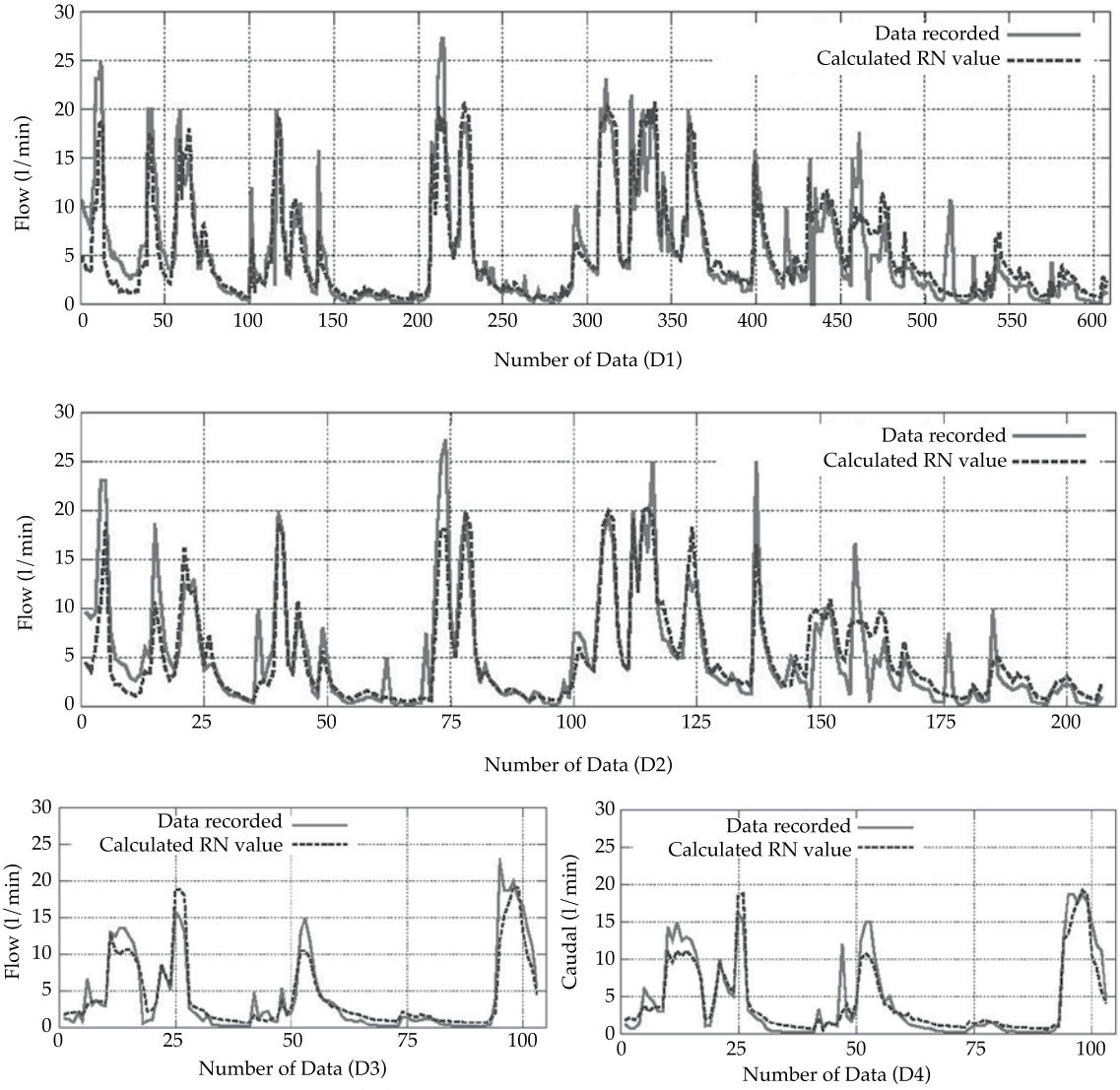

Figure 4. Prediction with the neural network of filtrated flow based on data measured in the dam for all data sets.

temperature is not among them. The gauge studied collected filtrated water at a height between 590 and 550 meters, the zone named in the study. The lowest height is 535 at the foot of the dam and the crest is at 632. The upper portion of the filtration study area is 42 meters below the ground surface. The portion most sensitive to thermal changes corresponds to the top meters of the rock stratum (Guidicini and De Andrade, 1988). Therefore, since the study zone is so deep it is logical that thermal air changes will not have an appreciable effect on filtration. In addition, the load in an arch dam is transmitted to the land primarily from the effect of the arch. While this affects the permeability of the zone, it is unlikely that it would be appreciable in the foundation area, where filtration is collected by the gauge which was analyzed.

Another factor to be analyzed is the RMSE values when predicting the four data subsets. They are very similar to each other for each one of the eight iterations which indicates the absence of over-training and the generalization capability of the different networks. In addition, in nearly all cases, the error values for subsets D3 and D4 were less than those for D1 and D2, which is another indication of the generalization capability. Remember that subset D3 is only used once a network is selected among those determined by each iteration and does not intervene in the calculations executed in the iterations.

The comparison among different iterations of networks, that is, with different architectures, is performed with the AIC, whose value depends on both the RMSE as well as the network structure. The information criterion also depends on the number of data in each set and, therefore, for the same network structure, there is an appreciable difference among the criterion values calculated with the four data subsets. Table 3 shows that subset D3 reaches its minimum value in the fifth iteration, as do subsets D4 and D2, but not D1. Nevertheless, it is important to mention that the difference between the criterion value in the fifth iteration and the sixth (where the minimum occurs) is only 2.2%.

Conclusions

As a pilot case, a neural network model was used to predict flows filtrated through the foundation of an arch dam. These flows were recorded by a gauge. The water flows through a solid rock medium which is typically very difficult to characterize because of the large number of joints and its heterogeneous character. In addition, filtration is governed by complex physical laws. Therefore, neural networks have been able to generate a model to predict filtrated flows which meets the expectations for simplicity as well as generalization and prediction capabilities. The results obtained create possibilities to include these models in the set of tools available to monitor structural behavior.

In addition, the determination of relevant variables makes it possible to interpret the phenomenon modeled. For example, inertia in the response of the dam can be analyzed based on rate of change in levels. The resulting model also makes it possible to study the influence of each of the external variables on the filtrated water flow. Thus, it may be possible to more quickly identify a considerable diversion of filtrated flow due to assumed damage resulting from a given combination of external actions within a normal range. In conclusion, the modeling of the behavior of dams using artificial neural networks is a useful tool for typical works involving the exploration of dams. The methodology presented was applied to filtrated flow through a gauge but can easily be extended to other response variables of the structure.

Acknowledgements

We would like to thank the government of Spain's Ministry of the Environment and Rural and Marine Environment (Ministerio de Medio Ambiente y Medio Rural y Marino del Gobierno de España) for its financing through the research project "Study of the Safety of Dams and Identification of Risk Scenarios using Intelligent Systems" (Estudio de la Seguridad de Presas e Identificación de Escenarios de Riesgo mediante Sistemas Inteligentes" (SEPRISIS)), number 048/RN08/04.5 .

The authors also wish to thank Ofiteco and the Catalana Water Agency for providing data from the La Baells dam.

Received: 25/04/13
Accepted: 09/09/13

References

AHMADI-NEDUSHAN, B. and CHOUINARD, L.E. Use of artificial neural networks for real time analysis of dam monitoring data. *Proceedings of the Annual Conference of the Canadian Society for Civil Engineering*, Moncton, Nouveau-Brunswick, Canada, June, 2003.

ARTIS-ORTUÑO, M., SURIÑACH-CARALT, J. y LÓPEZ-BAZO, E. *Análisis económico regional. Nociones de la cointegración*. Barcelona: Antoni Bosch, 2009, pp. 192.

ASCE. *Guidelines for instrumentation and measurements for monitoring dam performance*. Reston, Virginia: American Society of Civil Engineers, 2000, 712 pp.

BEALE, M. and HAGAN, M. *Neural network toolbox 7. User's Guide*. Natick, MA, USA: The MathWorks, 2012, 422 pp.

CAMPOS, P.L., GADEA, J., SORIANO, J., MARTÍN, A. y CALDERÓN, V. Reactividad álcali-sílice y álcali-silicato en pizarras. *Estudios Geológicos*. Vol. 66, núm. 1, enero-julio, 2010, pp. 91-98.

COMI, C., FEDELE, R., and PEREGO, U. A chemo-thermo-damage model for the analysis of concrete dams affected by alkali-silica reaction. *Mechanics of Materials*. Vol. 41, No. 3, March, 2009, pp. 210-230.

FLOOD, I. Neural networks in civil engineering: a review. In *Civil and structural Engineering Computing*. Topping, B.H.V. (editor). Stirlingshire, UK: Saxe-Coburg Publications, 2001, pp. 185-209.

GALÁN-MARTÍN, D., MARTÍNEZ-MARÍN, R., MARCHAMALO-SACRISTÁN, M., and SÁNCHEZ-SOBRINO, J.A. Control of Movement for Concrete-Reinforced Dams using DGPS and Comparison with Auscultation Methods. Application at the La Aceña (Spain) dam. *Water Technology and Sciences*. Vol. II, No. 3, July-September, 2011, pp. 159-176.

GARSON, G.D. Interpreting neural-network connection weights. *AI Expert*. Vol. 6, No. 4, April, 1991, pp. 46-51.

GEDEON, T.D. Data Mining of Inputs: Analyzing Magnitude and Functional Measures. *International Journal of Neural Systems*. Vol. 8, No. 2, April, 1997, pp. 209-218.

GUIDICINI, G. and DE ANDRADE, R.M. Seasonal Oscillation of Uplift Pressures in Hydraulic Structure Foundations Due to Environmental Thermal Variations. In *Rocks Mechanics and Power Plants*. Romana, M. (editor), Rotterdam: Balkema, 1988, pp. 467-472.

GUTIÉRREZ, A.J. *Diseño de procesos en ingeniería química*. Barcelona, España: Reverté, 2003, 272 pp.

HASSOUN, M. *Fundamentals of artificial Neural Networks*. Cambridge: The MIT Press, 1995, 511 pp.

HAYKIN, S. *Neural Network: a comprehensive Foundation*. 2nd ed. Upper Saddle River, USA: Prentice Hall PTR, 1998, 842 pp.

HECHT-NIELSEN, R. *Neurocomputing*. New York: Addison-Wesley Publishing Company, 1990, 433 pp.

ICOLD. *Methods of Analysis for the Prediction and the Verification of Dam Behaviour*. Swiss Committee on Dams, Baden, Suiza, 2003.

JAMAL, S.H., HUSSAIN, M.A., AROUA, M.K., and YAAKOP, D. Artificial Neural Network Models Applied to Chemical Engineering: a Review. *Trends in Chemical Engineering*. Vol. 10, 2006, pp. 1-15.

JOGHATAIE, A. and DIZAJI, M.S. Nonlinear Analysis of Concrete Gravity Dams by Neural Networks. *Proceeding of the World Congress on Engineering*. Vol. 2, July, 2009.

KALIN, L., ISIK, S., SCHOONOVER, J.E., and LOCKABY, B.G. Predicting Water Quality in Unmonitored Watersheds Using Artificial Neural Networks. *Journal of Environmental Quality*. Vol. 39, No. 4, 2010, pp. 1429-1440.

KALINLI, A., ACAR, M.C., and GÜNDÜZ, Z. New Approaches to Determine the Ultimate Bearing Capacity of Shallow Foundations Based on Artificial Neural Networks and Ant Colony Optimization. *Engineering Geology*. Vol. 117 No. 1-2, January, 2011, pp. 29-38.

KIM, Y.S. and KIM, B.T. Prediction of Relative Crest Settlement of Concrete-Faced Rockfill Dams Analyzed Using an Artificial Neural Network Model. *Computers and Geotechnics*. Vol. 35, No. 3, May, 2008, pp. 313-322.

KUNG, G.T.C., HSIAO, E.C.L., SCHUSTER, M., and JUANG, C.H. A Neural Network Approach to Estimating Deflection of Diaphragm Walls Caused by Excavation in Clays. *Computers and Geotechnics*. Vol. 34, No. 5, September, 2007, pp. 385-96.

LI, F., WANG, Z.Z., and LIU, G. Towards an Error Correction Model for Dam Monitoring Data Analysis Based on Cointegration Theory. *Structural Safety*. Vol. 43, July, 2013, pp. 12-20.

LI, P., LU, W., LONG, Y., YANG, Z., LI, J. Seepage Analysis in a Fractured Rock Mass: The Upper Reservoir of Pushihe Pumped-Storage Power Station in China. *Engineering Geology*. Vol. 97, No. 1, March, 2008, pp. 53-62.

MARENGO-MOGOLLÓN, H. Análisis de riesgo de falla en presas, estadísticas y parámetros de referencia. *Hydraulic Engineering in Mexico*. Vol. II, No. 6, May-August, 1996.

MARTÍN DEL BRÍO, B. y SANZ-MOLINA, A. *Redes neuronales y sistemas borrosos: introducción teórica y práctica*. Zaragona, España: Ra-ma, 1997, 387 pp.

MARTÍN, A., GADEA, J., CAMPOS, P.L., CALDERÓN, V., GARCÍA-CALLEJA, M.A., and RODRÍGUEZ, A. Evaluación de la reactividad árido-álcali en diversos áridos silicatados. Alternativas para minimizar esta reacción. *Estudios Geológicos*. Vol. 66, No. 1, 2010, pp. 99-103.

MATA, J. Interpretation of Concrete Dam Behavior with Artificial Neural Network and Multiple Linear Regression Models. *Engineering Structures*. Vol. 33, No. 3, March, 2011, pp. 903-910.

MEIRELES, M.R.G., ALMEIDA, P.E.M., and SIMOES, M.G.A. Comprehensive Review for Industrial Applicability of Artificial Neural Networks. *IEEE Transactions on Industrial Electronics*. Vol. 50, No. 3, June, 2003, pp. 585-601.

MUSTAFA, M., REZAUR, R., RAHARDJO, H., and ISA, M. Prediction of Pore-Water Pressure Using Radial Basis Function Neural Network. *Engineering Geology*. Vol. 135-136, May, 2012, pp. 40-47.

PADMINI, D., ILAMPARUTHI, K., and SUDHEER, K. Ultimate Bearing Capacity Prediction of Shallow Foundations on Cohesionless Soils Using Neurofuzzy Models. *Computers and Geotechnics*. Vol. 35, No. 1, January, 2008, pp. 33-46.

PRADHAN, B. and LEE, S. (2010). Landslide Susceptibility Assessment and Factor Effect Analysis: Backpropagation Artificial Neural Networks and Their Comparison with Frequency Ratio and Bivariate Logistic Regression Modelling. *Environmental Modelling & Software*. Vol. 25, No. 6, June, 2010, pp. 747-759.

RAFIQ, M.Y., BUGMANN, G., and EASTERBROOK, D.J. Neural Network Design for Engineering Applications. *Computers & Structures*. Vol. 79, No. 17, July, 2001, pp. 1541-1552.

RANKOVIC, V., GRUJOVIC, N., DIVAC, D., MILIVOJEVIC, N., and NOVAKOVIC, A. Modelling dam Behaviour Based on Neuro-Fuzzy Identification. *Engineering Structures*. Vol. 35, February, 2012, pp. 107-113.

REN, L. and ZHAO, Z. An Optimal Neural Network and Concrete Strength Modeling. *Advances in Engineering Software*. Vol. 33, No. 3, March, 2002, pp. 117-130.

SINGH, Y., BHATIA, P.K., KAUR, A., and SANGWAN, O. Application of Neural Networks in Software Engineering: A Review. In *Information Systems, Technology and Management*. PRASAD, S.K. *et al*. (editors). Berlin: Springer Berlin Heidelberg, 2009, pp. 128-137.

STOJANOVIC, B., MILIVOJEVIC, M., IVANOVIC, M., MILIVOJEVIC, N., AND DIVAC, D. Adaptive system for dam behavior modeling based on linear regression and genetic algorithms. *Advances in Engineering Software*. Vol. 65, Noviembre, 2013, pp. 182-190.

TAYFUR, G., SWIATEK, D., WITA, A., and SINGH, V.P. Case Study: Finite Element Method and Artificial Neural Network Models for Flow through Jeziorsko Earthfill Dam in Poland. *Journal of Hydraulic Engineering*. Vol. 131, No. 6, June, 2005, pp. 431-440.

YANQING, W. Multi-Level Fracture Network Model and FE Solution for Ground Water Flow in Rock Mass. *Journal of Hydraulic Research*. Vol. 43, No. 2, 2005, pp. 202-207.

YUSUF-ERZIN, S.D., GUMASTE, S.D., GUPTA A.K., and SINGH, D.N. Artificial Neural Network (ANN) Models for Determining Hydraulic Conductivity of Compacted Fine-Grained Soils. *Canadian Geotechnical Journal*. Vol. 46, No. 8, 2009, pp. 955-68.

ZHAO, Z., ZHANG, Y., and LIAO, H. Design of Ensemble Neural Network Using the Akaike Information Criterion. *Engineering Applications of Artificial Intelligence*. Vol. 21, No. 8, December, 2008, pp. 1182-1188.

Institutional Address of the Authors

David Santillán
Miguel Ángel Toledo

Departamento de Ingeniería Civil: Hidráulica y Energética
Escuela Técnica Superior de Ingenieros de Caminos, Canales y Puertos
Universidad Politécnica de Madrid
28040, Madrid, España
david.santillan@upm.es

Jesús Fraile-Ardanuy

Departamento de Tecnologías Especiales Aplicadas a la Telecomunicación
Escuela Técnica Superior de Ingenieros de Telecomunicación,
Universidad Politécnica de Madrid
28040, Madrid, España

Click here to write the autor

Evapotranspiration Partitioning with Stable Isotopes for Ecohydrological Studies

• Tonantzin Tarin • Enrico A. Yépez* • Jaime Garatuza-Payán •
Instituto Tecnológico de Sonora, México
*Corresponding Author

• Christopher J. Watts • Julio C. Rodríguez •
Universidad de Sonora, México

• Enrique R. Vivoni • Luis A. Méndez-Barroso •
Arizona State University, USA

Abstract

TARIN, T., YÉPEZ, E.A., GARATUZA-PAYÁN, J., WATTS, C.J., RODRÍGUEZ, J.C., VIVONI, E.R. & MÉNDEZ-BARROSO, L.A. Evapotranspiration Partitioning with Stable Isotopes for Ecohydrological Studies. *Water Technology and Sciences* (in Spanish). Vol. V, No. 3, May-June, 2014, pp. 99-116.

The purpose of the emergent discipline of ecohydrology is to generate knowledge to understand processes that are fundamental to ecosystems in terms of the dynamics of the hydrological cycle. During the rainy season, which coincides with high temperatures in semi-arid zones, a variety of ecological processes are triggered involving land surface-atmosphere water exchange through evapotranspiration (*ET*). Although different methodologies exist to calculate *ET*, it is complicated to identify the proportion of its components, evaporation in soil (*ES*) and transpiration of the vegetation (*T*) at congruent scales. The objective of the present work is to identify the ratio *T*/*ET* for one day during the rainy season in a semiarid ecosystem in northwestern Mexico using stable isotopes as tracers of different components of *ET*. The value of the *T*/*ET* ratio was 59 ± 6% on July 24, 2007, but a significant variation was shown between the morning and the afternoon, decreasing from 86 ± 21% in the morning to 46 ± 9% in the afternoon. These results indicate that the vegetation is more active in the morning, contributing more to *ET* than in the afternoon. By using stable isotopes, *ET* can be separated into its components at the ecosystem level, thereby contributing to knowledge about the ecohydrology.

Keywords: Keeling graphs, evaporation, transpiration, turbulent correlation, Sonora.

Resumen

TARIN, T., YÉPEZ, E.A., GARATUZA-PAYÁN, J., WATTS, C.J., RODRÍGUEZ, J.C., VIVONI, E.R. & MÉNDEZ-BARROSO, L.A. Partición de la evapotranspiración usando isótopos estables en estudios ecohidrológicos. Tecnología y Ciencias del Agua. *Vol. V, núm. 3, mayo-junio de 2014, pp. 99-116.*

La ecohidrología como disciplina emergente pretende generar conocimiento para entender procesos fundamentales de los ecosistemas en función de la dinámica del ciclo hidrológico. Durante la temporada de lluvias, que coincide con las altas temperaturas en las zonas semiáridas, se desencadenan diversos procesos ecológicos relacionados con el intercambio de agua entre la superficie terrestre y la atmósfera, vía evapotranspiración (ET). A pesar de que existen diferentes metodologías para estimar ET, conocer la proporción de sus componentes, evaporación del suelo (Es) y transpiración de la vegetación (T), en escalas congruentes es todavía complicado. El presente trabajo tiene como objetivo conocer la proporción de T/ET durante un día de la temporada de lluvias en un ecosistema semiárido del noroeste de México, usando isótopos estables como trazadores de los diferentes componentes de la ET. Durante el 24 de julio de 2007 se obtuvo que la proporción T/ET fue de 59 ± 6%, pero mostró una variación importante entre la mañana y la tarde, ya que la T/ET fue de 86 ± 21% por la mañana y decayó a 46 ± 9% en la tarde. Estos resultados apuntan a que durante la mañana la vegetación se mantiene más activa, contribuyendo más a la ET vía T, en contraste con lo que se observa en la tarde. Con el uso de isótopos estables es posible separar la ET en sus componentes en nivel de ecosistema, lo cual permite el avance del conocimiento ecohidrológico.

Palabras clave: *gráficos de Keeling, evaporación, transpiración, correlación turbulenta, Sonora.*

Introduction

Evapotranspiration (ET) is a key process in the climate system and the only one through which water is returned from the land surface to the atmosphere in the form of water vapor (Jung *et al.*, 2010). The importance of ET is such that two-thirds of annual precipitation returns to the atmosphere through this process (Wang and Dickinson, 2012). In arid and semi-arid regions, 90% or even 100% of precipitation is evapotranspired (Wilcox *et al.*, 2003). Nevertheless, little knowledge exists about the factors that affect ET rates and the variability of its components— evaporation from soil (Es) and transpiration (T) at the ecosystem level (Newman *et al.*, 2006). From a ecohydrological perspective, it is important to understand the movement of water through these routes and its implications for the hydrological cycle, as well as its influence on ecosystem processes (Huxman *et al.*, 2005). Different methodologies and approaches exist to separate ET into its components. For example, porometry and fixed cameras coupled with infrared gas analyzers enable obtaining simple and accurate measurements of *T* at the leaf level (Wang and Yakir, 2000; Yepez *et al.*, 2005). Automated techniques based on thermal balances using sap flow sensors are used to measure transpiration at the individual level (trees or shrubs; Plaut *et al.*, 2012, Reyes-García *et al.*, 2012). Nevertheless, scaling these two techniques to the ecosystem level is complicated because of the heterogeneity of the functioning and spatial distribution of the vegetation (Williams *et al.*, 2004). Meanwhile, *Es* can be calculated with flow cameras placed on the surface of the soil (Raz-Yaseef *et al.*, 2010) as well as with lysimeters (Wenninger *et al.*, 2010), but good spatial representation is lacking for surfaces as heterogeneous as soil. While models exist to calculate the components of *ET*, they require other calculations, such as local meteorology, soil properties, the xylem function (Plaut *et al.*, 2012), the dynamics of vegetation (Reynolds *et al.*, 2000; Vivoni, 2012b; Méndez- Barroso *et al.*, 2014) and the distribution of roots (Manzoni *et al.*, 2013), thereby greatly increasing the level of complexity. In general, these methodologies are problematic when it comes to temporal and spatial representations of the individual components of *ET*, complicating the interpretation at an ecosystem scale and requiring a combination of techniques to achieve this goal (Wilson *et al.*, 2001; Williams *et al.*, 2004).

On the other hand, the Eddy covariance technique is an important tool to study gas exchange with vegetation cover. This method directly measures the net exchange of CO_2 and vapor (*ET*) between land ecosystems and the atmosphere (Baldocchi, 2003). These measurements have a large is continuous and direct temporal resolution for *ET* above the ecosystem canopy, but do not provide details of the contributions of its components (Baldocchi *et al.*, 2001). The use of stable isotopes in combination with other techniques has enabled separating *ET* into its components (Table 1). In particular, an increasing number of studies over recent years has combined stable isotopes and hydrometeorological tools, such as the *EC* technique and the physics of the soil, to calculate the ratio of transpiration to evapotranspiration for studies of ecosystems (Reynolds *et al.*, 2000, Huxman *et al.*, 2005; Yepez and Williams, 2009) (Table 1). Thus, a useful alternative to separte the flow of *ET* (T/ET) can be obtained for studies at the ecosystem scale by combining *EC* measurements with stable isotopes of the different components involved in *ET*, as tracers of the hydrological cycles (Wang and Yakir, 2000; Yepez *et al.*, 2003). This complex circulation can be understood by analyzing

Table 1. Investigations that Contribute to Knowledge about the Partitioning of Evapotranspiration.

Authors	Location	Study Field	*T/ET* %	Type of *ET* partitioning
Moreira *et al*., 1997	Amazons	Forest, pasture	60-80	Stable isotopes/meteorology
Brunel *et al*., 1997	Sahel, Africa	Sagebrush forest	20	Stable isotopes/meteorology
Ferretti *et al*., 2003	Central plains, United States	Pasture	40-75	Stable isotopes/balance of masses
Yepez *et al*., 2003	Arizona, United States	Mesquite	50-85	Stable Isotopes/*EC*
Williams *et al*., 2004	Morocco	Olive crops	72-86	Stable isotopes/*EC*/sap flow
Lai *et al*., 2005	Pacific Northwest, United States	Conifer Forest	85	Stable isotopes/*EC*/sap flow
Yepez *et al*., 2005	Sonora Desert, Mexico	Pasture	22-43	Stable isotopes/static cameras
Yamanaka and Tsunakawa, 2007	Japan	Scrubland	80	Stable isotopes/micrometeorology
Yepez *et al*., 2007	Arizona, United States	Mesquite	5-100	Stable isotopes/*EC*
Xu *et al*., 2008	Wolong, China	Oak scrub	74-96	Stable isotopes/meteorology
Rothfuss *et al*., 2010	Environmental Research Observatory, France	*Festuca arundinacea*	0-95	Stable isotopes/balance of masses
Wang *et al*., 2010	Biosphere 2, Arizona, United States	Mesquite	61-83	Stable isotopes/CRDS
Wenninger *et al*., 2010	UNESCO-IHE laboratory, Holland	*Eragrostis tea (Zucc.)*	70	Stable isotopes/lysimeters
Bijoor *et al*., 2011	California, United States	Wetlands, *Typha latifolia*	17-96	Stable isotopes/EC
Sutanto, 2012	UNESCO-IHE laboratory, Holland	Pasture	77	Stable isotopes/balance of masses/ lysimetry

Where the vortex correlation technique is represented by *EC* (Eddy Covariance) and laser spectroscopy as CRDS (*Eddy covariance*) y la espectroscopia láser como CRDS (*Conventional Cavity Ring Down Spectroscopy*).

samples of atmospheric water vapor and the soil and plants in an ecosystem, and their isotopic composition (*i.e.*, ^{18}O or ^{2}H) (Griffis, 2013).

Nevertheless, this methodology has some disadvantages, including sample handling and laboratory analysis, as well as the high cost of sample processing and the isotope analyzer equipment. Therefore, *T/ET* calculations are normally performed with a low temporal resolution. Since the *T/ET* calculation contributes to linking the water balance with the activities of the plants at the ecosystem level, an improved capacity to calculate *T/ET* contributes to understanding how biotic and abiotic factors affect the rates at which the water is recirculated into the atmosphere and the relationship with the productivity of ecosystems during gas exchanges (Wang and Yakir, 2000,; Yepez *et al*., 2007; Yepez and Williams, 2009). In this context, the present investigation aimed to calculate the contribution of *T* to total *ET* using stable water isotopes and the Eddy

covariance technique based on a case study in the semi-arid scrubland of northwestern Mexico. Because of the large amount of precipitation in this region after the dry season, *T* is expected to be the dominant flow in the total *ET*, since the vegetation is undergoing a growth period when its productivity is highest productivity.

Isotopic Theory

Isotopes are atoms with nuclei that are identical to the number of protons but with a different number of neutrons. The proportion of stable isotopes of an element is represented with the delta notation (δ), in ‰ per mil units (Sharp, 2007):

$$\delta = \left[\left(\frac{R_{\text{sample}}}{R_{\text{standard}}}\right) - 1\right] \times 1\,000 \qquad (1)$$

where R_{sample} and $R_{standard}$ are molar ratios of heavy isotopes to light isotopes in the sample and standard, respectively (V-SMOW: Viena-Standart Mean Ocean Water, for water isotopes; Ehleringer *et al*., 2000). Molar ratios (*R*) are expressed as a function of the isotopic abundance ratio, for example $^{2}H/^{1}H$ or $^{18}O/^{16}O$. Many of the values are negative and only indicate a lower number of heavy isotopes in relation to the standards. The more negative the value the poorer the heavy isotopes in the sample and the more positive the value the richer the sample will be in heavy isotopes with respect to the standard (Sharp, 2007).

ET Partitioning

The isotopic model to calculate the fraction of *T* that contributes to total *ET* is based on the balance of masses (Yakir and Sternberg, 2000), equation (2):

$$\frac{T}{ET} = \frac{\left(\delta_{ET} - \delta_{Es}\right)}{\left(\delta_{T} - \delta_{Es}\right)} \times 100 \qquad (2)$$

where *T*/*ET* represents the proportion of transpiration that contributes to *ET*, δ_{ET} is the isotopic composition of *ET*, δ_{Es} is the isotopic composition of evaporation from soil and δ_{T} is the isotopic composition of transpiration. The different isotopic signatures obtained when analyzing the flows of *E* and *T* are the fundamental basis for separating *ET* into its components (Wang and Yakir, 2000). To calculate δ_{ET}, measurements of a moisture concentration gradient are combined with the isotopic composition of the respective water vapor samples. Based on this, Keeling plots are generated of the isotopic mixture (Pataki *et al*., 2003), which graphs the values of the inverse of the moisture concentration gradient (on *X*) and the isotopic composition of the vapor on the gradient (δ on *Y*), thereby identifying δ_{ET} as the *Y* intercept of the line with the best fit (Yepez *et al*., 2003). These graphs integrate vertical vapor flow on a spatial scale that varies according to the heights at which the vapor is collected, with the same logic used to determine the contribution area using the Eddy covariance technique (Williams *et al*., 2004). Using this technique, it is assumed that: 1) no water vapor is lost from the ecosystem that is not caused by the turbulence in the atmospheric parcel under study, and 2) *Es* and *T* are the only sources of water with different isotopic compositions (Yakir and Sternberg, 2000).

To determine the isotopic composition of evaporation from the soil (δ_{Es}), the modified equation by Craig and Gordon is used (1965), which relates the relative moisture at the evaporation front with the processes that are key to the change in the isotopic composition of the water subject to evaporation, including kinetic isotope fractionation and equilibrium (Wang and Yakir, 2000):

$$\delta_{Es} = \frac{\alpha^* \delta_L - h\delta_a - \varepsilon^* - (1-h)\varepsilon_k}{(1-h) + (1-h)\left(\frac{\varepsilon_k}{1\,000}\right)} \qquad (3)$$

where δ_L is the isotopic composition of the liquid water at the evaporation front (first 5 to 10 cm of depth in the soil); δ_a is the isotopic composition of the atmospheric water vapor in the first 10 cm above the soil level; α^* is the equilibrium isotope fractionation, dependent on the temperature (for 18O a* = (1.137(106 / Tk2) - 0.4156(103 / Tk) - 2.0667) / 1000 + 1] (*Tk* = temperature in °K), expressed as $\varepsilon^* = (1-\alpha^*)$ x 10^{-3} (9.8 ‰ for oxygen at 20°C; Majoube, 1971); ε_k is the kinetic fractionation factor (16.4 ‰ for oxygen, Cappa *et al*., 2003) *h* is the value of relative moisture normalized to the temperature at the evaporation front. In general, this expression denotes the isotopic change that occurs when water evaporates, since during the phase change from liquid water to vapor, the light isotopes tend to leave the soil and the heavy isotopes accumulate.

The isotopic composition of the transpiration flow (δ_T) in an ecosystem can occur in a isotopic steady state (ISS), in which the isotopic composition of *T* is equal to that of the water in the plant's xylem (δ_s) of the plant, since that water is the source of water for the leaves and the leaves do not accumulate water isotopes during dynamic transpiration (Yakir y Sternberg, 2000; Xiao *et al*., 2012). Nevertheless, according to Farquhar and Cernusak (2005), with changing environmental conditions, transpiration may not reach a isotopic steady state (non-ISS), which can seriously affect the calculation of *T*/*ET*(equation 2). An alternative for determining δ_T is to use the isotopic composition of foliar water (δ_f), not modeled as in equation (4), collected over key periods of the day and substitute this value with δ_L in equation (3) to calculate the isotope fractionation from the phase change in the stomatal cavity (Lai *et al*., 2005). Nevertheless, this strategy is only an approximation of the real value of the reservoir that is exposed to evaporation, since the total water from the leaf is mixed with the unevaporated water (for example, veins) and conserves the isotopic composition of the original source (for example, the stem). Therefore, it does not necessarily represent the isotopic composition of the evaporation sites on the leaf (Farquhar and Cernusak, 2005; Lai *et al*., 2005). Nevertheless, since it is very difficult to identify (and therefore to measure) the water at the exact evaporation sites on the leaf to adequately calculate δ_T, several authors have chosen to model the isotopic enrichment of foliar water at the evaporation sites in non-ISS and based on that result calculate δ_T with equation (3) (Farquhar and Cernusak, 2005; Xiao *et al*., 2012). For example, Lai *et al*. (2005) and Yepez *et al*. (2007) used the Dogmann *et al*. (1974) model, which takes into account the time the water is recycled in the leaf in function of the transpiration rate and environmental conditions to predict the isotopic composition of foliar water, and model δ_T based on that approximation (Farquhar and Cernusak, 2005).

To this end, first δ_{ss} (*t*) needs to be calculated, which is the isotopic composition of the water in the leaf in ISS, modeled with a modification of Craig and Gordon (Yakir and Stenberg, 2000):

$$\delta_{ss} = \delta_s + \varepsilon_{eq} + \varepsilon_k + h(\delta_a - \varepsilon_k - \delta_s) \qquad (4)$$

where most of these symbols are described in equation (3), and δ_a is now the isotopic composition of the vapor near the leaf, and *h* is the relative moisture normalized to the temperature of the leaf.

Then the isotopic composition of the foliar water in the isotopic non-steady state (non-ISS) is calculated as follows:

$$\delta_{en}(t) = \delta_{ss}(t) - \left[\delta_{ss}(t) - \delta_{en}(t-1)\right]\exp\left(\frac{-\Delta t}{\tau\varsigma}\right) \qquad (5)$$

where δ_{en} (t) and δ_{en} (t-1) are the isotopic composition of foliar water in non-ISS during a determined time t and time (t – 1); δ_{ss} (t) is the isotopic composition of the leaf in ISS conditions for time 1; Δt is the time interval in seconds; $t = W/T_{leaf}$ is the residence time of water in the leaf, where W is the molar concentration of water in the leaf and T_{leaf} is the transpiration time (mmol $m^{-2}s^{-1}$) of each species. The ς is related to $\alpha^*\alpha_k(1-h)$, where α_k is the kinetic fractionation factor (1.023; Cappa *et al*., 2003) and α^* and h are likewise represented in equation (3). The term T_{leaf} is based on the relation of the stomatal conductance and the vapor pressure deficit (VPD), such that the isotopic composition of transpiration δ_T in non-*ISS* conditions is calculated by replacing δ_{en} (t) with δ_L (t) in equation (3).

From this perspective, it is important to note that Xiao *et al*. (2012) conducted a comparative analysis among the Craig and Gordon (1965; equation (4)), Dogmann *et al*. (1974; equation (5)), and Farquhar and Cernusak (2005) models and concluded that the best way to represent water composition in the leaf is under ISS conditions (Craig and Gordon, 1965) with studies at the canopy and ecosystem scale. This conclusion is based on the fact that the Farquhar and Cernusak (2005) and Dogmann *et al*. (1974) models are complex since they require a significant number of biotic parameters that control enrichment at the leaf level and the variability expressed does not have a large impact on the isotopic composition of the foliar water at the ecosystem level.

Methodology

Description of the Site

The study was performed in a semi-arid ecosystem in northwestern Mexico at 29.741 north latitude and -110.5337 west longitude

Figure 1. Location of the study zone.

and approximately 630 masl (Figure 1). The ecosystem is dominated by seasonal rainfall during summer from the North American monsoon in July, August and September, which can represent up to 70% of the total yearly rainfall (Adams and Comrie, 1997; Watts *et al*., 2007). The average rainfall between 1974 and 2009 was 511 mm and the annual average temperature was 21.3°C. The predominant species are mezquite (*Prosopis velutina*), ocotillo (*Fouquieria macdougalii*), huinolo (*Acacia cochliacantha*), torote (*Jatropha cordata*), chicura (*Ambrosia cordifolia*), gutaño (*Mimosa distachya*) y palo verde (*Parkinsonia praecox*). Most of the species lose their leaves during the dry season and they return when the rainfalls begin at the end of June or beginning of July. The type of soil is silty sand with 70% sand, 17% silt and 13% clay.

En el sitio de estudio hay una torre micrometeorológica equipada con un sistema para medir flujos turbulentos con la técnica de covarianza de vórtices (*Eddy Covariance*) (Moncrieff *et al*., 2000). En breve, los intercambios turbulentos de momento, calor, vapor de agua, CO_2 y, en general,

cualquier cantidad escalar, matemáticamente se definen como la covarianza entre el escalar en cuestión (inercia, temperatura, concentración de vapor de agua y de CO_2) y la velocidad vertical del viento (Watts *et al*., 2007).

There is a micrometeorological tower in the study site with a system for measuring turbulent flows using Eddy covariance (Moncrieff *et al*., 2000). Briefly, the turbulent exchanges for inertia, heat, water vapor CO_2 and, in general, any scalar amount are mathematically defined as the covariance between the scalar in question (inertia, temperature, water vapor concentration and CO_2) and the vertical wind speed (Watts *et al*., 2007).

Specifically, vertical water flow is defined as the covariance between the vertical wind speed and the H_2O concentration multiplied by mean air density (Baldocchi, 2003). Simultaneous measurements of water vapor are performed with a gas analyzer that directly measures the concentration of water in the atmosphere near the surface or vegetation cover. The systems consists of a gas analyzer (LI-7500, LI-COR, Lincoln, NE, USA) and a sonic 3-D anemometer (CSAT3, Campbell Sci., Logan, UT, USA) which take measurements at a frequency of 10 Hz. These sensors are controlled by a datalogger CR5000 (Cambell Sci., Logan, UT, USA) programmed to calculate average flows every 30 minutes. The sensors are installed in a 9 meter high tower which also has sensors that measure net radiation (NR-LITE-L NR1, Campbell Sci., Logan, UT, USA), wind speed and direction (Wind Monitor, R.M. Young, MI, USA) and precipitation (TR-52USW, Texas Ele., Dallas, TX, USA). During the study period, the relative moisture and temperature were measured at heights of 0.1, 2.5, 4.5 and 9 mm with HMP45D (Vaisala, Helsinki, Finland). This data was used to calculate the vapor concentration at the different levels.

Sample Collection for the Partitioning of T/ET

The study was performed July 24, 2007 during North America monsoon season. Water vapor, soil and stem samples were collected. The water vapor samples were simultaneously collected during two periods in the morning and two in the afternoon at four different heights (0.1, 2.5, 4.5 and 9 m). The collection of air vapor consisted of circulating air through a system of valves and hoses circulating through the air in four different crystal traps (one for each heights). The traps were approximately 30 cm longs and 0.9 in diameter with a inside tube of 6 cm, filled with crystal balls 0.3 cm in diameter to increase the tortuosity of the flow. During collection, the set of traps remained submerged in a glass with ethanol at -80 °C, after the periodic addition of liquid nitrogen to freeze the samples in the traps (Helliker *et al*., 2002). The air circulation was regulated with a flow controller at 500 $ml \cdot min^{-1}$, at which rate 30 to 50 µl was collected in each trap, depending on the air moisture (Yepez *et al*., 2003). In a system with multiple species, which is the case of the study herein, a simple average of δ_S values of the species studied is used to represent the δ_T value, assuming ISS conditions (Yepez *et al*., 2003). To this end, stems were collected from three to four individuals from the three species most representative of the vegetation: *F. macdougalii*, *A. cochliacantha* and *P. praecox*. To calculate δ_L, 12 soils samples were randomly collected around the micrometeorological tower at a depth of 5 cm in micro-sites with and without vegetation cover. The averages of the isotopic compositions of the 12 samples was calculated. The samples were placed in 25 ml hermetic vials, sealed with Parafilm® and kept on ice until reaching the laboratory, where they remained frozen at -2 °C. Later, in the laboratory, the water contents of the samples were extracted (>

95%) using cryogenic distillation (West *et al*., 2006). The water extracted from each sample was deposited in separate 2 ml vials and analyzed in a DLT-100 laser spectroscope (Los Gatos Research, Inc.). Molar oxygen ratios ($^{18}O/^{16}O$) were obtained from each sample and the δ was calculated using equation (1), with an accuracy in the range of 0.4 ‰ in $\delta^{18}O$, with respect to the standard reference for LGR on the V-SMOW scale.

Data Analysis

The data from the isotopic analysis are presented for three periods: 1) morning from 7:00 to 12:00 h; 2) afternoon from 12:00 to 17:00 h and 3) complete day from 7:00 to 17:00 h. The micrometeorological and EC data were sampled during daylight hours from 6:00 to 18:00 h. To obtain δ_{ET}, the inverse of the moisture concentration [1/H2O] was calculated (measured in mg per m^{-3} of air) at the different heights with temperature and moisture sensors. This was graphed against the isotopic concentration of the water vapor at the corresponding heights to obtain isotope mixture graphs for each period. With the water from the soil samples analyzed, the value δ_L was used and δ_{Es} was calculated, applying equation (3). To obtain δ_T, first δ_{SS} was calculated with equation (4) and the isotopic enrichment of the foliar water was calculated with equation (5).

To determine T_{leaf} for each species, stomatal conductance values were used (g), which were measured with a porometer (SC- 1 Leaf Porometer Systems, Decagon Devices, Pullman, Wa). This value of g was related with the VPD (calculated with the micrometeorology from the tower), based on which T_{leaf} was obtained. To calculate the residence time of the water in the leaf, W values of 5.3, 9.8 and 10.9 mol m^{-2} were used for *A. cochliacantha*, *P. praecox* and *F. macdougalii*, respectively. With the value of T_{leaf} and W, the recycled time t of the water in the leaf was calculated (equation (5)). Considering the comparison of the models in ISS and non-ISS (Dogmann *et al*., 1974; Figure 5), and the arguments proposed by Xiao *et al*. (2012), to minimize the complexity of estimating δ_T in non-ISS, it was possible to represent δ_T as a simple average of the isotopic compositions of the stems from the three species mentioned in this study; in ISS, the value of δ_T did not change during the day.

T/ET was obtained by applying equation (2) in the morning, afternoon and full day periods. The statistic model developed by Phillips and Gregg (2001) was also applied, which calculates the isotopic error (ios-error), taking into account the standard error of the y intercept in the linear regression of the mixture graphs and the variability in δ_T and δ_{Es}.

Results

July 24, 2007 was a sunny day, although during the early morning a rain event of 0.5 mm occurred and two days earlier an event of 11m occurred (Fig ure 2). The highest net radiation during the study day, 643 W m^{-2}, occurred at 14 h, while daylight hours were between 6:00 and 19:00h (Figure 3). The environmental conditions had a minimum

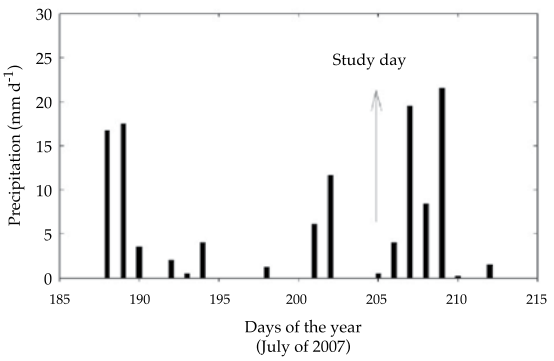

Figure 2. Total daily precipitation in July, 2007.

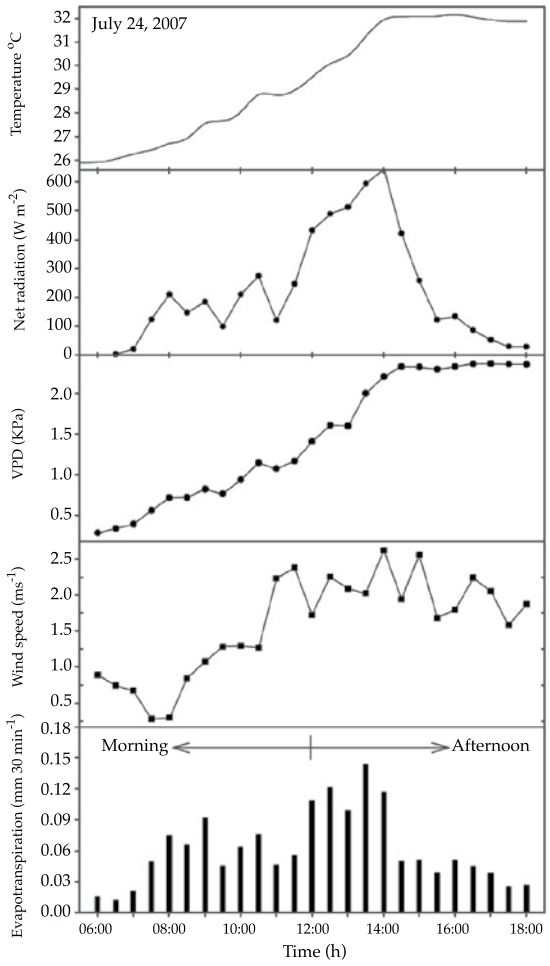

Figure 3. Environmental variation day 205 of 2007. The top figure shows the total evapotranspiration each half hour. The next down shows wind speed (m s^{-1}), followed by vapor pressure deficit (DPV) and the bottom shows net radiation (W m^{-2}).

pressure vapor deficit of 0.22 kPa before sunrise and a maximum of 2.37 kPa after noon, and remained in that range the rest of the afternoon (from 13:00 to 18:00 h).

Separation of the ET components

The isotopic compositions of the components of *ET*, δ_{Es} and δ_T, as well as the mixture (δ_{ET}) were determined. After calculating δ_{ES} with the Craig and Gordon model (equation (3)), the liquid water clearly became considerably poorer in heavy isotopes when evaporating (Table 2). The values of δ_L were -5.0 ± 0.48‰ of $\delta^{18}O$ for both periods and for the morning δ_{Es} was -26.6‰, while in the afternoon it was -25.2‰ of $\delta^{18}O$. δ_{Es} becomes significantly lighter than δ_L during both periods, with a difference in δ_{Es} between the two periods of 1.4‰ of $\delta^{18}O$. On average, the value of δ_{Es} was $\delta^{18}O$ = -25.9‰ (±0.69) during the afternoon of July 24, 2007. With the Keeling graphs, the isotopic composition of *ET* was obtained—δ_{ET} (Figure 4). The isotopic concentration of δ_{ET} was more enriched with heavy isotopes in the morning as compared to the afternoon, with values of 2.0‰ (±6.7) and -10.5 ‰ (±3.0) of $\delta^{18}O$, respectively (Table 3). The isotopic composition of *ET* on average during the entire day was -6.28‰ (±1.2) of $\delta^{18}O$.

No significant differences were observed with the isotopic modeling of foliar water in ISS and non-ISS (Figure 5). The isotopic composition of foliar water from the three

Cuadro 2. Parámetros involucrados en la determinación de la composición isotópica de la evaporación del suelo, aplicando el modelo de Craig y Gordon, 1965 (ecuación (2)). Todos los valores isotópicos son de $\delta^{18}O$.

Day 205 of 2007								
Period	***m***	***Ts* (°C)**	***Ts* (°K)**	δ_a **(‰)**	δ_L **(‰)**	α*	α_K	δ_{Es}
Morning	0.8	29.2	302.3	-15.6	-5.0	1.0090	1.0189	-26.6
Afternoon	0.6	34.9	308.1	-18.8	-5.0	1.0086	1.0189	-25.2

Where m is the relative soil moisture, *Ts* in °C and in °K; δ_a is the istopic composition of atmospheric vapor at the evaporation front of the soil (0.1 m); δ_L is the isotopic composition of water in the soil at 5 cm; α* is the equilibrium fractionation factor; α_K is the kinetic frationation factor and δ_{Es} is the isotopic composition of the evaporation from the soil.

Table 3. Statistics from Keeling Graphs shown in Figure 4.

Period	*n*	r^2	Gradient	*S*	Intercept δ_{ET}	*s*
Full Day	18	0.85	-190.85	20.50	-6.28	1.20
Morning	10	0.48	-348.30	127.36	2.04	6.74
Afternoon	8	0.57	-127.73	45.39	-10.45	2.94

Standard error of the regression of the intercept, gradient and squared error (r^2) were obtained. Confidence level of 95%.

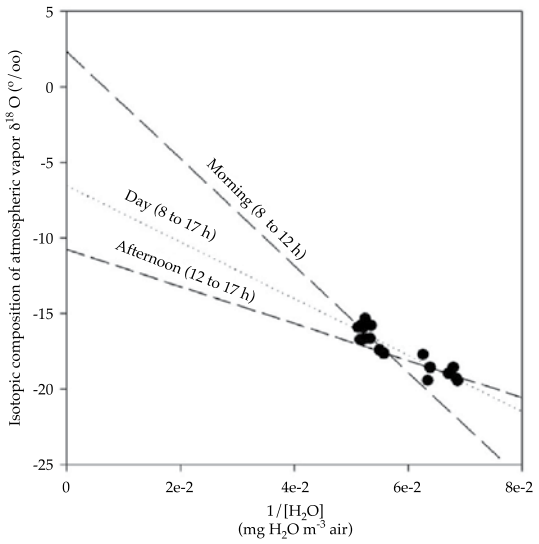

Figure 4. Keeling graphs for morning and afternoon periods for day 205 of 2007.

species was observed to vary by -0.5‰ of $\delta^{18}O$ during the first period, 6:00 am. Based on the comparison of the ISS and non-ISS models (Figure 5) and the arguments proposed by Xiao *et al*. (2012), the present study accepts that the transpiration of the three species studied occurs in the isotopic steady state. Therefore, the composition of the vegetation's original water source was used to calculate δ_T. To this end, a simple average was taken of the values observed in the three species (Table 4). This strategy resulted in a value of 7.1‰ (± 4.9) of $\delta^{18}O$, which regardless of its variability, is considerably more enriched in heavy isotopes than the isotopic composition of δ_{Es} (Table 5), where δ_T and δ_{Es} have different isotopic compositions.

It is notable that the values of δ_{ET} are different when considering the observations for the entire day, or only those for the morning or only the afternoon. For example, the values of δ_{ET} are closer to δ_T in the morning and more similar to δ_{Es} in the afternoon, while the full day period presents intermediate values (Figure 4). *T*/ET can be calculated based on these differences and the application of equation (1) (Table 5). In this case, the results of *T*/*ET* show a high contribution by ***T*** during the morning period, since this flow represents 86 ± 21% of the *ET*. T/ET falls considerably during the afternoon period, when *T* represents only 46 ± 9% of *ET*. If we take into account all the observations in the mixture graph to calculate δ_{ET}, in this ecosystem *T* would represent 59 ± 6% of the ET during this day.1

The depth of water that evapotranspired during the study day was obtained based on the continuous estimates of the EC of the flow of water (*ET*). The actual ET was 1.58 mm for the full day, 0.73 mm in the morning (5 to 12 h) and 0.85 mm in the afternoon (12 to 18 h; Figure 6). To obtain the depth of water transpired with the previous values, *T*/*ET* was multiplied by *ET*, resulting in 0.62 ± 0.15 mm for the morning period, 0.39 ± 0.08 mm for the afternoon and 0.93 ± 0.10 mm for the full daylight period.

Discussion

Direct measurements of ET using the Eddy covariance technique do not provide

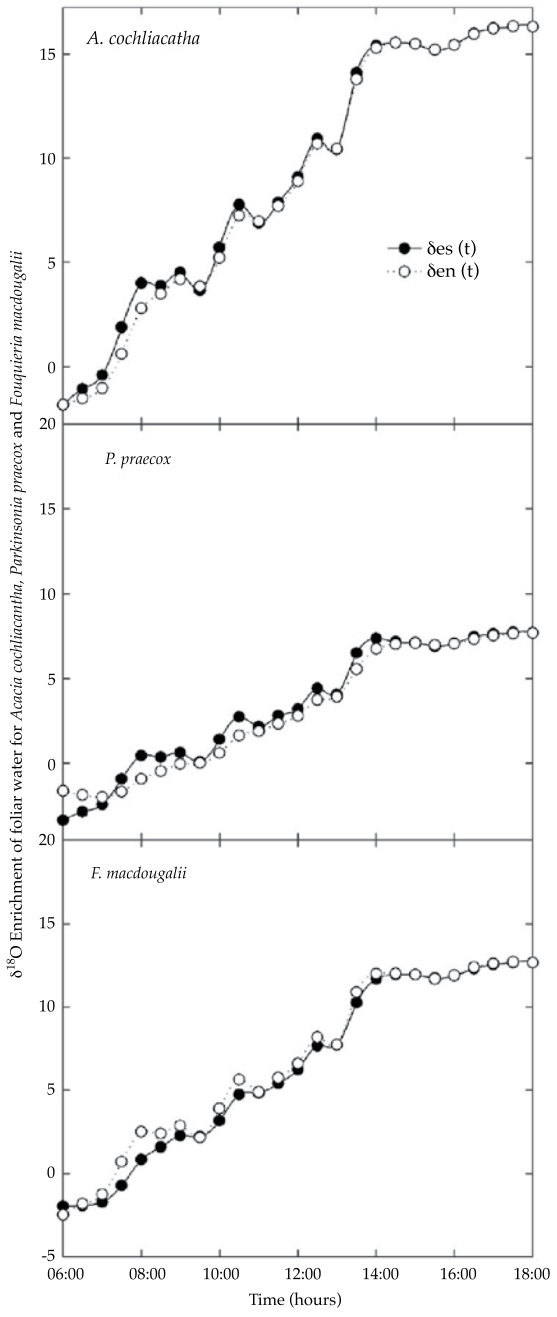

Figure 5. Daytime trend for isotope enrichment of foliar water; δ_{es} is the isotope enrichment calculated in steady isotopic state; δ_{en} is foliar enrichment in non-isotopic steady state conditions.

information about the relative contributions of evaporation from the soil and transpiration (Wilson *et al.*, 2001). Rather, identifying these proportions depends on functional

Table 4. Isotopic Composition of Water for Xylem in three species representative of xerophyllum shrub in Sonora.

Species	δs
Acacia cochliacantha	15.1
Parkinsonia praecox	8.0
Fouquieria macdougalii	-1.7
δ_{ir} (*ISS*)	7.1
s	4.86

Simple average of the isotopic compositions of water from xylem in three species representative of a semi-arid ecosystem in Sonora; *s* represents the standard error.

information from ecohydrological studies of ecosystems (Newman *et al.*, 2006). To advance in this area, stable water isotopes in combination with meteorological techniques to separate ET into its components serves as a useful tool to generate knowledge about ecohydrological processes (Yepez *et al.*, 2007). The isotopic fractionation that occurs in ecosystems during the transport of water from the liquid phase to a gas is the basis for separating ET into its components. The isotopic fractionation that occurs during the change in the physical stage (liquid-vapor) results in a more negative isotopic composition for evaporation from soil than for the liquid phase of the soil. Meanwhile, the absorption of water by roots during transpiration does not present isotopic fractioning and in stable conditions the isotopic composition of the flow of the transpiration can be equal to the original source of the plants' water (Table 5; Yakir and Sternberg, 2000). The objective of this work was to separate ET into its components in a semi-arid ecosystem in Sonora. The results show that the components of the ET flow can be separated based on stable water isotopes from different reservoirs (soil, plants and atmosphere) in a semi-arid ecosystem, in combination with direct measurements of ET. The isotopic analysis resulted in T/ET values which were comparable to estimates from

Table 5. Isotopic Components for Partitioning of Evapotranspiration into *T*/*ET*: isotopic compositions of evapotranspiration..

Period	δ_T	*s*	δ_{Es}	*S*	δ_{ET}	*s*	*T/ET (SSI)*	Iso-error
Day (8 to 17 h)	7.11	4.86	-25.93	0.69	-6.38	1.20	0.59	0.06
Morning (8 to 12 h)	7.11	4.86	-26.62	0.69	2.30	6.74	0.86	0.21
Afternoon (12 to 17 h)	7.11	4.86	-25.24	0.69	-10.50	2.94	0.46	0.09

Where δ_T is the isotopic composition of *T* of three representative species; δ_{Es} is the isotopic composition of *Es*; δ_{ET} is the isotopic composition of *ET*; *T*/*ET* is the proportion of T contributing to total *ET*; s is the standard error of the samples, and Iso-error is the isotopic error (Phillips and Gregg, 2001).

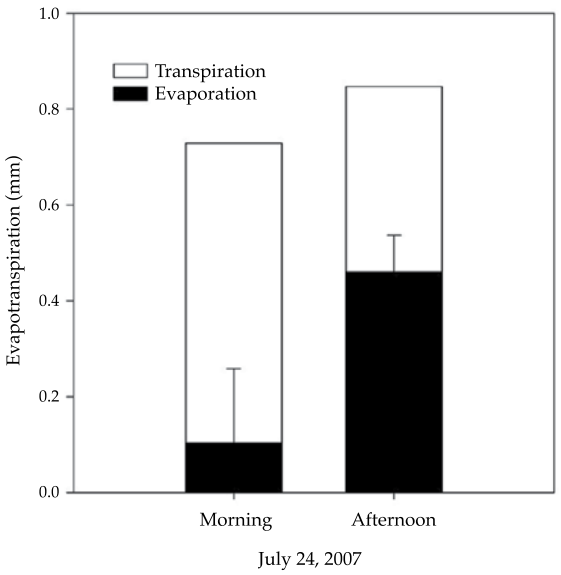

Figure 6. Total evapotranspiration partitioned into transpiration of the vegetation. The standard errors in the bars representing transpiration are based on variation in the sources, previously calculated with the Iso-error.

other ecosystems (Tables 1 and 5). Unlike these studies, the results herein suggest that the separation of ET using Keeling graphs offers a suitable temporal resolution for studying the possible variations in the proportions of the components of ET during a single day. For example, the results of this study shows that *T* is dominant during the morning period, while *Es* is more dominant in the afternoon (Figure 6). The values between 80 and 100% of T/ET during the morning suggest a high transpiration rate, which suggests high physiological activity by the vegetation during this period (Huxman *et al*., 2005). According to Figure 3, the environmental conditions present in the morning were less extreme for the vegetation to perform its physiological activities (Bond *et al*., 2007), whereas maximum radiation (644 W m2), temperature (32 °C) and PVD (2.4 kPa) occurred in the afternoon. The environmental conditions present in the afternoon may induce stress in the vegetation (Pockman and Sperry, 2000), such that the T/ET proportion falls considerably in the afternoon, since *E* represents up to 46% of ET and a flow of as much as 0.39 mm. In the afternoon, the high radiation affecting the soil in the ecosystem generates more heat and increases the temperature. Therefore, the flow due to evaporation from the soil is considerably higher (Vivoni *et al*., 2008), coinciding with a depression in the stomatal conductance of the plants. These differences between the morning and the afternoon have significant implications, helping to identify the periods limiting the environmental conditions that regulate the transport of vertical water through the different routes that contribute to ET, and providing elements to more accurately calculate the water balances of an ecosystem.

The present work reflects ecohydrological implications of the relationship between the biological part of land ecosystems and the water cycle; in particular, the influence of the dynamics between precipitation and ET on

the productivity of ecosystems (Yepez *et al*., 2007), as well as the influence of biological process on hydrological processes such as ET (Newman *et al*., 2006). It can be inferred from the results that high photosynthetic activity occurs during the morning when most of the water is transported by the flow of transpiration, since during stomatal aperture there is a significant balance between the loss of water and assimilated carbon dioxide (Nobel, 2009).

In arid and semi-arid ecosystems such as northern Mexico, the availability of water in the soil is the primary limiting resource for plants and microorganisms in the soil. Under arid conditions with high temperatures, evaporation can represent significant vertical flow (Zhao *et al*., 2011). The loss of water through this route controls the residence time of the water in the soil (Raz-Yaseef *et al*., 2010) and therefore the availability of water for vegetation and microorganisms (Yépez and Williams, 2009). This is important because both plants and the microorganisms in the soil use the water available in the soil for their metabolic activities. When water is available, the microorganisms perform processes such as the decomposition of organic matter and heterotrophic respiration, which emits large amounts of CO_2 into the atmosphere (Chapin *et al*., 2002). In this study, in the afternoon when *Es* is the largest component of *ET*, significant amounts of water would be lost to the atmosphere, which would not contribute to primary productivity, though it would contribute to the regulation of the respiration of the ecosystem.

Knowledge about ecohydrological processes makes it possible to improve the modeling of better scenarios (and validate them locally) in order to predict the response of ecosystems to climate change (Vivoni, 2012a; Vargas *et al*., 2012). For example, the study performed by Dominguez *et al.* (2008) uses climatological models to show how ET plays an important role in land ecosystems in the recirculation of water during the rainy season, since the amount of water evapotranspired in a region contributes to the following rainfalls or is redistributed to other regions. Nevertheless, the relative contribution of the components of ET in terms of its influence on atmospheric recirculation processes is not known. Understanding this water-soil-vegetation relationship is crucial to understanding the anthropogenic impact on the main flows in the water cycle (Jung *et al*., 2010). Technologies such as stable isotopes and continuous measurements of ET provide more information about the variation in *T* and *Es*. Discerning between hydrological processes controlled by the availability of water and ecosystem processes (primary-photosynthesis-cover vegetation-microbial activity) contributes to an understanding of this ecohydrological dynamic (Yepez *et al*., 2007). This provides valuable information for validating and constructing models of processes, making it possible to generate ecosystem response scenarios with a large temporal and spatial resolution without neglecting functioning mechanisms (Lawrence *et al*., 2011; Newman *et al*., 2006; Vivoni, 2012b; Méndez-Barroso *et al*., 2014). Including these observations in a monitoring network scheme would result in obtaining fundamental elements for managing water resources in accordance with its distribution and in the context of climate change (Vargas *et al*., 2013).

Suppositions and Observations regarding the ET Separation Model

Modeling the values of δ_{Es} with the Craig and Gordon (1965) approach can create difficulties with regard to the representation of the boundary layer of the evaporation front of the soil because of the complexity involved in identifying the front during wet

and dry periods (Konukcu *et al*., 2004; Yepez *et al*., 2005). This study was performed two days after an 11 mm rainfall event and 0.5 mm of precipitation occurred during the previous early morning hours. Therefore the soil humidity conditions in the surface maintained an evaporation front of 0.05 to 0.1 m.

It is important to mention that when determining δ_T, even when the isotopic composition of the transpiration of the vegetation at the level of the leaf can be measured, taking into account biological aspects that affect the foliar enrichment of the water (Dogmann *et al*., 1974; Farquhar and Cernusak, 2005), it has recently been argued that at the parcel or ecosystem level the supposition that transpiration occurs in an isotopic steady state (for example, $\delta_T = \delta_s$) is valid in some cases (Xiao *et al*., 2012). Measurements and models described at the leaf level have shown that the dynamics in the isotopic composition of the foliar water, which controls δ_T in highly changeable extreme conditions, could fall outside the isotopic steady state (Yakir and Sternberg, 2000; Farquahar and Cernusak, 2005). This could represent an error of up to 20% in the final calculation of T/ET (Yepez *et al*., 2005 y 2007). The results from the work herein from modeling several shrub species, in isotopic enrichment without considering the isotopic steady state using the Dogmann equation (1974), suggest that foliar isotopic enrichment occurred in the isotopic steady state (Figure 6) regardless of the changing environmental conditions observed during the study day. It could therefore be assumed with certainty that the isotopic composition of the water from a stem is a good representation of the isotopic composition of transpiration (Yakir y Sternberg, 2000; Lai *et al*., 2005; Yepez *et al*., 2007). Although the analysis of these observations is outside the scope of the present work, it is relevant because this behavior suggests that microphyll leaf species in semi-arid zones transpire in an isotopic steady state, thereby providing elements to simplify future studies.

The use of Keeling graphs contributes a large amount of information about the components of the flow of ET, since it assumes only two sources of contribution to the atmospheric parcel (Yakir and Sternberg, 2000) and also shows δ_{ET} to be similar to the isotopic composition of the predominant source (δ_{Es} or δ_T), according to different isotopic signatures. Nevertheless, this methodology is only a snapshot approximation of the isotopic composition of *ET* at the moment in which the air vapor samples are collected and only represents the integrated flow of *ET* (Yepez *et al*., 2005). In addition, this technique has not yet been used to examine the short-term dynamic and its application is limited to after a wet event occurs in the ecosystem (Williams *et al*., 2004). Knowledge about the isotopic variability of the components of ET is expected to improve with the advance of continuous measurements of atmospheric vapor using laser spectroscopy (Good et al., 2012).

Conclusions

The isotope analysis of water from different reservoirs (plant, soil and atmosphere) in an ecosystem using graphs of vapor isotope mixtures (Keeling graphs) makes it possible to identify the relative contributions to the evapotranspiration (*ET*) of the ecosystem by the vegetation's transpiration (*T*) and evaporation from the soil (*Es*). This separation is possible because δ_{Es} and δ_T and the mixture values δ_{ET} have different isotopic signatures that provide a balance of masses. In the semi-arid scrublands of Sonora, the separation of *ET* indicated that transpiration during the morning contributed to roughly 86 ± 21% of the *ET* on a rainy summer day, while the

contribution by *Es* and *T* was similar in the afternoon, each one representing 50% of the total *ET*. This first estimate of *T*/*ET* in this ecosystem suggests that the affect of the vegetation on the recirculation of water is relevant. This information can provide elements to better understand the effect of the variation in order to predict the possible response patterns of ecosystems to climate change. It also clearly indicates that the use of stable isotopes in ecohydrological studies represents a new tool to contribute to knowledge about the hydrological cycle of an ecosystem.

Acknowledgements

This work was made possible by financing from the Conacyt project (CB2009- 132188), PROMEP ITSON-503 and PROFAPI-ITSON 2013. We are very thankful to the students who helped to collect the samples and data during the 2007 field campaign, especially Lluvia Vargas for assistance with the calculation of *W* for equation (4). Finally, thank you to Conacyt for support through the postgraduate grant 232184 provided to Tonantzin Tarin.

Received: 15/08/12
Accepted: 28/08/13

References

ADAMS, D.K. and COMRIE, A.C. The North American Monsoon. *Bulletin of the American Meteorological Society*. Vol. 78, No. 10, 1997, pp. 2197-2213.

BALDOCCHI, D., FALGE, E., GU, L., OLRSON, R., HOLLINGER, D., RUNNING, S., ANTHONI, P., BERNHOFER, CH., DAVIS, K., EVANS, R., FUENTES, J., GOLDSTEIN, A., KATUL, G., LAW, B., LEE, X., MALHI, Y., MEYERS, T., MUNGER, W., OECHEL, W., PAW, U.K., PILEGAARD, K., SCHMID, P., VALENTINI, R., VERMA, S., VESALA, T., WILLSON, K., and WOFSY, S. FLUXNET: A New Tool to Study the Temporal and Spatial Variability of Ecosystem-Scale Carbon Dioxide, Water Vapor, and Energy Flux Densities. *Bulletin of the American Meteorological Society*. Vol. 82, No. 11, 2001, pp. 2415-2434.

BALDOCCHI, D.D. Assessing the Eddy Covariance Technique for Evaluating Carbon Dioxide Exchange Rates of Ecosystems: Past, Present And Future. *Global Change Biology*. Vol. 9, 2003, pp. 479-492.

BIJOOR, N.S., PATAKI, D.E., ROCHA, A.V., and GOULDEN, M.L. The Application of $\delta^{18}O$ and δD for Understanding Water Pools and Fluxes in a Typha Marsh. *Plant, Cell & Environment*. Vol. 34, No. 10, 2011, pp. 1761-1775.

BOND, B.J., MEINZER, F.C., and BROOKS, J.R. *How Trees Influence the Hydrological in Forest Ecosystems. Hydroecology and Echohydrology: Past, Present and Future*. Ciudad Ltd, Chichester, UK: John Wiley & Sons, 2007, pp. 7-35.

BRUNEL, J.P., WALKER, G.R., DIGHTON, J.C., and MONTENY, B. Use of Stable Isotopes of Water to Determine the Origin of Water Used by the Vegetation and to Partition Evapotranspiration. A Case Study from HAPEX-Sahel. *Journal of Hydrology*. Vol. 188, No. 189, 1997, pp. 466-481.

CAPPA, C.D., HENDRICKS, M.B., DEPALO, D.J., COHEN, R.C. Isotopic Fraction of Water during Evaporation. *Journal of Geophysical Research*. Vol. 108, 2003, pp. 4525.

CHAPIN, F.S., MATSON, P.A., and MOONEY, H.A. *Principles of Terrestrial Ecosystem Ecology*. New York: Springer-Verlag, Inc., 2002, pp. 123-149.

CRAIG, H. and GORDON, L.I. Deuterium and Oxygen-18 Variations in the Ocean and the Marine Atmosphere. In: Tongiori, E. (Ed.). *Proceedings of the Conference on Stable Isotopes in Oceanographic Studies and Paleotemperatures*. Laboratory of Geology and Nuclear Science, Pisa, 1965, pp. 9-130.

DOGMANN, G., NORNBERG, H.W., FORSTEL, H., and WAGENER, K. On the Enrichment of H218O in the Leaves of Transpiring Plants. *Radiat Environmental Biophysics*. Vol. 60, 1974, pp. 41-52.

DOMINGUEZ, F., KUMAR, P., and VIVONI, E.R. Precipitation Recycling Variability and Ecoclimatological Stability- A Study using NARR Data. Part II: North American Monsoon Region. *Journal of Climate*. Vol. 21, No. 20, 2008, pp.5187.

EHLERINGER, J.R., RODEN, J., and DAWSON, T.E. *Assessing Ecosystem-Level Water Relations through Stable Isotope Ratio Analyses. Methods in Ecosystem Science*. New York: Springer, 2000, pp. 181-198.

FARQUHAR, G.D. and CERNUSAK, L.A. On the Isotopic Composition of Leaf Water in the Non-Steady State. *Functional Plant*. Vol. 32, 2005, pp. 293-303.

FERRETTI, D.F., PENDALL, E., MORGAN, J.A., NELSON, J.A., LECAIN, D., and MOSIER, A.R. Partitioning Evapotranspiration Fluxes from a Colorado Grassland Using Stable Isotopes: Seasonal Variations and Ecosystem Implications of Elevated Atmospheric CO_2. Ratio. *Plant and Soil*. Vol. 254, 2003, pp. 291-303.

GOOD, S., SODERBERG, K., WANG, L., and CAYLOR, K. Uncertainties in the Assessment of the Isotopic Composition of Surface Fluxes: A Direct Comparison of Techniques using Laser-Based Water Vapor Isotope Analyzers. *Journal of Geophysical Research*. Vol. 117, 2012, D1530, doi:10.1029/2011JD017168.

GRIFFIS, T.I. Tracing the Flow of Carbon Dioxide and Water Vapor between the Biosphere and Atmosphere: A Review of Optical Isotope Techniques and their Application. *Agricultural and Forest Meteorology*. Vol. 174, No. 175, 2013, pp 85-109.

HELLIKER, B.R., RODEN, J.S., COOK, C., EHLERINGER, J.R. A Rapid and Precise Method for Samplig and Determining the Oxygen Isotope Ration of Atmospheric Water Vapor. *Rapad. Comun. Mass Spectr*. Vol. 16, 2002, pp.929-932.

JUNG, M., REICHSTEIN, M., CIAIS, P., SENEVIRATNE, S., SHEFFIELD, J., GOULDEN, M.L., BONAN, G., CESCATTI, A., CHEN, J., JEU, R., DOLMAN, J., EUGSTER, W., GERTEN, D., GIANELLE, D., GOBRON, N., HEINKE, J., KIMBALL, J., LAW, B.E., MONTAGNANI, L., MU, ., MUELLER, B., OLESON, K., PAPALE, D., RICHARDSON, A.D., ROUPSARD, O., RUNNING, S., TOMELLERI, E., VIOVY, N., WEBER, U., WILLIAMS, C., WOOD, W., ZAEHLE, S., and ZHANG, K. Recent Decline in the Global Land Evapotranspiration Trend due to Limited Moisture Supply. *Nature*. Vol. 467, 2010, pp. 951-954.

KONUKCU, F., ISTANBULLUOGLU, A., and KOCAMAN, I. Determination of Water Content in Drying Soils: Incorporating Transition from Liquid Phase to Vapor Phase. *Australian Journal of Soil Research*. Vol. 42, 2004, pp. 1-8.

LAI, C.T., EHLERINGER, J.R., BOND, B.J., and PAW, U.K.T. Contributions of Evaporation, Isotopic Non-Steady State Transpiration and Atmospheric Mixing on the $\delta^{18}O$ of Water Vapor in Pacific Northwest Coniferous Forests. *Plan, Cell and Environment Ltd.* Vol. 29, No. 1, 2005, pp. 77-94.

LAWRENCE, D.M., OLESON, K.W., FLANNER, M.G., THORNTON, P.E., SWENSON, S.C., LAWRENCE, P.J., ZENG, X., YANG, Z.L., LEVIS S., SAKAGUCHI, K., BONAN, G.B., and SLATER, A.G. Parameterization Improvements and Functional and Structural Advances in Version 4 of the Community Land Model. *Journal of Advances in Modeling Earth Systems*. Vol. 3, 2011, doi: 10.1020/2011MS000045.

MAJOUBE, M. Fractionnement en oxygene-18 et en deuteriumentre l'eau et sa vapaeur. *J. of. Chim. Phys*. Vol. 68, 1971, pp. 1423-1436.

MANZONI, S., VICO, G., PORPORATO, A., KATUL, G. Biological Constraints on Water Transport in the Soil-Plant-Atmosphere System. *Advances in Water Resources*. Vol. 51, 2013, pp. 292-304.

MÉNDEZ-BARROSO, L.A, VIVONI, E.R., ROBLES-MORUA, A., YEPEZ, E.A., RODRIGUEZ, J.C., WATTS, C.J., GARATUZA-PAYAN, J., and SAIZ-HERNANDEZ, J.A. A Modeling Approach Reveals Differences in Evapotranspiration and its Partitioning in Two Semiarid Ecosystems in Northwest Mexico. *Water Resources Research*. Vol. 15, 2014, doi:10.1002/2013WR014838.

MONCRIEFF, J.B., JARVIS, P.G., VALENTINI, R., CANOPY FLUXES. In SALA, O.E., JACKSON, R.B., MOONEY, H.A., HOWARTH, R.W. (Editors). *Methods in Ecosystem Science*. New York: Springer-Verlag, 2000, pp. 161-180.

MOREIRA, M., STERNBERG, L., MARTINELLI, L., VICTORIA, R.L., BARBOSA, E.M., BONATES, L.C.M., and NEPSTAD§, D.C. Contribution of Transpiration to Forest Ambient Vapor based on Isotopic Measurements. *Global Change Biology*. Vol. 3, No. 5, 1997, pp. 439-450.

NEWMAN, B.D., WILCOX, B.P., ARCHER, S.R., BRESHEARS, D.D., DAHM, C.N., DUFFY, C.J., MCDOWELL, N.G., PHILLIPS, F.M., SCANLON, B.R., and VIVONI, E.R. Ecohydrology of Water-Limited Environments: A Scientific Vision. *Water Resources Research*. Vol. 42, No. 6, 2006, pp. 1-15.

NOBEL, P.S. *Physicochemical and Environmental Plant Physiology*. 4th Edition. San Diego: Academic Press, 2009.

PATAKI, D.E., EHLERINGER, J.R., FLANAGAN, L.B., YAKIR, D., BOWLING, D.R., STILL, C.J., BUCHMANN, N., KAPLAN, J.O., and BERRY, J.A. The Application and Interpretation of Keeling Plots in Terrestrial Carbon Cycle Research. *Global Biogeochemical Cycles*. Vol. 17, No. 1, 2003, pp. 1-14.

PHILLIPS, D.L. and GREGG, J.W. Uncertainty in Source Partitioning using Stable Isotopes. *Oecologia*. Vol. 127, 2001, pp. 171-179.

PLAUT J.A., YEPEZ, E.A., HILL, J., PANGLE, R., JOHNSON, J., SPERRY, J.S., POCKMAN, W.T., and McDOWELL, N.G. Hydraulic Limits on Water Use under Experimental Drought in a Piñon-Juniper Woodland. *Plant Cell & Environment*. Vol. 9, 2012, pp. 1601-1617.

POCKMAN, W.T. and SPERRY, J.S. Vulnerability to Xylem Cavitation and the distribution of Sonora Desert Vegetation. *American Journal of Botany*. Vol. 87, No. 9, 2000, pp. 1287-1299.

RAZ-YASEEF, N., ROTENBER, E., and YAKIR, D. Effect of Spatial Variations in Soil Evaporation caused by Tree Shading on Water Flux Partitioning in a Semi-Arid Pine Forest. *Agricultural and Forest Meteorology*. Vol. 150, No. 1, 2010, pp. 454-462.

REYES-GARCIA, C., ANDRADE, J.L., SIMÁ, J.L., US-SANTAMARIA, R., and JACKSON, P.C. Sapwood to Heartwood Ratio Affects Whole-Tree Use in Dry Forest Legume and Non-Legume Trees. *Trees*, 2012, doi: 10.1007/s00468-012-0708-5.

ROTHFUSS, Y., BIRON, P., BRAUD, I., CANALE, L., DURAND, J.L., GAUDET, J.D., RICHARD, P., VAUCLIN, M., and BARIAC, T. Partitioning Evapotranspiration Fluxes Into Soil Evaporation and Plant Transpiration Using Water Stable Isotopes under Controlled Conditions. *Hydrological Processes*. Vol. 24, No. 22, 2010, pp. 3177-3194.

SHARP, Z. Principles of Stable Isotope Geochemistry. USA: Pearson Prentice Hall TM, 2007.

SUTANTO, S.J. Partitioning of Evaporation into Transpiration, Soil Evaporation and Interception:

A Combination of Hydrometric Measurements and Stable Isotope Analyses. *Hydrology and System Sciences Discussion*. Vol. 9, 2012, pp. 3657-3690.

VARGAS, R., LOESCHER, H.W., ARREDONDO, T., HUBER-SANNWALD, E., LARA-LARA, R., and YEPEZ, E.A. Opportunities for Advancing Carbon Cycle Science in Mexico: Towards a Continental Scale Understanding. *Environmental Science and Policy*. Vol. 21, 2012, pp. 84-93.

VARGAS, R., YÉPEZ, E.A., ANDRADE, J.L., ANGELES, G., ARREDONDO, T., CASTELLANOS, A.E., GARATUZA-PAYAN, J., GONZÁLEZ DEL CASTILLO, E., OECHEL, W., RODRÍGUEZ, J.C., SÁNCHEZ-AZOFEIFA, A., VIVONI, E.R., and WATTS, C.J. Progress and Opportunities for Measurements of Water and Greenhouse Gas Fluxes in Mexican Ecosystems: MexFlux. *Atmosfera*. Vol. 26, No. 3, 2013, pp. 84-93.

VIVONI, E.R., MORENO, H.A., MASCARO, G., RODRIGUEZ, J.C., WATTS, C.J., GARATUZA-PAYAN, J., and SCOTT, R.L. Observed Relation between Evapotranspiration and Soil Moisture in the North American Monsoon Region. *Geophysical Research Letters*. Vol. 35, 2008, L22403.

VIVONI, E.R. Spatial Patterns, Processes and Predictions in Ecohydrology: Integrating Technologies to Meet the Challenge. *Ecohydrology*. Vol. 5, No. 3, 2012a, pp. 235-241.

VIVONI, E.R. Diagnosing Seasonal Vegetation Impacts on Evapotranspiration and its Partitioning at the Catchment Scale during SMEX04-NAME. *Journal of Hydrometeorology*. Vol. 13, 2012b, pp. 1631-1638.

WANG, L., CAYLOR, K.K., VILLEGAS, J.C., BARRON-GAFFORD, G.A., BRESHEARS, D.D., HUXMAN, T.E. Partitioning Evapotranspiration Across Gradients of Woody Plant Cover: Assessment of a Stable Isotope Technique. *Geophysical Research Letters*. Vol. 37, No. 9, 2010, pp. 1-7.

WANG, K. and DICKINSON, R.E. A Review of Global Terrestrial Evapotranspiration: Observation, Modeling, Climatology, and Climatic Variability. *Reviews of Geophysics*. Vol. 50, 2012, RG2005, doi: 10.1029/2011RG000373.

WANG, X.F. and YAKIR, D. Using Stable Isotopes of Water in Evapotranspiration Studies. *Hydrological Processes*. Vol. 15, No. 8, 2000, pp. 203-1421.

WATTS, C.J., SCOTT, R.L., GARATUZA-PAYAN, J., RODRIGUEZ, J.C., PRUEGER, J.H., KUSTAS, W.P., and DOUGLAS, M. Changes in Vegetation Condition and Surface Fluxes during NAME 2004. *Journal of Climate*. Vol. 20, No. 9, 2007, pp. 1810-1820.

WENNINGER, J., BEZA, D.T., and UHLENBROOK, S. Experimental Investigations of Water Fluxes within the Soil-Vegetation-Atmosphere System: Stable Isotope Mass-Balance Approach to Partition Evaporation and Transpiration. *Physics and Chemistry of the Earth*. Parts A/B/C. Vol. 35, No. 13-15, 2010, pp. 565-570.

WEST, A.G., PATRICKSON, S.J., and EHLERINGER, J.R. Water Extraction Times for Plant and soil Materials used in Stable Isotope Analysis. *Rapid Communication in Mass Spectrometry*. Vol. 20, 2006, pp. 1317-1321.

WILCOX, B.P., SEYFRIED, M.S., and BRESHEARS, D.D. The Water Balance on Rangelands. In B.A. Stewart and T.A. Howell (editors). *Encyclopedia of Water Science*. New York: Marcel Dekker, 2003, pp. 791-794.

WILLIAMS, D.G., CABLEB, W., HULTINEB, K., HOEDJESC, J.C.B., YEPEZ, E.A., SIMONNEAUXA, V., ER-RAKID, S., BOULETA, G., BRUINC, DE H.A.R., CHEHBOUNIA, A., HARTOGENSISC, O.K., and TIMOUKA, F. Evapotranspiration Components Determined by Stable Isotope, Sap Flow and Eddy Covariance Techniques. *Agricultural and Forest Meteorology*. Vol. 125, No. 3-4, 2004, pp. 241-258.

WILSON, K.B., HANSON, P.J., MULHOLLAND, P.J., BALDOCCHI, D.D., and WULLSCHLEGER, S.D. A Comparison of Methods for Determining Forest Evapotranspiration and its Components: Sap-flow, Soil Water Budget, Eddy Covariance and Catchment Water Balance. *Agricultural and Forest Meteorology*. Vol. 106, 2001, pp. 153-158.

XIAO, W., LEE, X., WEN, X., SUN, X., and ZHANG, S. Modeling biobphysical Control Son Canopy Foliage Water 18O Enrichment in Wheat and Corn. *Global Change Biology*. 2012, doi: 10.1111/j.13 *et al*., 2012.02648.x.

XU, Z., YANG, H., LIU, F., AN, S., CUI, J., WANG, Z., and LIU, S. Partitioning Evapotranspiration Flux Components in a Subalpine Shrubland based on Stable Isotopic Measurements. *Botanical Studies*. Vol. 49, 2008, pp. 351-361.

YAMANAKA, T. and TSUNAKAWA, A. Isotopic Signature of Evapotranspiration Flux and its use for Partitioning Evaporation/Transpiration Components. *Water*. Vol. 3, 2007, pp. 11-21.

YAKIR, D. and STERNBERG, L.S. The Use of Stable Isotopes to Study Ecosystem Gas Exchange. *Oecologia*. Vol. 123, 2000, pp. 297-311.

YEPEZ, E.A., WILLIAMS, D.G., SCOTT, R.L., and LIN, G. Partitioning Overstory and Understory Evapotranspiration in a Semi-Arid Wood-Land Ecosystem from the Isotopic Composition of Water Vapor. *Agricultural and Forest Meteorology*. Vol. 119, 2003, pp. 53-68.

YEPEZ, E.A., HUXMAN, T.E., IGNACE, D.D., ENGLISH, N.B., WELTZIN, J.F., CASTELLANOS, A.E., and WILLIAMS, D.G. Dynamics of Transpiration and Evaporation following a Moisture Pulse in Semiarid Grassland: A Chamber-Based Isotope Method for Partitioning Flux Components. *Agricultural and Forest Meteorology*. Vol. 132, No. 3-4, 2005, pp. 359-376.

YEPEZ, E.A., SCOTT, R.L., CABLE, W.L., and WILLIAMS, D.G. Intraseasonal Variation in Water and Carbon Dioxide Flux Components in a Semiarid Riparian Woodland. *Ecosystems*. Vol. 10, 2007, pp. 1100-1115.

YEPEZ, E.A. and WILLIAMS, D.G. *Precipitation Pulses and Ecosystem Carbon and Water Exchange in Arid and Semi-Arid Environments. Perspectives in Biophysical Plant Ecoplysiology: A Tribute to Park S. Nobel*. México, DF: UNAM, 2009, pp. 337-361.

ZHAO, Y., PETH, S., HALLETT, P., WANG, X., GIESE, M., GAO, Y., and HORN, R. Factors Controlling the Spatial Patterns of Soil Moisture in a Grazed Semi-Arid Steppe Investigated by Multivariate Geostatistics Group. Vol. 48, 2011, pp. 36-48.

Institutional Address of the Authors

Mtra. Tonantzin Tarin
Dr. Enrico A. Yépez
Dr. Jaime Garatuza-Payán

Departamento de Ciencias del Agua y del Medio Ambiente
Instituto Tecnológico de Sonora
5 de Febrero 818 Sur, Colonia Centro
85000 Ciudad Obregón, Sonora, México
Teléfono: +52 (644) 4100 900, extensiones 2107, 1328
tonantzin.tarin@gmail.com
enrico.yepez@itson.edu.mx
jaime.garatuza@itson.edu.mx

Dr. Christopher J. Watts

Departamento de Física
Universidad de Sonora
Blvd. Encinas y Rosales, Colonia Centro
83000 Hermosillo, Sonora, México
Teléfono: +52 (662) 2592 108
cwatts@correo.fisica.uson.mx

Dr. Julio C. Rodríguez

Departamento de Agricultura y Ganadería
Universidad de Sonora
Blvd. Encinas y Rosales, Colonia Centro
83000 Hermosillo, Sonora, México
Teléfono: +52 (662) 2130 954
Fax: +52 (662) 2138 006

Dr. Enrique R. Vivoni
Dr. Luis A. Méndez-Barroso

School of Earth and Space Exploration
Arizona State University
Tempe, AZ 85287, USA
Teléfono: +1 (480) 727 3575
vivoni@asu.edu
luis.mendez-barroso@asu.edu

Click here to write the autor

Removal of Solids from Wastewater from the Fishmeal Industry

• Dulce María Arias-Lizárraga* • Evaristo Méndez-Gómez •
Instituto Tecnológico de Mazatlán, México
*Autor de correspondencia

Abstract

ARIAS-LIZÁRRAGA, D.M. & MÉNDEZ-GÓMEZ, E. Removal of Solids from Wastewater from the Fishmeal Industry. *Water Technology and Sciences* (in Spanish). Vol. V, No. 3, May-June, 2014, pp. 117-125.

The fishmeal company Maz Industrial S.A. de C.V., located in Mazatlan, Sinaloa, Mexico pours its wastewater into the Urías estuary. This effluent has a high organic matter load and contains proteins, fats and oils, resulting in an environmental impact and economic loss from not being reused. As much as 11.44 t d^{-1} which could be reused in production is wasted. In order to evaluate the removal of organic matter during the pre-treatment phase of these wastewaters, coagulation, flocculation and sedimentation tests were conducted using natural and innocuous organic polymers, chitosan as a primary coagulant and sodium alginate and tannic acid to assist in anionic coagulation. With 300 mgl^{-1} of chitosan and 20 mgl^{-1} of sodium alginate, 91.84% of total suspended solids (TSS) was removed and 90.83% of volatile suspended solids (VSS). With 200 mgl^{-1} of chitosan and 20 mgl^{-1} of tannic acid, 97.78% TSS was removed and 97.79% of volatile suspended solids (VSS). Given the removal efficiencies obtained in this investigation and considering that the precipitate recovered using these biopolymers is not toxic, it is possible to scale the recovery of organic matter to the industry level for reuse in the production of fishmeal, facilitate conventional biological treatment of the organic matter remaining in the pretreated wastewater and reduce the environmental impact of discharges with a high organic load.

Keywords: Removal, fishmeal industry, coagulation, chitosan, tannic acid, sodium alginate.

Resumen

ARIAS-LIZÁRRAGA, D.M. & MÉNDEZ-GÓMEZ, E. Remoción de sólidos en aguas residuales de la industria harinera de pescado empleando biopolímeros. Tecnología y Ciencias del Agua. *Vol. V, núm. 3, mayo-junio de 2014, pp. 117-125.*

La industria productora de harina de pescado Maz Industrial S.A. de C.V, ubicada en Mazatlán, Sinaloa, México, vierte sus aguas residuales hacia el estero de Urías con una alta carga de materia orgánica, que contiene proteínas, grasas y aceites, lo cual, además del impacto ambiental que ocasiona, representa una pérdida económica por no recuperarla, llegando a desperdiciar hasta 11.44 t d^{-1}, que puede retornarse a la producción. A fin de evaluar la remoción de materia orgánica en la fase de pretratamiento de dichas aguas residuales, se hicieron pruebas de coagulación, floculación y sedimentación, utilizando polímeros orgánicos naturales e inocuos; quitosán como coagulante primario, y alginato de sodio y ácido tánico como ayudantes de coagulación aniónicos. Con la mezcla de 300 mgl^{-1} de quitosán con 20 mgl^{-1} de alginato de sodio se logró una remoción de 91.84% de sólidos suspendidos totales (SST) y 90.83% de sólidos suspendidos volátiles (SSV) y con la mezcla 200 mgl^{-1} de quitosán con 20 mgl^{-1} de ácido tánico se obtuvieron remociones del 97.78% de SST y 97.79% de SSV. Con las eficiencias de remoción conseguidas en esta investigación y tomando en cuenta que el precipitado sedimentado con el empleo de estos biopolímeros no es tóxico, es posible escalar la recuperación de la materia orgánica en el ámbito industrial, para retornarla hacia el tren de elaboración de harina de pescado, facilitar el tratamiento biológico convencional del remanente de materia orgánica en el agua residual pretratada y reducir el impacto ambiental que ocasiona la descarga con alta carga orgánica.

Palabras clave: *remoción, industria harinera de pescado, coagulación, quitosán, ácido tánico, alginato de sodio.*

Introduction

The prime material used by the fishmeal industry in Mazatlan, Sinaloa Mexico includes sardines, anchovies, tuna remains, tilapia, northern kingfish (*Menticirrhus saxatilis*) and other fish and shrimp scraps. For each 1000 kg of the prime material processed, 212 kg of fishmeal is produced, and 108 kg of oil and 680 kg are discarded through wastewater (Cabrera, 2002). Wastes from the production of fishmeal are the most questionable

environmental material in terms of the large amount of pollution created (Galarza *et al*., 2001). Different wastewater effluents are generated through its production, such as water from pumping, typically brackish, blood water or stickwater, or condensed and cooling water (Cabrera, 2002; Méndez, 2009) —effluents containing high amounts of protein, fats and oils which are eventually discarded with poor or no treatment and discharged into receptor bodies. One such case is the Maz Industrial S.A. de C.V. plant, which is the subject of this study. The liquid wastes from this plant end up in Urias estuary in Mazatlan, Sinaloa where it has altered the water column and the sediment and caused physical, chemical, biological and ecological imbalances (Ahumada *et al*., 2004). Some of the effects on the receptor body include changes in salinity, decreased dissolved O_2, increased biochemical oxygen demand (BOD_5), increased nutrients, high sulfur and ammonium loads and increased temperature. Together, these generate eutrophication, causing death of benthic, plankton and nekton organisms (Pacheco *et al*., 2009).

Three steps are involved in the treatment of wastewater, including those produced by the fishmeal industry.

1. Pretreatment. In this stage, sedimented and suspended solids are removed through screens, sand filters, settlers, oil and fat traps, flotation and on occasion sedimentation with coagulation-flocculation. The latter process is commonly used to increase the sedimentation of suspended particles.
2. Secondary treatment. In this stage, biological processes are usually applied with microorganisms that use organic pollutants as food (Sumathi, 2004). Chemical or physical digestion may also be used, although the waste resulting from their application generates new pollutants.
3. Tertiary treatment. A variety of chemical, electrochemical, physical and biological processes can be applied to remove untreated substances remaining from the second stage, including recalcitrant substances (Rodríguez *et al*., 2006).

The coagulation and flocculation process typically applied in the pretreatment stage consists of destabilizing suspended particles, provoking them to collide, adhesion, increased size, agglutination, increased density and, as a consequence, sedimentation. After the particles are sedimented, they can be easily removed (Metcalf, Eddy, Inc., 2003). A large variety of organic and inorganic substances can be used as coagulants and flocculants in the pretreatment of the wastewater. Those most used are alum (aluminum sulfate) and ferric salts (ferric chloride). In the case of inorganic substances, synthetic polymers (usually polyacrylamides) are most commonly used because they are easily obtained in the market and are low cost (Lafleur *et al*., 2008). Nevertheless, when using these substances, the resulting sediment becomes toxic, as occurs with the use of aluminum salts (aluminum sulfate) and ferric salts (ferric chloride). This prevents the use of the sedimented organic matter since it can cause cancer in animals fed with meals containing such substances (ATSDR, 2008), results in the accumulation of metal in the food chain and contributes to the development of Alzheimer in humans (Fuentes *et al*., 2008; Linn *et al*., 2008) if recovered and returned to the meal production process and added to foods. On the other hand, if the organic matter is not used and is disposed of in receptor bodies, it becomes an environmental pollution problem and an economic loss for the industry.

A good substitute for the toxic polymers currently used for the sedimentation of the

organic matter present in this type of water may be natural polymers derived from chitin, such as chitosan (poli [B-(1,4)-2- amino-2-desoxi-D-glucopiranosa]). This substance is abundant in arthropod animals, including crustaceans, and shrimp in particular (Mohd *et al*., 2008). Chitosan has cationic characteristics and therefore its molecules bond to the negatively charged surfaces through ionic bonds or hydrogen bridges (Mohd y Puteh, 2007). As a result, it has been widely used as a coagulant (Mohd *et al*., 2008). Chitosan is innocuous and biodegradable. It is commercially manufactured from the deacetylation Chitin extracted from the shells of shrimp. Another very well known natural polymer which is used industrially is sodium alginate, an anionic polyelectrolyte extracted from certain brown algae species (Aguilar *et al*., 2002), primarily *Ascophyllum, Laminaria* (Europe), *Lessonia* (South America), *Ecklonia* (South Africa), *Durvillaea* (Australia and Chile) and *Macrocystis* (California and Baja California) (McHugh, 2002). Sodium alginate is considered non-toxic and has a large number of applications both in the pharmaceutical as well as food industries. It is also efficient for the flocculation of suspended particles in aqueous solutions and is therefore frequently used in the pretreatment of wastewater (Kirchmer *et al*., 1975). Another group of non-toxic natural polymers used in low concentrations are tannins, polyphenol substances produced by superior plants which have the ability to form coagulant complexes with proteins, polysaccharide, nucleic acids and steroids (Marroquín, 2008). They have therefore received a good amount of attention for use in wastewater treatment because of their anionic behavior in solution and their high capacity for coagulation, flocculation and sedimentation (Linn *et al*., 2008).

In addition to being innocuous, biodegradable and having a large number of applications, chitosan, alginates and tannins can be used as coagulants and flocculants in water containing organic and inorganic waste. They have therefore been used widely in the pretreatment of industrial wastewater, food packaging (Roussy *et al*., 2005), production of palm oil (Sumathi, 2004; Mohd and Puteh, 2007), textiles (Mohd *et al*., 2008), paper manufacturing (Linn *et al*., 2008), the oil industry (Razali *et al*., 2010), food processing (Bough and Landes, 1979; Markham *et al*., 1990) and in the fishing industry (Wibowo *et al*., 2006; Pacheco *et al*., 2009; Méndez, 2009) where no sediment obtained added toxicity.

The present investigation proposed evaluating the feasibility of treating wastewater from the fishmeal industry with innocuous organic and biodegradable polymers such as chitosan.

The contribution after this study lies in the economic feasibility of the integral use of shells from shrimp, which are used in large quantities by this type of company. Chitosan can be produced from these, which in small quantities enables commercializing the excess and thereby acquiring a coagulation aid — either sodium alginate or tannic acid.

The objective of this investigation was to evaluate the efficiency of removing total and volatile suspended solids by applying chitosan as a primary coagulant and sodium alginate or tannic acid as coagulation aids in the pretreatment of wastewater from the fishmeal industry.

Methodology

This study evaluated the ability of chitosan combined with sodium alginate or tannic acid to enable coagulation and sedimentation of organic matter contained in wastewater from the fishmeal company Maz Industrial, S.A. de C.V . The pH was controlled at 6.5 with 5 M sodium hydroxide or 5 M Hydrochloric acid and the temperature was maintained at

42 °C (Mohd and Puteh, 2007).

The optimal dosage of the coagulant (chitosan) was first determined by measuring the size of the flocculant, since this is a determinant of the efficiency of the sedimentation of suspended particles. If an overdosage occurs of the coagulant or the particles they become unstable, resulting in deficient flocculation (Linn *et al*., 2008).

To evaluate the flocculant size, chitosan dosages of 100, 200, 300, 400, 500 and 600 mgl^{-1} were evaluated in a conventional six-paddle jar test apparatus (Phipps & Bird, Inc), with 1 liter of homogenized samples of wastewater taken from the Maz Industrial company. The sample with the coagulant was mixed using rotation at a velocity of 250 rpm for 2 minutes, followed by slow mixing with a rotation of 30 rpm for 3 minutes, according to the adapted Roussy *et al*. (2005), Mohd and Puteh (2007), Mohd *et al*. (2008), Linn *et al*. (2008) and Méndez (2009) techniques . Lastly, an aliquot was taken and placed in a ring slide and the size of the flocculants was measured with a binocular compound microscope using a 25X objective lens and a 10X ocular lens, the latter with a 1 000 μ ocular micrometer (Méndez, 2009).

After finishing this analysis, the data were statistically evaluated for normality (Lilliefors) and homoscedasticity (Barttlet), and a one-way variance analysis was later performed to determine whether significant differences existed among the flocculants formed by applying the different dosages of chitosan. A Tukey analysis was performed *a posteriori* (Zar, 1984).

After obtaining the optimal dosage of the coagulant (chitosan), the efficiency of coagulation, flocculation and sedimentation of organic matter was evaluated using mixtures of chitosan-sodium alginate and chitosan-tannic acid. The tests were conducted in a Phipps & Bird Inc. six-paddle jar test, in which the wastewater and the selected dosage of the coagulant (chitosan) were mixed using rotation at a velocity of 250 rpm for 2 minutes. When completing this period, concentrations of 10, 20, 30, 40, 50 and 60 mgl-1 of the coagulation aid (sodium alginate or tannic acid) were added, after a flocculation period, with a rotation velocity of 30 rpm for 30 minutes. Lastly, they were left at rest without rotation for 30 minutes, according to the adapted Roussy *et al*. (2005), Mohd and Puteh (2007), Mohd *et al*. (2008), Linn *et al*. (2008) and Méndez (2009) techniques. At the end of this period samples were taken to measure TSS and VSS using the gravimetric technique according to that established by the norm NMX-AA-034-SCFI-2001.

After determining TSS and VSS removal percentages, each test was statistically evaluated taking the removal percentages as non-parametric since they are not normal data, with a significance of 0.05. A two-way variance analysis was then applied according to the Kruskal-Wallis method for non-parametric data in order to determine whether there were significant differences between the dosages tested with chitosan-sodium alginate and chitosan-tannic acid. When significant differences were found, the Student-Newman-Keuls (SNK) multiple comparisons test was performed (Zar, 1984).

Results and Discussion

The water used for the different tests contained high amounts of solids. On average, TSS was 14 040.22 mgl^{-1} and VSS was 12 665.03 mgl^{-1}, pH was 6.5 ± 0.1 and temperature was 42 ± 0 °C.

Optimal Chitosan Dosage

In the first series of experiments, 6 coagulation-flocculation tests were conducted to evaluate the effect of chitosan on the destabilization

of particles and the formation of flocculants, observing that the dosage of 200 y 300 mgl^{-1} resulted in the largest sized flocculants recorded, with 1.20 and 1.20 mm in diameter, respectively. When increasing the dosage to 400, 500 and 600 mgl^{-1}, a reduction in the size of the flocculant was observed, with a diameter of 0.57 mm (Figure 1).

The theory establishes that the graphic efficiency model for cationic polymers such as chitosan reach their optimal point in a small concentration range (Guidas, 1998), since an overdosage of the polymer has a negative effect on the physio-chemical coagulation-flocculation process. This coincides with the results of the present investigation, which found that the size of the flocculant decreased when increasing the dosage from 200 to 300 mgl^{-1}. Based on the flocculation values obtained, a variance analysis was performed for all of the dosages tested, finding statistically significant differences ($p > 0.05$). Therefore, the Tukey test was performed with the same information to determine the dosages for which there were differences. No significant differences were found between the dosages (200 and 300 mgl^{-1}) that produced the largest flocculants ($p > 0.05$) while significant differences were found ($p > 0.05$) when comparing those to dosages of 100, 400, 500 and 600 mgl^{-1} (Table 1).

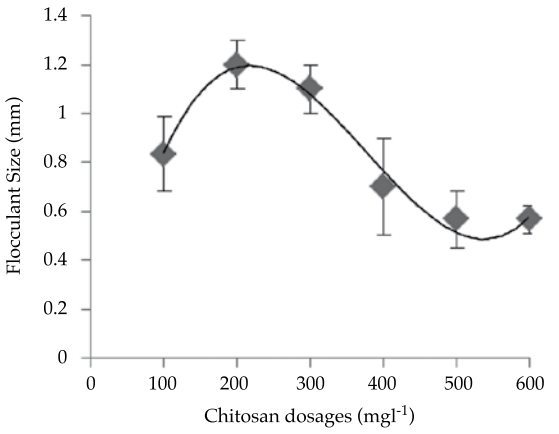

Figure 1. Flocculant size using different chitosan doses.

Efficiency of Chitosan-Sodium Alginate

Next, the tests to study the effect of variations in the concentration of sodium alginate, mixed with 200 mgL^{-1} of chitosan when used as a coagulation aid, resulted in removal percentages of 84.91% for TSS and 85.65% for VSS when dosing with 50 mgL^{-1} of sodium alginate.

It was also observed that small flocculants resulted from both rapid and slow mixing. These flocculants formed a compact sediment after sedimentation. Removal efficiency increased when raising the dosages of sodium alginate from 10 to 50 mgL^{-1}. Nevertheless, the removal percentage for TSS as well as VSS decreased when adding 60 mgL^{-1} (Figures 2 and 3).

Next, a test was performed using the same sodium alginate dosages but with a concentration of 300 mgl^{-1}. Flocculants with sizes similar to those obtained using a dosage of 200 mgl^{-1} resulted. After the settling period, a compact sediment was observed with the first dosages, resulting in a removal percentage of 91.57% for TSS and 90.35% for VSS with 300 mgl^{-1} of chitosan and 10 mgl^{-1} of sodium alginate. The removal percentages were 91.84% for TSS and 90.83% for VSS with 300 and 20 mgl^{-1} of alginate. Meanwhile, when using a concentration of 30 mgl^{-1} again with 300 mgl^{-1} of chitosan the particles remained agglomerated without settling after the time assigned to coagulation and flocculation, thereby resulting in 0% removal. This may be related to an overdosage of the sodium alginate polymer.

The results obtained for removal of TSS and VSS when testing with 200 mgl^{-1} of chitosan and 10, 20, 30, 40, 50 and 60 mgl^{-1}

Table 1. Flocculant size values: average, standard deviation and results frmo the Tukey test obtained by adding chitosan as a coagulant-flocculant ($\alpha = 95\%$)*.

Chitosan dosage (mgl^{-1})	Average size ± standard deviation (mm)
100	0.83 ± 0.15^{bc}
200	1.20 ± 0.10^{d}
300	1.10 ± 0.10^{d}
400	0.70 ± 0.20^{ab}
500	0.57 ± 0.12^{a}
600	0.57 ± 0.06^{a}

*Different letters indicate significant differences ($\alpha = 0.05$).

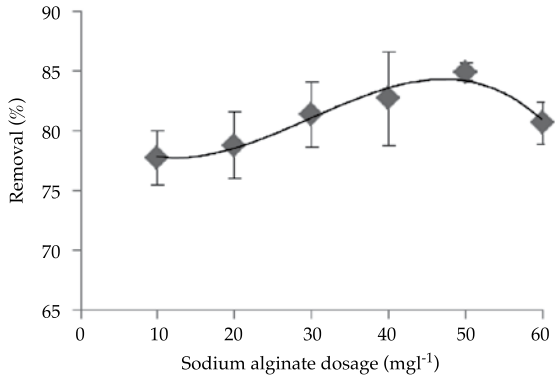

Figure 2. Removal efficiency for TSS with 200 mgl^{-1} of chitosan and sodium alginate.

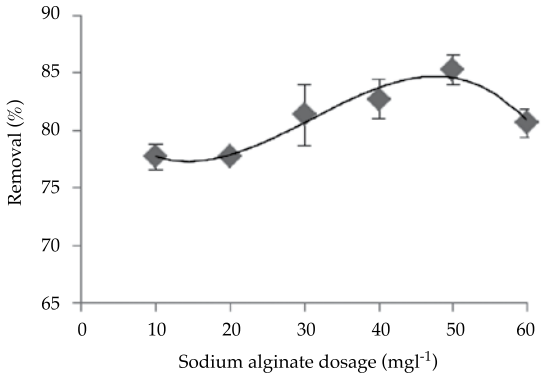

Figure 3. Removal efficiency for VSS with 200 mgl^{-1} of chitosan and sodium alginate.

of tannic acid resulted in a removal of up to 97.78% of TSS and 97.79% of VSS (Figures 4 and 5). The generation of sediments with small compacted lumps was also observed.

When comparing removals of TSS and VSS obtained with the two mixtures —chitosan-sodium alginate and chitosan-tannic acid— the non-parametric two-way Kruskal- Wallis analysis indicated significant differences between the mixtures and dosages ($p > 0.05$). An interaction was also observed between each combination of polymers with the dosage used, demonstrating that the removal efficiency depends on the concentration of the polymer mixture. Later, when performing a multiple comparison using the SNK the chitosan-tannic acid combination was statistically higher than the chitosan-alginate ($p > 0.05$; 95% significance level) (Table 2).

When directly comparing the percentages obtained for the removal of total suspended solids, the chitosan-alginate removed as much as 92% while the chitosan-tannic acid mixture removed 92%. In both cases, the removal obtained was more efficient than expected for pretreatment with conventional coagulation and flocculation, for which a maximum removal efficiency for SST is pre-calculated as ranging from 70 to 90% (Metcalf, Eddy, Inc., 1991; Fair *et al.*, 1993).

In earlier works in which chitosan, alginate or tannic acid have been used, such

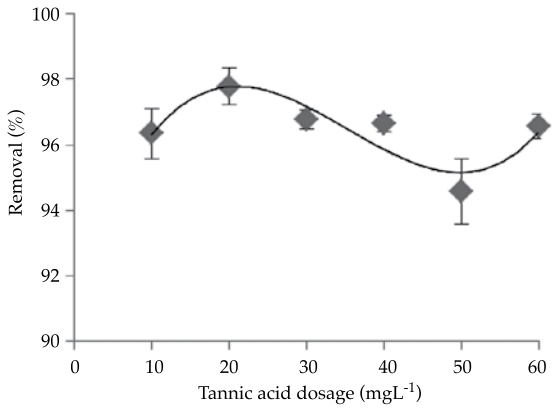

Figure 4. Removal efficiency for TSS with a mixture of 200 mgl^{-1} of chitosan and various tannic acid dosages.

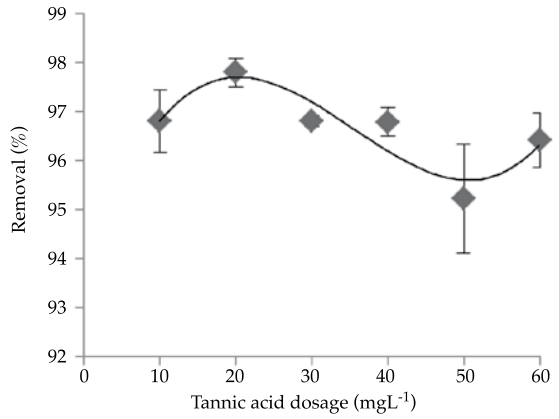

Figure 5. Removal efficiency for VSS with a mixture of 200 mgl^{-1} of chitosan and various tannic acid dosages.

as those by Sumathi (2004) and Mohd and Puteh (2007), more than 99% removal of total suspended solids was obtained when evaluating chitosan as an adsorbent and coagulant to remove suspended solids in the treatment of wastewater from the palm oil manufacturing industry. Meanwhile, the study by Markham *et al*. (1990) reported 95% removal of TSS from discharges from a butchery, and Razali *et al*. (2010) also reported 95% removal of suspended solids from wastewater from the petrochemical industry using chitosan. These results can be compared with those obtained using chitosan-tannic acid, since it shows greater efficiency than expected, when considering a high initial organic load and high variability in the physical and chemical characteristics of both the suspended as well as dissolved particles in the effluents from the fishmeal industry.

When comparing the efficiencies obtained with both mixtures tested in this investigation with similar studies of wastewater from seafood processing industries, the latter reported lower efficiencies than those obtained herein. For instance, Méndez (2009) reported 57% removal of total suspended solids when using 250 mgl^{-1} of chitosan as a flocculant and 50 mgl^{-1} of the inorganic coagulant ferric chloride (FeCl3) as aids for the sedimentation of organic particles in wastewater from the fishmeal industry. In another similar investigation, Pacheco *et al*. (2009) applied chitosan with a centrifuge process to wastewater from the fishmeal industry in Guaymas, Sonora. They obtained a removal of 58.88% of total suspended solids, as compared to the investigation herein which achieved a removal efficiency between 92 and 98% of TSS when combining chitosan with other innocuous and biodegradable polymers, which also made it possible to return the sediment that formed to the production of the fishmeal.

Conclusions

When evaluating sedimentation efficiency using these natural and biodegradable polymers, an experimental removal of organic matter of 91.84% from wastewater from the fishmeal industry was achieved with 300 mgl^{-1} of chitosan and 20 mgl^{-1} of sodium alginate, and 97.78% with the

Table 2. Average values and standard deviations for TSS and VSS removal percentages obtained with the two natural polymer combinations. Different letters indicate significant differences ($\alpha = 0.05$).

Parameter		Combination	
		Chitosan-sodium alginate	Chitosan-tannic acid
TSS	Removal (%)	$80.86 \pm 2.92_b$	$96.44 \pm 1.05_a$
VSS		$80.88 \pm 2.91_b$	$96.63 \pm 0.83_a$

mixture of 200 mgl^{-1} of chitosan and 20 mgl^{-1} f tannic acid, measured in TSS.

The use of natural substances tested in this investigation not only prevents harm to the environment caused by inorganic or synthetic coagulants and flocculants but also makes it possible to recover the organic matter for the fishmeal production train. For the case study herein of Maz Industrial, this would result in a recovery of up to 98% of the 11.44 t d^{-1} of organic matter discharged into the receptor body, equal to 283 sacks of fishmeal weighing 50 kg each.

Acknowledgments

Thank you to the Maz Indsutrial S.A. de C.V. fishmeal processing company of Mazatlan, Sinaloa, for facilitating the collection of samples and their support of conducting this project.

Received: 25/01/13
Accepted: 27/09/13

References

AHUMADA, R., RUDOLPH, A., and CONTRERAS, S. Evaluation of Coastal Waters Receiving Fish Processing Waste: Lota Bay as a Case Study. *Environmental Monitoring and Assessment*. Vol. 90, No. 1-3, 2004, pp. 89-99.

AGUILAR, M.I., SAENZ, J., LLORENS, M., SOLER, A., y ORTUÑO, J.F. *Tratamiento físico-químico de aguas residuales: coagulación-floculación*. Murcia, España: Universidad de Murcia, 2002, pp. 160-162.

ATSDR. *Toxicological Profile for Aluminum*. Atlanta: U.S. Department of Health and Human Services, Public Health Service, Agency for Toxic Substances and Disease Registry, 2008, 305 pp.

BOUGH, W. and LANDES, D. Treatment of Food-Processing Wastes with Chitosan and Nutritional Evaluation of Coagulated by Products. In *Proceedings of the First International Conference on Chitin/Chitosan* (reprinted). Muzzarelli, R.A.A. and Pariser, E.R. (editors), 1979, pp. 218-230.

CABRERA, C. *Estudio de la contaminación de las aguas costeras en la bahía de Chancay: propuesta de recuperación*. Tesis. Lima: Universidad Nacional Mayor de San Marcos, 2002.

FAIR, M., GEYER, J., and OKUN, D. *Purificación de aguas y tratamiento y remoción de aguas residuales*. México, DF: Ed. Limusa-Wiley, S.A., 1993, 764.

FUENTES, L., CONTRERAS, W., PEROZO, R., MENDOZA, I., y VILLEGAS, Z. Uso del quitosano obtenido de *Litopenaeus schmitti* (Decapoda: *Penaeidae*) en el tratamiento de agua para consumo humano. *Multiciencias*. Vol. VIII, 2008, pp. 282-283.

GALARZA, E., GONZÁLEZ, L., y NESTOROVIC, D. *El costo ambiental de hacer negocios en Perú, reporte final. Proyecto Andino de Competitividad*. Quito: Centro de Investigación del Pacífico, 2001.

GUIDAS, B. *Étude de la performance du chitosane comme coagulant pour l'enlèvement du cuivre et de la turbidité des eaux usées*. Tesis. Montreal: Université de Montreal, National Library of Canada, 1998.

KIRCHMER, C.J., ARBOLEDA, J.V. y CASTRO, M. *Polímeros naturales y su aplicación como ayudantes de floculación*. Lima: Centro Panamericano de Ingeniería Sanitaria y Ciencias del Ambiente, 1975.

LAFLEUR, C., FORTIER, J., KHAROUNE L., et KHAROUNE, M. *Évaluation d'un procédé de coagulation floculation au chitosane pour l'enlèvement du phosphore dans les effluents piscicoles*. Québec: Société de Développement de l'Industrie Maricole Inc. École de Technologie Supérieure, 2008.

LINN, H., TINT K., and MYA, O. *Treatment of Wastewater in Recycled Paper Industry using Biopolymers. International Conference on Sustainable Development: Issues and Prospects for the GMS*. Myanma: Department of Chemical Engineering, Mandalay Technological University, 2008.

MARKHAM, W., REID, J., and COFFMAN, G. *Recovery of Fats and Proteins from Food Processing Wastewaters with Alginates*. United States Patent, Patent Number 4993087, 1990.

MARROQUÍN, A. *Obtención del extracto tánico por maceración dinámica de la corteza de árboles jóvenes de cuatro especies forestales, a nivel laboratorio*. Tesis. Nueva Guatemala de

la Asunción: Universidad de San Carlos de Guatemala, Facultad de Ingeniería, 2008.

McHUGH, D.J. *Perspectivas para la producción de algas marinas en los países en desarrollo*. FAO Circular de Pesca. Núm. 968. Roma: FAO, 2002, 30 pp.

METCALF, EDDY, INC. *Wastewater Engineering Treatment, Disposal and Reuse*. Third edition. New York: McGraw Hill, 1991, 550 pp.

METCALF, EDDY, INC. *Wastewater Engineering Treatment and Reuse*. Fourth edition. New York: McGraw-Hill. 2003, 479 pp.

MÉNDEZ, O. I. *Diseño e implementación de mejoras al proceso de tratamiento aplicado a las aguas residuales provenientes de la producción de harina de pescado*. Tesis. Mazatlán, México: Instituto Tecnológico de Mazatlán, 2009, 77 pp.

MOHD, A. and PUTEH, M. Pre-Treatment of Palm Oil Mill Effluent (POME): A Comparison Study using Chitosan and Alum. *Malaysian Journal of Civil Engineering*. Vol. 19, No. 2, 2007, pp. 128-141.

MOHD, A., LI, T., and NOOR, Z. Coagulation and Flocculation Treatment of Wastewater in Textile Industry using Chitosan. *Journal of Chemical and Natural Resources Engineering*. Vol. 4, No. 1, 2008, pp. 43-53.

NMX-AA-034-SCFI-2001. *Norma Oficial Mexicana. Análisis de agua. Determinación de sólidos y sales disueltas en aguas naturales, residuales y residuales tratadas. Método de prueba*. México, DF: Secretaría de Comercio y Fomento Industrial, Diario Oficial de la Federación, 1° de agosto de 2001.

PACHECO, R., LEYVA, P., CARVALLO, G., GARCÍA, L., y MÁRQUEZ, V. Efecto de la concentración de quitosano y pH sobre la remoción de sólidos en agua de cola de la industria sardinera. *Interciencia*. Vol. 34, núm. 4, 2009, pp. 274-279.

RAZALI, M., YUNUS, R.M., JEMAAT, Z., and ALIAS, S. Monoethanolamina Wastewater Treatment Via Adsorption Method: A Study on comparison of Chitosan, Activated Carbon, Alum and Zeolite. *Journal of Applied Sciences*. Vol. 10, No. 21, 2010, pp. 2544-2550.

RODRÍGUEZ, A., LETÓN, P., ROSAL, R., DORADO, M., VILLAR, S. y SANZ, J. *Tratamientos avanzados de aguas residuales industriales*. Madrid: CEIM, 2006.

ROUSSY, J., CHASTELLAN, P., VAN VOOREN, M., and GUIBAL, E. Treatment of Ink-Containing Wastewater by Coagulation/Flocculation using Biopolymers. *Water SA*. Vol. 31, No. 3, 2005, pp. 369-376.

SUMATHI, S. *Removal of Residue Oil from Palm Oil Mill Effluent (POME) using Chitosan*. Thesis. Pahang, Malaysia: University Sains Malaysia, 2004.

WIBOWO, S., VELÁZQUEZ, G., SAVANT, V., and TORRES, J. Effect of Chitosan Type on Protein and Water Recovery Efficiency from Surimi Wash Water Treated with Chitosan Alginate Complexes. *Biosource Technology*. Vol. 98, No. 3, 2006, pp. 665-671.

ZAR, H. *Biostatical Analysis*. Department of Biological Sciences. Second edition. New Jersey: Northern Illinois University, Prentice Hall, 1984, pp. 79-186.

Institutional Address of the Authors

Ing. Dulce María Arias-Lizárraga
Dr. Evaristo Méndez-Gómez

Instituto Tecnológico de Mazatlán
Corsario 1 núm. 203, Colonia Urías
82070 Mazatlán, Sinaloa, México
Teléfono: +52 (669) 9838 400
dulce_dem06@hotmail.com
evaristo3@hotmail.com

Click here to write the autor

The decline in the lagoon of San Juan Epatlan, Puebla, Mexico.

Photo: Guadalupe Balbuena Marín.

Geometric and Kinematic Characterization of a Spray Using the PTV Optical Technique

• Humberto Salinas-Tapia •
Universidad Autónoma del Estado de México

• Cruz Octavio Robles-Rovelo* • Dagoberto Chávez-Carlos •
• Carlos Francisco Bautista-Capetillo •
Universidad Autónoma de Zacatecas

*Corresponding Author

Abstract

SALINAS-TAPIA, H., ROBLES-ROVELO, C.O., CHÁVEZ-CARLOS, D. & BAUTISTA-CAPETILLO, C.F. Geometric and Kinematic Characterization of a Spray Using the PTV Optical Technique. *Water Technology and Sciences* (in Spanish). Vol. V, No. 3, May-June, 2014, pp. 127-142.

Natural or induced phenomena involving the movement of drops drive the analysis to determine soil loss from erosion and changes that could occur in the infiltration rate as a result of the energy with which they impact the soil surface. The diameter and velocity define the magnitude of the effect. To characterize these variables, a variety of techniques have been applied (water-sensitive paper, flour, oil immersion, optics and photography). The present investigation uses particle tracking velocimetry (PTV) to characterize the drops emitted by a spray flow. The development of PTV partly arose from the analysis of the sedimentation velocity in biphasic flows, which requires tracer particles to evaluate a phenomenon. Nevertheless, the experimental characteristics of the work required omitting the use of these elements, and therefore adjustments to the scheme proposed by Salinas et al. (2006) were indispensable. The drops were produced at a constant hydraulic pressure of 175 kPa and the photographs were taken at a distance of 4.5 m with three different sprayer heights. The information collected (diameters and velocities) enabled constructing velocity vector fields. The results presented are based on the analysis of 1 582 drops, for which mean diameters of 0.39, 0.55 and 0.34 mm and velocities of 4.02, 3.70 and 3.63 ms-1 were obtained, with heights of 0.5, 1.0 and 1.5 m, respectively.

Keywords: Characterization of drops, optical technique, PTV, diameter, velocity, statistical analysis.

Resumen

SALINAS-TAPIA, H., ROBLES-ROVELO, C.O., CHÁVEZ-CARLOS, D. & BAUTISTA-CAPETILLO, C.F. Caracterización geométrica y cinemática de un chorro pulverizado empleando la técnica óptica PTV. Tecnología y Ciencias del Agua. *Vol. V, núm. 3, mayo-junio de 2014, pp. 127-142.*

Los fenómenos naturales o inducidos que involucran el movimiento de gotas motivan análisis para determinar aspectos como la pérdida de suelo por erosión o los cambios que pudieran ocurrir en la tasa de infiltración debido a la energía con la que impactan sobre la superficie del suelo. El diámetro y la velocidad definen la magnitud del efecto. Para caracterizar estas variables se han aplicando diversas técnicas (papel sensible al agua, harina, inmersiones en aceite, ópticas y fotografía). En este sentido, la presente investigación emplea velocimetría por rastreo de partículas (PTV) en la caracterización de gotas emitidas por un pulverizador de flujo. PTV ha encaminado parte de su desarrollo al análisis de la velocidad de sedimentación en flujos bifásicos donde se requiere del sembrado de partículas trazadoras para evaluar el fenómeno; sin embargo, las características experimentales del trabajo obligaron a omitir el uso de estos elementos, por lo que fue indispensable hacer adecuaciones al esquema propuesto por Salinas et al. (2006). Las gotas se originaron a una presión hidráulica constante de 175 kPa, las fotografías se capturaron a una distancia de 4.5 m con tres alturas diferentes del pulverizador. La información recolectada (diámetros y velocidades) posibilitó la construcción de campos vectoriales de velocidad. Los resultados presentados derivan del análisis de 1 582 gotas, con las que se obtuvieron valores medios de 0.39, 0.55 y 0.34 mm en diámetro, y 4.02, 3.70 y 3.63 ms^{-1} en velocidad, para alturas de 0.5, 1.0 y 1.5 m, respectivamente.

Palabras clave: *caracterización de gotas, técnica óptica PTV, diámetro, velocidad, análisis estadístico.*

Introduction

Physical phenomena (natural or induced) in which there is movement of a fluid can best be explained when theory and experimentation are joined to represent processes occurring within the event. In this context, a stream of water that is dispersed by high pressure forms drops with diverse characteristics, such as diameter and velocity, resulting in their following different trajectories from the point of origin. The experimental determination of the magnitude of these variables depends on factors that include the hydraulic operating conditions and the environmental characteristics of the region. Ballistic theory is used to predict this (Vories *et al*., 1987; Dechmi, 2002; Playán *et al*., 2006). Because of the complexity of analyzing the movement of drops, ballistic models consider three hypotheses (Dechmi, 2002): 1) the stream of water separates into individual drops with different diameters and which move independently through the air; 2) the aerodynamic drag coefficient does not depend on the height, angle of inclination, wind speed or diameter of the device; 3) the diameter of the drop determines the maximum distance it travels.

Various techniques have been proposed (water-sensitive paper, flour, oil immersion, high- and low-speed photography, among others) to experimentally evaluate the third hypothesis (Jones, 1956; Magarvey, 1956; Eigel and Moore, 1983; Hauser *et al*., 1984; Kohl and DeBoer, 1984; Kincaid *et al*., 1996). Some were first used to measure the size and distribution of raindrops, and others to evaluate drops generated by irrigation sprinkler systems (Cruvinel *et al*., 1996; Cruvinel *et al*., 1999; Salles *et al*., 1999; Sudheer and Panda, 2000; Montero *et al*., 2003). According to Cruvinel *et al*. (1996), the first evidence of the use of six techniques to measure the size and distributions of drops was documented in 1895. Two optical methods were applied at the end of the 20th century to determine their diameter. The first was based on the analysis of light diffraction generated by drops illuminated by a laser light beam (Kincaid *et al*., 1996). The second, known as optical disdrometer, measures the diameter of a particle based on the attenuation of an infrared light beam during the fall of the water particles (Hauser *et al*., 1984; Montero *et al*., 2003). Meanwhile, Sudheer and Panda (2000) proposed another method of analysis using high-speed photography combined with digital techniques, demonstrating that the processing of images would offer an improved technique, particularly to determine the relation between the distribution of the size of drops and the operating pressure and characteristics of the sprinkler heads. Recently, Salvador *et al*. (2009) proposed a technique using low-speed photography which shows the trajectory of drops, where digital processing can determine the length, angle, diameter and speed of fall. Nevertheless, obtaining reliable results with this technique requires too much time and one part of the process relies on personal criteria in the discrimination of the drops.

The analysis of various phenomena involving fluid mechanics, such as hydraulics, has significantly advanced thanks to the development of measurement techniques that use the principle of optics to evaluate the characteristics desired in the case study analyzed. These techniques are divided into intrusive and non-intrusive. The former includes the hot-wire anemometry (HWA) technique and the latter includes laser doppler anemometry (LDA), laser induced fluorescence (LIF), doppler global velocimetry (DGV) and phase doppler anemometry (PDA). Their limitation is that they are used

to analyze small flow regions. Meanwhile, thanks to the development of high-speed photographic cameras and the emergence of sophisticated laser light equipment, non-intrusive techniques have evolved over the past 20 years, including particle image velocimetry (PIV) and particle tracking velocimetry (PTV) for two-dimensional analysis, such as the stereo-PIV (S-PIV) technique and digital holography to analyze flows in 3D (Adrian, 1991; Jensen, 2004).

PIV and PTV are the optical techniques commonly used in hydraulics and fluid mechanics to determine the properties of a flow, such as velocity, temperature, pressure, turbulence, vorticity, density and size of particles (Van Dyke, 1982; Smits and Lim, 2000). These techniques have been focused on measuring velocity fields in different types of fluids using tracer particles (Adrian 1989; Adrian, 1991; Westerweel, 1993; Raffel *et al*., 1998).

Individual particle tracking (PTV) algorithms are used for low density particles in the flow region analyzed. For the case of images with high particle density, algorithms such as cross-correlation and autocorrelation (PIV))(Virant and Dracos, 1997; Ido *et al*., 2002) are locally applied to the area of interest and they are developed using the convolution theorem with the inverse Fourier transform (Crunivel *et al*., 1996) or other methods such as the Hough transform or the convex envelope when particles overlap (Sang and Yu, 2004). Nevertheless, these processes take more time to analyze the images than the PTV technique.

PTV is based on operating principles for the acquisition of high-speed images and spatial resolution. It uses a charge couple device (CCD) over a flow region seeded with tracer particles (density similar to that of the fluid). The region is illuminated with a sheet of light from a double-cavity pulsed laser. The light is dispersed when making contact with the tracers and recorded by the sensor of the camera. Each pulse illuminates the same particle at different times and, thus, it can be observed in the same image at two different positions. Then, by means of digital processing, the distance separating each pair of particles is measured and their velocity is determined according to the time between each pulse of light. The above procedure is automated using algorithms developed in a programming language, which facilitates and standardizes the analysis (Prasad, 2000; Salinas *et al*., 2006). Although this technique has been used primarily to study the sedimentation velocity of non-cohesive particles (sand) (Salinas and García, 2011; Flores and López, 2012), some authors suggest the possibility of implementing it to determine the characteristics of water drops generated by a spray flow, air bubbles (cavitation) or solid particles that move through a mixing tank (Sang and Yu, 2004; Salinas *et al*., 2011).

Low-speed photographic techniques have been use to analyze the movement of isolated drops, as occurs with rain or sprinkler irrigation (Bautista *et al*., 2009; Salvador *et al*., 2009), while optical techniques such as PIV or PTV have been used in investigations of biphasic flows with sedimentary particles (spherical and non-spherical) at low velocities (< 16 cms^{-1})(Salinas *et al*., 2006; Salinas and García, 2011). Nevertheless, the investigations by Salvador *et al*. (2009) and Bautista *et al*. (2009) have the following drawbacks:

a) A large amount of photographs are needed (500-2 000 images) since a considerable percentage are not usable because they do not contain drops. The decision to include or eliminate an image is made based on the analyst's criteria and a detailed examination of the photograph. The diameter and trajectory

of the drop must therefore be clearly visible in the image.

b) The parameters that characterize the drop (diameter, length and fall angle) are obtained manually, which causes errors of perception.

c) The characterization of each drop requires between 4 and 7 min (Salvador *et al*., 2009; Bautista *et al*., 2013), while Salinas and García (2011) use the PTV technique to calculate the fall velocity of sedimentary particles in a fluid in movement and report the advantage of obtaining instantaneous pairs of images (2 to 5 ms). In addition, because of the principle behind the technique, when using light pulses the position of the drop at two successive points in time can be recorded on the same image. Digital processing of the image is used to generate a two-dimensional velocity vector map of a multiphase flow field (the solid part is the tracers and the fluid is liquid or gas) at a specific instant in time, by calculating movement through individually tracing the drops.

As a result of the high use of pressurization in irrigation systems, interest has increased in developing techniques to characterize drops that travel through the air under different hydraulic and environmental conditions because of the effect of these factors on the kinetic energy with which the drops impact the surface of the soil, or the loss due to evaporation or drag. In addition, reliable models are sought that are efficient in terms of the time required to determine diameters and velocities. Based on the above, this investigation describes the kinetics and geometry of drops generated by a spray flow under controlled conditions. The objective is to implement the PTV algorithm developed by Salinas *et al*. (2006) to characterize a set of drops captured at different heights with respect to the ground surface and thereby construct two-dimensional velocity fields based on the information recorded by a series of photographs taken at high speed.

Materials and Methods

The investigation was conducted at the Inter-American Water Resource Center (Centro Interamericano de Recursos del Agua (CIRA, Spanish acronym)) of the Autonomous University of the State of Mexico (Universidad Autónoma del Estado de México (UAEMex, Spanish acronym)). Figure 1 presents the experimental equipment used.

A spray flow was used to generate water drops. They were characterized by a particle tracking velocity (PTV) system installed at the CIRA's Flow Imaging Laboratory. The hydraulic device used to create the spray flow stream contained four components: 1) a cylindrical device with a capacity of 0.8 m^3; 2) a ½ HP Myers hydropneumatic equipped with a pressure regulator tank and a 600 kPa Fimet brand ABS radial manometer; 3) a conical spray gun (60 mm diameter with 150 orifices, Truper brand); 4) PVC tubing (20 mm diameter; 1.6 m tall; inclination angle of 60°with respect to the horizontal (θ)). The PTV velocimetry system contained five elements: a) JAI brand coupled charge device (digital camera) with a temporal resolution of 30 to 250 squares per second and a spatial resolution of 1600 x 1200 pixels, equipped with a Nikkor 50 mm lens, with processing algorithm; b) Nd:YAG New Wave brand 15 mJ double-cavity pulse laser; c) optical accessories (mirrors and lens); d) signal synchronizer to control the image acquisition sequence with laser light pulses; e) PTV-SED v. 1.0 algorithm to process the images, developed by Salinas *et al*. (2006). The stages involved in its functioning are shown in Figure 2.

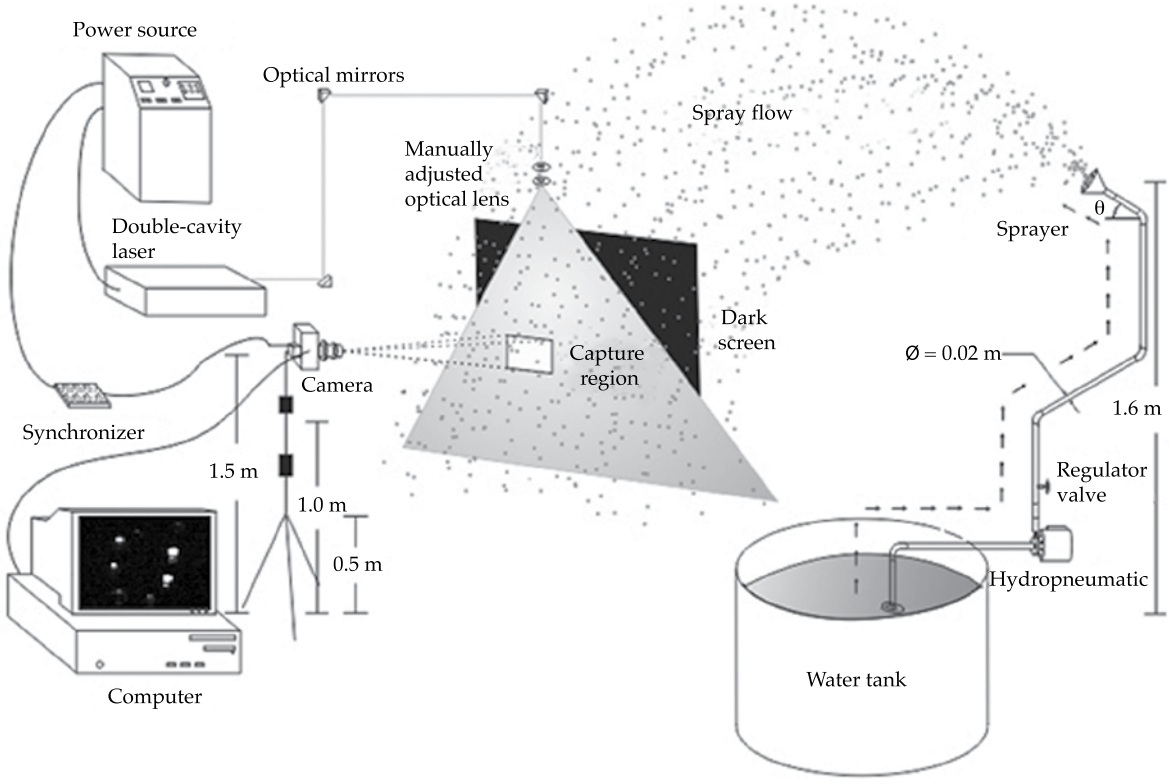

Figure 1. Experimental setup. PTV system (computer, laser, synchronizer, optical equipment camera and acquisition positions) and hydraulic system (feed tank, hydropneumatic and sprayer).

Image Acquisition and Processing

A hydraulic pressure of 175 kPa was used to generate the drops. The images were acquired at three different heights (H1 = 1.5 m; H2 = 1.0 m; H3 = 0.5 m) at a distance of 4.5 m from the sprayer. According to the principle involved in the PTV technique, tracers are generally used to determine the fluid velocity fields and visualize the flow behavior. Nevertheless, because of the nature of this experiment and since the PTV algorithm has been applied to characterize solid particles larger than the tracers (Salinas and García, 2011), the water drops in this experiment functioned as tracers; that is, they diffracted the laser light and were recorded by the camera's sensor. Therefore, the tests were conducted at night in order to control the lighting in the area of analysis, which was illuminated with a double-cavity pulse laser. This contrast makes the information in the images visible for digital processing (Salinas *et al.*, 2006). The light beam was diverted to the visualization area with optical mirrors (placed at 45°), along a horizontal-vertical-horizontal-vertical trajectory (Figure 1). Once the beam was placed at the site, a light sheet needed to be created. This was accomplished with the combination of two lenses (one spherical and the other cylindrical), thereby obtaining an illuminated area larger than that covered by the camera (60 x 40 mm). The camera was installed perpendicularly to the light sheet (region of analysis) at a distance of 1.0 m. The thickness of the

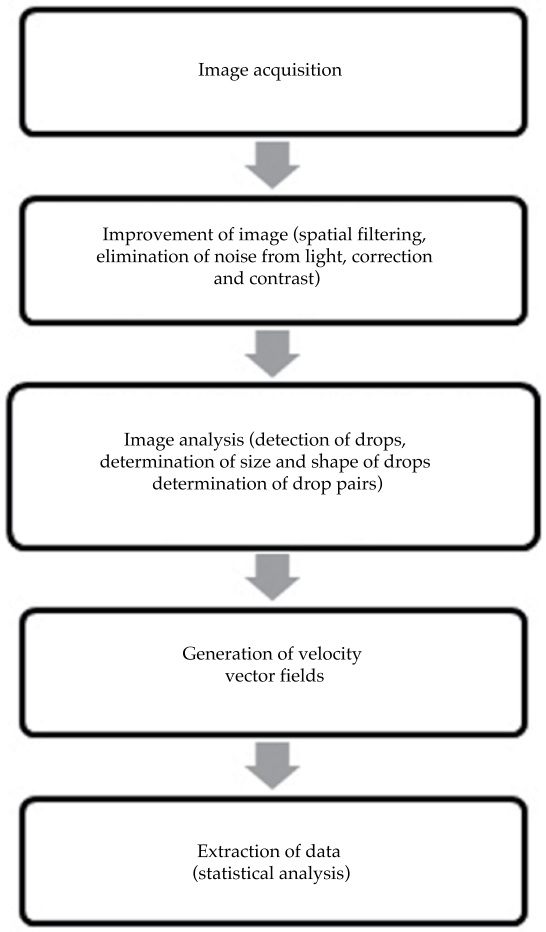

Figure 2. Characterization of drops with the PTV-SED v 1.0 algorithm.

laser light sheet was adjusted to 3.0 mm to ensure that the drops included in the characterization were on the same plane of analysis. To capture the drops on the images using the PTV technique, the laser frequency (light pulses) and the camera frequency (number of images per second) needed to be synchronized so that the laser would be pulsed each time at which an image would be captured. This processes was conducted with a signal synchronizer manipulated by a computer. This research conducted several tests to mark the times between the laser light pulses (Δt) in order to determine the position of the drops generated at two different times on the same image. The exposure time (t_{exp}) required to detect the largest number of drops was also defined. For this experiment, Δt = 0.4 ms and t_{exp} = 20 ms were chosen (Figure 4a). It is worth mentioning that to fulfill these time requirements, the camera needed to be synchronized with the laser light source so that the two pulses would coincide with the exposure time and ensure that the position of the drops for each light pulse would be recorded on the same image. This made it possible to process the images in order to calculate the movement, size and velocity of the water drops.

To determine the characteristics of the drops (diameter, position and velocity), the PTV-SED v 1.0 algorithm was used, which was originally developed to study the velocity of sedimentary particles in biphasic flows (Salinas *et al*., 2006). It is important to mention that the algorithm needed to be adjusted to determine the geometry of the drops since it detects irregular (sediment) particles and the drops have a uniform geometry. It functions according to two sequential and automated sequences (Figure 2). In the first, the quality of the image is improved through spatial filtering (eliminating the intensity of the light). That is, eliminating the noise generated by excess light or reflection not controlled during image acquisition, which is caused by random changes in the brightness or color of the image produced by the camera's sensor when acquired. This ensures that the particles detected are clearly visible and identifiable by the PTV-SED v. 1. 0 algorithm (Figure 3). The second procedure involves five stages to detect the drops in each pulse (Figure 4b): 1) maximum and minimum intensities are identified to determine their size; 2) a circular area is formed based on its geometry, which is evaluated according to the intensity of each pixel: 3) the centroid of each double-pulsed drop recorded on the image is obtained, which is also a function of the

intensity of the pixels; 4) the coordinates (x,y) of the centroids of the drops are calculated to later determine the distances between them $(\Delta x, \Delta y)$ and; 5) the velocity vector (u, v) is obtained with the following equation:

$$u = \frac{\Delta x}{\Delta t} \quad v = \frac{\Delta y}{\Delta t} \qquad (1)$$

To perform the stages mentioned above, initial parameters needed to be established based on the acquisition conditions. To determine the magnification factor, a calibration image was taken at the three heights analyzed. This was done by placing a ruler divided into cm in the region of analysis (at 1 m from the camera) before acquisition. This factor was determined by measuring the distance in pixels equivalent to 1 cm in the image. The algorithm was then introduced ensuring that the data from the processing were in centimeters. This resulted in 115, 116 and 122 px cm^{-1} for the set of images taken at 0.5, 1.0 and 1.5 m, respectively. The separation between laser light pulses used in the experimentation was Δt = 0.4 ms. The maximum and minimum thresholds depended on the amount of brightness or color in the images and the amount of light dispersed by a drop. These values were recorded in RGB, between 0 and 255 (Salinas *et al.*, 2006). To identify the particles, 25 images taken at the three heights analyzed were visualized. For each group, the distances and angles separating the double-pulsed drops were measured, thereby finding ranges of separation of 15-24, 12-24 and 15-35 px at H1, H2 and H3,

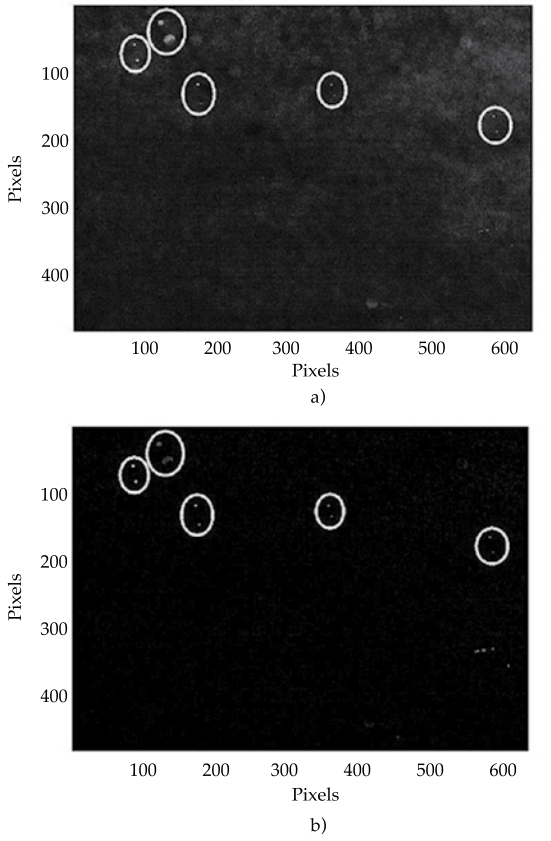

Figure 3. Spatial filter to improve the quality of the image. a) Photograph with distortion from excess illumination; b) photograph processed with the PTV-SED v. 1.0 algorithm.

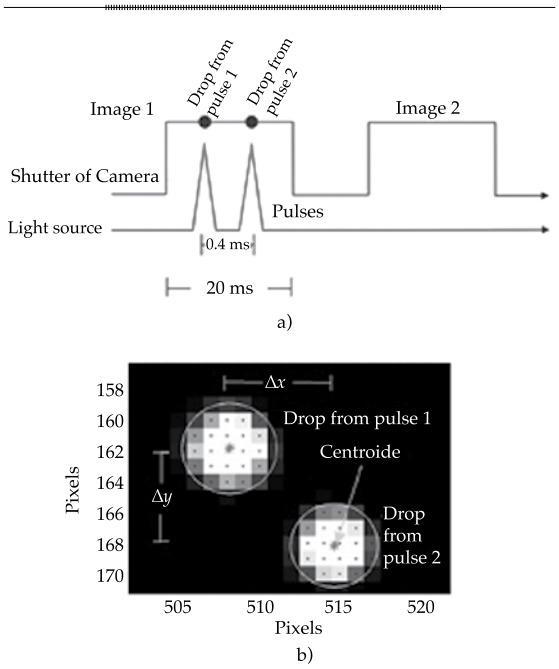

Figure 4. Time interval between light pulses and drops identified. a) Camera and laser frequencies; b) double-pulsed drops, movement in Δt and centroid.

respectively. In addition, the angle of all the drops was defined in a range of 65 and 90°.

Although the acquisition times were nearly instantaneous, some images detected drops that were not completely visible in the second pulse, indicating that they left the plane of analysis. Therefore, the diameter of the drop and its centroid could not be accurately determined. This occurred primarily because the trajectories of the drops generated by the spray presented a dispersed behavior in space. Although the illuminated drops were detected, the diameter was not correct and the velocity was also different (Figure 5). Therefore, to ensure that the data were correct, MatLap algorithms were used to discriminate the drops for which the difference between diameter 1 and 2 exceeded 10%. Roughly 30% of the drops were thereby eliminated. In order to generalize and statistically analyze the information, equivalent diameters were obtained based on the arithmetic mean of the diameters 1 and 2 of the double-pulsed drops.

Statistical Analysis of the Drops

After processing the images, a statistical analysis was performed with MatLab based on the information collected. Centrality and dispersion parameters were determined, including the arithmetic mean ($\bar{x}$), standard deviation (S) and coefficient of variation (*CV*) (equations (2), (3) and (4), respectively) for equivalent diameters and velocities corresponding to each group of images. Specifically for the diameter, the volumetric mean (D_v) corresponding to equation (5) was also determined as well as the mean of 50% of accumulated volume.

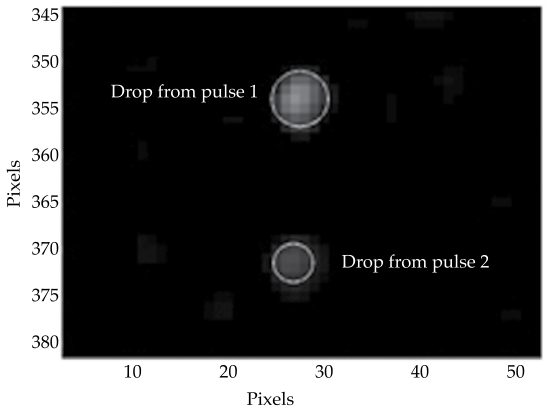

Figure 5. Drops outside the plane of analysis. In this case the difference between diameters is over 10%.

$$\bar{x} = \frac{\sum_{i=1}^{n} x_i}{n} \tag{2}$$

$$S = \sqrt{\frac{\sum_{i=1}^{n} \left(x_i - \bar{x}\right)}{n-1}} \tag{3}$$

$$CV = \frac{S}{\bar{x}} \tag{4}$$

$$D_V = \frac{\sum_{i=1}^{n} d_i^4}{\sum_{i=1}^{n} d_i^3} \tag{5}$$

To obtain the mean of 50% of the accumulated volume (D_{50}), the diameters resulting from each set of images were separately sorted in ascending order. The volume was then calculated and the diameter of the drop corresponding to 50% of total accumulated volume was selected.

In the above formulas, x represents the data analyzed (diameter or velocity) n is the total number of data and d is the diameter of the drop (mm).

Velocity Fields

The PTV-SED v. 10 algorithm provided information that describes the kinematic

behavior of the drops when falling. These data were generated for each observation height in order to create two-dimensional velocity vector fields by applying algorithms developed in MatLab to the data resulting from the processing. Each vector map presents: the magnitude, direction and sense of the drops; the position (x,y) in cm of their respective centroids with respect to the origin of the image; and the resulting velocity of each double-pulsed drop in cms^{-1} units.

Validation of the PTV Optical Technique

Some errors occurred in the processing of the images, which were promptly identified.

These were:

a) Synchrony of equipment, that is, the camera captures the drops when the region of analysis is illuminated. Different tests were conducted to obtain the optimal times between separation of light pulses and image exposure in order to acquire the largest number of drops.
b) The magnification and sharpness of the images, for which the camera's focus and capture distance were adjusted.
c) The main source of error was the detection of pairs of particles in the processing of the images. To solve this problem, two detection criteria were followed —the minimum and maximum distance a particle traveled and the direction. Therefore, these parameters were calibrated for each run to detect the corresponding pair for each drop. In addition, according to the application of the algorithm to non-cohesive sediments, the degree of error in the results was less than 10%. Therefore, when performing the statistical analysis and determining the diameters of the drops that criterion was used and the drops that had a difference of more than 10% between the initial and final diameter were eliminated. As can be observed, this is much less than the permitted degree of error.

Results and Discussion

To evaluate the characteristics of the drops, a set of 1 685 images was obtained and divided into three subsets (H1, H2 and H3), containing 541, 572 and 572 images, respectively. Before analyzing these with the PTV-SED v. 1.0 algorithm, a manual visualization procedure was used to select those images that contained drops, since the experimental conditions generated images

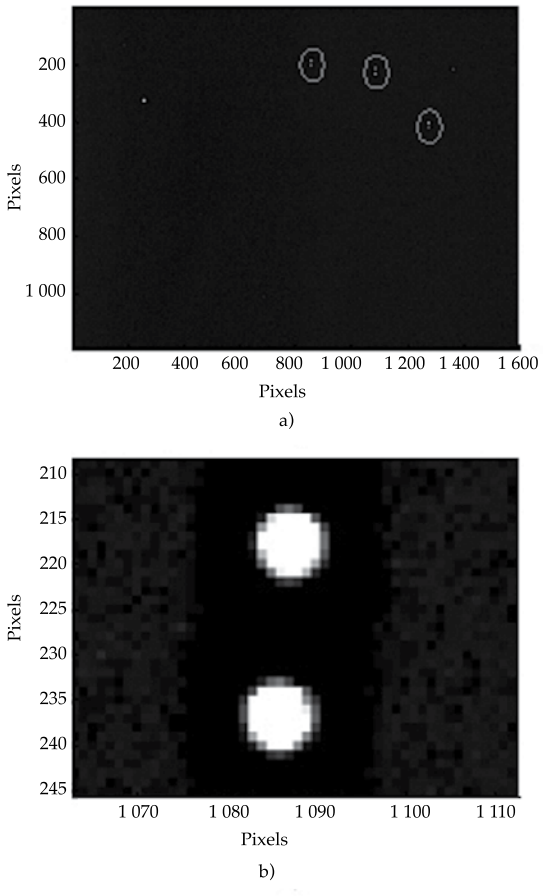

Figure 6. Images acquired: a) image with a low density of a drops; b) close-up of the image of a double-pulsed drop.

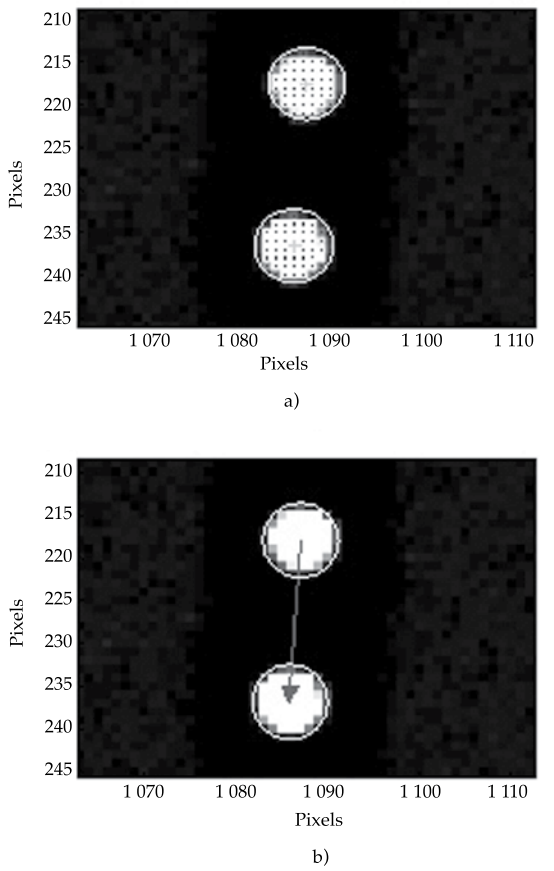

Figure 7. Detection of the drops and velocity vector: a) determination of the centroid of the drops; b) diameter of drops a velocity vector, based on the centroid of each drop.

without data which poses a cycling problem in the functioning of the algorithm.

Thus, 40% of images were eliminated, which did not contain information. From the remaining, an average of two drops were obtained (Figure 6a), with which a group of 1 582 was created (658 drops in H1, 448 in H2 and 476 in H3). Figure 6b shows a close-up of a drop recorded at the two consecutive times in the same image. After obtaining the images with valid information, they were processed to determine the diameter and centroid of the drop for each pulse (Figure 7a). The velocity was also calculated based on the distance traveled (Δx, Δy) over time Δt (equation (1), Figure 7b).

It is worth mentioning that the processing time was 4.2 s to determine the characteristics of each drop, including their velocity. This is significantly different than the results reported by Salvador *et al*. (2009) and Bautista *et al*. (2013) who indicated between 4 and 7 minutes per drop.

As determined, the images were acquired at three heights from the ground surface, maintaining the hydraulic pressure and observation distance constant. The statistical analysis was performed under these conditions and with equations (2) and (5). These results are shown in Table 1. With regard to the diameters, ranges of 0.10 to 0.58 mm, 0.10 to 0.83 mm and 0.09 to 0.59 mm were found at heights of 0.5, 1.0 and 1.5 m, respectively. The minimum diameters were virtually equal, while the maximum diameters increased 30.12% with a change in height from 0.5 to 1.0 m and decreased 28.92% when the height of the camera was moved from 1.0 to 1.5 m. In terms of the values of D_v and D_{50}, they were equal for H2 and H3, while D_v was 2.3% less than D_{50} in the case of H1. Nevertheless, when comparing the arithmetic diameters, the differences were greater. At heights of 0.5, 1.0 and 1.5 m, D_v and D_{50} were 17.0, 21.4 and 19.99% larger than $\bar{x}$, respectively. In addition, a relationship could not be determined between the height of the camera and the differences in values obtained for the arithmetic volumetric diameter and for 50% of the accumulated volume, since there was no trend indicating that the diameter increased or decreased with respect to the vertical position of the camera. This finding differs from that reported by Bautista *et al*. (2013), who reported changes in the diameter of the drops at different heights in a sprinkler system. This discrepancy may be related to the spray device used in this investigation. Figure 8a shows the frequency of the diameters. Those with the highest detection had diameters between 0.4 and 0.5

Table 1. Characteristics of diameters and velocities obtained, per observation height.

Variable	Parameters	Observation height (m)		
		0.5	1.0	1.5
Diameter (mm)	$\bar{x}$	0.39	0.55	0.34
	D_v	0.47	0.70	0.42
	D_{50}	0.47	0.70	0.43
	S	0.12	0.25	0.11
	CV	0.01	0.06	0.01
	D_{min}	0.10	0.10	0.09
	D_{max}	0.58	0.83	0.59
Velocity (ms^{-1})	$\bar{x}$	4.02	3.70	3.63
	S	0.49	0.50	0.36
	CV	0.24	0.25	0.12
	V_{min}	3.02	2.59	3.15
	V_{max}	5.46	4.97	4.89

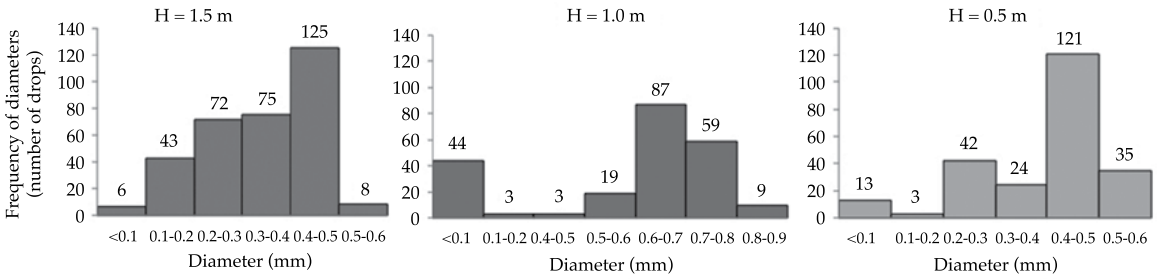

a)

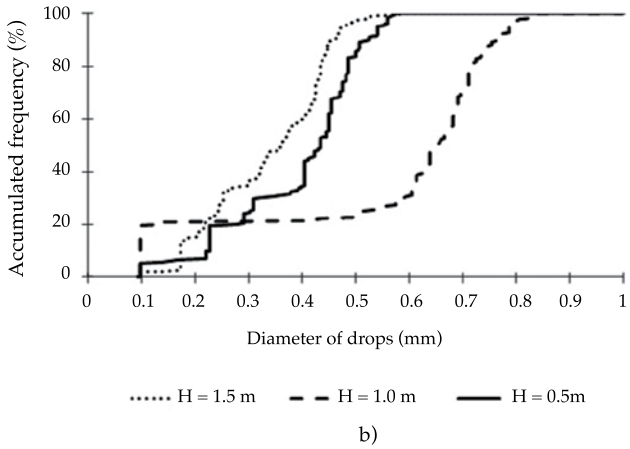

b)

Figure 8. Behavior of drop diameters at different heights: a) frequency histogram for different heights H; b) accumulated frequency.

mm (125 drops), 0.6 and 0.7 mm (87 drops) and between 0.4 and 0.5 mm (121 drops) for each set (H1, H2, H3), respectively. The diameters detected at H2 were 30.76% larger than those at H1 and H3. Figure 8b shows the accumulated frequency of the diameter of the drops captured at the three heights. The behavior indicates a greater number of small diameters at a camera height of 1.5 m, followed by 0.5 m and lastly 1.0 m. In general, the number of drops of a particular diameter varied by roughly 10% between heights of 0.5 and 1.5 mm, and did not exceed 0.6 mm. This condition did not occur at 1.0 m, where the accumulated frequency did not exceed 20% for drops between 0.1 and 0.6 mm. Meanwhile, the rate of the accumulated frequency for the 0.6 mm diameter was 32% per 0.1 mm increase in the diameter of the drop, up to 0.9 mm.

The statistical analysis of the fall velocity of the drops (Table 1) resulted in mean of values of 3.63, 3.70 and 4.02 ms^{-1} at heights H1, H2 and H3, respectively. The ranges for each case were 3.02 to 5.46 ms^{-1} ($S = 0.36$ ms^{-1}), 2.59 to 4.97 ms^{-1} ($S = 0.50$ ms^{-1}) and 3.15 to 4.89 ms^{-1} ($S = 0.49$ ms^{-1}), respectively. An increase was observed in the mean velocity of the drops as the observation height decreased: 1.89% when decreasing from 1.5 to 1.0 m and 23.63% from 1.0 to 0.5 m. Figure 9 shows the frequency of the velocities for the heights analyzed. The maximum ranges detected were 3.7 to 3.8 ms^{-1} (53 drops), 3.5 to 3.7 ms^{-1} (26 drops) and 3.5 to 3.6 ms^{-1} (46 drops) at heights of 1.5, 1.0 and 0.5 m, respectively. Thus it was possible to construct the velocity vector field with the information obtained for each particle analyzed. Figure 10 presents the field for groups H1, H2 and H3, and shows the magnitude, direction and sense of the drops included. Comparing these vector maps was difficult since studies of similar phenomena found in the literature do not report this type of information.

It was evident that most of the vectors moved vertically, corresponding to the position in which the drops were captured, that is, when they were falling. Nevertheless, some (Figure 10b) had an inclination of roughly 45%, which is attributed to the position of the sprayer (30° with respect to the vertical), as observed by Salvador *et al*. (2009) and Bautista *et al*. (2009). In addition, the diameter-velocity relationship was key to the study of the energy with which the drops impacted the surface. Figure 11 shows the correspondence between these two variables and hydraulic pressure, observation distance and observation height. It is worth mentioning that some authors (Mang and Joss, 2000; Salvador *et al*., 2009) have proposed exponential and logarithmic expressions to explain the trend between diameter and velocity. In the work herein a correlation between these variables could not be found because only one observation point from the sprayer was used. To evaluate this, it is therefore necessary to apply the PTV technique at different distances and with different characteristics of the device used to generate the drops.

Conclusions

This investigation described the application of the PTV optical technique for the visualization of flows to characterize drops generated by a stream subject to the effect of high hydraulic pressures. Its implementation to analyze this type of physical phenomena was novel, since it had only been used in studies related to the sedimentation velocity of non-cohesive particles. An important advantage of this methodology over techniques that use low-speed photography is the time it takes to acquire images with valid drops and the factors required for their processing. The acquisition time improves over 200% and processing time per drop

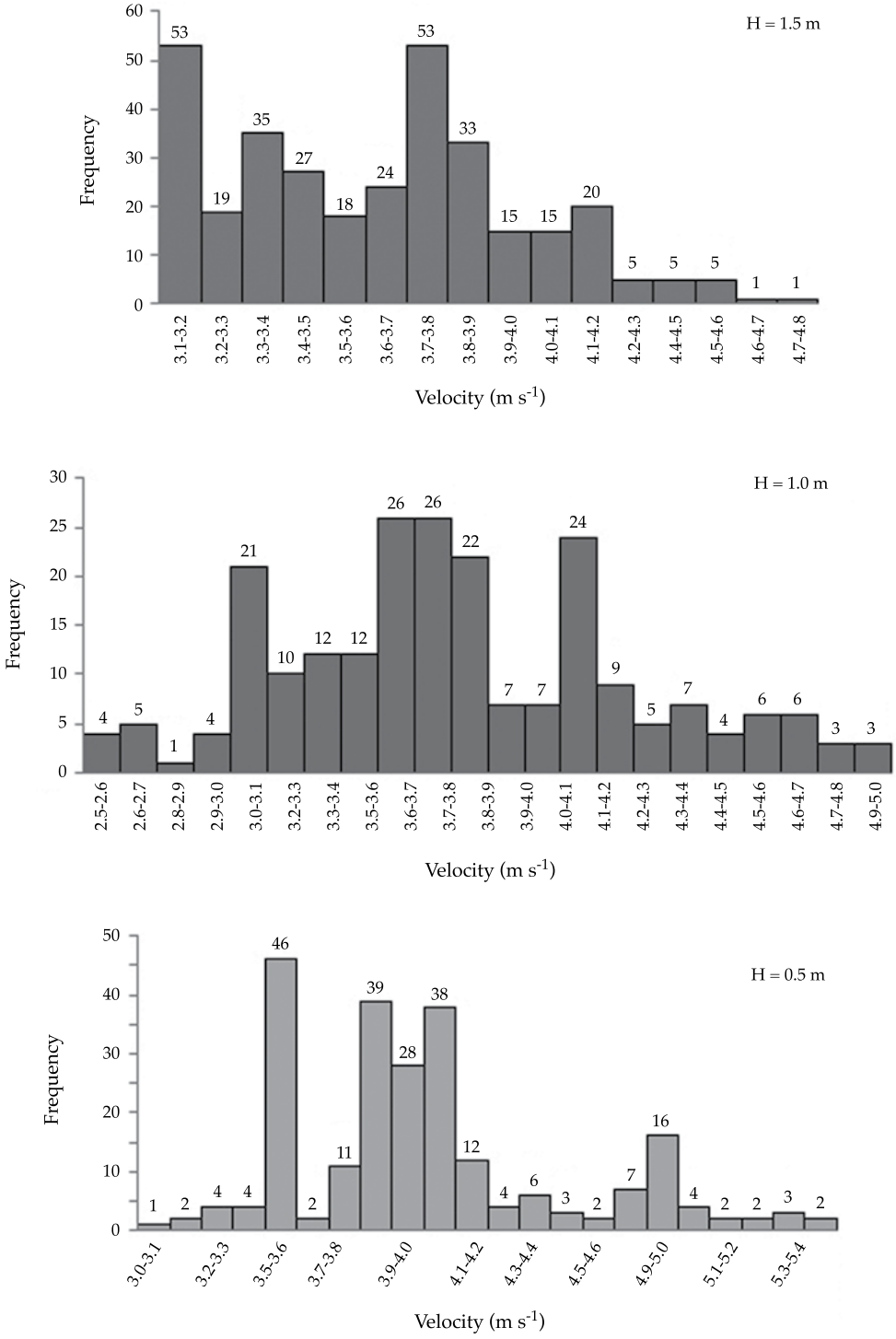

Figure 9. Frequency histograms of the velocities of drops at different heights.

analyzed is roughly 80 times less. The most important contribution by this work is its capacity to obtain diameters and velocities (magnitude, direction and sense) for a set of drops generated automatically, recorded at 4.5 m from the emitter at heights of 0.5,

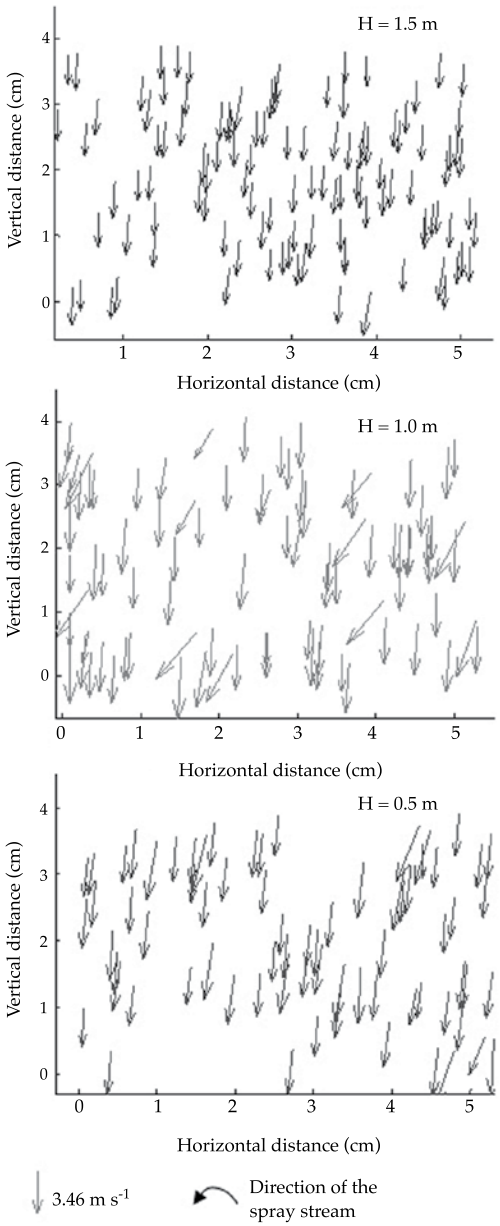

Figure 10. Velocity vectors per observation height: 1.5, 1.0 and 0.5 m.

1.0 and 1.5 m and with a hydraulic pressure of 175 kPa. This shows that the technique can be applied to future studies of drops generated by a sprinkler system. The above experimental conditions identified diameters between 0.09 and 0.83 mm and velocities between 2.5 and 5.5 ms^{-1}. The mean values

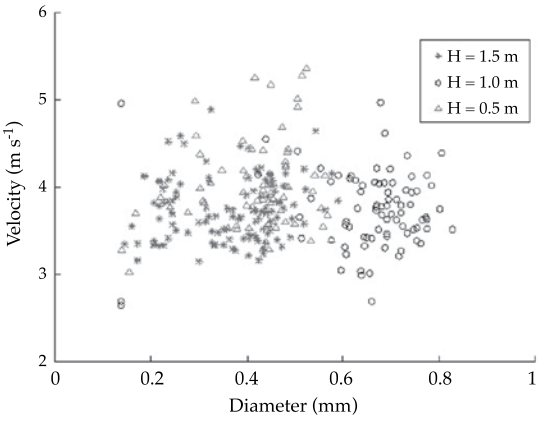

Figure 11. Relation of equivalent diameters *versus* resulting velocities.

of the diameter and velocity were 0.39 mm, 4.02 ms^{-1}; 0.55 mm, 3.70 ms^{-1} and 0.34 mm, 3.63 ms^{-1} for heights of 0.5, 1.0 and 1.5 m, respectively. The results of this work were based on a total of 1 685 acquired images, of which only 955 contained valid drops, thereby obtaining a total of 1 582 drops which were analyzed in order to characterize their diameters and velocity. The objective was to validate the technique for later use in the characterization of drops generated by sprinkler irrigation systems in order to determine diameter-velocity relationships for diverse combinations of diameter heads, sprinkler heights, fall distances, hydraulic operating pressures and environmental conditions.

Acknowledgements

Thank you to the Centro Interamericano de Recursos del Agua (Inter-American Water Resources Center) of the Autonomous University of the State of Mexico and the Masters in Applied Engineering in Hydraulic Resources of the Autonomous University of Zacatecas. Thank you to Conacyt for the grant to Cruz Octavio Robles Rovelo for masters studies. This investigation follows the first-last author emphasis norm.

Received: 25/04/2013
Accepted: 05/09/2013

References

ADRIAN, R.J. Engineering Applications of Particle Image Velocimeters. *Proc. SPIE* 1404, ICALEO'89, Optical Methods in Flow and Particle Diagnostics, October 01, Orlando, Florida, 1989, pp. 56-71.

ADRIAN, R.J. Particle Imaging Techniques for Experimental Fluid Mechanics. *Annual Reviews Inc., Fluid Mechanics*. Vol. XXIII. Urban, USA: Department of Theoretical and Applied Mechanics, University of Illinois, 1991, pp. 261-304.

BAUTISTA, C.F., SALVADOR, R., BURGUETE, J., MONTERO, J., TARJUELO, J.M., ZAPATA, N., GONZÁLEZ, J., and PLAYÁN, E. Comparing Methodologies for the Characterization of Water Drops Emitted by an Irrigation Sprinkler. *Transaction of the ASABE*. Vol. LII, No. 5, 2009, pp. 1493-1504.

BAUTISTA, C.F., MÁRQUEZ, V.H., JÚNEZ, F.H. y PLAYÁN, E.J. Characterization of drops emitted by a two-nozzle impact sprinkler using a photographic technique. *Water Technology and Sciences*. Vol. IV, No. 5, 2013, pp. 147-164.

CRUVINEL, P.E., MINATEL, E., MUCHERONI, M., VIEIRA, S., and CRESTANA, S. An Automatic Method Based on Image Processing for Measurements of Drop Size Distribution from Agricultural Sprinklers. *Anais do IX SIBIGRAPI*, Sao Paulo, Brazil, 1996, pp. 39-46.

CRUVINEL, P.E., VIEIRA, S., CRESTANA, S., MINATEL, R., MUCHERONI, M., and NETO, A. Image Processing in Automated Measurements of Raindrop Size and Distribution. *Comput. Electron. Agric*. Vol. XXIII, No. 3, 1999, pp. 205-217.

DECHMI, F. *Gestión del agua en sistemas de riego por aspersión en el valle de Ebro: análisis de la situación actual y simulación de escenarios*. Tesis doctoral. Zaragoza, España: Universidad de Lleida, diciembre de 2002.

EIGEL, J.D. and MOORE, I.D. A Simplified Technique for Measuring Raindrop Size and Distribution. *Trans. Am. Soc. Agric. Eng*. Vol. XXVI, No. 4, 1983, pp. 1079-1084.

FLORES, G.L. y LÓPEZ, R.B. *Análisis hidrodinámico de un sistema de recirculación de agua para uso en acuacultura utilizando técnicas óptimas PIV y PTV*. Tesis de Licenciatura en Ingeniería Civil. Toluca, México: Facultad de Ingeniería, Universidad Autónoma del Estado de México, 2012.

HAUSER, D., AMAYENC, P., NUTTEN, B., and WALDTEUFEL, P. A New Optical Instrument for Simultaneous Measurement of Raindrop Diameter and Fall Speed Distributions. *J. at Ocean. Technol*. Vol. I, No. 3, 1984, pp. 256-269.

IDO, T., MURAI, Y., and YAMAMOTO, F. Post-Processing Algorithm for Particle-Tracking Velocimetry Based on Ellipsoidal Equations. *Exp. Fluids*. Vol. 32, 2002, pp. 326-336.

JENSEN, K.D. Flow Measurements. *J. of the Braz. Soc. of Mech. Sci. & Eng*. Vol. XXVI, 2004, pp. 400-419.

JONES, D.M. *Rainfall Drop-Size Distribution and Radar Reflectivity*. Fort Monmouth, New Jersey: Illinois State Water Survey, Meteorology Laboratory, Research Report No. 6, 1956, pp. 20.

KINCAID, D.C., SOLOMON, K.H., and OLIPHANT, J.C. Drop Size Distributions for Irrigation Sprinklers. *Trans. of ASAE*. Vol. XXXIX, No. 3, 1996, pp. 839-845.

KOHL, R.A. and DeBOER, D.W. Drop Size Distributions for a Low Pressure Spray Type Agricultural Sprinkler. *Trans. Am. Soc. Agric. Eng*. Vol. XXVII, No. 6, 1984, pp. 1836-1840.

MAGARVEY, R.H. Stain Method of Drop Size Determination. *J. Meteorol*. Vol. XIV, 1956, pp. 182-184.

MANG, M.L. and JOSS, J. An Optical Disdrometer for Measuring Size and Velocity of Hydrometeors. *J. at Ocean. Technol*. Vol. XVII, 2000, pp. 130-139.

MONTERO, J., TARJUELO, J.M., and CARRIÓN, P. Sprinkler Droplet Size Distribution Measured with an Optical Spectropluviometer. *Irrigation Sci*. Vol. I, No. 22, 2003, pp. 47-56.

PLAYÁN, E., ZAPATA, N., FACI, J.M., TOLOSA, D., LACUEVA, J.L., PELEGRÍN, J., SALVADOR, R., SÁNCHEZ, I., and LAFITA, A. Assessing Sprinkler Irrigation Uniformity using a Ballistic Simulation Model. *Agric. Water Manag*. Vol. LXXXIV, No. 1-2, 2006, pp. 89-100.

PRASAD, A.K. Particle Image Velocimetry. *Exp. Fluids*. Vol. LXXIX, No. 1, 2000, pp. 51.

RAFFEL, M., WILLERT, C.E., and KOMPENHANS, J. *Particle Image Velocimetry*. New York: Ed. Springer, 1998.

SALLES, C., POESEN, J., and BORSELLI, L. Measurement of Simulated Drop Size Distribution with an Optical Spectro-Pluviometer: Sample Size Considerations. *Earth Surface Processes Landforms*. Vol. XXIV, No. 6, 1999, pp. 545-556.

SALINAS, T.H., GARCÍA, A.J., MORENO, H.D., and BARRIENTOS, G.B. Particle Tracking Velocimetry (PTV) Algorithm for Non-Uniform and Non-Spherical Particles. *Proceedings, Electronics, Robotics and Automotive Mechanics Conference, CERMA*. Núm. 2, Cuernavaca, Morelos, México, del 26 al 29 de septiembre de 2006, pp. 322-327.

SALINAS, T.H. y GARCÍA, A.J. Experimental formula for the settling velocity of sediments in cross-flow. *Water Technology and Sciences* therefore Hydraulic Engineer in Mexico. Vol. II, No. 2, 2011, pp. 175-182.

SALVADOR, R., BAUTISTA, C., BURGUETE, J., ZAPATA, N., SERRETA, A., and PLAYÁN, E. A Photographic Method for Drop Characterization in Agricultural Sprinklers. *Irrigation Sci*. Vol. XXVII, February, 2009, pp. 307-317.

SANG, Y.L. and YU, D.K. Sizing of Spray Particles using Image Processing Technique. *KSME International Journal*. Vol. XVIII, No. 6, 2004, pp. 879-894.

SMITS A.J. and LIM T.T. *Flow Visualization: Techniques and Examples*. Singapore: Ed. Imperial College Press, 2000, 396 pp.

SUDHEER, K.P. and PANDA, R.K. Digital Image Processing for Determining Drop Sizes from Irrigation Spray Nozzles. *Agric. Water Manag*. Vol. XLV, 2000, pp. 159-167.

VAN DYKE, M. *An Album of Fluid Motion*. Stanford: Ed. Parabolic Press, 1982, 176 pp.

VIRANT, M. and DRACOS, T. 3D PTV and Application on Lagrangian Motion. *Meas. Sci. Technol*. Vol. 8, 1997, pp. 1539-1552.

VORIES, E.D., VON BERNUTH, R.D., and MICKELSON, R.H. Simulating Sprinkler Performance In Wind. *J. Irrig. and Drainage Div. ASCE*. Vol. CXIII, No. 1, 1987, pp. 119-130.

WESTERWEEL, J. *Digital Particle Image Velocimetry. Theory and Application*. Ph. D. Thesis. Delft: University of Technology, the Netherlands, 1993.

Institutional Address of the Authors

Dr. Humberto Salinas Tapia

Profesor-investigador del CIRA
Centro Interamericano de Recursos del Agua (CIRA)
Universidad Autónoma del Estado de México
Carretera Toluca-Ixtlahuaca, km 14.5
San Cayetano de Morelos
50295 Toluca, Estado de México, México
Teléfono: +52 (722) 2965 550 y 51/180 6191 y 92, extensión 103
hsalinast@uaemex.mx

M.I. Cruz Octavio Robles Rovelo
M.I. Dagoberto Chávez Carlos
Dr. Carlos Francisco Bautista Capetillo

Universidad Autónoma de Zacatecas
Av. Ramón López Velarde 801, Col. Centro
98000 Zacatecas, Zacatecas, México
Teléfono: +52 (492) 9222 001
corr03@hotmail.com
dago_chc@hotmail.com
baucap@uaz.edu.mx

Technical Note

Effects of Hurricane *Wilma* on the Aquifer in the Yucatan Peninsula, Mexico

• Eduardo Graniel-Castro* • Jazmín Yam-Caamal •
Universidad Autónoma de Yucatán, México
*Corresponding Author

Abstract

GRANIEL-CASTRO, E. & YAM-CAAMAL, Y. Effects of Hurricane Wilma on the Aquifer in the Yucatan Peninsula, Mexico. *Water Technology and Sciences* (in Spanish). Vol. V, No. 3, May-June, 2014, pp. 143-149.

Environmental and climate changes worldwide have increased the number of hurricanes, for example, Gilberto in 1988, Opal and Roxana in 1995 and *Isidore* in 2002, and *Emily* and *Wilma* in 2005. These natural phenomena have caused floods, power outages, loss of crops and damages to housing and roads in the state of Yucatan, Mexico. In October 2005, hurricane Wilma passed through the Yucatan with 314.3 mm in precipitation, causing the hydraulic loads of the aquifer to increase 1.5 m, lowering the saline interface in wells 9 m (1B and 2C), which returned to their position in January due to the heterogeneity of the karstic subsoil. The direction of the groundwater flow was southeast to northwest and did not change as a result of hurricane *Wilma*. Pollutants existing before the hurricane were diluted in most of the wells, except 2A, in which nitrates increased due to organic matter accumulated from floods in the area. In general, hurricanes in the Yucatan are beneficial to the aquifer due to the recharge of water and dilution of existing pollutants, although they are not beneficial to the population because of damage to infrastructure.

Keywords: Dynamic, karstic, saline interface, hurricane *Wilma*, Yucatan, water quality.

Resumen

GRANIEL-CASTRO, E. & YAM-CAAMAL, Y. Efectos del huracán Wilma al acuífero de la península de Yucatán, México. Tecnología y Ciencias del Agua. *Vol. V, núm. 3, mayo-junio de 2014, pp. 143-149.*

Los cambios ambientales y climáticos en el mundo han incrementado el número de huracanes, como Gilberto en 1988, Opal y Roxana en 1995, Isidore *en 2002, y* Emily *y* Wilma *en 2005. Estos fenómenos naturales han causado inundaciones, interrupción del servicio eléctrico, pérdida de cosechas, y daños en la infraestructura habitacional y carretera en el estado de Yucatán, México. En octubre de 2005, el huracán* Wilma *pasó por Yucatán con una precipitación de 314.3 mm, ocasionando que las cargas hidráulicas del acuífero ascendieran 1.5 m y la interfase salina fuera desplazada hacia abajo unos 9 m en los pozos (1B y 2C), regresando en enero a su posición anterior debido a la heterogeneidad del subsuelo cárstico. La dirección del flujo subterráneo fue de sureste a noroeste y no cambió por el huracán* Wilma. *Se presentó el efecto de dilución de los contaminantes existentes antes del huracán en la mayoría de los pozos, excepto el 2A, en el cual se incrementaron los nitratos debido a la materia orgánica acumulada por las inundaciones de la zona. En general, los huracanes en Yucatán resultan benéficos para el acuífero debido a la recarga de agua que diluye la contaminación existente, aunque no para la población, por los daños en las infraestructuras.*

Palabras clave*: dinámica, carst, interfase salina, huracán* Wilma, *Yucatán, calidad de agua.*

Introduction

The dynamics of coastal aquifers are influenced by extreme precipitation caused by hurricanes which alter the fresh-saltwater interface. Therefore, it is very important to identify their effects on aquifers, such as the Yucatan coastline, Mexico. This area lies in the trajectory of hurricanes in the Atlantic and the Caribbean, including *Isidore* in 2002 and *Emily* and *Wilma* in 2005.

The karstic characteristics of the subsoil and the virtually flat topography (SARH, 1989) of the area result in most of the rainfall infiltrating the aquifer, causing the water level to increase, the saline interface to reach lower depths and the quality of the groundwater to change. Therefore, it is very important to

understand the effect of hurricanes passing through the region on the vertical and spatial changes in the saline interface and the quality of the groundwater.

During hurricane *Wilma*, extreme precipitation measuring 200 mm occurred over two days. This caused the eastern coastal area to flood and some of the wells to become artesian. The study area is located on the northwest coast between San Felipe and El Cuyo in the state of Yucatan. It covers an inland area of 20 km and contains 6 observation wells located on two transects perpendicular to the coastline (transect 1: San Felipe-Panaba; Transect 2: El Cuyo-Colonia Yucatan), at 5, 10 and 15 km from the coast and at depths of 20, 30 and 40 m, increasing as the distance from the coastline increases (Figure 1).

The climate in the coastal region has three seasons: rainy (June-October), dry (February-May) and northern winds (November-January) (CNA, 1997). The average precipitation is 1 058 mm and the average temperature is 26.6°C (CNA, 2005).

The aquifer is made up of massive mollusk limestone, white to cream in color from the Pleistocene-Holocene period, with outcroppings along a somewhat wide band on the coast. It is highly permeable and therefore very sensitive. A relatively wide strip in the area is made up of sand dunes and coquineferous limestone soil. It contains lacustrine soil composed of sands, clays and calcareous mud and is somewhat permeable (CNA, 1997).

Topographic depressions exist between the transects, often found 5 m below the plain because of a series of faults and fractures. In some sites, the static level surfaces form lagoons locally known as "sabanitas" (Tinajero *et al*., 1981; Back and Lesser, 1981).

The water table depth is only a few meters and presents hydraulic loads ranging between 2 and 5.5 m, resulting in a hydraulic gradient of the order of 0.50 cm/km due to the type of material and the physical characteristics of the terrain (MTA, 2003; Vera, 2005; Carrillo- Cauich, 2006; Yam, 2006). The water in the aquifer is calcium bicarbonate, except for Well 2A which is chloride and sodic (IMTA, 2003). The objective of this study was to determine the effects of hurricane *Wilma*

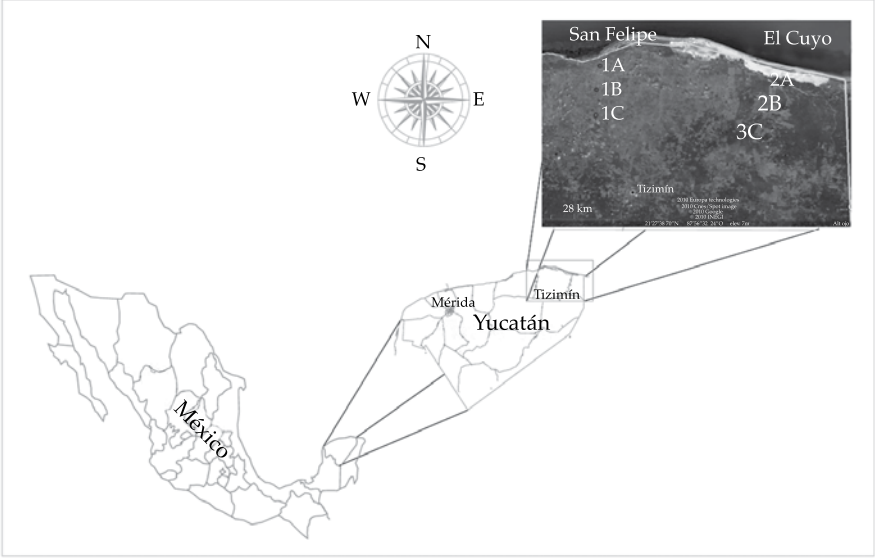

Figure 1. Location of study zone.

on the quantity and quality of water in the Yucatan aquifer.

Methodology

The study was conducted from September 2005 to January 2006. Three field campaigns were performed every two months. In situ measurements included the depth of the static level and water quality indicators (temperature, hydrogen potential, electrical conductivity, dissolved oxygen and redox potential). Water samples were collected at depths that varied according to the electrical conductivity, which had to be less than 2 500 mS/cm since a salty flavor begins to occur due to the presence of salts that can cause health problems. The water samples were analyzed at the Engineering School of the Autonomous University of Yucatan (UADY, Spanish acronym) according to standard methods (APHA, 1992). The following were determined: calcium (Ca^{++}), magnesium (Mg^{++}), sodium (Na^{+}), potassium (K^{+}), bicarbonates (HCO_{3}^{-}), sulfate ($SO_{4}^{=}$), chloride (Cl^{-}), nitrates (No^{3}), total kendal nitrogen (KTN), ammoniacal nitrogen (NH3), organic nitrogen (N_{org}) and nitrates (NO_{2}). Before analyzing the results, the percentage of error was estimated based on the calculation of ionic balance. The electrical conductivity was considered when analyzing the behavior of the saline interface, since this reflects the ability of the water to transmit electrical current and is directly proportional to the salt contents of the water (López and Mena, 1988).

Results and Discussion

The direction of the flow of groundwater is southeast to northwest, discharging into the sea. Its direction did not change as a result of hurricane *Wilma* (Figure 2). The hydraulic gradients ranged between 0.11 and 0.32 m/km, and the hydraulic loads varied between 1.65 and 6.69 m. During hurricane *Wilma* the hydraulic load increased 0.50 masl and 1.5 masl in Wells 1C and 2B, respectively, and returned to their original levels in January of 2006 (Figure 3).

Temperature, dissolved oxygen and hydrogen potential did not significantly change due to the hurricane and presented normal conditions. The analysis of the electrical conductivity showed fresh water in Wells 1B and 2B and saltwater throughout 2A (Figure 4).

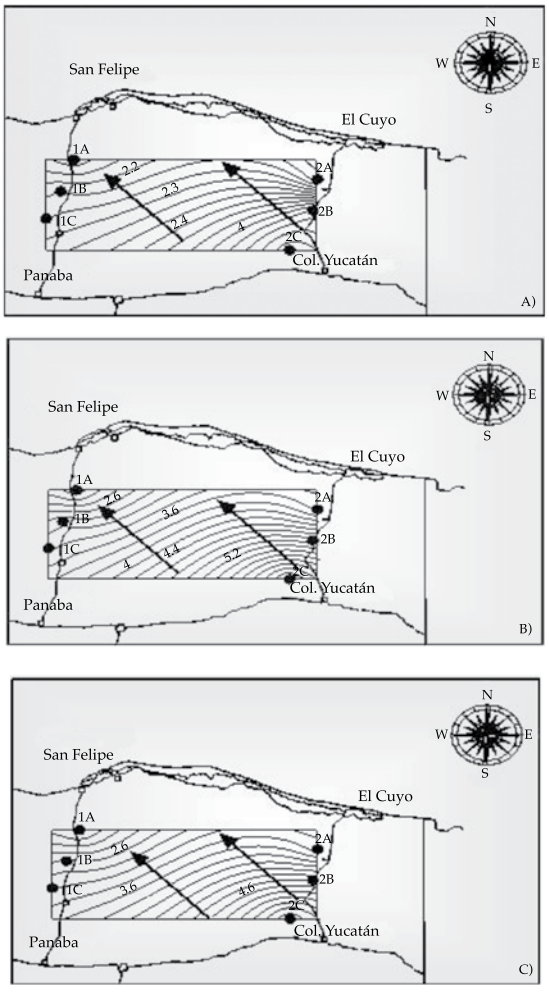

Figure 2. Direction of groundwater flow: a) September 2005, b) November 2005 and c) January 2006.

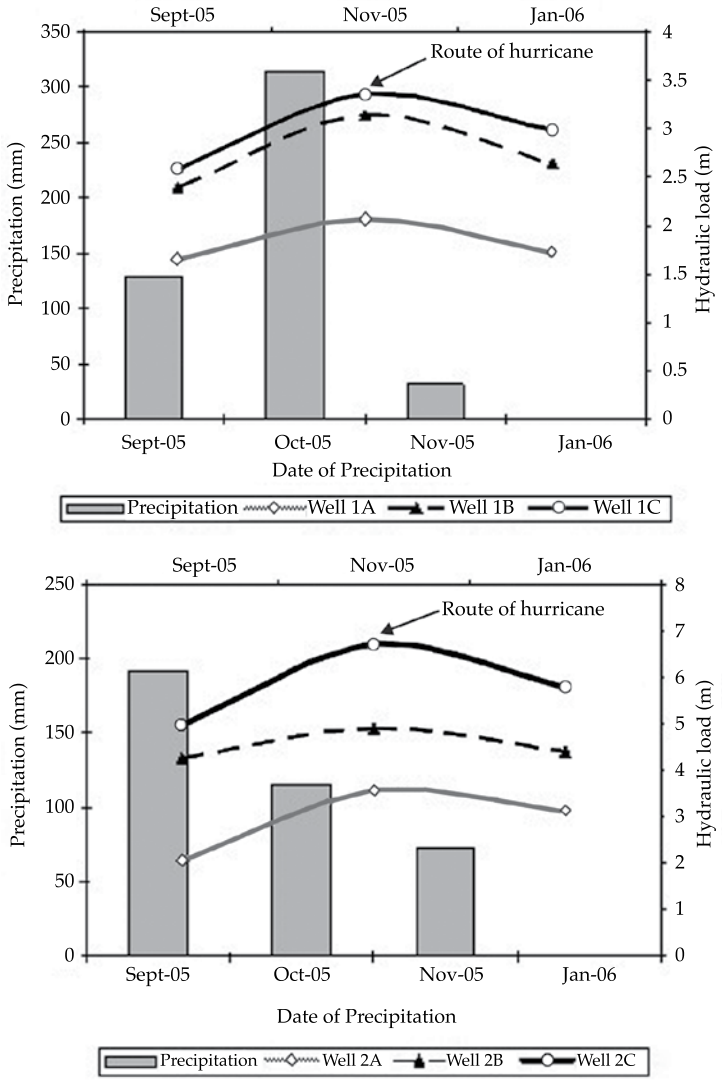

Figure 3. Variation in hydraulic load (m) and precipitation (mm).

In Well 1A, the saline interface began at a depth of 15 m, and in 1C it began at 26 m, moving downward 1 m in November 2005 due to the increased hydraulic load (0.50 masl). In Well 2C, the roof of the saline intrusion was located at a depth of 30 m in September 2005 and January 2006, and at 39 m in November. A movement was observed of 9 m due to the increase in the hydraulic load (1.5 masl).

According to the potential redox (Eh) (Figure 5), Wells 1B, 2A and 2C had anaerobic conditions after the hurricane, with a trend towards better quality over time. These values decreased in Wells 1A, 1C and 2B, while the aerobic conditions remained stable.

The ionic balance error in the results of the laboratory analysis was less than 10%. In transect 1, Ca, Na, Cl, NO_3 and HCO_3 decreased after the hurricane, and Mg, K and SO_4 increased due to the drifting of surface material. In transect 2, Ca, Mg, K, HCO_3 and $S0_4$ increased as the hurricane passed and Na, Cl and NO_3 decreased due to dilution (Figure 6).

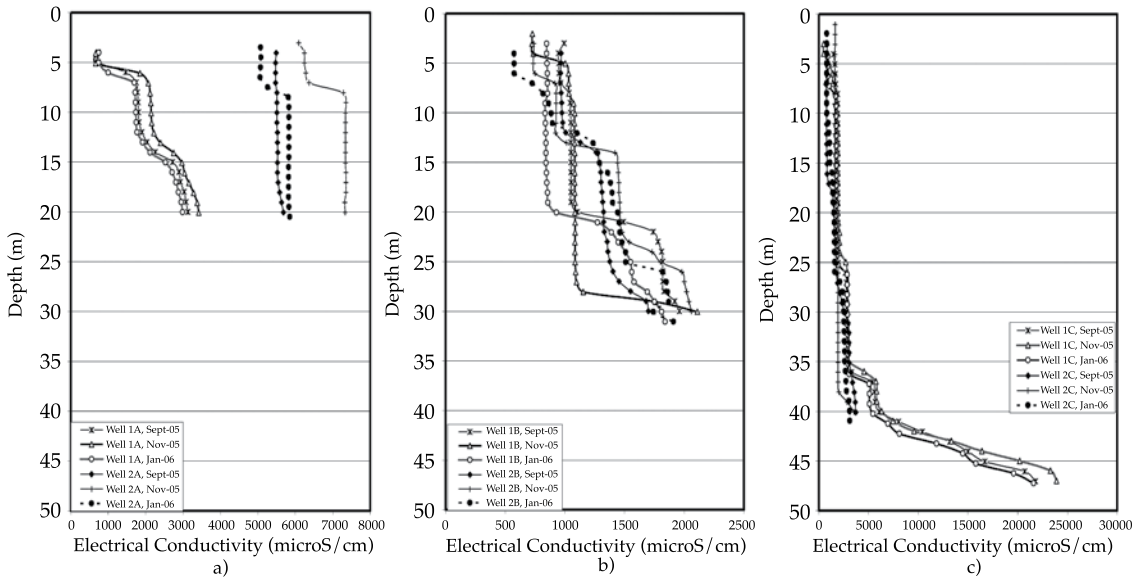

Figure 4. Electrical conductivity profiles: a) Wells 1A, and 2A b) 1B and 2B and c) 1C and 2C.

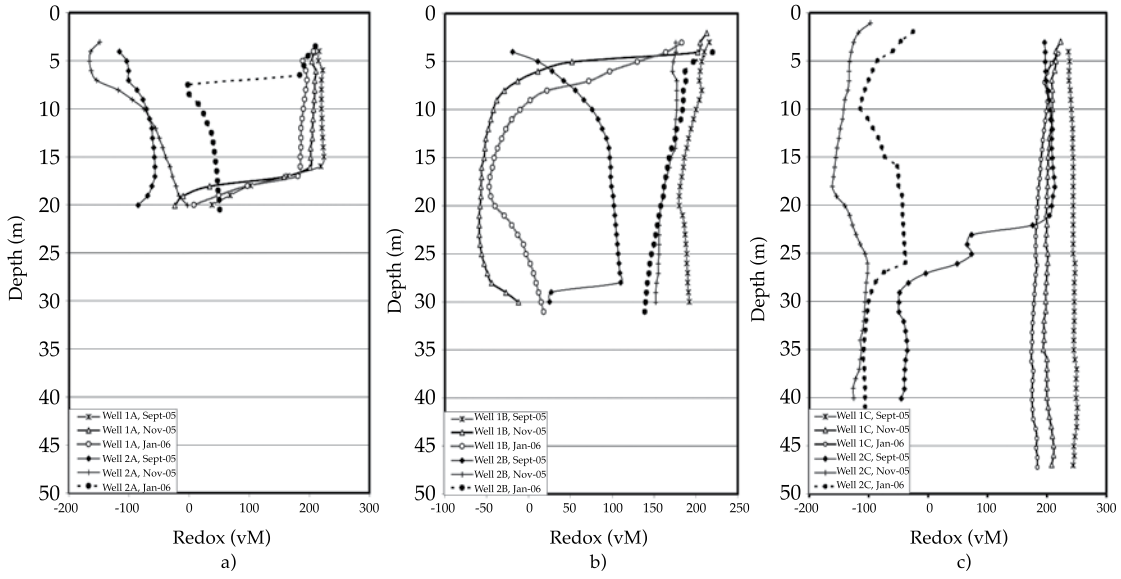

Figure 5. Redox profiles: a) Wells 1A and 2A, b) 1B and 2B and c) 1C and 2C.

Conclusions

The direction of the groundwater flow in the northeastern coastal area of the Yucatan is southeast to northwest and did not change direction as a result of hurricane *Wilma*.

The hydraulic loads increased 1.5 m in some of the wells and returned to their original levels in January 2006. The largest hydraulic loads were found in the El Cuyo-Colonia Yucatán transect, where there are fractures, faults and dissolution. The

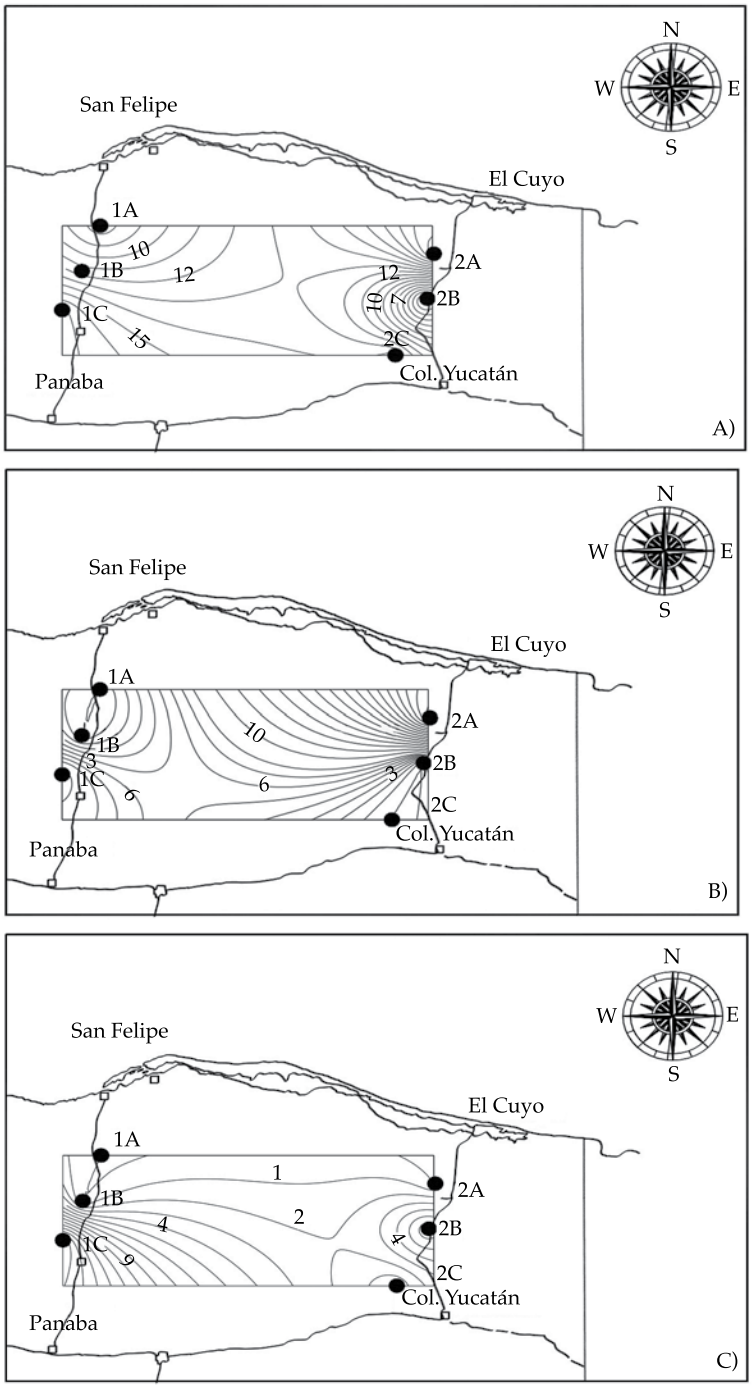

Figure 6. Isoconcentrations of nitrates in mg/l: a) September 2005, b) November 2005 and c) January 2006.

hydraulic load increases and the saline interface reaches lower depths as the distance of the wells from the coast increases. The roof of the saline intrusion moved downward 9 m in Wells 1B and 2C and 1 m in Well 1C, returning in January 2006 to the levels they had before the hurricane.

El techo de la intrusión salina en los pozos 1B y 2C fue desplazado hacia abajo 9 m, y en el pozo 1C se desplazó hacia abajo 1 m, regresando en enero 2006 a sus posiciones antes del huracán.

In the aquifer, dilution occurred of the pollutants present in most of the wells, except for 2A, in which the nitrates increased due to the infiltration of organic matter accumulated from the flood which occurred in that area.

In general, hurricanes passing over the Yucatan are favorable to the aquifer because of the recharge provided by the large volume of water that infiltrates as well as because of the dilution of pollution. Nevertheless, overall they are not beneficial to the population because of damages to infrastructure and harm to the health of the inhabitants.

Acknowledgements

The authors thank the Fondo Mixto Conacyt-Gobierno del Estado de Yucatán (Conacyt-Government of the State of Yucatan Mixed Fund) for support of the project YUC-2003-CO2-027, called "Characterization of the Dynamics of the Saline Interface and Water Quality in the Coastal Aquifer in the Yucatan State ("Caracterización de la dinámica de la interfase salina y de la calidad del agua en el acuífero costero del Estado de Yucatán"). Thank you to the National Water commission, Regional Yucatan Peninsula Management, and the Engineering School at the Autonomous University of Yucatan for their support of this work.

Received: 04/02/2011
Accepted: 05/11/2013

References

APHA, AWWA, WEF. Standard Methods for the Examination of Water and Wastewater. 18 th edition. Washington, DC: American Public Health Association, 1992.

BACK, W. and LESSER J.M. Chemical Constraints of Groundwater Management in the Yucatan Peninsula, Mexico. Elsevier Scientific Publishing Company, Amsterdam. *Journal of Hidrology*. Vol. 51, 1981, 119-130.

CARRILLO-CAUICH, M.E. *Estudio hidrogeológico de la costa nororiental de Yucatán*. Tesis de licenciatura. Facultad de Ingeniería de la Universidad Autónoma de Yucatán, Mérida, Yucatán, 2006.

CNA. *Diagnóstico de la Región XII, Península de Yucatán*. Subdirección General de Programación, Gerencia de Planeación Hidráulica, Gerencia Regional de la Península de Yucatán, Mérida, Yucatán, 1997.

CNA. *Datos climatológicos*. México, DF: Comisión Nacional del Agua, 2005.

IMTA. *Definición de las reglas de operación del acuífero costero de la península de Yucatán*. Reporte técnico. Jiutepec, México: Instituto Mexicano de Tecnología del Agua, 2003.

LÓPEZ, G. y MENA, I. *Aspectos metodológicos en el estudio de la intrusión salina* [en línea]. 1988. Disponible en World Wide Web: http://www.igme.es/internet/ web_aguas/ igme/publica/libro41/lib41.htm.

SARH. *Sinopsis geohidrológica del estado de Yucatán*. México, DF: Secretaría de Agricultura y Recursos Hidráulicos, Subsecretaría de Infraestructura Hidráulica, Dirección General de Administrativo y Control de Sistemas Hidrológicos, 1989, 50 pp.

TINAJERO, G.J., VELÁZQUEZ, A.L. y ZÚÑIGA, O.D. Hidrogeología e hidrogeoquímica regional de la península de Yucatán, México. Cap. II.2 del proyecto CPNH-IAS 8104. En *Estudio de las características geohidrológicas del acuífero en el área de Mérida Yucatán*. Secretaría de Agricultura y Recursos Hidráulicos, México, 1981.

VERA, I. *Estudio de la dinámica de la interfase salina y características fisico-químicas del acuífero nororiental del estado de Yucatán*. Tesis de maestría. Universidad Autónoma de Yucatán, Mérida, Yucatán, 2005, 85 pp.

Institutional Address of the Authors

Dr. Eduardo Graniel-Castro
Ing, Jazmín Yam-Caamal

Facultad de Ingeniería
Universidad Autónoma de Yucatán
Av. Industrias No Contaminantes por Anillo Periférico Norte s/n
97310 Mérida, Yucatán, México
Teléfono: +52 (999) 9300 550, extensión 1028
Fax: +52 (999) 9300 559
graniel@uady.mx
jaztere@hotmail.com

Click here to write the autor

Effects of drought on water bodies, San José de la Laguna, Durango, Mexico.

Photo: Óscar Alonso Barrón.

Nota técnica

Evaluación de los métodos de obtención de curvas IDF para México

• Francisco Manzano-Agugliaro* • Antonio Zapata-Sierra •
• Juan Francisco Rubí-Maldonado •
Universidad de Almería, España
*Autor de correspondencia

• Quetzalcoatl Hernández-Escobedo •
Universidad Veracruzana, México

Resumen

MANZANO-AGUGLIARO, F., ZAPATA-SIERRA, A., RUBÍ, J.F. & HERNÁNDEZ-ESCOBEDO, Q. Evaluación de métodos de obtención de curvas IDF para México. Tecnología y Ciencias del Agua. *Vol. V, núm. 3, mayo-junio de 2014, pp. 151-161.*

En este trabajo se evalúan los métodos de obtención de curvas IDF para México: Wencel modificado, Chen, Chen modificado, Témez y Témez modificado. Los datos proceden de 63 estaciones automáticas (EMAS), distribuidas por todo el país, con registros cada 10 minutos y durante siete años como mínimo. Para el análisis se han diferenciado estaciones de costa cuando están a 50 km o menos de esa zona, y las demás como de interior. Se han valorado para cada una de las estaciones, todos los parámetros de los métodos de cálculo de curvas IDF mencionados, para duraciones entre 10 minutos y 24 horas, y para periodos de retorno de 2 a 500 años. Se ha comprobado que cuando se tienen registros de lluvia cada 10 minutos o menos, se recomienda el método de Wencel; cuando se tienen registros de lluvia horarios, se aconseja el método de Chen; cuando los datos de lluvia son diarios, para duraciones menores de 2 h, se necesita el método de Témez modificado; para duraciones de más de 2 h, el mejor es el de Chen modificado para las zonas del interior y Témez modificados para las zonas costeras.

Palabras clave: *México, IDF, lluvia extrema, costa, interior, Wencel, Chen, Témez.*

Abstract

MANZANO-AGUGLIARO, F., ZAPATA-SIERRA, A., RUBÍ, J.F. & HERNÁNDEZ-ESCOBEDO, Q. Assessment of Obtaining IDF Curve Methods for Mexico. *Water Technology and Sciences* (in Spanish). Vol. V, No. 3, May-June, 2014, pp. 151-161.

This paper assesses the methods of obtaining IDF curves for the country of Mexico: modified Wencel, Chen, modified Chen, Témez and modified Témez. The data came from a total of 63 automated weather stations distributed throughout the country, recording data every 10 minutes for a minimum of 7 years. For the analysis, stations 50 km or less from the coast were identified as coastal and the remaining as inland. For each station, all of the parameters for the methods mentioned to calculate the IDF curves were evaluated for durations of 10 minutes to 24 hours, and return periods of 2 to 500 years. It was shown that when rainfall records for 10 minutes or less are used the Wencel method is recommended, and when the records are hourly the Chen method is recommended. When rainfall data are daily for durations under 2 h, the modified Temez method is required, and for durations of more than 2 h the best method is the modified Chen for inland areas and modified Temez for coastal areas.

Keywords: Mexico, IDF, extreme rainfall, coastal, inland, Wencel, Chen, Témez.

Introducción

El dimensionamiento de estructuras hidráulicas se basa en la inundación de diseño (Singh y Hao, 2011). El nivel del desempeño deseado se determina a menudo por medio del daño potencial y la severidad de los riesgos del clima que podrían provocar las fallas, el mal funcionamiento o la estructura de sobreflujo en cuestión (Soro *et al*., 2010). De tal modo, en el caso del manejo de agua de lluvia, la dimensión de diversos componentes del sistema de infraestructura (cajas de tubos y saneamiento de canales) se basa en el periodo de retorno de los eventos de lluvias extremas (Monhymont y Demarée, 2007); (Segond *et al*.,

2007). Esta información se expresa a menudo como las curvas de intensidad-duración-frecuencia (IDF) obtenidas del estudio estadístico de eventos extremos.

Para el país de México existe un mapa de curvas IDF desarrollado por la Secretaría de Comunicaciones y Transportes (SCT, 1990); en la literatura existen estudios tales como Campos (1990) que obtuvo curvas IDF de Cazadero, Zacatecas, aplicando las ecuaciones de Bell y Chen, lluvias intensas diseminadas; también Pereira-Díaz *et al*. (2004) en un estudio preliminar ajustaron las ecuaciones de Sherman (1931), Wenzel (modificada por Chow *et al*., 1988) y Koutsoyiannis *et al*. (1998) a las intensidades de 11 tormentas severas registradas durante el periodo 1999-2002. Todos estos estudios muestran la necesidad de registros continuos de precipitación para las grandes ciudades, para usar la lluvia extrema en el diseño urbano.

El objetivo de este artículo es evaluar los diferentes procedimientos para obtener las relaciones IDF para México, con base en dos enfoques: el método de referencia y el método empírico, con el fin de determinar primero si hay diferencias en el comportamiento entre área geográficas costeras e interiores o en tierra adentro, y si es así, cuál es el modelo más apropiado a cada zona, dependiendo de los datos de lluvia disponibles.

Datos y métodos

Datos

Para evaluar los diferentes métodos con los que se obtienen los cocientes IDF en áreas costeras e interiores, se usaron registros de la red de estaciones de clima automáticas (EMA) administradas por la Coordinación General del Servicio Meteorológico Nacional (CGSMN) con transmisión de satélite. Esta red tiene 133 estaciones automáticas instaladas a lo largo del país. El tiempo de la serie de registros de esta red de estaciones es variable dependiendo de la estación, por lo que se han seleccionado 63 estaciones con un conjunto de registros que se limita entre 1999 y 2008 (vea la figura 1). Se ha permitido la selección de estas 63 estaciones para este trabajo con conjuntos de datos de un periodo mínimo de 8 años, para los cuales corresponde el 86%, incrementándose hasta 90% cuando la edad mínima de la serie es de 7 años. Los trabajos realizados en otros países usan también periodos cortos de series para analizar estos fenómenos si estos no se arreglan para series más largas, por ejemplo Lam y Leung (1994) en Hong Kong (China) o Zapata-Sierra *et al*. (2009) en España, ya que una duración similar de las series da resultados similares para series más largas. Para México, Escalante y Reyes (2004) han observado que para registros más largos que 20 años la *R* (razón de la lluvia para 1 a 24 horas) se vuelve estable, y Mendoza-Resendiz *et al*. (2013) usan series de datos de duración de 7 años para el cálculo de lluvias sintéticas.

Los registros de precipitación utilizados en este trabajo se elaboraron por medio de la altura de precipitación (mm) en 10 minutos (GMT), para cada estación, cada mes y año del periodo de estudio. Así, se ha tenido un total de 105 120 registros por estación y año. La tabla 1 lista las estaciones incluidas en el estudio, y la tabla 2 ofrece su clasificación en la zona costera (C) o interior (I) y el periodo de datos usados. La figura 1 muestra la distribución espacial de las 63 estaciones climáticas automáticas en México.

Análisis de intensidad-duración-frecuencia

Algunos autores proponen el uso de la distribución doble de Gumbel en áreas donde existe la posibilidad de lluvia con dos diferentes mecanismos de generación

Figura 1. Localización en México de las estaciones de lluvia (EMA) estudiadas.

Tabla 1. Valores calculados para los parámetros de las siguientes ecuaciones: Wenzel, Chen, Chen modificada y Témez modificada.

	Wenzel (1)				Chen (2)			Chen modificada (3)			Témez modificada (5)	
Estación	**a**	**b**	**c**	**d**	a_1	b_1	c_1	a_{24}	b_{24}	c_{24}	α_1	β_1
Acapulco	65.90	0.113	0.786	0.422	1.220	0.236	0.654	10.64	0.242	0.655	0.973	-0.222
Agustín	21.28	0.167	0.543	-0.125	1.040	-0.053	0.580	6.29	-0.054	0.578	1.005	-0.370
Álamos	60.78	0.124	1.135	0.533	1.922	0.691	1.225	41.60	0.637	1.159	0.980	-0.172
Altamira	112.85	0.136	1.044	0.997	2.067	1.040	1.047	29.16	1.032	1.041	0.955	-0.164
Alvarado	74.24	0.139	0.422	0.105	1.029	0.032	0.397	3.28	0.022	0.379	0.990	-0.297
Angamacutiro	49.61	0.139	1.241	0.404	2.223	0.663	1.433	82.59	0.648	1.410	0.995	-0.170
Atlacomulco	49.32	0.139	1.224	0.511	2.274	0.790	1.397	80.97	0.809	1.422	0.986	-0.164
Bahía Ángeles	12.40	0.232	1.016	0.145	1.239	0.134	0.976	27.61	0.134	0.977	1.006	-0.238
Basaseachi	41.79	0.157	0.955	0.268	1.252	0.238	0.927	21.81	0.237	0.926	0.992	-0.219
Cabo San Lucas	71.24	0.239	1.108	0.936	2.269	1.042	1.119	42.04	1.056	1.130	0.959	-0.158
Calakmul	119.01	0.097	1.215	1.119	3.841	1.619	1.429	89.46	1.629	1.436	0.957	-0.144
Campeche	95.12	0.082	0.800	0.716	1.251	0.468	0.694	8.44	0.391	0.618	0.958	-0.203
Cancún	131.39	0.204	0.615	0.696	1.173	0.319	0.495	5.10	0.311	0.487	0.956	-0.229
Cd. Alemán	147.15	0.084	1.043	1.332	2.277	1.348	1.027	23.31	1.202	0.937	0.945	-0.157
Cd. Constitución	36.08	0.149	0.625	0.343	0.891	0.112	0.477	5.01	0.109	0.473	0.974	-0.250
Cd. del Carmen	65.08	0.165	0.920	0.632	1.481	0.529	0.865	16.38	0.511	0.846	0.966	-0.191
Celestún	87.76	0.111	1.194	0.903	2.948	1.262	1.355	70.20	1.262	1.356	0.963	-0.151
Cerro Cat	39.63	0.117	0.793	0.692	1.258	0.450	0.692	9.87	0.454	0.695	0.959	-0.205
Chapala	54.09	0.169	1.221	0.470	2.317	0.730	1.393	72.39	0.719	1.379	0.989	-0.167

Tabla 1 (continuación). Valores calculados para los parámetros de las siguientes ecuaciones: Wenzel, Chen, Chen modificada y Témez modificada.

Chetumal	69.68	0.138	0.721	0.488	1.150	0.274	0.629	7.32	0.249	0.597	0.967	-0.226
Chinatú	49.18	0.147	1.145	0.492	1.985	0.656	1.245	52.05	0.646	1.233	0.984	-0.174
Chinipas	98.40	0.150	1.306	0.903	5.279	1.643	1.703	198.91	1.684	1.738	0.967	-0.140
Cozumel	118.90	0.201	0.656	1.063	1.267	0.541	0.510	5.35	0.531	0.503	0.944	-0.212
CPGM	81.48	0.104	0.821	0.598	1.295	0.418	0.742	9.96	0.363	0.680	0.964	-0.206
ENCB	77.86	0.147	1.448	0.975	19.361	2.532	2.354	1 180.37	2.584	2.408	0.969	-0.127
Guachochi	47.88	0.131	1.005	0.522	1.541	0.520	0.999	24.77	0.515	0.993	0.976	-0.188
Gustavo DO	17.53	0.209	0.613	0.181	1.054	0.076	0.555	6.20	0.072	0.547	0.986	-0.271
Huamantla	83.01	0.160	1.337	0.594	4.234	1.210	1.759	186.42	1.161	1.704	0.985	-0.148
Huejutla	163.64	0.128	1.063	1.700	3.022	1.825	1.093	34.20	1.814	1.087	0.939	-0.150
Huimilpan	107.06	0.123	1.426	1.231	24.123	2.955	2.319	985.90	2.939	2.307	0.960	-0.124
IMTA	84.61	0.136	1.143	0.794	2.567	1.047	1.271	56.09	1.047	1.272	0.966	-0.159
Izúcar	130.50	0.219	1.323	1.439	7.681	2.367	1.688	275.13	2.509	1.776	0.952	-0.129
Jalapa	48.85	0.115	0.729	0.239	1.086	0.137	0.674	8.62	0.125	0.652	0.985	-0.250
Joicotepec	23.20	0.191	0.702	0.013	1.074	0.004	0.688	9.65	0.003	0.686	1.000	-0.309
Los Colomos	66.62	0.115	1.428	0.597	7.893	1.548	2.142	466.06	1.561	2.155	0.988	-0.140
Maguarichi	27.64	0.148	0.986	0.137	1.199	0.129	0.972	22.93	0.125	0.961	1.005	-0.244
Matamoros	119.93	0.160	1.259	1.165	5.260	1.862	1.574	147.19	1.902	1.602	0.957	-0.139
Mérida	101.20	0.121	0.906	0.587	1.420	0.484	0.855	13.82	0.412	0.773	0.968	-0.196
Mexicali	13.90	0.240	0.961	0.280	1.263	0.231	0.895	22.18	0.238	0.907	0.992	-0.217
Nevado	19.21	0.113	0.553	0.288	1.075	0.117	0.490	4.61	0.105	0.472	0.977	-0.264
Pachuca	25.87	0.161	1.017	0.225	1.299	0.227	1.011	24.35	0.204	0.959	0.999	-0.220
Palenque	102.30	0.211	0.983	0.693	1.675	0.642	0.943	24.24	0.646	0.948	0.965	-0.181
Pinotepa	129.17	0.183	0.941	1.137	1.873	0.992	0.880	15.86	0.920	0.830	0.947	-0.172
Psa. Abelardo	10.90	0.181	0.669	0.097	1.069	0.047	0.635	7.98	0.044	0.629	0.994	-0.283
Psa. Allende	25.91	0.157	0.741	0.037	1.100	0.019	0.722	11.65	0.015	0.709	1.000	-0.298
Psa. El Cuchillo	213.00	0.141	1.177	1.918	5.827	2.557	1.391	74.71	2.426	1.332	0.939	-0.137
Presa Emilio LZ	19.22	0.141	0.643	0.485	1.094	0.232	0.544	6.10	0.234	0.547	0.966	-0.237
Presa La Cangrejera	180.94	0.148	0.831	1.068	1.496	0.764	0.723	10.55	0.751	0.714	0.946	-0.187
Presa Madín	60.96	0.135	1.001	0.587	1.579	0.577	0.989	24.72	0.578	0.991	0.971	-0.184
Pto. Ángel	103.28	0.124	1.065	1.020	2.328	1.135	1.109	34.62	1.129	1.104	0.955	-0.161
Río Lagartos	246.83	0.215	0.880	2.162	2.114	1.691	0.752	10.92	1.613	0.720	0.929	-0.168
Río Tomatlán	123.85	0.114	0.944	1.004	1.808	0.898	0.901	17.37	0.861	0.873	0.951	-0.175
San Quintín	10.64	0.200	0.764	0.135	1.095	0.077	0.717	10.55	0.071	0.702	0.994	-0.266
Sian Kaan	41.90	0.118	0.226	-0.173	1.033	-0.033	0.259	1.87	-0.046	0.234	1.016	-0.334
SMN	97.80	0.123	1.361	1.078	10.937	2.282	2.003	371.11	2.214	1.963	0.963	-0.132
Sta. Rosalía	63.74	0.231	0.718	0.819	1.258	0.453	0.585	7.16	0.447	0.580	0.952	-0.210
Tantakin	78.95	0.194	0.797	0.674	1.261	0.430	0.686	9.78	0.424	0.680	0.960	-0.205
Tezontle	46.27	0.158	0.944	0.480	1.356	0.412	0.894	19.98	0.422	0.907	0.976	-0.198
Tizapán	37.70	0.177	0.724	0.306	1.144	0.172	0.655	8.68	0.167	0.648	0.979	-0.242
Tuxpan	322.25	0.176	1.413	1.925	31.190	3.884	2.186	853.75	3.689	2.124	0.946	-0.118
Urique	58.09	0.091	1.043	0.548	1.674	0.596	1.070	27.58	0.560	1.025	0.976	-0.181
UTT	41.74	0.156	1.339	0.447	3.273	0.920	1.708	156.39	0.911	1.698	0.996	-0.157
Zacatecas	68.35	0.206	1.508	0.817	28.599	2.509	2.628	1 216.78	2.184	2.342	0.978	-0.126

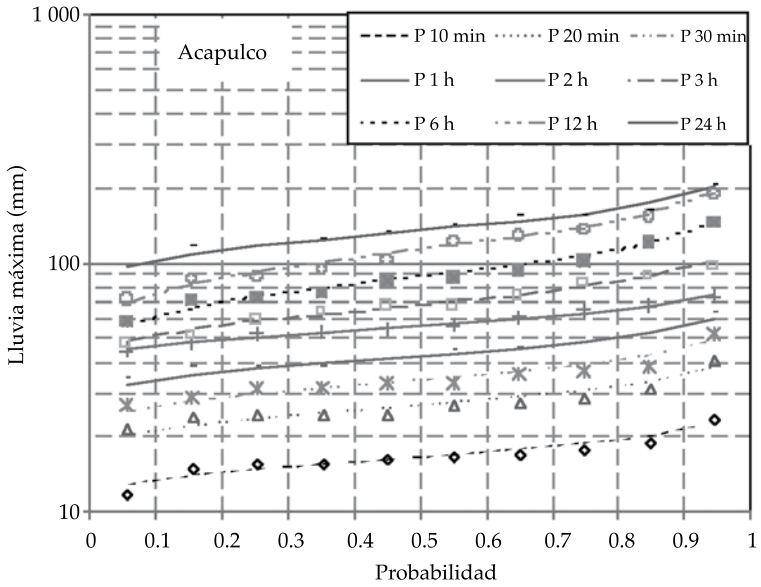

Figura 2. Ejemplo de valores máximos medidos (+) y datos estimados de Gumbel (---) para diversas duraciones, contra la probabilidad en la estación de Acapulco.

(Guichard Romero *et al*. 2009). Pero como en las regiones centrales de México se ha encontrado un mejor ajuste para la distribución de Gumbel (Domínguez-Mora *et al*. 2013), y por el hecho de que en el caso las series de datos cortas dicha distribución de Gumbel ofrece buenos resultados (Tung y Wong, 2013), ésta es la que se ha elegido. La figura 2 muestra un ajuste a la distribución Gumbel para los datos observados (máximo anual) en la estación de Acapulco. En cada estación, el análisis de frecuencia se efectuó utilizando la lluvia anual máxima para cada una de las duraciones de lluvia elegidas, ajustando cada serie a una distribución Gumbel utilizando el método de máxima probabilidad (Zapata-Sierra, *et al*., 2009).

Para los periodos de retorno T = 2, 5, 10, 25, 50 y 100 años, los valores de la altura de lluvia, R_t^T, se obtuvieron para cada relación de lluvia considerada, t, y las intensidades correspondientes, r_t^T.

Relaciones de intensidad-duración-frecuencia

Las relaciones de IDF pueden describirse matemáticamente por medio de diversas expresiones (Wenzel 1982). La más común, conocida también como método de referencia, que agrupa las diferentes curvas de intensidad-duración para los diversos periodos de retorno en una sola fórmula es la ecuación (1), la cual se aplica a lugares con observatorios que mantiene registros de duración de lluvia entre 10 min y 24 h:

$$r_t^T = \frac{a\,T^b}{t^c + d} \qquad (1)$$

donde r_t^T es la intensidad media (mm h^{-1}) para la duración t (min) y el periodo de retorno T (años), y a, b, c y d son los parámetros por determinar mediante el ajuste.

En los casos donde solo se disponen datos de lluvia de 24 horas, se efectuaron

estudios de caracterización de lluvia regional analizando las razones entre la lluvia de corta duración y la lluvia durante una 1 h y/o 24 h (Bell, 1969; Chen, 1983; Froehlich, 1993 y 1995). Empleando mapas de lluvias de isoyetas para grandes regiones en los Estados Unidos, Chen (1983) obtuvo una razón entre la altura de la lluvia para 1 h y 24 h, independientemente del periodo de retorno, (R_1^T/R_{24}^T), que varía muy poco de acuerdo con la ubicación geográfica, cambiando entre valores de 0.1 y 0.6, con un valor promedio de 0.4.

Las ecuaciones utilizadas en este trabajo son, Chen (1983):

$$r_t^T = \frac{a_1 r_1^T}{\left(t + b_1\right)^{c_1}} \qquad (2)$$

donde $a = a_1 r_1^T$, $b = b_1$ y $c = c_1$. Los parámetros de ajuste a_1, b_1 y c_1 pueden obtenerse de los datos de lluvia conocidas de una estación dada utilizando técnicas de optimación y el método de mínimos cuadrados.

La ecuación modificada de Chen:

$$r_t^T = \frac{a_{24} r_{24}^{10} \log\left\{10^{2-x}\left[ln\left(\frac{T}{T-1}\right)\right]^{-(x-1)}\right\}}{\left(t + b_{24}\right)^{c_{24}}} \qquad (3)$$

donde $x = R_{24}^{100} / R_{24}^{10}$. Estas ecuaciones permiten obtener las razones IDF de datos de lluvia de 24 horas, Témez, 1987:

$$r_t^T = r_{24}^T \left(\frac{r_1^t}{r_{24}^T}\right)^{\frac{28^{0.1} - t^{0.1}}{28^{0.1} - 1}} \qquad (4)$$

donde t es la duración de la lluvia en h.

La ecuación de Témez modificada (Zapata-Sierra *et al.*, 2009):

$$r_t^T = r_{24}^T \left(\frac{r_1^t}{r_{24}^T}\right)^{\alpha_1 + \beta_1 ln\, t} \qquad (5)$$

donde los coeficientes α_1 y β_1 pueden determinarse utilizando técnicas de optimación basadas en los datos de intensidad observados.

Resultados

Cada uno de los parámetros estudiados de las ecuaciones se obtuvieron mediante técnicas de optimación, siendo el error cuadrático mínimo para los datos de cada estación utilizando el análisis de frecuencia, aquí y después de los datos observados.

Primero, la ecuación de Wenzel (1) se ajustó a los datos de intensidad de lluvia obtenidos de cada estación por medio de análisis de frecuencia ("datos observados"), obteniendo valores para los parámetros a, b, c y d expresados en la tabla 1. Después se procedió a estimar los valores de intensidad de lluvia para las diferentes duraciones y periodos de retorno aplicando la ecuación de Chen (2), con los coeficientes a_1, b_1 y c_1 determinados utilizando técnicas de optimación; la ecuación modificada de Chen (3), aplicando los coeficientes a_{24}, b_{24} y c_{24}; y la ecuación de Témez (4) y su ecuación modificada (5), optimizando los parámetros α_1 y β_1. Los valores para los parámetros en las ecuaciones (1), (2), (3) y (5) determinados mediante optimación se muestran en la tabla 1.

Con el fin de comparar las estimaciones hechas mediante cada procedimiento se definió un coeficiente de variación (CV) como la razón entre la raíz cuadrada del error cuadrático medio y la media de los valores de lluvia observados:

$$CV = \frac{\sqrt{\frac{\sum_{i-1}^{n}\left(x_{i_0} - x_{i_c}\right)^2}{n}}}{\frac{\sum x_{i_0}}{n}} \qquad (6)$$

Tabla 2. Resultados resumidos (coeficiente de variación CV) obtenido para duraciones de lluvia de menos de 24 h. Se remarca en negritas el CV más bajo obtenido en cada EMA Zona: C = estación costera, I = estación tierra adentro.

Id	Estación	Zona	Periodo	Wenzel (1)	Chen (2)	Chen mod. (3)	Témez (4)	Témez mod. (5)
Aca	Acapulco	C	1999-2008	**0.0102**	0.0276	0.0282	0.0119	0.0113
AMe	Agustín	I	2003-2008	0.0131	0.0092	0.0110	0.0721	**0.0056**
Ala	Álamos	I	1999-2005	0.0106	**0.0084**	0.0193	0.0526	0.0198
Alt	Altamira	C	1999-2008	**0.0088**	0.0131	0.0143	0.0546	0.0203
Alv	Alvarado	C	2000-2008	0.0111	0.0067	0.0245	0.0154	**0.0017**
Ang	Angamacutiro	I	2000-2008	0.0082	**0.0078**	0.0115	0.0563	0.0207
Aco	Atlacomulco	I	2000-2008	0.0097	0.0118	**0.0073**	0.0628	0.0217
BLA	Bahía Ángeles	C	2000-2007	0.0208	0.0181	0.0179	0.0184	**0.0101**
Bas	Basaseachi	I	1999-2008	0.0099	**0.0095**	0.0098	0.0111	0.0125
CSL	Cabo San Lucas	C	2000-2007	**0.0186**	0.0211	0.0196	0.0654	0.0227
Ckl	Calakmul	I	2003-2008	**0.0115**	0.0127	0.0119	0.0763	0.0238
Cam	Campeche	C	2000-2008	**0.0131**	0.0139	0.0338	0.0232	0.0135
Can	Cancún	C	2000-2007	0.0136	0.0137	0.0187	0.0098	**0.0097**
CAl	Cd. Alemán	I	2000-2008	**0.0128**	0.0165	0.0281	0.0557	0.0205
CCo	Cd. Constitución	I	2000-2007	0.0095	0.0408	0.0423	**0.0038**	0.0074
CCa	Cd. del Carmen	C	2000-2006	0.0136	**0.0095**	0.0159	0.0333	0.0162
Cel	Celestún	C	2000-2008	**0.0090**	0.0134	0.0133	0.0714	0.0229
CCt	Cerro Cat	C	2000-2007	**0.0091**	0.0123	0.0107	0.0223	0.0133
Cha	Chapala	I	1999-2008	0.0135	**0.0097**	0.0121	0.0603	0.0214
Che	Chetumal	I	1999-2008	**0.0086**	0.0110	0.0247	0.0108	0.0106
Chi	Chinatú	I	2000-2008	0.0081	**0.0074**	0.0102	0.0519	0.0199
Chp	Chinipas	I	1999-2008	0.0086	0.0116	**0.0077**	0.0875	0.0256
Coz	Cozumel	I	1999-2008	0.0138	0.0140	0.0185	0.0168	**0.0116**
CPGM	CPGM	I	2003-2008	**0.0060**	0.0062	0.0269	0.0220	0.0134
ENCB	ENCB	I	2001-2008	0.0115	0.0147	**0.0086**	0.1075	0.0285
Gua	Guachochi	I	2000-2008	0.0078	**0.0074**	0.0096	0.0372	0.0170
GDO	GustavoDO	I	2000-2006	0.0155	0.0167	0.0211	0.0149	**0.0051**
Hua	Huamantla	I	2000-2007	**0.0095**	0.0096	0.0142	0.0832	0.0249
Hue	Huejutla	I	2000-2008	**0.0125**	0.0129	0.0139	0.0591	0.0215
Hpn	Huimilpan	I	2000-2007	0.0126	**0.0100**	0.0111	0.1055	0.0282
IMTA	IMTA	I	1999-2008	0.0102	0.0063	**0.0061**	0.0636	0.0217
IzM	Izúcar	I	2000-2007	0.0170	0.0207	**0.0147**	0.0970	0.0278
Jal	Jalapa	I	2000-2008	0.0091	0.0077	0.0185	0.0079	**0.0077**
Joc	Joicotepec	I	1999-2006	0.0132	0.0118	0.0130	0.0517	**0.0007**
LCo	Los Colomos	I	2000-2008	0.0094	0.0062	**0.0057**	0.0938	0.0263
Mag	Maguarichi	I	1999-2006	0.0099	**0.0087**	0.0124	0.0209	0.0088
Mat	Matamoros	C	2000-2008	0.0100	0.0117	**0.0084**	0.0844	0.0254
Mer	Mérida	C	2000-2008	0.0074	**0.0058**	0.0277	0.0297	0.0153
Mex	Mexicali	I	2000-2008	0.0203	0.0210	0.0181	0.0136	**0.0135**
Nev	Nevado	I	2000-2008	0.0090	**0.0042**	0.0203	0.0069	0.0055
Pach	Pachuca	I	2000-2008	0.0126	**0.0088**	0.0212	0.0099	0.0126

Tabla 2 (continuación). Resultados resumidos (coeficiente de variación CV) obtenido para duraciones de lluvia de menos de 24 h. Se remarca en negritas el CV más bajo obtenido en cada EMA Zona: C = estación costera, I = estación tierra adentro.

Pal	Palenque	I	2003-2008	0.0145	0.0141	**0.0128**	0.0433	0.0185
PiNa	Pinotepa	C	2003-2008	**0.0114**	0.0118	0.0236	0.0447	0.0187
PALR	Psa. Abelardo	C	2000-2007	0.0113	0.0111	0.0151	0.0275	**0.0037**
PAll	Psa. Allende	I	2000-2008	0.0108	0.0106	0.0160	0.0468	**0.0019**
PECu	Psa. El Cuchillo	I	2000-2007	**0.0080**	0.0091	0.0155	0.0733	0.0241
PELZ	Psa. Emilio LZ	C	2000-2008	0.0134	0.0128	0.0113	**0.0063**	0.0089
PLCa	Psa. La Cangrejera	C	2000-2007	**0.0098**	0.0115	0.0153	0.0317	0.0156
PMad	Psa. Madín	I	2000-2008	**0.0071**	0.0088	0.0081	0.0399	0.0175
PuA	Pto. Ángel	C	2000-2008	**0.0068**	0.0077	0.0090	0.0570	0.0207
RLag	Río Lagartos	C	2000-2008	**0.0149**	0.0171	0.0259	0.0393	0.0182
RTom	Río Tomatlán	C	2000-2008	0.0073	**0.0050**	0.0149	0.0425	0.0179
SQtin	San Quintín	C	2001-2007	0.0143	0.0143	0.0204	0.0230	**0.0059**
Sian	Sian Kaan	C	2000-2007	0.0154	0.0043	0.0391	0.0160	**0.0016**
SMN	SMN	I	1999-2007	0.0095	0.0075	**0.0068**	0.0960	0.0268
SRos	Sta. Rosalía	C	2001-2008	0.0172	0.0189	0.0212	0.0196	**0.0129**
Tan	Tantakin	I	2003-2008	0.0150	0.0174	0.0196	0.0230	**0.0138**
Tez	Tezontle	I	2000-2008	0.0100	0.0130	**0.0078**	0.0288	0.0154
Tiz	Tizapan	I	1999-2008	0.0105	0.0103	0.0143	**0.0044**	0.0089
Tux	Tuxpan	C	2000-2007	0.0134	0.0159	**0.0098**	0.1059	0.0290
Uri	Urique	I	2000-2008	0.0064	**0.0034**	0.0158	0.0421	0.0178
UTT	UTT	I	1999-2007	0.0128	**0.0085**	0.0087	0.0737	0.0235
Zac	Zacatecas	I	2000-2008	0.0162	**0.0160**	0.0214	0.1167	0.0301

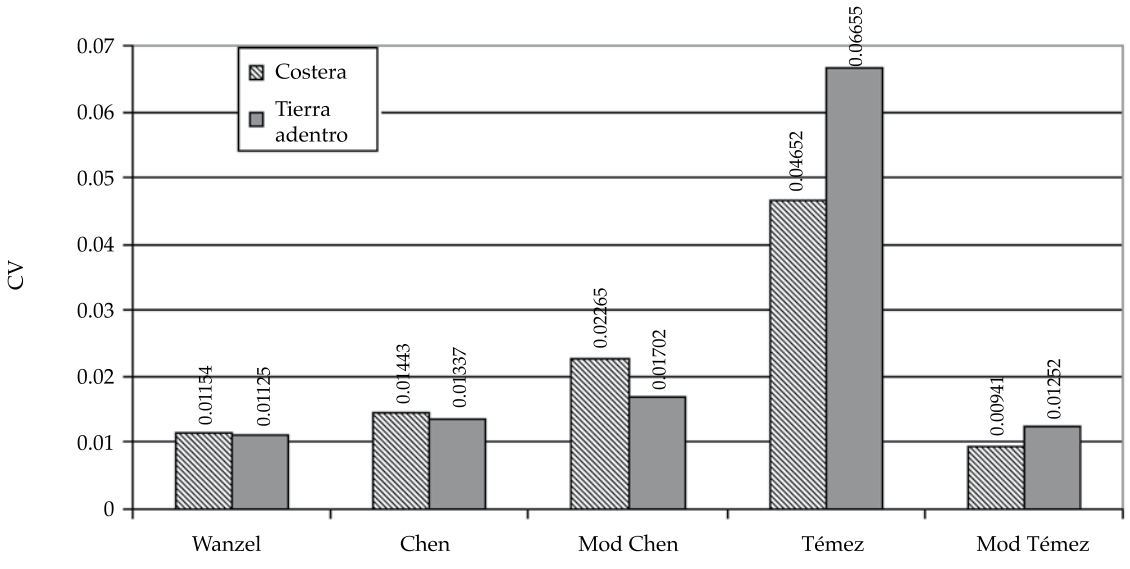

Figura 3. Valores del coeficiente de variación (CV) y de desviación estándar (de) obtenidos con ecuaciones diferentes para duraciones de lluvia de menos de 2 horas en las estaciones costeras estudiadas.

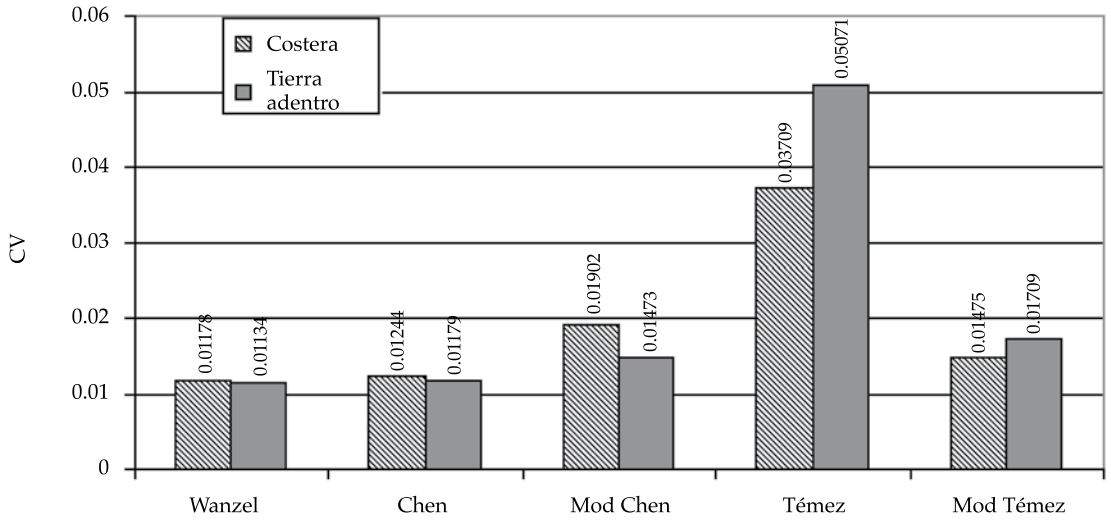

Figura 4. Coeficiente de variación (CV) obtenido con las diferentes ecuaciones de duraciones de lluvia de 24 h en estaciones tierra adentro y costeras estudiadas.

donde x_{i0} son los valores obtenidos para las alturas de lluvia de las diferentes duraciones de lluvia y periodos de retorno, x_{ic} son las alturas de lluvia calculadas para las diferentes duraciones (10 min a 24 h) y periodos de retorno (2 a 100 años) y n es el número de datos de lluvia empleados en cada ecuación.

Las ecuaciones de Témez modificadas (5) y Chen modificada (3) requieren el uso de parámetros calculados para un área cercana. Esto puede hacerse utilizando los parámetros obtenidos en este trabajo (tabla 1).

La tabla 2 muestra los valores de los coeficientes de variación (en negritas se indica el CV más bajo de cada EMA) obtenido con las diferentes expresiones para generar el conjunto completo de 10 minutos a 24 h de las alturas de lluvia para diferentes periodos de retorno. Observamos que las ecuaciones (1), (2) y (5) son aquellas con el mayor número de estaciones con el valor mínimo de CV. La ecuación de Témez (4) es la que ofrece los peores resultados, superando en algunos casos los valores de CV de 0.1.

Las figuras 3 y 4 muestran los valores promedio de CV obtenidos en estaciones costeras y tierra adentro, correspondientes a los dos periodos estudiados, menores que 2 horas y menores que 24 horas. En todos los casos, se observa que la ecuación de Témez obtiene los CV mayores, y entonces no se recomienda usarla sin la particularización propuesta en la ecuación (4).

Debido a la duración de los datos, los resultados obtenidos para las duraciones entre 10 minutos a 24 horas y para un periodo de retorno entre 2 a 500 años, correspondieron a 7 años; la validez respaldada por estas estimaciones está limitada a la duración de una serie de datos. Pero donde no existe otra información, en este caso se proporciona alguna guía para el diseño hidrológico.

Conclusiones

Las conclusiones que se obtuvieron en este trabajo para las duraciones de los datos de al menos 7 años fueron las siguientes:

El método de Wenzel por lo general muestra los mejores resultados según se espera, lo cual justifica su uso cuando se dispone de datos de lluvia a corto plazo tales como cada 10 minutos, lo cual no siempre es posible. Para estos casos, este trabajo muestra que las ecuaciones son más apropiadas dependiendo del área geográfica de México, en la costa o tierra adentro, donde los datos de lluvia se disponen para un tiempo mayor.

La ecuación de Chen proporciona muy buenos resultados para las duraciones de lluvia entre 2 h y 24 h, pero requiere datos de lluvia máxima de una hora. Estos datos pueden ser más accesibles pero no dispersos, salvo para estaciones relativamente modernas. En el caso de disponer solo de datos de lluvia de 24 horas (la situación más común), las modificadas de Témez son las mejores ecuaciones para estimación de la lluvia de corta duración (< 2 h) necesaria para obtener curvas IDF.

Para las duraciones más largas que 2 h y para la zona costera, la mejor ecuación siempre es la de Témez modificada. Mientras que para el área tierra adentro dependiendo de la duración de la lluvia que se va a estimar debe usarse la ecuación de Témez modificada para duraciones menores que 2 horas y la de Chen modificada para duraciones más largas.

Recibido: 20/06/12
Aceptado: 25/10/13

Referencias

BELL, F.C. Generalized Rainfall-Duration-Frequency Relationships. *J. Hydraulic Division*. Vol. 95, No. HY1, 1969, pp. 311-327.

CAMPOS, D.F. Procedimiento para obtener curvas I-D-T a partir de registros pluviométricos. *Ingeniería hidráulica en México*. Vol. 5, núm. 2, 1990, pp. 39-52.

CHEN, C.L. Rainfall Intensity-Duration-Frequency Formulas. *Journal of Hydraulic Engineering*. Vol. 109, No. 12, 1983, 1603-1621.

CHOW, V.T., MAIDMENT, D.R., and MAYS, L.W. *Applied Hydrology*. New York: McGraw-Hill, 1988, 572 pp.

DOMÍNGUEZ-MORA, R., ARGANIS-JUÁREZ, M.L., MENDOZA-RESÉNDIZ, A., CARRIZOSA-ELIZONDO, E., ECHAVARRÍA-SOTO, B. Storms Generator Method that Preserves their Historical Statistical Characteristics. Application to Mexico City Basin Daily Rainfall Fields. *Atmosfera*. Vol. 26, No. 1, 2013, pp. 27-43.

ESCALANTE, C.A. y REYES, L. Influencia del tamaño de muestra en la estimación del factor de lluvia. *R. Información Tecnológica*. Vol. 15, No. 4, 2004, pp. 105-110, doi: 10.4067/S0718-07642004000400015.

FROEHLICH, D.C., Short-Duration-Rainfall Intensity Equations for Drainage Design. *J. Irrigation and Drainage Engineering*. Vol. 119, No. 5, 1993, pp. 814-828.

FROEHLICH, D.C. Intermediate-Duration-Rainfall Intensity Equations. *Journal of Hydraulic Engineering*. Vol. 121, No. 10, 1995, pp. 751-756.

GUICHARD-ROMERO, D., DOMÍNGUEZ-MORA, R., FRANCÉS-GARCÍA, F. y GARCÍA-BARTUAL, R. Análisis de la densidad de estaciones en zonas de lluvias convectivas. Caso del Mediterráneo español. *Ingeniería Hidráulica en Mexico*. Vol. 24, núm. 3, 2009, pp. 35-49.

KOUTSOYIANNIS, D., KOZONIS, D., and MANETAS, A. A Mathematical Framework for Studying Rainfall Intensity-Duration-Frequency Relationships. *Journal of Hydrology*. Vol. 206, No. 1-2, 1998, pp. 118-135.

LAM, C.C., and LEUNG, Y.K. *Extreme rainfall Statistics and Design Rainstorm Profiles at Selected Locations in Hong Kong*. Hong Kong: Royal Observatory, 1994.

MENDOZA-RESENDIZ, A., ARGANIS-JUAREZ, M., DOMINGUEZ-MORA, R., and ECHAVARRIA, B. Method for Generating Spatial and Temporal Synthetic Hourly Rainfall in the Valley of Mexico. *Atmospheric Research*. No. 132-133, 2013, pp. 411-422

MONHYMONT, B., and DEMARÉE, G.R. Intensity-Duration-Frequency Curves for Precipitation at Yangambi, Congo, Derived by Means of Various Models Of Montana Type. *Hydrol. Sci. J*. Vol. 51, 2007, pp. 239-253.

PEREYRA-DÍAZ, D., PÉREZ-SESMA, J.A. y GÓMEZ-ROMERO, L. Ecuaciones que estiman las curvas intensidad-duración-período de retorno de la lluvia. *GEOS*. Vol. 24, núm. 1, 2004, pp. 46-56.

SCT. *Isoyetas de intensidad-duración-frecuencia. República mexicana*. México, DF: Subsecretaría de Infraestructura de la Secretaría de Comunicaciones y Transportes, 1990, 495 pp.

SEGOND, M.L., NEOKLEOUS, N., MAKROPOULOS, C., ONOF, C., and MAKSIMOVIC, C. Simulation and Spatio-Temporal Disaggregation of Multi-Site Rainfall Data for Urban Drainage Applications. *Hydrol. Sci. J*. Vol. 52, 2007, pp. 917-935.

SHERMAN, C.W. Frequency and Intensity of Excessive Rainfall at Boston, Mass. *Trans. Am. S.C.E.* Vol. 95, 1931, pp. 951-960.

SINGH, V.P. and HAO, Z. Entropy-Based Probability Distribution for IDF Curves. World Environmental and Water Resources Congress 2011: Bearing Knowledge for Sustainability. *Proceedings of the 2011 World Environmental and Water Resources Congress*, Palm Springs, California, USA, American Society of Civil Engineers, 2011, pp. 1265-1272.

SORO, G.E., GOULA, BI T.A., KOUASSI, F.W., and SROHOUROU, B. Update of Intensity-Duration-Frequency Curves for Precipitation of Short Durations in Tropical Area of West Africa (Cote D'ivoire). *Journal of Applied Sciences*. Vol. 10, No. 9, 2010, pp. 704-715.

TÉMEZ, J.R. *Cálculo hidrometeorológico de caudales máximos en pequeñas cuencas naturales*. Madrid: Dirección General de Carreteras, MOPU, 1987.

TUNG, Y.K., and WONG, C.L. Assessment of Design Rainfall Uncertainty for Hydrologic Engineering Applications in Hong Kong. *Stochastic Environmental Research and Risk Assessment*. Vol. 27, No. 6, 2013, pp. 1-10.

WENZEL, H.G. Rainfall for Urban Stormwater Design. In *Urban Storm Water Hydrology*. Kibler, D.F. (editor). Washington, DC: Water Resources Monograph, 7, AGU, 1982.

ZAPATA-SIERRA, A.J., MANZANO-AGLUGIARO, F., and AYUSO-MUÑOZ, J.L. Assessment of Methods for Obtaining Rainfall Intensity-Duration-Frequency Ratios for Various Geographical Areas. *Spanish Journal of Agricultural Research*. Vol. 7, No. 3, 2009, pp. 699-705.

Dirección institucional de los autores

Dr. Francisco Manzano Agugliaro
Dr. Antonio Zapata Sierra
Dr. Juan Francisco Rubí Maldonado

Facultad de Ingeniería
Universidad de Almería
La Cañada de San Urbano
04120 Almeria, España
Teléfono: +34 (950) 015 693
fmanzano@ual.es
ajzapata@ual.es
rubimal@ual.es

Dr. Quetzalcóatl Hernández Escobedo

Facultad de Ingeniería
Universidad Veracruzana
Campus Coatzacoalcos
Av. Universidad Veracruzana km 7.5,
96535 Col. Santa Isabel
Coatzacoalcos, Veracruz, México
Teléfono: +52 (921) 2115 700, extensión 59223
qhernandez@uv.mx

Click here to write the autor

Technical Note

Estimate of the Magnitudes of Ruptures of Earth or Rockfill Dams Using a Statistical Method

• Daniel Francisco Campos-Aranda •
Profesor jubilado de la Universidad Autónoma de San Luis Potosí, México
*Corresponding Author

Abstract

CAMPOS-ARANDA, D.F. Estimate of the Magnitudes of Ruptures of Earth or Rockfill Dams Using a Statistical Method. *Water Technology and Sciences* (in Spanish). Vol. V, No. 3, May-June, 2014, pp. 163-176.

Studies of dam safety define emergency plans and strategies to mitigate risks in underwater areas. These studies involve the estimate of the magnitudes of dam ruptures, which include the geometry of the failure breach, the time it took to develop and peak discharge flow. Three approaches to estimating these characteristics exist: (1) the *statistical method* which applies empirical equations obtained through regression, (2) the *hydraulic method* which numerically simulates the development of the failure breach, taking into account hydraulic mechanisms and flow erosion and (3) the *experimental method* or laboratory method which uses models at reduced or actual scale. This work applies the statistical approach based on 28 empirical equations which have been established as most reliable or having the least uncertainty. Two hypothetical numerical applications are described— the first for a small dam with failure due to overtopping and the second for a dam of medium height which failed due to internal erosion that caused filtrations. Both applications follow two analytical approaches depending on the available information. It is concluded that the collection of the 28 empirical equations makes it possible to establish the probable values for the magnitudes associated with the failure of earth or rockfill dams, as well as variation intervals.

Keywords: Earth dam, rockfill dam, overtopping, piping, failure breach, time to develop breach, peak discharge flow.

Resumen

CAMPOS-ARANDA, D.F. Estimación de las magnitudes asociadas con el rompimiento de presas de tierra o enrocamiento a través del método estadístico. Tecnología y Ciencias del Agua. *Vol. V, núm. 3, mayo-junio de 2014, pp. 163-176.*

Los estudios de seguridad de presas definen los planes de emergencia y las estrategias de mitigación de riesgos en sus áreas localizadas aguas abajo. Tales estudios abarcan la estimación de las magnitudes originadas por el rompimiento de su cortina, las cuales incluyen la geometría de la brecha de falla, el tiempo de desarrollo de ésta y el gasto máximo de descarga. Existen tres enfoques de estimación de las características citadas: (1) el método estadístico, *que aplica ecuaciones empíricas obtenidas por regresión; (2) el* método hidráulico, *el cual simula numéricamente la formación de la brecha de falla, tomando en cuenta los mecanismos hidráulicos y de erosión del flujo, y (3) el* método experimental *o de laboratorio que utiliza modelos reducidos o a escala real. En este trabajo se aplica el enfoque estadístico basado en 28 ecuaciones empíricas que se han establecido como las más confiables o de menor incertidumbre. Se describen dos aplicaciones numéricas hipotéticas: la primera en una presa pequeña que falla por desbordamiento; la segunda en una presa de mediana altura, cuya falla se debe a la erosión interna que generan las filtraciones; en ambas aplicaciones se siguen dos planteamientos de análisis, función de la información disponible. Se concluye que la recopilación expuesta de 28 ecuaciones empíricas permite establecer los valores probables de las magnitudes asociadas con la falla de presas con cortinas de tierra o de enrocamiento, así como sus intervalos de variación.*

Palabras clave: *cortinas de tierra, cortinas de enrocamiento, desbordamiento, tubificación, brecha de falla, tiempo de formación de la brecha, gasto máximo de descarga.*

Introduction

Beginning in the 1980s, interest in the safety of dams began to grow worldwide, with the key objective to reduce the loss in human lives and material damages downstream caused by their failure and rupture. Though dams actually fail infrequently, their consequences are generally catastrophic (NWS, 2002).

More than 800 000 dams have been built worldwide, as well as thousands of kilometers of breakwaters and dikes for cities and regions of economic importance. History also shows that hundreds of dams have failed over the centuries, and that currently sections of dikes or breakwaters rupture every year due to overtopping or other causes (Zagonjolli, 2007). Dramatic examples include New Orleans, United States in August 2005 from hurricane Katrina, and the Chalco region in the Valley of Mexico with the periodic failure of the dikes in the La Compañía River or channel.

In general, all dams are subject to aging and as a result become more dangerous since they are more susceptible to failures due to deficient operations or overtopping associated with sedimentation. The latter occurs primarily in small dams, which represent the majority. In addition, the old dams were designed with little information and may have been built with less strict criteria than those of today. For example, design norms and construction of earth dams establish that the base as well as the wall must meet very precise control standards related to seepage, pressure and stability, as well as hydrological safety measures against overtopping. Nevertheless, the failure of earth dams has not substantially decreased (Singh, 1996).

In addition, more extreme flood conditions are likely to occur in existing dams because of the effects of climate change. Therefore, they should be studied by modeling their failure or rupture. This involves two key calculations: (1) an outflow hydrograph, characterized by the peak flow, which is a function of the geometry of the failure and the time for it to develop; and (2) the flood wave (produced by the failure) moving downstream towards the valley and/or floodplains (Singh, 1996; Chinnarasri *et al*., 2004).

Three approaches are used to calculate the magnitudes associated with the failure of a dam: (1) *statistical*, oriented towards developing empirical regression equations; (2) *hydraulic methods*, which numerically simulate the information related to the failure breach, taking into account hydraulic mechanisms and the erosion of the flow; and (3) *experimental methods* or laboratory tests using reduced or real scale models, and that make it possible to verify the results of the other two approaches or generate new empirical relations (Chinnarasri *et al*., 2004; Zagonjolli, 2007).

The objective of this work is to present the regression equations that have been determined to be the most reliable, or having the least uncertainty, for the calculation of the geometric characteristics of a failure breach, the time for it to form and the resulting peak discharge flow. These 28 empirical equations are composed of three groups, according to the degree of uncertainty. Two hypothetical numerical applications are described. The first applies to a small dam which fails because of overtopping and the second to a dam of medium height with a failure due to internal erosion generated by seepage (tunneling). Both applications follow two types of analyses according to the available information. Based on the results, the magnitudes associated with the failure or rupture of a dam with earth walls are determined, as well as the confidence intervals.

Compiling of Empirical Equations

Information about Dam Failures

A dam wall can fail gradually or suddenly. The type of failure depends particularly on the wall material. Generally, those made of concrete fail instantly while those made of earth or rock do so gradually. Earth walls are the most common (homogenous, mixed and rockfill), and their failures have been more widely documented, with quick durations of 15 minutes to 3 hours as well as prolonged periods of 3 to 12 hours or more (Singh, 1996).

Various researchers have presented the methods they have used to calculate the empirical equations they have proposed, including Hagen (1982), MacDonald and Langridge-Monopolis (1984), Costa (1985, 1988), Froehlich (1995a, 2008), and Xu and Zhang (2009).

Dimensions and Calculations

Generally, the magnitudes of dam failures or ruptures can be divided into two groups: geometric parameters and hydrographs. Geometric failures correspond to a failure breach (typically trapezoidal) with five geometric parameters: maximum width (b_M), medium width (b), bottom or minimum width (b_m), depth or height of the breach (Hb), and slopes of the sides (z). Figure 1 indicates the overall geometric elements of a failure breach. The hydrographic parameters include the time a failure lasts (Tf) and the peak discharge flow (Qp). Tf for rupture from overtopping is the time from the beginning of the rapid rise downstream until the lateral erosion of the wall ceases (Chinnarasri *et al*., 2004). Failures due to internal erosion from seepage begin with the collapse of the dam's crest to the subsequent lateral formation of the breach (Xu and Zhang, 2009).

Basic data are needed to apply most of the empirical equations, such as the following geometric characteristics or hydraulics of the dam (NWS, 2002):

1. *Hydraulic height* (H_h) or *wall height* (H_c) is the distance, in meters, from the level of the channel at the wall to the maximum height of the stored water.
2. *Storage Volume* (V_a) is the maximum storage space in the dam, in m^3, below the maximum level reachable by the water, including any excess storage.

The first definition establishes that $H_h = H_c$, therefore three simplifications are implied: (1) the floor or bottom of the failure breach reaches the channel, that is, the entire height of the wall is eroded; (2) for failures from tunneling, the water level reaches the dam's crest; and (3) failures from overtopping, the water depth over the crest is not considered. When the bottom of the failure breach does not reach the channel and the actual level reached by the water at the beginning of the failure is known, the discharged volume (V_w) should be defined by the failure breach and the water depth above the bottom of the breach, H_w. In Figure 1, H_f is the height of the bottom of the breach and H_d is the hydraulic load above the crest.

Other information needed to verify the estimates performed includes: (1) the *length of the wall* (L_c), the total horizontal distance, in meters, measured along the wall axis at the crest, that is, between the edges of the crest, which enables verifying the maximum width (b_m) of the breach, and should be less than L_c; and (2) the *wall volume* (V_c), which should be greater than the estimate of the volume of eroded material (V_e) in the failure breach. It is also necessary to know the *type of wall* in order to apply the most recent empirical equations.

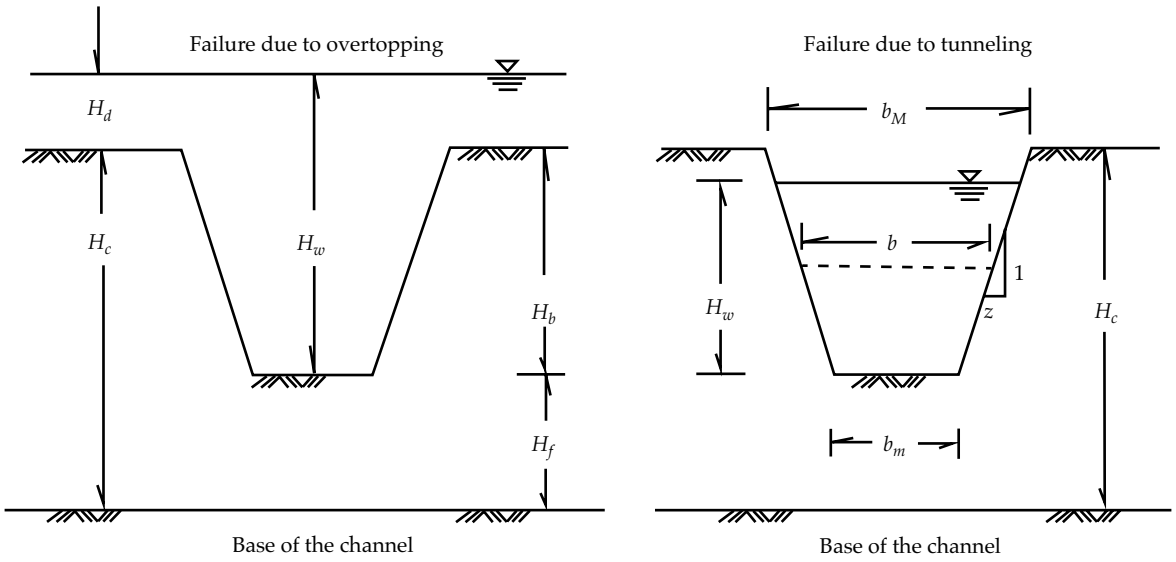

Figura 1. Elementos geométricos generales de una brecha de falla (Froelich, 2008; Xu y Zhang, 2009).

Exhaustive Compilation and Selection of Empirical Equations

An exhaustive search through all the references cited led to the creation of a list of 52 empirical equations. The first selection consisted of eliminating those applicable to natural dams caused by landslides or the obstruction of rivers (Walder and O'Connor, 1997). Another elimination was based on the similarity of formulas in relation to their coefficients and/or exponents, leaving only those representative of one type of equation. Next, based on a sampling of dams or reservoirs analyzed in Mexico (Campos-Aranda, 2013), magnitudes representative of wall heights were defined as well as capacities to perform numerical comparisons and to eliminate formulas with dispersed results or those that were clearly incorrect. This led to the selection of only 28 empirical equations, shown below in chronological order and grouped into three estimates b, T_f and Q_p.

List of Variables Used

To facilitate a quick understanding of each of the 28 empirical formulas that will be shown, a *list of the variables involved* are presented below.

B_i = control variable (I varies from 1 to 5).
b_M = maximum width of the failure breach, in meters.
b = medium width of the failure breach, in meters.
b_m = minimum width or width of the bottom of the failure breach, in meters.
C_b = empirical constant, function of V_a, dimensionless.
ICW = impermeable core wall.
Db = type of failure from overtopping.
g = acceleration of gravity equal to 9.81 m/s^2.
H_b = height of breach or depth from the crest of the wall, in meters.
H_c = height of the wall, distance from the channel to its crest, in meters.

H_d = hydraulic load above the crest of the wall, in meters.
H_f = height above the channel of the bottom of the breach, in meters.
H_h = hydraulic height, distance from the channel to the maximum height of the stored water, in meters.
HM = type of homogeneous wall or graduated materials (mixed).
H_r = height of the reference wall equal to 15 meters.
H_w = depth of water above the bottom of the breach, in meters.
k_0, k_1 = factor by type of failure, dimensionless.
L_c = length of the wall, measured along the axis of the crest, in meters.
CW = concrete wall.
Q_p = peak discharge flow, in m^3/s.
Qp = peak discharge flow, according to the envelope curve, in m^3/s.
V_a = storage volume or maximum water capacity, with excess storage, in m^3.
V_c = wall volume, in m^3.
V_e = volume of eroded wall material, in m^3.
V_w = volume discharged due to the failure breach, in m^3.
v_i = control variable (i varies from 1 to 5).
Tb = type of failure due to tunneling.
T_f = failure duration, in hours.
T_r = reference failure time equal to 1 hour.
z = slopes of the sides of the failure breach, dimensionless.

Estimate of the Width of the Failure Breach

For the case of 23 dams with failures due to overtopping and walls made of earth material (homogeneous, mixed and rockfill), with or without revetting of the slopes, and observed values of b that varied from 5 to 170 meters, Zagonjolli (2007) found that the mean square error (MSE) for equation (2) was 30% less than that for formula (1), originally proposed by the US Bureau of Reclamation en 1988:

$$b = 3.0 \cdot H_h \quad (1)$$

$$b = 4.6 \cdot H_h - 5.7 \quad (2)$$

Meanwhile, Van Thun and Gillette (1990), cited in NWS (2002) and by Wahl (2004), analyzed 57 dam failures and proposed the following formula:

$$b = 2.5 \cdot H_h + C_b \quad (3)$$

in which C_b is a constant function of the stored volume (V_a) in millions of m^3 (Mm^3), with the following values: 6.10 with Va < 1.233 Mm^3; 18.3 when V_a ranges between 1.233 and 6.165 Mm^3; 42.7 when V_a ranges from 6.165 to 12.330 Mm^3 and 54.9 with V_a > 12.330 Mm^3.

Based on the uncertainty analysis of the empirical equations conducted by Wahl (2004), Reed and Halgren (2011) recommend those found by Froehlich (1995b), which for b is:

$$b = 0.1803 \cdot k_0 \cdot (H_b)^{0.190} \cdot (V_a)^{0.320} \quad (4)$$

in which k_0 is the factor for the type of failure, with a value of 1.40 for overtopping and 1.00 for tunneling. H_b is the height or depth of the breach in meters (Figure 1).

Froehlich (2008) established and presented a registry of 74 failures which includes 69 data for medium breach widths. The following expression was found for these values:

$$b = 0.270 \cdot k_1 \cdot H_b^{0.040} \cdot V_w^{0.320} \quad (5)$$

where b is in meters; k_1 is dimensionless and the value of failures due to overtopping is 1.30 and 1.00 due to other types, such as tunneling; V_w is the volume of water stored

above the bottom of the breach, in m^3, and therefore defines the outflow hydrograph. Froehlich (2008) also specifies that the slope z (Figure 1) is approximately 1.00 for failures due to overtopping and 0.70 for other types.

Xu and Zhang (2009) present two empirical equations, one complete and another simplified, for the five following characteristics: H_b, b_M, b, T_f and Q_p. Since dimensionless variables are used, first H_b must be calculated. In the equations, $H_r = 15$ meters is the reference height for the walls, whose types may be: (1) impermeable core, (2) concrete screen; and (3) homogeneous or made of graduated (mixed) materials. In addition, they establish the main predictive variable as the *erodibility* of the wall, classified as high, medium or low. Some of the equations take into account the type of failure, that is, overtopping or erosion from seepage (tunneling). To obtain their empirical equations, they selected the variables based on the adjusted coefficient of determination. Their first three complete and simplified equations made it possible to estimate *H*b, *b*M and *b*. Equations(6), (7) and (8) correspond to the complete and (9), (10) and (11) to the simplified equations (Table 1).

Estimate of time of formation of failure breach

MacDonald y Langridge-Monopolis (1984) were the first to propose an empirical graphic relationship on logarithmic paper to estimate T_f in hours, as a function of the volume of eroded wall material (V_e), in m^3. In addition, they defined the *breach formation factor* as the product of the hydraulic height times the discharged water volume ($H_h \cdot V_w$), which makes it possible to estimate V_e. Wahl (2004) has presented these relations as potential equations:

$$T_f = 0.0179 \cdot V_e^{0.364} \qquad (12)$$

where V_e is estimated with the following expressions for walls made of homogenous earth and graduated (mixed) materials, as well as others (rockfill and embankments with a concrete screen or impermeable core):

$$(V_e)_H = 0.0261 \cdot (H_h \cdot V_w)^{0.769} \qquad (13)$$

$$(V_e)_{OT} = 0.00348 \cdot (H_h \cdot V_w)^{0.852} \qquad (14)$$

Here again, Reed and Halgren (2011) adopted the formula proposed by Froehlich (1995b) according to results from Wahl (2004):

$$T_f = 0.00254 \cdot (H_b)^{-0.90} \cdot (V_w)^{0.53} \qquad (15)$$

With dimensionless analysis and processing of 23 data Froehlich (2008) establishes the following formula:

$$T_f = 0.0176 \cdot \left(\frac{V_w}{g \cdot H_b^2} \right)^{1/2} \qquad (16)$$

Lastly, the complete and simplified equations found by Xu and Zhang (2009) for failure time are (17) and (18) in Table 1, whose T_r is 1 hour.

Estimate of Peak Discharge Flow

Hagen (1982), cited by Wahl (2004) and Zagonjolli (2007), analyzed 18 dam failures due to overtopping and found that the product of H_h times V_a or V_w, called the *dam factor*, is related to the peak discharge flow (Q_p). The observed peak flows varied from 730 to 83 000 m^3/s, while the dam factor ranged from 2.90 to 48 000 Mm^4. Its envelope equation is:

$$\boldsymbol{Qp} = 0.5404 \cdot (H_h \cdot V_w)^{0.50} \qquad (19)$$

Figure 1. General geometric elements of a failure breach (Froelich, 2008; Xu and Zhang, 2009).

Equation no.	Complete equations	Control variables (v)	Wall type (v_3)			Failure type (v_4)		Erodibility (v_5)		
			ICW	CW	HM	Db	Tb	High	Medium	Low
(6)	$\frac{H_b}{H_c} = 0.453 - 0.025 \cdot \left(\frac{H_c}{H_r}\right) + B_1$	$B_1 = v_3 + v_4 + v_5$	0.145	0.176	0.132	0.218	0.236	0.254	0.168	0.031
(7)	$\frac{b_M}{H_b} = 1.062 \cdot \left(\frac{H_c}{H_r}\right)^{0.092} \cdot \left(\frac{V_w^{1/3}}{H_w}\right)^{0.508} \cdot exp\ (B_2)$	$B_2 = v_3 + v_4 + v_5$	0.061	0.088	–0.089	0.299	–0.239	0.411	–0.062	–0.289
(8)	$\frac{b}{H_b} = 0.787 \cdot \left(\frac{H_c}{H_r}\right)^{0.133} \cdot \left(\frac{V_w^{1/3}}{H_w}\right)^{0.652} \cdot exp\ (B_3)$	$B_3 = v_3 + v_4 + v_5$	–0.041	0.026	–0.226	0.149	–0.389	0.291	–0.140	–0.391
(17)	$\frac{T_f}{T_r} = 0.304 \cdot \left(\frac{H_c}{H_r}\right)^{0.707} \cdot \left(\frac{V_w^{1/3}}{H_w}\right)^{1.228} \cdot exp\ (B_4)$	$B_4 = v_3 + v_4 + v_5$	–0.327	–0.674	–0.189	–0.579	–0.611	–1.205	–0.564	0.579
(30)	$\frac{Q_p}{\sqrt{g \cdot V_w^{5/3}}} = 0.175 \cdot \left(\frac{H_c}{H_r}\right)^{0.199} \cdot \left(\frac{V_w^{1/3}}{H_w}\right)^{-1.274} \cdot exp\ (B_5)$	$B_5 = v_3 + v_4 + v_5$	–0.503	–0.591	–0.649	–0.705	–1.039	–0.007	–0.375	–1.362
–	**Ecuaciones simplificadas**									
(9)	$\frac{H_b}{H_c} = C_1 - 0.025 \cdot \left(\frac{H_c}{H_r}\right)$	$C_1 = v_5$						1.072	0.986	0.858
(10)	$\frac{b_M}{H_b} = 0.996 \cdot \left(\frac{V_w^{1/3}}{H_w}\right)^{0.558} \cdot exp\ (C_2)$	$C_2 = v_4 + v_5$				0.258	–0.262	0.377	–0.092	–0.288
(11)	$\frac{b}{H_b} = 5.543 \cdot \left(\frac{V_w^{1/3}}{H_w}\right)^{0.739} \cdot exp\ (C_3)$	$C_3 = v_4 + v_5$				–1.207	–1.747	–0.613	–1.073	–1.268
(18)	$\frac{T_f}{T_r} = C_4 \cdot \left(\frac{H_c}{H_r}\right)^{0.654} \cdot \left(\frac{V_w^{1/3}}{H_w}\right)^{1.246}$	$C_4 = v_5$						0.038	0.066	0.205
(31)	$\frac{Q_p}{\sqrt{g \cdot V_w^{5/3}}} = 0.133 \cdot \left(\frac{V_w^{1/3}}{H_w}\right)^{-1.276} \cdot exp\ (C_5)$	$C_5 = v_4 + v_5$				–0.788	–1.232	–0.089	–0.498	–1.433

Legend:

ICW = impermeable core; CW = concrete wall; HM = mixed homogeneous materials; Db = overtopping; Tb = tunneling.

Walder and O'Connor (1997) indicate that the *envelope curves* define the upper limit of Q_p in the graphs, which show its value as a function of H_h, V_w or $(H_h \cdot V_w)$ and whose only purpose is to make it possible to quickly and conservatively estimate Q_p. The envelope curves have no physical significance and only have been established to show the upper limits of the historical observations.

MacDonald and Langridge-Monopolis (1984) analyzed the failure of 42 dams, 30 with homogeneous walls and 12 with mixed and rockfill walls with concrete screens. Their heights ranged from 6 to 93 meters. They defined two regression equations between Q_p and the breach formation factor. The latter is the envelope curve.

$$Q_p = 1.154 \cdot \left(H_h \cdot V_w\right)^{0.412} \quad (20)$$

$$\boldsymbol{Qp} = 3.850 \cdot \left(H_h \cdot V_w\right)^{0.411} \quad (21)$$

Costa (1985), also cited by Wahl (2004) and Zagonjolli (2007), analyzed 31 historical dam failures, whose heights varied from 1.8 to 83.8 meters with storage volumes at the time of the failure between 3 800 m^3 and 700 Mm^3. No distinction was made in terms of type of failure or type of wall. Their two equations with least uncertainty according to the Wahl (2004) study are:

$$\boldsymbol{Qp} = 2.634 \cdot \left(H_h \cdot V_w\right)^{0.440} \quad (22)$$

$$Q_p = 0.981 \cdot \left(H_h \cdot V_w\right)^{0.420} \quad (23)$$

Zagonjolli (2007) graphically did not find significant differences between equations (20) and (23). Froehlich (1995a,b) studied 22 historical failures of dams with heights from 3.7 to 86.9 meters and volumes V_w ranging from 92 500 m^3 to 660 Mm^3, finding:

$$Q_p = 0.607 \cdot \left(H_w\right)^{1.240} \cdot \left(V_w\right)^{0.295} \quad (24)$$

As a historical reference, Froehlich (1995a) cited the formula proposed by the US Soil Conservation Service in 1985 for walls with earth materials and values of H_h greater than 31.4 meters:

$$Q_p = 16.60 \cdot \left(H_h\right)^{1.85} \quad (25)$$

Walder and O'Connor (1997) address the issue of *natural dams*, that is, those formed by processes involving storage of water from the obstruction of a channel, most commonly from landslides and the flow of stems and branches. These authors present three regression equations and their respective envelope curves for dams created from obstruction and those constructed *ex professo*. The formulas for the constructed dams are:

$$Q_p = 2.50 \cdot \left(H_h\right)^{2.340} \quad (26)$$

$$Q_p = 1.16 \cdot \left(V_w\right)^{0.460} \quad (27)$$

$$Q_p = 0.61 \cdot \left(H_h \cdot V_w\right)^{0.430} \quad (28)$$

$$\boldsymbol{Qp} = 2.90 \cdot \left(H_h \cdot V_w\right)^{0.430} \quad (29)$$

Walder and O'Connor (1997) indicated that their formulas were based on the data collected by Costa (1988). These authors reported that the estimates of Q_p obtained with the regression equations are probably less than the actual discharge flow from the breach failure because many of the measurements were taken below the dam and their values were not corrected for movement and reduction of the flood wave.

This also justifies the use of envelope curves to bound the value of Q_p. The last two complete and simplified equations by Xu and Zhang (2009) are (30) and (31) (Table 1) and enable estimating Q_p.

Factors with the Most Influence on the Estimates

Erodibility of the wall is the most important factor influencing the estimate of most of the simplified equations found by Xu and Zhang (2009). A high erodibility leads to a rapid development of the failure breach, which results in larger failure dimensions, higher peak discharge flow and shorter formation time. The *storage form ratio* ($V_w^{1/3}/H_w$) has also been observed to play a large role in all of their equations, except for the first two which estimate the depth of the breach (H_b).

With regard to this ratio, two types of dams or reservoirs exist: *low* with a shorter wall height and large storage, that is, plain reservoirs that result in large $V_w^{1/3}/H_w$ values; and *high* dams with a considerably high wall and smaller storage volume, that is, canyon reservoirs with small $V_w^{1/3}/H_w$. For two dams with the same storage value, where one is high and one low, the former will generate a larger discharge flow due to more potential energy, as observed in equations (30) and (31) where the flow Q_p decreases as $V_w^{1/3}/H_w$ increases. T_f decreases as Q_p increases and increases as $V_w^{1/3}/H_w$ increases (equations (17) and (18)).

Various researchers have found that the peak flow can occur before the width of the failure breach reaches is maximum. Xu and Zhang (2009) indicate that in high dams the peak discharge flow is very likely to occur sooner than in low dams, and that the width of the failure breach in low dams will larger because the lateral erosion continues with a relatively high reservoir level.

It has also been found that failures due to overtopping create larger breach widths than those caused by rupture due to erosion from seepage (tunneling). This is likely to be associated primarily with failures from overtopping commonly caused by floods supplying large volumes of water to the reservoir, which raise the level above the wall crest, increasing $V_w^{1/3}/H_w$. Meanwhile, for failures due to tunneling, water is released from the reservoir and the storage levels are less at the beginning of the process as well as after the collapse of the erosion tunnel that creates the breach failure.

Uncertainty Values Associated with the Various Empirical Equations

Table 2 presents the estimates based on Wahl (2004) for the uncertainty of 11 of the 28 empirical equations selected, indicating the mean error of the estimate in logarithmic cycles ($\bar{e}$), the uncertainty interval range ($\pm 2S_e$) and the logarithmic cycles, where S_e is the standard deviation of the errors and the interval variation or confidence interval (CI), which correspond to $10^{\bar{e}-2S_e}$ and $10^{\bar{e}+2S_e}$. These approximately define the 95% confidence interval when multiplied by the value obtained with the respective empirical equation. The 10 empirical equations proposed by Xu and Zhang (2009) are presented in the last two columns of Table 2 (only those established by these authors).

Grouping of Empirical Equations

Three groups were created with the 28 empirical equations applied to constructed dams, since they only require information related to water storage level and stored volume before the failure. The first group is composed of 7 equations which were not verified by Wahl (2004) and therefore their calculations do not have confidence intervals. The second group contains 11 equations, reported in Table 2, which were studied by

Table 2. Uncertainty estimates for the empirical equations indicated, according to Wahl (2004) and Xu and Zhang (2009).

Equation number (variable to be calculated)	$\bar{e}$	$\pm 2S_e$	95% Confidence Interval	Equation number (variable to be calculated)	95% Confidence Interval
(4) (b)	+0.01	± 0.39	0.40-2.40	(6) y (9) ($H_b < 50$ m)	0.79-1.20
(3) (b)	+0.09	± 0.35	0.37-1.80	(6) y (9) ($H_b > 50$ m)	0.74-1.25
(12) (T_f)	–0.21	± 0.83	0.24-11.0	(7) (b_M)	0.44-2.27
(15) (T_f)	–0.22	± 0.64	0.38-7.30	(10) (b_M)	0.45-2.22
(24) (Q_p)	–0.04	± 0.32	0.53-2.30	(8) (b)	0.43-2.36
(23) (Q_p)	–0.05	± 0.72	0.17-4.70	(11) (b)	0.44-2.30
(25) (Q_p)	+0.13	± 0.50	0.23-2.40	(17) (T_f)	0.30-3.35
(20) (Q_p)	+0.13	± 0.70	0.15-3.70	(18) (T_f)	0.34-2.97
(19) (***Qp***)	+0.43	± 0.75	0.07-2.10	(32) (Q_p)	0.30-3.35
(21) (***Qp***)	+0.64	± 0.70	0.05-1.10	(33) (Q_p)	0.33–3.02
(22) (***Qp***)	+0.64	± 0.72	0.04-1.22	–	–

Wahl (2004). The last group is composed of 10 empirical equations found by Xu and Zhang (2000) which are considered to be the most reliable because of the information incorporated in the control variables (B_i and C_i, Table 1) regarding the erodibility of the wall and its type, as well as type of rupture or failure.

Numerical Applications

Established hypothetical Cases and their Results

Two hypothetical numerical applications have been formulated to illustrate the results from the 18 empirical equations which are applicable when only the basic information that has been cited exists (H_c and V_a). The first corresponds to a relatively small dam with a wall height (H_c) of 13 meters, conservation water level (NAN) height of 10 meters and whose failure from overtopping resulted in a water depth above the crest of 1 m. H_w is therefore 14 meters since the failure breach is presumed to have reached the base of the wall at the level of the channel. The storage volume(V_a) is 15 Mm^3 at the level of conservation and 30 Mm^3 at the initial failure (V_w). The wall is homogeneous clay material considered to easily erode.

The second application is that of a failure of a medium high dam due to tunneling, with the following data: H_c = 45 m, H_w = 35 m, NAN height = 40 m, V_a = 140 Mm^3 and V_w = 80 Mm^3. The wall has an impermeable core and can be considered to be resistant to erosion (medium erodibility).

In the first application $k_0 = 1.40$ and $k_1 = 1.30$ in equations (4) and (5). The type of wall is H to estimate the erodibility volume with expression (13) and expressions (12), (15) and (16) are used to calculate T_f. Two analyses are proposed. The first uses the data that are easily available from the dam, that is, height of the NAN and conservation volume, for which H_h = 10 meters and V_w = 15 Mm^3. The second analysis uses the level before the failure and the respective storage volume, for which $H_h = H_w$ = 14 meters and V_w = 30 Mm^3. The results from applying the 18 empirical equations to each analysis are shown in Table 3, as well as the values adopted in each one.

For the second application, $k_0 = k_1 = 1.00$. In equations (4) and (5) the type of wall is OT, used to calculate the eroded volume with expression (14) and equations (12), (15) and

Table 3. Results from 18 equations indicated in the first numerical application: failure from overtopping and homogeneous erodible wall.

First analysis: H_h = 10.0 m and V_w = 15.0 Mm³			**Second analysis: H_h = 14.0 m and V_w = 30.0 Mm³**		
Equation number	**Estimated magnitude**	**Confidence interval**	**Equation number**	**Estimated magnitude**	**Confidence interval**
(4)	b = 77.4	30.9-185.6	(4)	b = 102.9	41.2-247.0
(3)	b = 79.9	29.6-143.8	(3)	b = 89.9	33.3-161.8
(2)	b = 40.3		(2)	b = 58.7	
(5)	b = 76.1		(5)	b = 96.3	
	b_{adop} = 75.0 m			b_{adop} = 95.0 m	
(13)	V_e = 50 589		(13)	V_e = 111 665	
(12)	T_f = 0.92	0.22-10.15	(12)	T_f = 1.23	0.30-13.54
(15)	T_f = 2.03	0.77-14.84	(15)	T_f = 2.17	0.82-15.83
(16)	T_f = 2.18		(16)	T_f = 2.20	
	$(T_f)_{adop}$ = 1.75 h			$(T_f)_{adop}$ = 2.00 h	
(24)	Q_p = 1 381	732-3 176	(24)	Q_p = 2 571	1 363-5 914
(23)	Q_p = 2 665	453-12 524	(23)	Q_p = 4 106	698-19 299
(25)	Q_p = 1 175	270-2 821	(25)	Q_p = 2 190	504-5 256
(20)	Q_p = 2 696	404-9 976	(20)	Q_p = 4 121	618-15 247
(19)	Qp = 6 619	463-13 899	(19)	Qp = 11 075	775-23 257
(21)	Qp = 8827	441-9 710	(21)	Qp = 13 478	674-14 826
(22)	Qp = 10 425	417-12 719	(22)	Qp = 16 400	656-20 008
(26)	Q_p = 547		(26)	Q_p = 1 202	
(27)	Q_p = 2 320		(27)	Q_p = 3 191	
(28)	Q_p = 2 000		(28)	Q_p = 3 114	
(29)	Qp = 9 509		(29)	Qp = 14 805	
	$(Q_p)_{adop}$ = 2 000 m³/s	425-6 500		$(Q_p)_{adop}$ = 3 500 m³/s	650-10 000
	$(Qp)_{adop}$ = 10 000 m³/s	450-12 000		$(Qp)_{adop}$ = 15 000 m³/s	700-20 000

(16) are used to estimate T_f. Two analyses are again proposed. The first is based on data that are easily available from the dam (height of the NAN and conservation volume), for which H_h = 40 meters and V_w = 80 Mm³. The second analysis is based on the level before the failure and the respective storage volume, for which Hh = H_w = 14 meters and V_w = 30 Mm³. The results from applying the 18 empirical equations to each analysis are shown in Table 5, as well as the values adopted for each one.

Tables 4 and 6 present the results from the application of the complete and simplified equations by Xu and Zhang (2009) for the first and second numerical applications.

Analysis of the Results

With regard to the results shown in Tables 3 through 6, corresponding to the two numerical applications presented and their respective approaches using available information, it is noteworthy that they all have similar orders of magnitude, in particular with respect to the estimates of width of the breach and peak discharge flow. Considering that the calculations shown

Table 4. Estimated quantities associated with the breaking of a dam with homogeneous shade of land, high erodibility and overflow flaw with the equations of Xu and Zhang (2009)

General data: H_c = 13.0 m; H_w = 14 m; V_w = 30.0 Mm³					
Complete equation			**Simplified equation**		
Equation number	**Estimated magnitude**	**Confidence interval**	**Equation number**	**Estimated magnitude**	**Estimated magnitude**
(6)	H_b = 13.5 m	10.6-16.2	(9)	H_b = 13.7 m	10.8-16.4
(7)	b_M =126.7 m	55.8-287.7	(10)	b_M =144.7 m	65.1-321.2
(8)	b = 97.1 m	41.8-229.2	(11)	b = 121.1 m	53.3-278.6
(17)	T_f = 1.72 h	0.52-5.76	(18)	T_f = 1.65 h	0.56-4.90
(30)	Q_p = 4 483 m³/s	1 345-15 018	(31)	Q_p = 5 653 m³/s	1 865-17 071

Table 5. Results from the 18 empirical equations indicated in the second numerical application: failure from tunneling and erosion-resistant wall.

First analysis: H_h = 40.0 m and V_w = 140.0 Mm³			**Second analysis H_h = 35.0 m and V_w = 80.0 Mm³**		
Equation number	**Estimated magnitude**	**Confidence interval**	**Equation number**	**Estimated magnitude**	**Confidence interval**
(4)	b = 146.9	58.8-352.7	(4)	b = 119.8	47.9-287.5
(3)	b = 154.9	57.3-278.8	(3)	b = 142.4	52.7-256.3
(2)	b = 178.3		(2)	b = 155.3	
(5)	b = 126.5		(5)	b = 105.2	
	b_{adop} = 150.0 m			b_{adop} = 130.0 m	
(14)	V_e = 703 130		(14)	V_e = 389 545	
(12)	T_f = 2.41	0.58-26.46	(12)	T_f = 1.94	0.47-21.34
(15)	T_f = 1.91	0.72-13.92	(15)	T_f = 1.60	0.61-11.67
(16)	T_f = 1.66		(16)	T_f = 1.44	
	$(T_f)_{adop}$ =2.00 h			$(T_f)_{adop}$ = 1.65 h	
(24)	Q_p = 14 889	7 891-34 244	(24)	Q_p = 10 697	5 669-24 602
(23)	Q_p = 12 187	2 072-57 280	(23)	Q_p = 9 109	1 549-42 813
(25)	Q_p = 15 273	3 513-36 655	(25)	Q_p = 11 930	2 744-28 632
(20)	Q_p = 11 980	1 797-44 326	(20)	Q_p = 9 004	1 351-33 314
(19)	$\boldsymbol{Qp}$ = 40 440	2 831-84 924	(19)	$\boldsymbol{Qp}$ = 28 595	2 002-60 050
(21)	$\boldsymbol{Qp}$ = 39 081	1 954-42 989	(21)	$\boldsymbol{Qp}$ = 29 393	1 470-32 332
(22)	$\boldsymbol{Qp}$ = 51 265	2 051-62 543	(22)	$\boldsymbol{Qp}$ = 37 789	1 512-46 103
(26)	Q_p = 14 020		(26)	Q_p = 10 258	
(27)	Q_p = 6 482		(27)	Q_p = 5 011	
(28)	Q_p = 9 485		(28)	Q_p = 7 041	
(29)	$\boldsymbol{Qp}$ = 45 094		(29)	$\boldsymbol{Qp}$ = 33 472	
	$(Q_p)_{adop}$ = 13 500 m³/s	2 500-40 000		$(Q_p)_{adop}$ = 10 000 m³/s	2 000-30 000
	$(\boldsymbol{Qp})_{adop}$ = 45 000 m³/s	2 250-62 000		$(\boldsymbol{Qp})_{adop}$ = 35 000 m³/s	1 500-45 000

Table 6. Calculation of magnitudes associated with rupture of a rockfill wall with impermeable core, medium erodibility and failure due to tunneling, with Xu and Zhang equations (2009).

General data: H_c = 45.0 m; H_w = 35 m; V_w = 80.0 Mm³					
Complete equation			Simplified equation		
Equation number	Estimated magnitude	Confidence interval	Equation number	Estimated magnitude	Confidence interval
(6)	H_b = 41.7 m	33.0-50.1	(9)	H_b = 41.0 m	32.4-49.2
(7)	b_M =138.0 m	60.7-313.2	(10)	b_M =116.3 m	52.3-258.1
(8)	b = 110.4 m	47.5-260.5	(11)	b = 86.6 m	38.1-199.1
(17)	T_f = 3.21 h	0.96-10.75	(18)	T_f = 3.09 h	1.05-9.18
(30)	Q_p = 15 794 m³/s	4 738-52 909	(31)	Q_p = 11 571 m³/s	3 819-34 946

in Tables 4 and 6 are the most reliable, it is important to note that the use of the 18 empirical equations results in values of b and T_f estimated with the first application, which is not the case with Q_p ; the opposite occurs in the second numerical application.

With regard to the results from the complete and simplified Xu and Zhang (2009) equations shown in Tables 4 and 6 for each numerical application, high erodibility is seen in the former which results in larger b and Q_p estimates. The opposite occurs in the second numerical application, possibly because of its medium erodibility.

Conclusions

First. The selection of empirical equations presented to calculate the magnitudes of dam failures due to rupture of a wall composed of earth materials (that is, the medium breach width (b) in meters, time for it to form (T_f) in hours and the peak discharge flow (Q_p) in m³/s) is a first approach to the study of dam or reservoir safety for the purpose of defining emergency plans and risk mitigation strategies for areas located downstream.

Second. The results shown in Tables 3 through 6 for the two numerical applications enable establishing the probable values of magnitudes b, T_f and Q_p, as well as their confidence intervals. Based on these estimates, it is possible to determine the *sensitivity analyses* to be studied with hydraulic models corresponding to the outflow hydrograph and the respective movement downstream, thereby defining flows, levels and estimated arrival time of the flood caused by the rupture or failure of a dam with a rockfill earth wall.

Third. In the process of selecting the results, the two following recommendations should be taken into account: (1) the 10 empirical questions developed by Xu and Zhang (2009) (shown in Table 1) are the most reliable because they were generated with a process to select regressors and they incorporate into their control variables (v_i) relevant information about the wall, type of failure and estimated erodibility ; (2) of the remaining 18 empirical equations, the 11 that present confidence intervals are most reliable since they showed less uncertainty according to the work by Wahl (2004).

Acknowledgements

Thank you to engineer Rodrigo Murillo Fernández, vice manager of Dam Safety at the National Water Commission (Comisión Nacional del Agua) whose personal communication with the author helped to formulate the first hypothetical numerical application.

Received: 03/09/12
Accepted: 07/08/13

Referencias

CAMPOS-ARANDA, D.F. Modelado empírico simple del rompimiento de presas pequeñas de tierra (hidrograma de salidas). *Ingeniería. Investigación y Tecnología*. Vol. XIV, núm. 3, julio-septiembre de 2013, pp. 377-388.

COSTA, J.E. *Floods from Dam Failures*. Open-File Report 85-560. Denver: US Geological Survey, 1985, 54 pp.

COSTA, J.E. Floods from Dam Failures. In *Flood Geomorphology*. Baker, V.R., Kochel, R.C., and Patton, P.C. (editors). New York: John Wiley, 1988, pp. 439-463.

CHINNARASRI, C.H., JIRAKITLERD, S., and WONGWISES, S. Embankment Dam Breach and Its Outflow Characteristics. *Civil Engineering and Environmental Systems*. Vol. 21, No. 4, 2004, pp. 247-264.

FROEHLICH, D.C. Peak Outflow from Breached Embankment Dam. *Journal of Water Resources Planning and Management*. Vol. 121, No. 1, January/February, 1995a, pp. 90-97.

FROEHLICH, D.C. Embankment Dam Breach Parameters Revisited. *Proceedings of the First International Conference on Water Resources Engineering*, San Antonio, Texas, August 14-18, 1995b. New York: ASCE, pp. 887-891.

FROEHLICH, D.C. Embankment Dam Breach Parameters and their Uncertainties. *Journal of Hydraulic Engineering*. Vol. 134, No. 12, December, 2008, pp. 1708-1721.

HAGEN, V.K. Re-evaluation of Design Floods and Dam Safety. *Proceedings of the 14th Congress of International Commission on Large Dams*. Vol. 1. Río de Janeiro, Brasil, 1982, pp. 475-491.

MacDONALD, T.C. and LANGRIDGE-MONOPOLIS, J. Breaching Characteristics of Dam Failure. *Journal of Hydraulic Engineering*. Vol. 110, No. 5, May, 1984, pp. 567-586.

NWS. *Dambreak Scenario Rules of Thumb used at LMRFC*. National Weather Service, 2002. Consultado en agosto de 2012. World Wide Web: www. nws.noaa.gov/…/dambeak_rules_of_thumb_v2.30.doc.

REED, S. and HALGREN, J. Validation of a New GIS Tool to Rapidly Develop Simplified Dam Break Models. *Proceedings of Association of Dam Safety, Officials Dam Safety*. Washington, DC, Sept. 25-29, 2011, 18 pp.

SINGH, V.P. *Dam Breach Modeling Technology*. Chapter 2: Dam Breaching. Dordrecht, The Netherlands: Kluwer Academic Publishers, 1996, pp. 27-40.

VON THUN, J.L. and GUILLETTE, D.R. *Guidance on Breach Parameters*. Unpublished internal document. Denver: US Bureau of Reclamation, 1990, 17 pp.

WAHL, T.L. Uncertainty of Predictions of Embankment Dam Breach Parameters. *Journal of Hydraulic Engineering*. Vol. 130, No. 5, May, 2004, pp. 389-397.

WALDER, J.S. and O'CONNOR, J.E. Methods for Predicting Peak Discharge of Floods Caused by Failure of Natural and Constructed Earthen Dams. *Water Resources Research*. Vol. 33, No. 10, October 1997, pp. 2337-2348.

XU, Y. and ZHANG, L.M. Breaching Parameters for Earth and Rockfill Dams. *Journal of Geotechnical and Geoenvironmental Engineering*. Vol. 135, No. 12, December, 2009, pp. 1957-1970.

ZAGONJOLLI, M. *Dam Break Modeling, Risk Assessment and Uncertainty Analysis for Flood Mitigation*. London: Taylor & Francis Group, 2007, 140 pp.

Author's address institutional

Dr. Daniel Francisco Campos Aranda

Profesor jubilado de la Universidad Autónoma de San Luis Potosí
Genaro Codina 240, Colonia Jardines del Estadio
78280 San Luis Potosí, San Luis Potosí, México
campos_aranda@hotmail.com

Click here to write the autor

Discussion

Technical notes and technical articles are open to discussion according to the following guidelines:

- The discussion will be written in the third person.
- The writer of the discussion shall use the term "commentator" when referring to oneself and the term "author" when referring to the one responsible for the technical note or article.
- The discussion shall be sent within 12 months of the last day of the quarter in which the a technical article or note was published.
- The length of the discussion may be extended by written request from the commentator.
- The discussion is to be presented according to the Guide for Collaborators published in this journal (omitting data referring to the length and abstract). In addition, the bibliographical citation of the technical notes or articles to which the discussion refers shall be included.
- The maximum length of the discussion is 4 journal pages (approximately 10 cuartillas, including figures and tables).
- The figures and tables presented by the commentator shall be progressively marked with Roman numbers and when citing those generated by the author the original numeration should be respected.
- The editors will suppress data that does not pertain to the subject of the discussion.
- The discussion will be rejected if it contains topics addressed by other sources, promotes personal interests, is carelessly prepared, raises controversy involving already established facts, is purely speculative or falls outside the purpose of the journal.
- The discussion will be published along with commentaries from the author or authors to which it refers.
- The discussion will be directed by the editor in chief.

Records video in the mountains of Cacahuatepec, Huaycatenango, Guerrero, Mexico.

Photo: Omar Fonseca Moreno.

Contributor's guide

The journal ***Tecnología y Ciencias del Agua*** invites specialists to collaborate with original technical articles or notes **related to water, that result from investigations and provide original contributions,** based on the disciplines of hydrology, hydraulics, water management, water and energy, water quality, and physical, biological and chemical sciences as well as political and social sciences, among others, according to the guidelines stated below.

PREPARATION OF THE ARTICLE

FORMAT

Font: Palatino throughout the entire document (body of text, tables and figures).

Font Size: Use 8, 9, 10 and 20 points, according to the following table:

8 points (Palatino)	9 points (Palatino)
• Tables. • Figures. • Acknowledgements.	• Name of authors. • Institution of authors. • Abstract. • *Abstract* and *keywords*. • Institutional address of the authors.
10 points (Palatino)	**20 points capital letters (Palatino)**
• Body of the text. • Title of the work in English.	• Title of the work in Spanish

Line Spacing: double-spaced.

Page Numbers: all pages shall be numbered.

Length

***Technical article*:** **30 pages** (numbered), including figures and tables.
***Technical note*:** **10 pages** (numbered), including figures and tables.

CONTENS

Contens

The article shall present significant contributions to scientific and technological knowledge pertaining to the specialty. It shall be based on finished works or those that have completed a development cycle. It shall show results from a series of experiences over 1 year or more of investigations and be supported by an adequate bibliographical review. **The basic structure of the text shall contain an introduction, the development and the conclusions.** The classic layout is preferable: abstract, introduction, methodology, results, discussion, conclusion and references.

Title

The title, written in Spanish and English, shall be informative and not exceed 12 words.

Abstract

The abstract, **written in Spanish and English**, shall be concise and provide a broad overview of the investigation (objective, method, results and conclusions) without exceeding 250 words.

Key Words

Eight words or key phrases (maximum) shall be provided **in Spanish and English** that facilitate the identification of the information.

Footnotes

Not admitted. The information is to be incorporated into the text.

Acknowledgements

To be included after the text and before the references.

Tables

- One page for each table.
- A list of all the tables cited shall be presented after the references.

Figures

- One page for each figure.
- All the names of the figures shall be included after the tables.
- They should be high-resolution (300 dpi).

Note: When the article is approved by the publication, the author shall send each figure in high-resolution (300 dpi) in JPG format.

References

- The entire bibliography must be referenced in the main body of the text.
- In the case of addressing scientific and technological topics that are common domain, works that denote the knowledge of the authors about the *state-of-art* shall be cited.
- Avoid self-citations to the extent possible
- International ISO-690 and ISO-690-2 standards are to be used as a basis. References to the literature used to develop the document are to be cited with last name of the author and date in parenthesis, for example, (Black, 1989), and ordered alphabetically by last name, ensuring that they are complete.

Examples of references:

Books

Last name of the author and initials in capital letters. Title of the book in capital/small letters and italics. Responsibilities related with the editorial work such as translating and editing. Edition (beginning with the second edition). Publication (city, publisher and year).

Example:

LEVI, E. *Tratado elemental de hidráulica*. Second edition. Jiutepec, Mexico: Instituto Mexicano de Tecnología del Agua, 1996, 303 pp.

When there are two or more authors:

GARCÍA R., E., GONZÁLEZ, R., MARTÍNEZ, P., ATHALA, J. and PAZ-SOLDÁN, G.A. *Guía de aplicación de los métodos de cálculo de caudales de reserva ecológicos en México*. Colección Manuales. Mexico: Convenio SGP-IMTA, 1999, 190 pp.

Titles of works or articles should not be translated. In the event a version exists in Spanish, it shall be indicated at the end of the original reference after the period.

Journals

Last name of the author and initials in capital letters. Title of the article in regular font, capital and small letters. Responsibilities related with the editorial work, such as translating and editing. Publication in capital/small letters and italics. Edition (volume, number, year, pages).

Example:

DÖLING, O.R. y VARAS, E. Operación de sistemas de recursos de agua multipropósito usando un modelo de simulación de procesos. *Ingeniería hidráulica en México*. Vol. XV, no. 2, May-August 2000, pp. 5-18.

Electronic Documents

Last name of the author and initials in capital letters. Title in capital/small letters and italics. Type of media in brackets. Responsibilities related with the editorial work, such as translating and editing (optional). Edition. City of publication. Publisher. Date of publication. Date of last review or update. Date in which the search was conducted in brackets. Series (optional). Notes (optional). Availability and access. Email.

Example:

CARROLL, L. *Alice's adventures in Wonderland* [online]. Textinfo ed. 2.1. Dortmund, Germany. WindSpiel, November 1994 [cited February 10, 1995]. Available in *World Wide Web*: http://www.germany.eu.net/books/carroll/alice.html.

Language

Spanish or English

Separation of numbers and use of decimal points

In *Tecnología y Ciencias del Agua*, the separation between thousands is denoted with a blank space. A decimal point is used to separate whole numbers from fractions. In this regard, refer to *Diccionario panhispánico de dudas*, edited by the Real Academia Española and the Asociación de Academias de la Lengua Española, in 2005, with respect to numeric expressions: "**the Anglo-Saxon use of the period is accepted, normal in some Hispano-American countries…: $\pi = 3.1416$.".**

Delivery of Article

Send the article in *Word* with the name of the authors and institutional address to revista.tyca@gmail.com, with copy to Elizabeth Peña Montiel, elipena@tlaloc.imta.mx.

General Information

The review process will begin once the material is received, during which it is possible that the manuscript could be rejected. If the text is suitable for review, having fulfilled the Editorial Policy and the Editorial Committee having determined so, it will proceed to the review stage.

Depending on the review process, the text may be accepted without changes, with minor changes, with extensive changes or rejected.

Once a work is published, the main author has the right to two journals and ten offprints free of charge.
In there are any questions, please write to Helena Rivas López, hrivas@tlaloc.imta.mx or Elizabeth Peña Montiel, elipena@tlaloc.imta.mx

Editorial Policy

Mission

Disseminate scientific and technical knowledge and advances related to water through the publication of previously unpublished articles and technical notes that provide original contributions.

Our Principles

- Impartiality
- Objectivity
- Honesty

Our Values

- Knowledge
- Experience
- Thematic expertise

Contents

Interdisciplinary, composed of previously unpublished articles and technical notes related to water, that result from research and provide original scientific and technological contributions or innovations, developed based on the fields of knowledge of diverse disciplines.

Topics Covered

Interdisciplinary, related to water, with priority topics in the following knowledge areas:

- Water and energy
- Water quality
- Physical, biological and chemical sciences
- Hydro-agricultural sciences
- Political and social sciences
- Scientific and technological development and innovation
- Water management
- Hydrology
- Hydraulics

Type of Contributions

Technical article: scientific document that addresses and communicates, for the first time, results from a successful investigation or innovation, whose contributions provide and increase current knowledge about the topic of water.

Technical note: text that addresses advances in the field of hydraulic engineering and professional practices in the field of water, while not necessarily making an original contribution in every case it must be a previously unpublished work.

Some of the articles submitted to the review process can result in being published as notes and vice versa. This will occur through a proposal and process of mutual agreement between the authors and the editor responsible for the topic. The article and the note have nearly the same structure (abstract, introduction, methodology, results, discussion, conclusion, references).

Review Process

The journal is governed by a rigorous review process which establishes that each article be analyzed separately by three reviewers who recommend its acceptance, acceptance with minor changes, acceptance with extensive changes, rejection or acceptance as a technical note with the required changes.

At least one of three reviewers will be sought from a foreign institution.

The reviewers may not belong to the same institution as the authors proposing the article for publication.

When the decisions are opposing or inconsistent, the involvement of other reviewers or the members of the Editorial Committee may be requested.

On occasion, the approval of an article will be decided by two reviewers in addition to the opinion of the editor of the corresponding topic or, the editor in chief.

A rejected article will not be accepted for a new review process.

The review process will be performed in such a way that neither the authors nor the reviewers know the names of the other party.

The review process is performed by high-level specialists and experts who are national and internationally renowned in their professional fields and have the ability to reliably evaluate, in a timely manner, the quality as well as the originality of contributions, in addition to the degree of scientific and technological innovation in the topic under which it is submitted for possible publication.

This participation is considered a professional contribution and will be performed as a courtesy.

The reviews have a "Guide for the Reviewer" provided by the journal's Editorial Department.

Final Ruling

The ruling resulting from the review process is not subject to appeal.

Authors

Works are published from authors of any nationality who present their contributions in Spanish; nevertheless, we all accept works in Spanish or English.

Responsibility of the Authors

Submitting a proposal for the publication of an article commits the author not to simultaneously submit it for consideration by other publications. In the event an article has been submitted to another media for eventual publication, the author agrees to do so with the knowledge of the Editorial Department, which will suspend the review process and inform the Editorial Committee of the decision by the authors.

Collaborators whose articles have been accepted will formally cede the copyright to ***Tecnología y Ciencias del Agua***.

The authors are responsible for the contents of the articles.

The author is responsible for the quality of the Spanish used. If the writing is deficient the work will be rejected. ***Water Technology and Sciences*** will only be responsible for the editorial management.

The author commits to making the changes indicated by the editor of the topic in the time frame establish by the editor. In the event these indications are not met, the article will be removed from the review process and be classified as rejected.

The author shall be attentive to resolving the questions and proposals presented by the editors and the editorial coordinator.

Each author shall approve the final printed proofs of their texts.

It is suggested that authors consult the "Guide for Collaborators."

Readers

Academics, investigators, specialists and professionals interested in the analysis, investigation and search for knowledge and solutions to problems related to water.

Reception of Articles

The reception of articles and notes is ongoing.

Time period

Bimonthly, appearing in the second month of the period.

Subscription and Distribution

The journal is distributed through paid and courtesy subscriptions.

Open Access

Water Technology and Sciences, previously ***Hydraulic Engineering in Mexico***, provides a digital version of all the material published since 1985.

Special editions and issues

Water Technology and Sciences will publish special numbers independently or in collaboration with other journals, professional associations or editorial houses with renowned prestige and related to water resources.

In addition, it will publish articles by invitation, acknowledging the professional advances of prominent investigators.

In both cases, the quality of the technical continents and scientific contributions will be reviewed.

Water Technology and Sciences is registered in the following national and international indices and abstracts:

• Thomson Reuters Science Citation Index® (ISI) • Expanded Thomson Reuters Research Alert® (ISI) • Índice de revistas mexicanas de investigación científica y tecnológica del Consejo Nacional de Ciencia y Tecnología (Conacyt) (2013-2018) • Sistema de Información Científica Redalyc (Red de Revistas Científicas de América Latina y El Caribe, España y Portugal), Universidad Autónoma del Estado de México • EBSCO (Fuente Académica Premier NISC; Geosystems, como Marine, Oceanographic and Freshwater Resources) • ProQuest (Cambridge Scientific Abstracts) • Elsevier (Fluid Abstracts: Process Engineering; Fluid Abstracts: Civil Engineering) • CAB Abstracts, CAB International • Latindex (Sistema Regional de Información en Línea para Revistas Científicas de América Latina, el Caribe, España y Portugal), Universidad Nacional Autónoma de México • Periódica (Índice de Revistas Latinoamericanas en Ciencias), Universidad Nacional Autónoma de México • Catálogo Hela (Hemeroteca Latinoamericana), Universidad Nacional Autónoma de México • Actualidad Iberoamericana, CIT-III, Instituto Iberoamericano de Información en Ciencia y Tecnología.

Other Sources

The journal can also be found archived in Google scholar.